9.1 HISTORICAL INTRODUCTION

(C. A. Lundquist and F. L. Whipple)

9.1.1 Initial Objectives of the SAO Satellite-Tracking Program

As the principal objective of its participation in the International Geophysical Year (IGY), the Smithsonian Astrophysical Observatory (SAO) conceived of and established a systematic program to observe positions of artificial satellites and to derive geophysical information from these observations (Whipple and Hynek, 1956, 1958a,b). The fundamental concepts for this program existed in the minds and studies of SAO Director Fred L. Whipple and his colleagues (see Ryan, 1952) well before President Eisenhower announced in 1955 that the United States would launch a scientific satellite during the IGY. These plans originated with Project Orbiter, followed by Project Vanguard, which in turn was superseded by the Army program that launched Explorer–I (5800101), the first United States satellite (Hayes, 1968). When this satellite attained its orbit on January 30, 1958, the SAO observation network and analytical apparatus were ready with partial operational status.

As stated in 1957, the principal objectives of this early SAO activity were (1) "to tie together the observing stations and the center of the geoid to a precision of the order of 10 m," (2) "to add appreciably to our knowledge of the density distribution of the earth, particularly in crustal volumes," and (3) to provide "the value of the [atmospheric] density a few kilometers above the initial perigee distance, and periodic effects or predictable cyclic effects that may occur in the earth's high atmosphere" (Whipple and Hynek, 1958a). The first two objectives evolved into similar, but more demanding, ones for subsequent programs, such as the National Geodetic Satellite Program (NGSP) (Rosenberg, 1968).

9.1.2 Establishment of the Baker-Nunn Network

To establish the required satellite observation capability, SAO initially developed a photographic system (Whipple and Hynek, 1958b). The basic tracking camera, named Baker-Nunn after its optical and mechanical designers, has f/1 Schmidt optics. During the first several years of field operation, a Norrman time standard, also named for its designer, provided epoch measurements. The Baker-Nunn tracking system has accuracies in the arc-second and millisecond range. Twelve stations with this equipment went into operation as a global network during the IGY.

With the passage of time, the Baker-Nunn network continued operation with only small changes (Whipple and Lundquist, 1967). The modes of camera operation required slight modification to accommodate a variety of satellite characteristics. A few stations were moved to higher latitudes because many satellites were launched into high-inclination orbits. A new, more accurate, time standard replaced the Norrman standard.

It is a tribute to the designers of the Baker-Nunn system that for nearly a decade the accuracy of the Baker-Nunn data exceeded the accuracies of the analytical treatment of these data and of the geodetic parameters derived from them. Indeed, Baker-Nunn observations contributed appreciably to the NGSP results reported here. By about 1966, however, the accuracy of the derived geodetic parameters began to approach that of the observations, thus motivating significant moves toward deployment of new tracking systems of superior accuracy.

9.1.3 Introduction of Laser Systems

When the accuracy of photographic methods began to pose a serious limit on future

geodetic investigations, laser systems to measure Earth-to-satellite ranges offered the best prospect for substantial reduction of measurement uncertainties. Range measurements with pulsed laser systems became possible in 1964 after the BE–B satellite (6406401), which carried an array of optical retroreflectors, was launched (Plotkin, 1964). In 1965, SAO and the General Electric Company began laser ranging experiments in conjunction with the Baker-Nunn system at Organ Pass, New Mexico (Anderson *et al.*, 1966).

Experience with the equipment at Organ Pass led to the specification and development of a greatly improved instrument, and the prototype model of this ruby-laser system began operating in late 1967 at Mt. Hopkins Observatory, Arizona (Lehr *et al.*, 1968). After appropriate tests of this prototype and after identification of design modifications indicated by them, SAO procured three additional laser ranging systems. In late 1970, these three units began operating at the SAO sites in Arequipa, Peru; Natal, Brazil; and Olifantsfontein, South Africa. The prototype remained at Mt. Hopkins.

These SAO instruments, and similar laser systems deployed by other groups, contributed the major data base used in the final NGSP results presented here. It is the improved accuracy of these data, relative to earlier observations, that allows further refinements of geodetic parameters.

9.1.4 Evolution of International Cooperation

The network of Baker-Nunn satellite-tracking stations was conceived by SAO as a cooperative international enterprise during the IGY. Its implementation depended crucially on agreements between SAO and appropriate scientific organizations in the nations hosting the stations. Many of these agreements have continued to the present, with occasional renewals and modifications as needed. The viability and success of such a network stem from a recognition that little can be accomplished on global problems by a single station working in isolation, whereas a well-coordinated global network can achieve much.

The cooperative aspects of the efforts coordinated by SAO naturally extend to the analysis and interpretation of the data. First, it has been a policy that data generated by the network are available to all network participants. Also, SAO data are eventually published or otherwise made available to the general scientific community. Second, several visiting scientists from host countries have been deeply involved at SAO in geodetic investigations that employ the network data (in particular, Veis, 1960, 1961, 1963a,b, 1965c, 1966a,b; Kozai, 1960, 1962a,b, 1963a,b, 1964; Giacaglia, 1973).

In recent years, cooperative efforts have increased further through various international observing campaigns. These campaigns involve a concerted effort among the several existing networks, as well as between individual stations. Such campaigns have been responsible for some of the most valuable data used in the analyses reported here. Thus, credit for the basic support behind these results must go to many nations, organizations, and individuals.

9.1.5 Cooperative Observing Programs

The first of the inter-network cooperative observing programs occurred in the spring of 1967 (Lundquist, 1967). The timing of this campaign followed the launch of Diademe–1 (D1C, 6701101), and Diademe–2 (D1D, 6701401), which carried retroflectors for laser ranging. The major participants—Centre National d'Etudes Spatiales (CNES), Goddard Space Flight Center (GSFC), and SAO—arranged an observing schedule to be followed by the stations of these three organizations. The arrangements emphasized the need to coordinate observations taken by the small number of laser instruments in operation at that time. Lasers were located at three CNES stations, in Haute Provence,

France; Colomb-Bechir, Algeria; and Stephanion, Greece; at a GSFC station in Greenbelt, Maryland; and at the SAO station in Organ Pass. The Baker-Nunn and other camera systems also participated.

For this observation campaign, intervals of favorable satellite visibility lasting several weeks were selected for the five satellites with retroreflectors. During each selected interval, all participating stations were dedicated to obtaining maximum tracking coverage of the designated satellite. This became known as the saturation-tracking mode. Such periods of high-density data are particularly valuable in determinations of longitude-dependent coefficients in the gravity field of the Earth.

SAO took the initiative in organizing a second, international, geodetic-satellite tracking effort in 1968, following the launch of GEOS–2 (6800201). GEOS–2 was the second satellite launched under the aegis of the NGSP and equipped with retroreflectors. Again, intervals of several weeks were designated for saturation tracking of the six retroreflector satellites. By 1968, a few more laser instruments were operational, and they participated in this observation campaign. The two CNES lasers were located at Haute Provence and at the SAO station in San Fernando, Spain; two NASA lasers were at Greenbelt and at Rosmund, North Carolina; and an SAO laser was located at Organ Pass.

A two-laser collocation experiment was conducted at the SAO Mt. Hopkins Observatory in 1969. A GSFC mobile laser system and the SAO prototype obtained simultaneous observations on GEOS–2, enabling an evaluation of system performance to be made.

The next observation campaign in this series was the International Satellite Geodesy Experiment (ISAGEX), organized by CNES in conjunction with the launch of PEOLE (7010901), a new retroreflector satellite in a low-inclination orbit. This effort extended from January 5 to August 31, 1971.

9.1.6 Evolution of Results

The results presented here by SAO, corresponding to the completion of the NGSP, are but the latest in a sequence of advances in the determination of geodetic parameters. This sequence started with the early works of Izsak (1963, 1964, 1966), Kozai (1963a,b, 1964), and Veis (1965c).

A major effort in 1966 resulted in the first Smithsonian Institution Standard Earth (SE) (Lundquist and Veis, 1966), the combined work of many authors. This was the first solution for geodetic parameters based on a combination of dynamical and geometrical data and analyses. The 1969 SE II (Gaposchkin and Lambeck, 1970) was the next milestone in the SAO series. This solution for geodetic parameters not only combined dynamical and geometric data, but also incorporated surface-gravity information and results from Jet Propulsion Laboratory's (JPL) Deep Space Net (DSN). This was also the first solution to employ some laser range data, resulting from the 1967 and 1968 observation campaigns. Finally, the solution presented here is again a combination of all the varieties of data used in the 1969 solution, laser range data playing a dominant role. The available surface-gravity data are more complete then they were in 1969 and, hence, bear strongly on the final results. Survey data are also included.

9.2 INSTRUMENTATION [1]

(M. R. Pearlman, J. M. Thorp, C. R. H. Tsiang, D. A. Arnold, C. G. Lehr, and J. Wohn)

9.2.1 Baker-Nunn Camera

9.2.1.1 Description of Technique

The Baker-Nunn camera photographs satellites against a star background. It can

[1] Also included in this part is material originally prepared by G. Veis, K. Lambeck, and K. L. Haramundanis. We are grateful to them for their contributions.

photograph either passive, Sun-illuminated satellites or active-satellite flashes under night-sky conditions. The *Smithsonian Astrophysical Observatory Star Catalog* has an average standard deviation in star position of 0".5 (epoch of 1963.5) (Staff, Smithsonian Astrophysical Observatory, 1966). The SAO field timing system is kept within 100 μsec or better of Universal Time Coordinated (UTC) as maintained by and referred to the United States Naval Observatory (USNO); hereafter, we shall express such time as UTC(USNO). With the use of the catalog and the timing system, the reduction technique can provide an accuracy of 2". Observations are routinely reduced at the observing station to an accuracy of 40" to 60".

The camera was originally designed to photograph very small satellites in poorly known orbits without the aid of active systems on the satellites themselves. For this reason, it has a fast optical system and a wide field of view. Pointing predictions need an accuracy of only several degrees.

9.2.1.2 Instrument Description

The Baker-Nunn is a three-axis camera designed according to the specifications of SAO for satellite tracking. The optical system was designed by James G. Baker; the mounting and mechanical system, by Joseph Nunn. The camera is approximately 2.5 m high and 3 m wide and weighs about 9000 kg. It combines an extremely fast f/1 optical system with a sophisticated film transport, and currently uses 55.6–mm Royal X extended red film (Kodak S0–338). It is best known for its light-gathering power and can photograph stars 3×10^4 fainter than those visible to the naked eye. The camera, which operates only at night, can photograph Sun-illuminated satellites as well as satellites with flashing lights.

9.2.1.2.1 CAMERA OPERATION

The Baker-Nunn camera (see fig. 9.1) is basically a Schmidt telescope with refinements designed to improve its optical performance. The focal ratio of the system is f/1 with an aperture of 508 mm (20 inches). This focal length gives a film scale of 406" mm^{-1}.

Light enters the camera through the three-element lens assembly (two positive and one negative), which corrects for spherical and chromatic aberrations, and is reflected from the 787–mm (31-inch) diameter, spherical pyrex mirror onto the photographic film. During exposure, tension is applied to the film to force it to conform to the shape of the backup plate, which is figured to the required aspherical focal surface.

A clamshell-type focal-plane shutter begins and ends the exposure, which is preset for 0.2, 0.4, 0.8, 1.6, or 3.2 sec. A barrel-type shutter rotating in front of the focal surface chops the star trails or satellite trail (depending on the operating mode) and provides five reference breaks for measurement. The chopping shutter is coupled to a set of timing points that close at the third break and trigger a time presentation, readable to 0.1 msec, which is recorded on the film. When the exposure is completed, the film is advanced until the next frame is positioned against the backup plate. For a $15°\times5°$ field, including time presentation, one frame is 152 mm of film. The film-transport mechanism, chopper shutter, and clamshell shutter are mechanically synchronized.

The camera is supported on a massive altitude-azimuth mount (see fig. 9.2) with a third mechanized tracking axis normal to the altitude axis. Both altitude and azimuth are manually set, normally to $\pm0°.2$, and clamped into position during photography. The camera then tracks along a great circle about the tracking axis at a prescribed rate. This motion approximates the apparent satellite motion over a short arc. Movement about the azimuth axis is limited only by the length of the power and slave-clock cables, which permits approximately 400° of freedom. Altitude is limited by stops at 20° and 160°, and track angle is limited by microswitches at 27° and 153°. Continuously variable angular velocities of 0 to 7000" sec^{-1} are available.

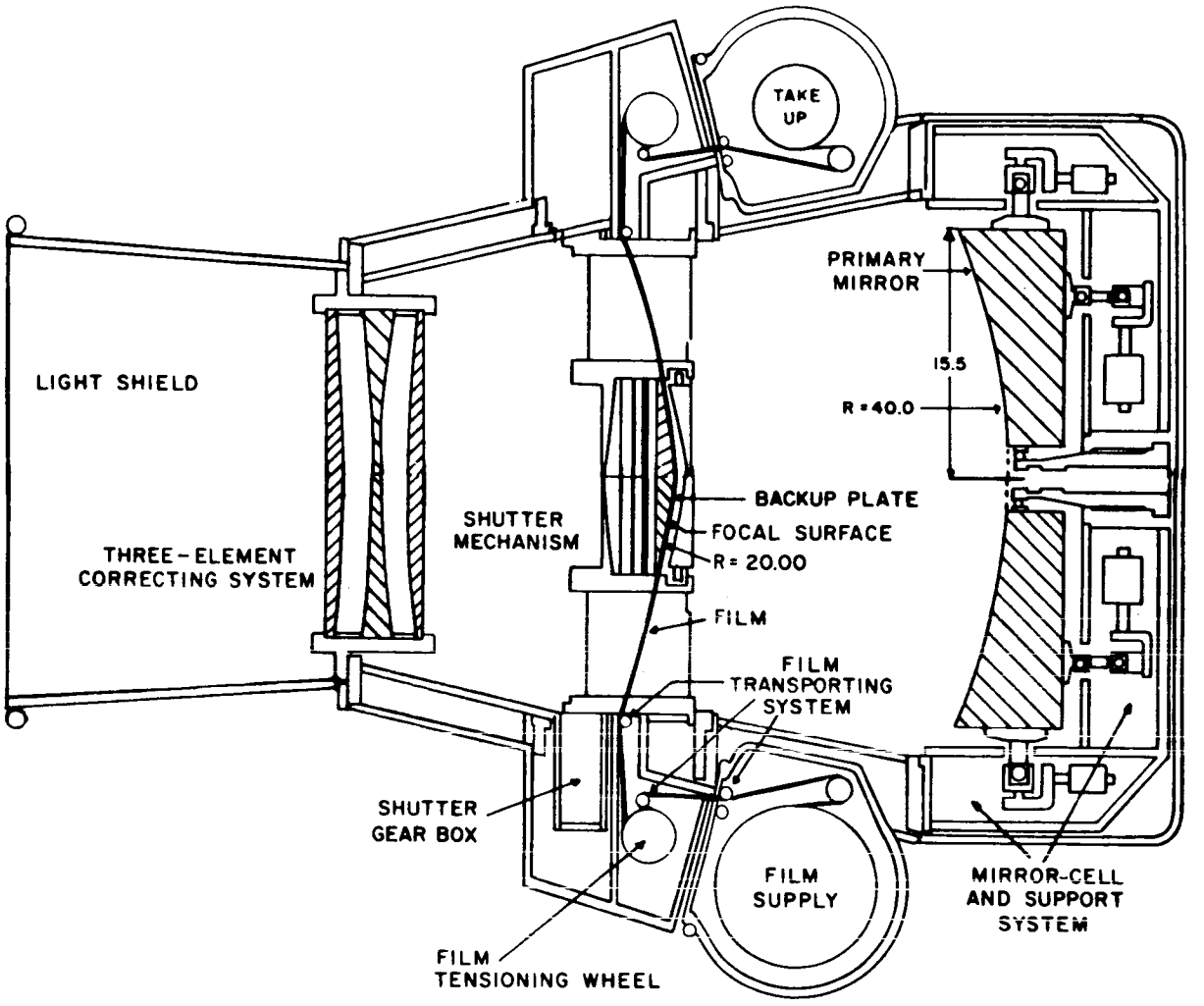

FIGURE 9.1.—Cross section of the Baker-Nunn camera.

9.2.1.2.2 OPTICS

The modified Schmidt optical system was chosen because it has a fast speed and a wide field of view and it yields good images over the entire field of view. To compensate for aberrations introduced by the spherical primary mirror, the camera has a three-element lens assembly, or corrector cell, mounted at the aperture stop. The cell has little focusing power but a strong spherical aberration approximately equal to and opposite that of the mirror. This permits a large field, fast speed, and good images. In the Baker-Nunn, no attempt has been made to flatten the focal surface: Instead, the film is made to conform to the curved focal surface. Chromatic aberration is minimized in the corrector cell by the use of two types of glass: Schott K2FS–2 glass on the two outer elements and Schott SK–14 glass on the inner element. The outer glass is subject to etching in the presence of water, and care must be taken in the field to keep the outer surface dry.

The mirror is very accurately supported by 12 counterweights and a center collimating post to position the mirror at the correct distance from the film. This supporting sys-

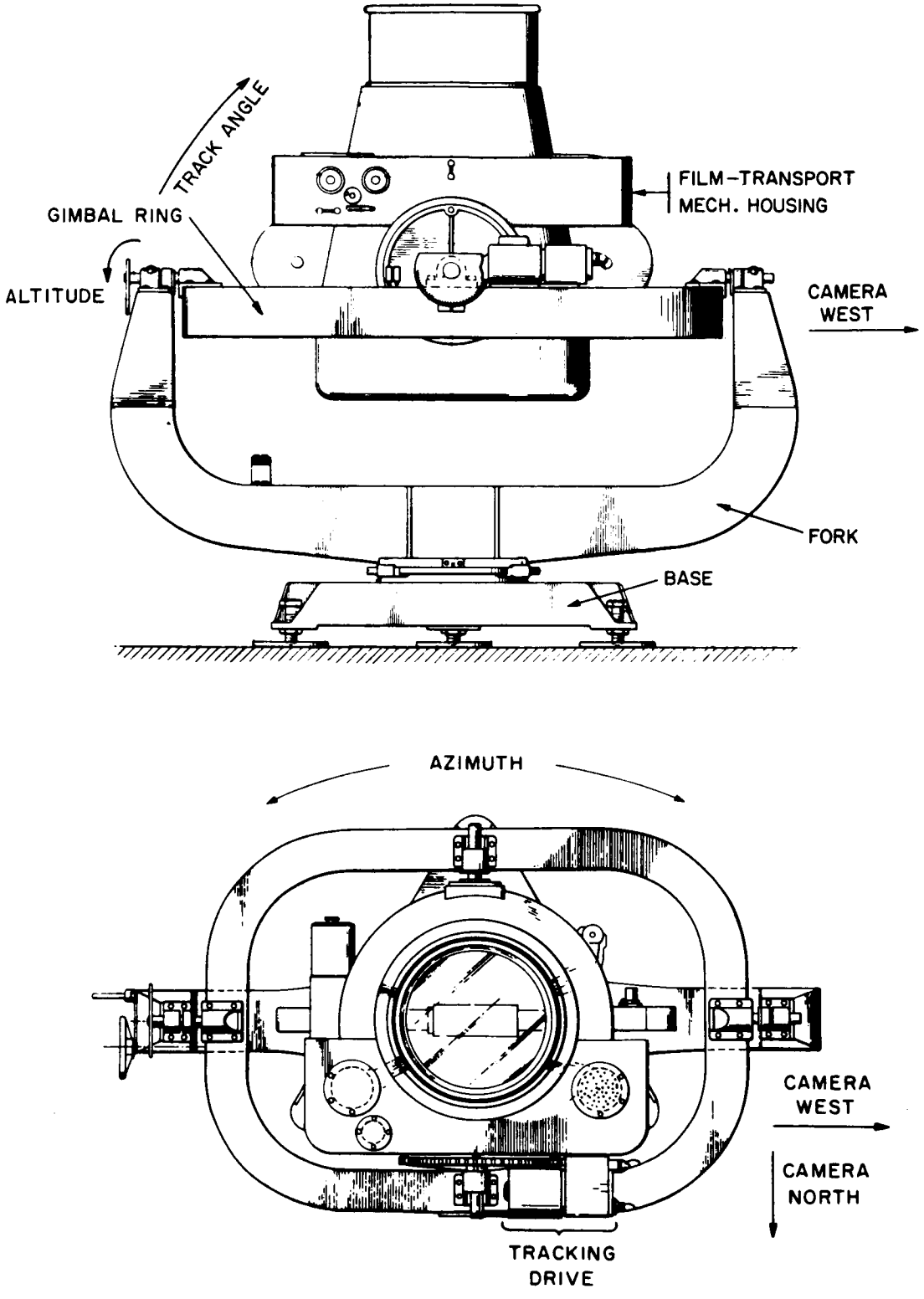

FIGURE 9.2.—Top and side views of the Baker-Nunn camera, showing three axes of rotation.

tem was designed to minimize image degradation due to temperature change and mechanical flexure.

9.2.1.2.3 MECHANICS

The operation of the camera depends on the synchronous operation of a gross (clamshell) shutter and a fast (chopping) shutter. These shutters and the film transport are mechanically linked and driven by a synchronous motor and a cycle-speed-selector transmission. Speeds of 2, 4, 8, 16, or 32 sec per cycle can be selected. There are two exposures per cycle with an effective exposure time of one-tenth the cycle. The system was originally designed to have both a tracking and a stationary exposure on each frame. However, this complicated the problems of reduction, and the camera is now operated either in the stationary mode or in the tracking mode for the entire arc photographed. The latter is used for faint satellites, and the former, for the brighter (visual) satellites.

The film is transported from a supply reel to a takeup reel by means of two drums and a system of idler rollers. The drums are powered by a system that applies tension, transports, and holds to the film during the camera's operation cycle. The drive that operates the shutters also operates the film transport in such a way that as the cycle period is decreased, the speed of transport increases. For example, for a 2-sec cycle, the film is exposed and transported at 1 frame sec^{-1}.

Timing of an event on the Baker-Nunn camera requires exact knowledge of the position of the chopping shutter at the moment the time display is triggered. The camera timing points are adjusted so that an epoch corresponding to the third passage of the shutter through the field of view is recorded on the film. The break in the image caused by the passage of the shutter is called a "chop." Figure 9.3 is a Baker-Nunn photograph in which the satellite, shown by the arrow, is being tracked by the camera and the star trails are chopped five times. During the third passage of the shutter, a strobe lamp with a collimating lens, located in the body of the camera, illuminates the chopping shutter, whose shadow is recorded on the film. The length of this shadow on the film is measured and used in the reduction process to calculate the angular position of the chopper.

The track-angle axis of the Baker-Nunn camera mount is driven by a reversible synchronous motor, a Graham variable-speed drive, and a multiplier transmission. The Graham drive allows a variation in speed from 0 to 70″ sec^{-1}. The transmission has three gearing ranges of 1, 10, and 100, allowing a total variation of 0 to 7000″ sec^{-1}. The lower the gear range, the more accurately the angular velocity can be set.

9.2.1.2.4 ELECTRONICS

For a proper sequencing of events, accurate exposure times, and accurate angular velocity, the camera must operate on precise 60–Hz power. Since this frequency is not available in many countries, the camera is operated on an amplified 60–Hz phase-shiftable reference signal from the station clock. By instantaneously increasing or decreasing the phase, the camera motors can be speeded up or slowed down. This procedure allows the center (third) chop to occur at a preset firing time and the camera to be synchronized for satellite-flash photography.

A display of the station clock is mounted on each camera at the point where film leaves the camera tube. On a demand pulse from the timing points, epoch is displayed and photographed by the camera. With the EECo clock, manufactured by the Electronic Engineering Company (EECo) of Santa Ana, California, time is displayed on the film in hours, minutes, seconds, and fractions to 0.0001 sec.

9.2.1.3 Accuracy and Error Budget

The accuracy of a satellite-position measurement with the Baker-Nunn camera is

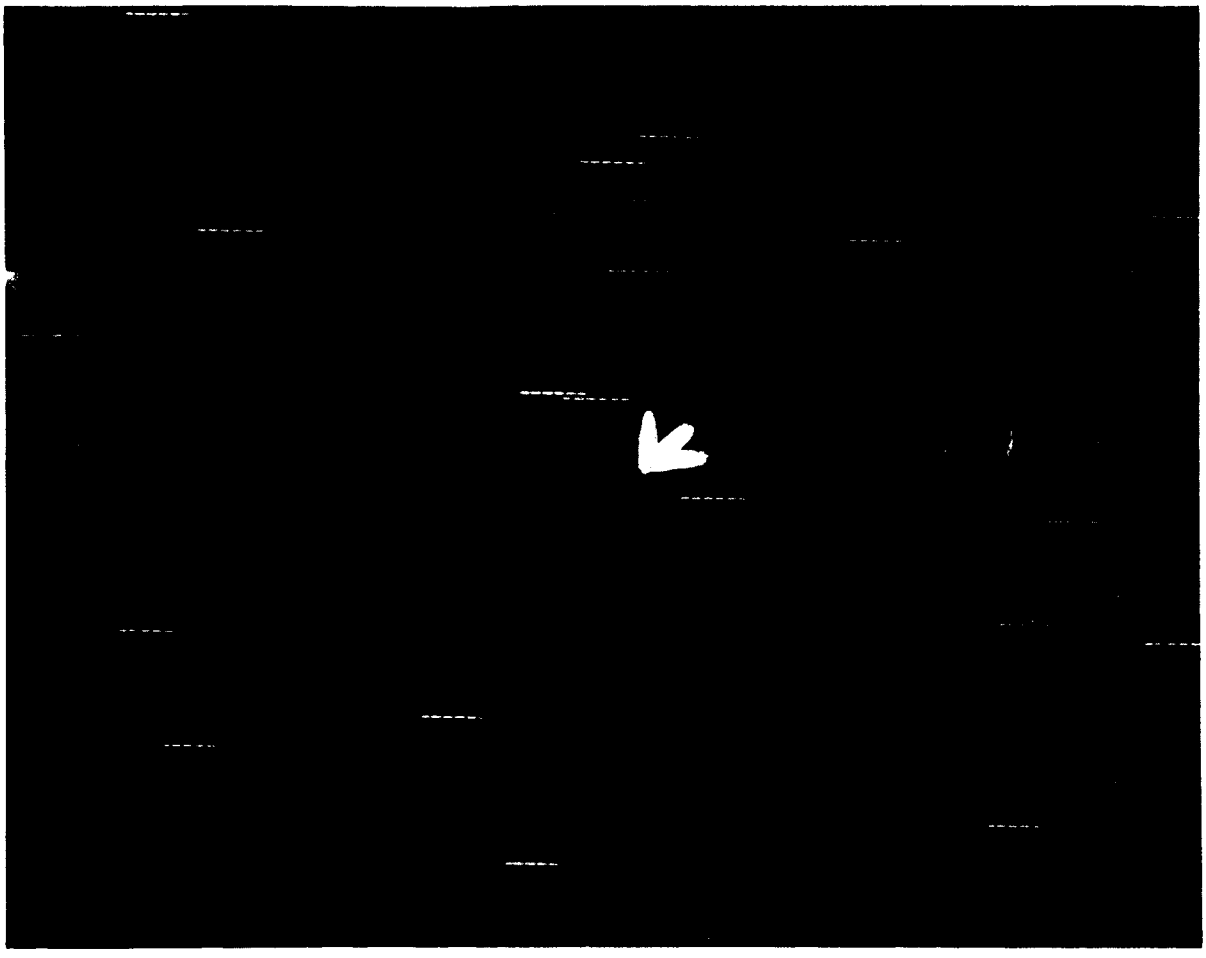

FIGURE 9.3.—Baker-Nunn photograph of satellite 6506301 (EG–RS–5). The satellite is indicated by the arrow, and the chopped star image tracks are in the background.

dictated primarily by (1) the film measurement and reduction procedure, (2) the accuracy of star positions, (3) atmospheric influences, and (4) the accuracy of timing maintained by the station clocks. In those cases where the great-circle approximation is an accurate representation of the satellite's apparent motion, the instrumentation introduces very minor errors in measurement. In those cases where the great-circle approximation may no longer be accurate, the accuracy of the observation is degraded because the satellite image may be spread. This condition may occur when long exposure times are required to obtain images of very faint satellites, or when the satellite angular velocity is very large.

9.2.2 Laser Ranging System

9.2.2.1 Description of Technique

A laser ranging system is an optical radar used to measure the distance from a ground station to a satellite. When accurate timing and appropriate corrections for range bias caused by the atmosphere are incorporated, this is one of the most accurate satellite-tracking techniques available.

The technique is made possible by the availability of Q-switched lasers that produce sharply defined pulses of nearly monochromatic high energy in a beam with a very low angle of divergence. Equally important is the availability of nanosecond-risetime elec-

tronics instrumentation to handle these optical signals. The fast-risetime, small-width pulses make time-interval measurements at nanosecond resolution possible on the basis of a single observation. The high degree of collimation enables the laser beam to hit the satellite with a significant amount of radiant energy. Finally, the technique requires optical retroreflectors on the satellite to ensure measurable return signals. The monochromatic nature of the laser output allows for efficient filtering to improve the signal-to-noise ratio.

The basic ranging system consists of a laser transmitter, a photoreceiver, a mount for the transmitter and receiver, and a time interval counter. The observed range time is the two-way time of flight of the laser pulse, measured by the time interval counter.

In operation, the laser beam is pointed to the predicted satellite position and is pulsed at specified times. During a normal satellite pass, the system makes many range measurements in order to take advantage of the satellite geometry and to permit accumulation of data for analysis.

9.2.2.2 Instrument Description

9.2.2.2.1 SMITHSONIAN ASTROPHYSICAL OBSERVATORY LASER SYSTEM

The SAO laser system (see fig. 9.4) was designed for the particular requirements and needs of the observatory's program in satellite geodesy. The system has a static-pointing mount (or pedestal) that is aimed by means of computed predictions of satellite azimuth and altitude. This method of steering permits the system to operate when the station is in daylight or the satellite is in the Earth's shadow, i.e., 24 hours per day. The static-pointing mount was selected because it is economical and operationally simple. The system operates routinely at 4 pulses min^{-1} and is capable of operating at rates as high as 10 pulses min^{-1}.

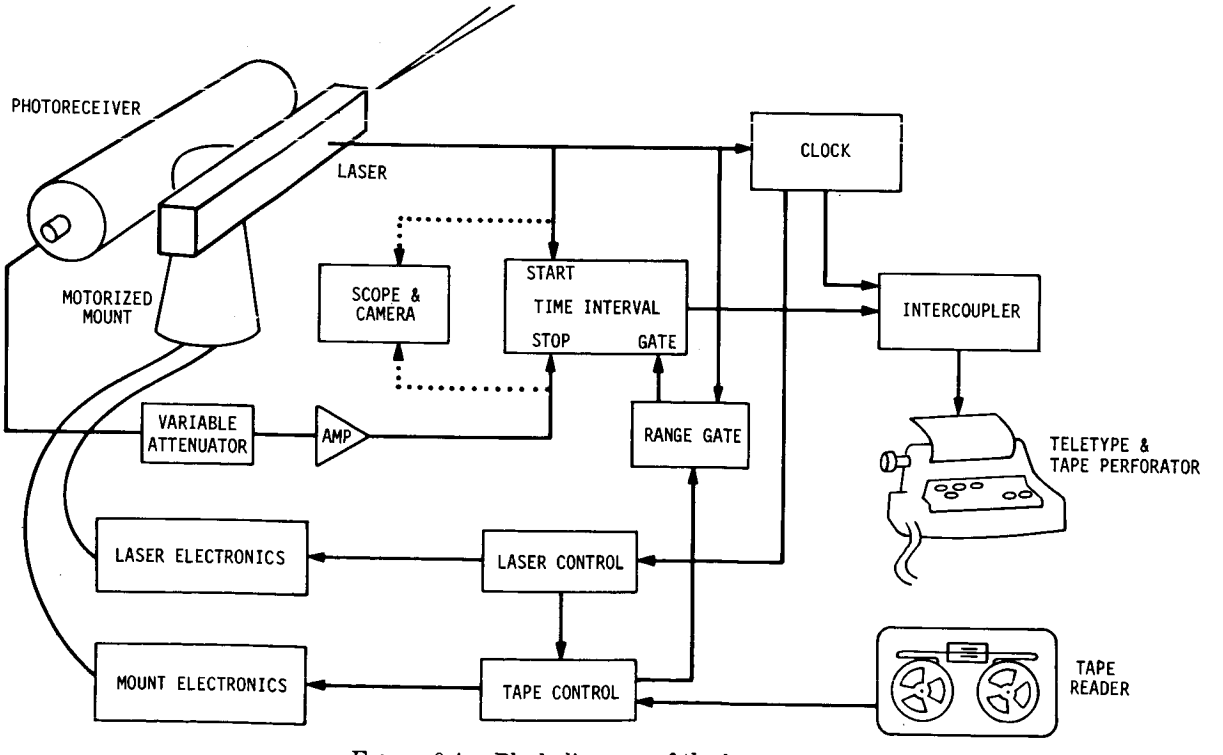

FIGURE 9.4.—Block diagram of the laser system.

The laser, built in an oscillator-amplifier configuration, generates an output of 5 to 7 joules in a 20–nsec pulse (half-power, full width). The laser transmitter system was produced by Spacerays, Inc., of Englewood, Colorado. The system uses a Pockels cell and a Brewster stack for a Q-switch and can maintain a pulse repetition rate of 10 ppm. Both the 0.85–cm (3/8-inch) diameter oscillator ruby rod and the 1.59–cm (5/8-inch) diameter amplifier rod are mounted in 15.24–cm (6-inch) double elliptical cavities, each containing two linear flashlamps. The optical cavity of the oscillator is formed by a flat rear mirror, with a reflectivity of 99.9 percent, and the uncoated front of the oscillator rod.

The oscillator output of 1 to 2 joules is coupled into the amplifier through a small beam-expanding telescope. The amplifier has a single-pass gain of about 4. Both ends of the amplifier rod are antireflective-coated.

The amplifier output is expanded to fill the 12.7–cm (5-inch) objective lens of a Galilean telescope. The telescope optics allows adjustment of the output beam divergence from a diameter of 0.5 to 5.0 mrad. Mounted at the output of the laser, ITT FW128 photodiodes pick up atmospherically scattered light from the outgoing pulse and send an electrical start signal to the time interval counter.

The optical elements of the laser are mounted on the machined upper surface of an aluminum I-beam, so that dimensional stability between the optical components will be maintained for all pointing orientations. Separate water-cooling systems are provided for the ruby rods and for the flashlamps. The coolant for the ruby rods is maintained at a temperature of $10° \pm 1°$ by thermostatically controlled cooling or heating elements. The lamp coolant is maintained within 10° C of the ambient air temperature. There is provision for applying nitrogen under pressure to the cavities, but experience has shown that this is not necessary. A cover over the I-beam is sealed, and desiccated air under slight pressure is circulated through the system.

The electronics of the laser transmitter are basically power supplies and pulse trigger circuits. The 1875–μf capacitor bank for the oscillator and amplifier lamps can be operated from 2000 to 4000 volts dc. Serial triggering of the lamps begins the discharge, which lasts slightly over 1 msec. Approximately 800 μsec after the lamp pulse begins, the system is Q-switched by quickly switching to ground the high-voltage input to the Pockels cell.

The ranging-system electronics consist of a clock, a firing control, a range gate control, and a time interval counter. The clock, synchronized to within ± 1 μsec of the station master clock, controls the firing time of the laser and provides the epoch of observation. The firing rate and the time of the laser firing are controlled by the laser control unit. The laser firing time can be shifted by a multiple of 0.001 sec, with a maximum of ± 10 sec, to account for the early or late arrival of a satellite at a predicted point in its orbit. The range gate control sends a delayed pulse of adjustable width to the counter so that the counter can be stopped only during a small interval of time about the predicted range time. The range gate provides protection against triggering by sky-background noise. The Eldorado 796 range counter is a time interval counter with 1-nsec resolution. It uses leading-edge, voltage, threshold discriminators on the start- and stop-signal lines. A start signal ranging from 5 to 20 volts is produced by the photodiode at the laser output. This signal is not processed or amplified before it reaches the start channel of the counter. The photomultiplier tube (PMT) output passes through a 0– to 50–db variable-step attenuator and a 32–db fixed-gain pulse amplifier before it reaches the stop-channel discriminator.

Stepping motors that point the mount are driven by position control electronics manufactured by Zehntel, Inc., Berkeley, California. Position information is maintained in the control units, which generate the appropriate number of drive pulses for the motors once a new azimuth or altitude position is demanded of the system.

The laser ranging system has a data subsystem that reads predicted satellite positions from punched paper tape and sends the information to the mount and laser control electronics and to the range gate. Azimuth and altitude pointing angles are given in thousandths of a degree; the range gate setting is specified in microseconds. The epoch for a predicted observation is displayed. Once the predictions start, operation continues automatically until the satellite pass is completed. Operation of the punched paper-tape reader is synchronized with the rest of the system by the laser control unit. Output data are also handled automatically by the data subsystem. The binary-coded-decimal (BCD) form of the epoch of firing and the range-time interval in nanoseconds is serialized, converted to Baudot code, and printed by an ASR32 Teletype machine. ASR32 punched tape can be fed directly into the radio communications system once a heading is put on each data pass. The input/output, clock, and control systems were designed and constructed by SAO.

The receiving telescope, made by Tinsley Laboratories, Inc., Berkeley, California, is a 50.8-cm (20-inch) Cassegrain system with additional optics designed to focus an image of the primary mirror on the photocathode of the PMT. The optics following the flat secondary mirror pass the collimated return signal through a 7-Å filter that is both tilt- and temperature-dependent. A micrometer tilt adjustment tunes the filter to compensate for effects of age and temperature. Adjustable field stops and a provision to insert combinations of neutral-density filters are available.

The photodetector, an RCA 7265, was chosen for its quantum efficiency of 4 percent or greater at 6943 Å. This PMT has a gain of 5×10^7 and a risetime of approximately 3 nsec as operated in the SAO system.

The azimuth-altitude static-pointing mount, also built by Tinsley, has a pointing accuracy of better than $\pm30''$. Verification of the mount position is made by viewing a goniometer in the mount; but under normal operations, the system is driven in an open-loop fashion from the electronic control unit. The stepping-motor drive-system gearing allows for slewing speeds of 2° sec^{-1} and positioning increments of 0°.001. The unit can be hand-cranked, but this limits the pulse repetition rate to 2 ppm, whereas the laser and the data subsystem have the capability to go to 10 ppm.

9.2.2.2.2 ATHENS LASER SYSTEM

The laser system in Athens was built as a cooperative project between the National Technical University and SAO and began operation in 1968.

The laser transmitter is a Q-switched ruby laser, manufactured by the TRG Company, now Hadron, Inc., Westbury, Long Island. The laser transmitter has a 1-joule, 24-nsec (half-power, full width) output pulse. The Q-switch is a rotating roof prism with a bleachable dye. The roof prism is driven by a synchronous motor at a speed of 30 000 rpm (500 rps). The bleachable dye is Kodak Cryptocyanine, a metal pthalocyanine, in an alcohol solution. The laser beam divergence of 5 mrad is reduced to 1 to 2 mrad with a 5-cm-diameter Galilean telescope.

The flashlamp power supply has a 900-μf capacitor bank with a maximum charging voltage of 975 volts (960 joules). A typical threshold is 560 joules when all optical components are in good condition and accurately aligned.

Photosensitive monitors are used both to start the ranging counter when the laser pulse leaves the transmitter and to monitor the output power. An RCA 931 PMT senses the light reflected from a glass plate oriented 45° to the beam. Its output is used to start the range counter. The power monitor is an EG&G SGD-100 semiconductor photodiode that senses the laser light scattered from the back of the rotating-prism Q-switch. The output of the photodiode is monitored on a high-speed oscilloscope.

The receiver of the system is a Cassegrain telescope with a 40.6-cm (16-inch) parabolic primary and a hyperbolic secondary. The system has a focal length of 6.55 m and

a focal ratio of 16. Incoming light first passes through a 10′ field stop at the focal plane and through a 20–Å interference filter and then falls directly on the PMT (RCA 7265), which is uncooled and operates at an anode voltage of 2400 volts.

The laser and photoreceiver are mounted on a modified surplus 3-inch gun mount, which is hand-cranked in altitude and azimuth by two observers. One observer tracks in azimuth and the other in altitude by observing the sun-illuminated satellite in the illuminated reticle of a 2.7–cm (5-inch) elbow telescope. Both observers sit directly on the mount and move with it as a system. This method of aiming the laser limits operations to times when the satellite is in sunlight and the station in darkness. Pulse detection is by leading-edge fixed-threshold discriminators.

The outgoing laser pulse starts a counter with 1–nsec resolution. The light pulse reflected from the satellite enters the receiving telescope and goes through the optical chain to the PMT, whose output is amplified and used to stop the counter. A range gate between the pulse amplifier and the ranging counter reduces the possibility of erroneous range measurements due to sky-background noise.

During operation, the laser fires every 30 sec—on the even minute and at 30 sec after the minute. Both the exact firing time of the laser and the range measurement are recorded with a camera system that automatically photographs the counter readings.

9.2.2.3 Accuracy and Error Budget

The accuracy of the laser systems can be discussed in terms of random and systematic error components. The former are those that are uncorrelated and appear as range scatter on a point-to-point basis, while systematic errors are correlated and vary regularly over a single pass or longer.

The random noise level of the systems has been computed from data on short-arc analyses taken during the International Satellite Geodesy Experiment (1971) and the Earth Physics Satellite Observation Campaign (1971 to 1973). This type of analysis generally detects only random errors, because systematic errors tend to be absorbed into the orbit parameters when they are adjusted in the least-squares-fitting procedures. The best-fitting curves for single transits were obtained by varying the mean anomaly, its first derivative, and the right ascension of the node. The standard deviation of the data varied from 30 to 120 cm, with a median of less than 60 cm. The dominant random-error component is due to the variation in size and shape of the return signals. The fixed-threshold, leading-edge pulse-detection system we are now using is very susceptible to such irregularities in return pulses. The return signals from the PMT may contain as few as 1 to 10 photoelectrons. They also may vary widely in size and shape during a single transit, owing primarily to scintillation from the satellite retroreflector array, irregularities in the laser beam pattern, and the statistical nature of the PMT detector. The expected random variation in the triggering times of the leading-edge threshold is a few nanoseconds (50 cm) for our transmitted pulse width of 20 nsec. Other random influences in the data, such as the least-count error in the counter and the random variability of the atmosphere, have smaller effects.

Systematic errors are considerably more difficult to grasp. However, the size of the systematic errors, per pass, has been estimated from performance and field tests. The ± 50–μsec uncertainty in epoch timing could be responsible for a systematic error of as much as 35 cm for some satellite-pass geometries. The models used by SAO and others compute the optical range correction due to tropospheric refraction from ground-based data. These models have an estimated systematic error of a few centimeters at zenith, with an approximate secant dependence for zenith angles down to about 70°. The residual error in current tropospheric-propagation-correction models is, on the average, probably about 4 cm per pass. The

geometry of the satellite and the placement of the retroreflectors relative to the satellite's center of mass are responsible for a systematic contribution of about 10 cm. This error is the result of uncertainties (1) in satellite attitude, (2) in retroreflector optical properties and placement, and (3) in the resultant return-signal shape and size from the entire satellite retroreflector array. The fixed-threshold, leading-edge detection system is probably responsible for systematic errors of about 3 nsec (50 cm) for a 20–nsec pulse width. This is in addition to the random variations and arises from systematic differences in the triggering point on the outgoing and the return pulses. Calibration on a fixed target is also an area where systematic influences are introduced through survey error and inaccuracies in the time interval measurement. It is estimated that systematic errors of about 10 cm may be introduced during calibration. If the sources of these errors are assumed to be independent, the total estimated influence, or root sum squared, is about 57 cm.

A two-laser collocation test was performed on satellite 6800201 (GEOS–2) at SAO's Mt. Hopkins Observatory, Arizona, from October 1969 to January 1970. SAO's laser there and a mobile laser system operated by National Aeronautics and Space Administration (NASA) participated. The objective was to determine the relative accuracy of two laser systems that were being used in the routine collection of satellite geodetic data. Since the two systems were built, calibrated, and operated by independent groups and since the instrumentation designs were different, the experiment gave a good estimate of the system-induced bias errors that can be expected. During the experiment, the two systems demonstrated a relative ranging accuracy of 1 to 2 m. In half the satellite passes, the difference in the range measurements of the two systems had a bias of less than 1.2 (see fig. 9.5). The sign of the bias changed several times during the 4-month experiment. At the time, it was felt that these bias components were primarily introduced into one or both of the systems during

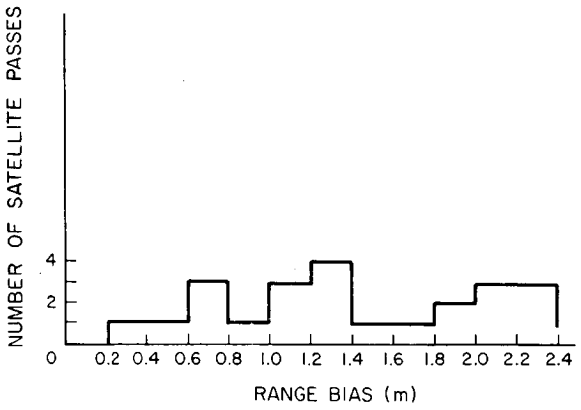

FIGURE 9.5.—Distribution of relative system biases.

the calibration procedure, which involved a determination of the system delay by ranging on a target at a known distance from each laser. Both systems have undergone significant modifications since the time of the collocation, and the systematic error in each has been substantially reduced.

9.2.3 Timing System

Each station has a timekeeping system to provide precise epoch data for each observation. The station clock is basically a crystal oscillator, a time accumulator, and a system of time and frequency monitoring aids. The clock has a dual-channel redundancy and a battery-backed power system to guard against loss of time continuity.

The clocks that were used in the Baker-Nunn network until the mid-1960's relied on a WWV-emitted time pulse and tone reference for both time and frequency settings. The active electronic components were vacuum tubes, and the time readout was in the form of rotating mechanical indicators and a rotating spot on an oscilloscope. Limitations on the stability and reading accuracy of the oscilloscope display led to the use of a fully electronic system featuring solid-state digital circuitry and a high-stability frequency standard.

The present clock has a Sulzer 5-MHz crystal oscillator stable to 1×10^{-10} day^{-1} and is generally kept within 5×10^{-10} of UTC

(USNO). It can be adjusted to 1×10^{-10}. The frequency of the oscillator is maintained through frequency and phase comparisons with stable VLF transmissions from stations such as NAA and NLF.

A locally generated 100–kHz signal is phase-locked to the VLF signal and then compared in phase to a 100–kHz reference signal from the clock. A relative phase position record is kept, which helps maintain station time to greater accuracies than is possible with the HF timing pulses.

The components of the EECo timing system are the clock's accumulator, the Sulzer oscillator, a VLF tracking receiver, a WWV receiver, a chart recorder to display the VLF/clock phase relationship, an oscilloscope (Tektronix 561A), and an ac–dc–ac battery-backed power system. Some stations have a secondary timing system, made up by duplicating most of these same elements. Other stations have a backup clock, consisting simply of an oscillator and a miniaturized digital counter.

The accumulator of the master clock system is a 100–kHz digital counter that offers a visual display of time in hours, minutes, seconds, and fractions of seconds to 10–μsec steps for precise timing control.

Timing at the stations is checked primarily by means of portable-clock trips. Although the VLF tracking receiver does not give epoch information, it does provide an accurate method of maintaining a record of time position relative to the setting obtained from the portable-clock comparison. Maintenance of accurate time between trips is facilitated in some locations by using the time tick of WWV and times sources of other agencies. The HF time signals offer the station a convenient time reference, but accuracies are limited to ±0.5 msec at best, owing to variations occurring over the long propagation paths to the stations.

At the laser stations, clocks routinely provide epoch to ±50 μsec (UTC) by means of portable-clock trips, which are conducted once a year on the average. During specific experimental periods, time has been corrected to ±25 μsec through extra care in VLF monitoring, more frequent checks by portable clocks, or other means of reference. The less stringent timing requirements at the camera stations (±100 μsec) are achieved through less frequent portable-clock trips.

9.2.4 SAO Satellite-Tracking Network

9.2.4.1 Sites

The first Baker-Nunn camera was sent to Organ Pass, New Mexico, at the observing site of the Harvard Meteor Program. The first successful observation was made November 26, 1957, just a month and a half after the launch of the first artificial earth satellite. The network had expanded by the following August to 12 operating Baker-Nunn stations. Table 9.1 shows the history of the Baker-Nunn sites to date.

After 8 years, it became apparent that higher accuracies were needed for future scientific projects. By March 1966, SAO had assembled, tested, and operated its first laser system. It consisted of a rented General Electric laser mounted on a 3-inch gun mount with a searchlight as receiver. This system operated successfully for over a year at the New Mexico site, during which time plans were formulated for a prototype laser system with components designed and built specifically for that purpose.

The prototype system was operating at Mt. Hopkins in December 1967. Three production laser systems, based on the design and experience gained with the prototype, were fielded in late 1970. In 1972, the Mt. Hopkins prototype was reworked to make it similar to the three production systems. Table 9.2 shows the history of the lasers to date. Figure 9.6 shows the present global distribution of stations, including the location of laser systems.

The present SAO sites that contain both a laser and a Baker-Nunn camera are Mt. Hopkins, South Africa, Peru, and Brazil. The last three stations are staffed and operated by SAO personnel with logistic support provided by cooperating agencies in each country: the Council for Scientific and

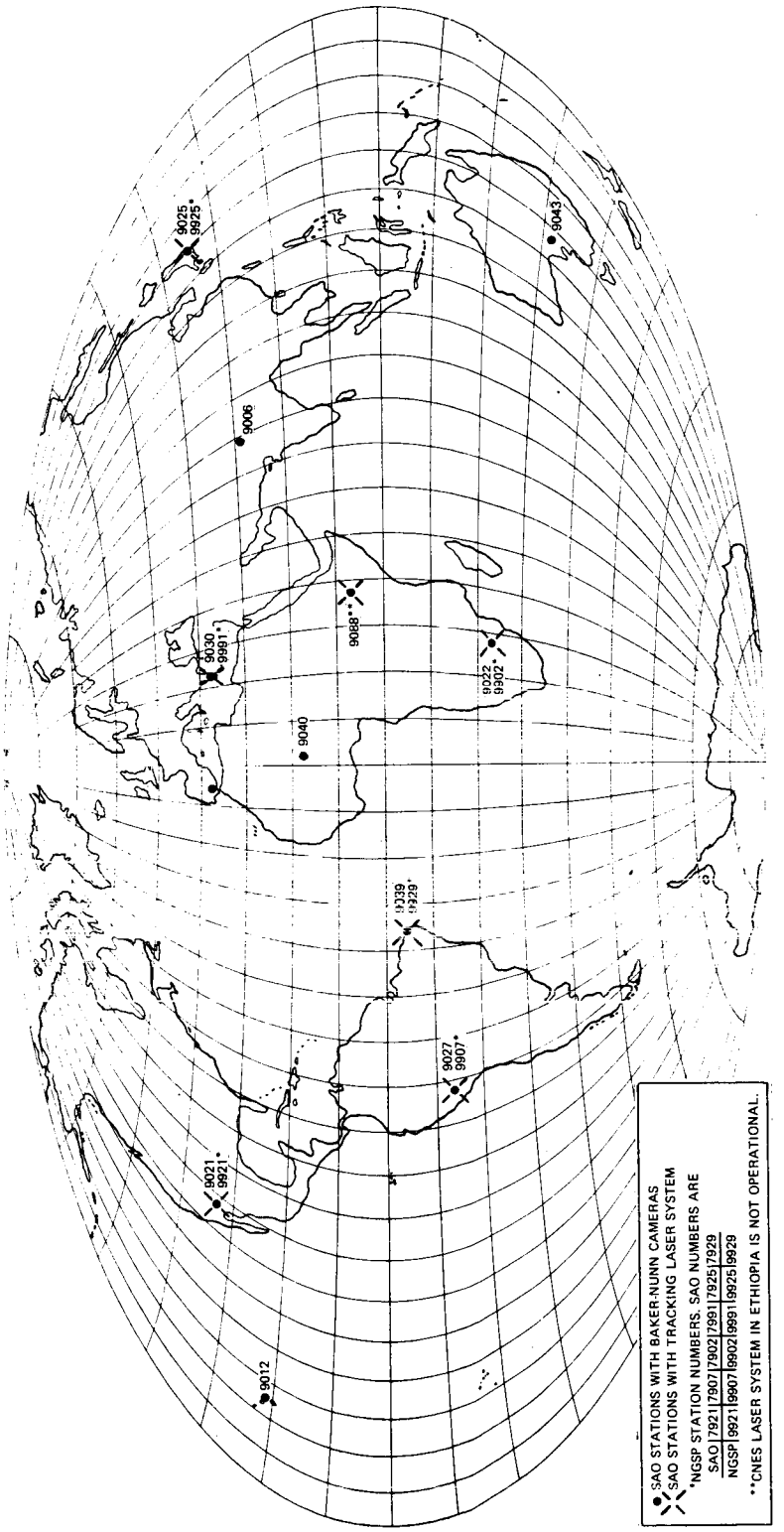

FIGURE 9.6.—SAO field stations.

Industrial Research in South Africa, the Instituto Geofisico del Peru and the Universidad Nacional de San Agustin in Peru, and the Instituto Nacional de Pesquisas Espaciais in Brazil.

The Baker-Nunn site in Maui, Hawaii, is staffed and operated by SAO personnel in conjunction with the University of Hawaii. The camera in Australia is operated by the Department of Supply of the Australian government. The stations in Spain, Ethiopia, and Greece are supported and operated jointly by the Smithsonian and cooperating agencies: the Spanish Naval Observatory in Spain, the Haile Selassie I University in Ethiopia, and the NTU in Greece. NTU also operates a laser system. A laser system belonging to the Centre National d'Etudes Spatiales (CNES) is currently located at Addis Ababa, Ethiopia.

The tracking station in Japan is operated by the Tokyo Astronomical Observatory and has, in addition to the Baker-Nunn camera, a laser system designed and built in Japan. The Baker-Nunn camera in India is operated by the Uttar Pradesh State Observatory.

A Baker-Nunn camera on loan to CNES has been used at several locations in Africa; it is currently in operation in Ouagadougou, Upper Volta.

Beginning in 1964, several Baker-Nunn cameras operated by the 7th Aerospace Squadron at ENT Air Force Base have participated in SAO satellite-tracking programs. The sites are listed in table 9.3. SAO scheduled observing times and provided predictions for simultaneous observations. These data have been included in the SAO analysis and are incorporated in the SAO data file.

9.2.4.2 Operations

The SAO Baker-Nunn cameras and laser systems receive new satellite predictions each week. The predictions are computed from up-to-date observations provided by the SAO network and by camera, MINITRACK, and laser system observations made by other agencies (see table 9.4).

The predictions for the Baker-Nunn camera consist of azimuth- and altitude-pointing angles, which need be accurate to only a few degrees, and tracking-angle rates to simulate the satellite motion (Cherniack and Gaposchkin, 1963). These predictions are generated from orbits computed with a simple model of the earth's gravity field. The short-periodic terms due to C_2 and the long-period terms due to the odd zonal harmonics are included. The secular rate of the apsidal line and the argument of perigee are determined from the data for each orbit. The orbits are generated with the Smithsonian's Differential Orbit Improvement (DOI) program (Gaposchkin, 1964) from observations covering a period of about 2 weeks.

The laser, on the other hand, requires azimuth- and altitude-predicted pointing angles accurate to within several minutes of arc and a predicted range propagation time accurate to within 20 μsec for a given epoch. Orbits for laser tracking predictions are also generated with the DOI program by using a gravity field with most of the tesseral harmonics through degree and order 16 and with a number of higher resonance terms. Lunar perturbations are also included. Again, orbits are computed from data covering a period of about 2 weeks. Predictions for satellites equipped with retroreflectors are made for passes that reach altitudes greater than 25°.

The success of the network has depended on the timely flow of data from the field, the development of pointing predictions from up-to-date data, and the use of these fresh predictions at the field stations. The rapid data-prediction cycle is most critical for the laser, which has stringent pointing requirements; however, it is also an important factor in the Baker-Nunn operation, especially for simultaneous observations between stations for geometric geodesy.

Until 1968, direct links by teletype between the field stations and Cambridge provided real-time communications. Since then, a combination of means has been used to give real-time or near real-time communications at each site. Peru and Brazil receive predic-

tions and send their camera and laser data by direct radio-teletype link operated by SAO personnel. These stations have prearranged contact times for data transmission. Atmospheric disturbances severe enough to affect the link are infrequent. The tracking sites in Hawaii, Japan, Spain, Greece, and Arizona use facilities of the United States military communications network for transmission and receipt of data. The first three stations have direct access to this network, while those in Greece and Arizona must pick up and deliver messages at local military bases. The stations in Australia and South Africa use the NASA data network (teletype). Predictions for the Ethiopia station are sent via NASA teletype link to CNES in France and are retransmitted on their lines to Ethiopia. CNES generates and sends predictions for their laser, located in Ethiopia, as well as predictions for the 12th Baker-Nunn camera, now in Upper Volta. Data are currently returned to Cambridge by Embassy mail. The site in India receives predictions from SAO via the United States Embassy in New Delhi and sends its data back by way of commercial cable.

For the Baker-Nunn camera, predictions cover a period of 1 week, with an extra day in case of transmission delays. At present, an average of 10 arcs is predicted per station per night. In the past, as many as 50 arcs were predicted for each station. Observations are reduced in the field to an accuracy of 40″ to 60″ and sent to Cambridge immediately for use in the prediction cycle. The camera film is sent by commercial mail for subsequent precise reduction (photoreduction).

Predictions for the laser system are in the form of punched paper tape, which is used directly to point the laser. Each predicted arc contains from 10 to 90 separate points (4 min^{-1}), depending on the geometry of the pass. Stations receive 40 to 100 predicted arcs per week for three satellites currently being tracked: GEOS–1, GEOS–2, and BE–C. All seven retroreflector-equipped satellites have been tracked. Satellite ranging data, system calibration data, and ground-based meteorological data are sent to SAO.

9.3 DATA AND DATA REDUCTION

(Søren W. Henriksen)

This section summarizes the data used in (1) deriving coordinates for the locations of various tracking stations (sec. 9.5.1) and in (2) determining the Earth's gravitational potential (sec. 9.5.2). Data relating to the former are summarized in section 9.3.1; those relating to the latter are summarized in section 9.3.2. The section also describes (sec. 9.3.3) the preprocessing applied to data from Baker-Nunn cameras and laser systems.

9.3.1 Data Used in Determining Coordinates

(G. M. Gaposchkin, J. Latimer, and G. Veis)

9.3.1.1 Geometric Method

The geometrical solution included two networks: 27 stations of the SAO network, including the U.S. Air Force's Baker-Nunn cameras and several European stations; and 48 stations of the National Ocean Survey (NOS) BC–4 network. Of the SAO group, 21 stations were also included in the dynamical solution. The SAO data block consisted of 5200 pairs of synthetic simultaneous observations (table 9.5), or about 50 000 individual direction observations processed at SAO. The satellites observed were 6102801 (MIDAS–4), 6303004, 6508901 (GEOS–1), 6605601 (PAGEOS), 6800201 (GEOS–2), and 6305501. The BC–4 data consisted of 2157 pairs of simultaneous events (photographs of PAGEOS). Each event generally consisted of seven directions and a covariance matrix from each of the two stations. When more than two stations observed the satellite simultaneously, we treated each station pair separately. The BC–4 data were obtained from the National Space Sciences Geodetic Satellite Data Service at the National Aeronautics and Space Administration/Goddard Space Flight Center (NASA/GSFC) (see ch. 1). The data

were acquired, reduced, and processed by the NOS. The standard deviations assigned to the directions are given in table 9.26b.

In geometric work, SAO observations refer to the equator and equinox of 1950.0. They are corrected for the effects of annual aberration, diurnal aberration, parallactic refraction, and planetary aberration and then converted to the terrestrial system of SAO, which is fundamentally defined by the mean pole of 1900–1905 of the International Polar Motion Service (IPMS) and by the meridian of the Mean Observatory and UT1 of the Bureau International de l'Heure (BIH). The BC–4 data are in the same reference system.

9.3.1.2 Data Used in Dynamic Method

The stations whose data were used in the dynamic method are listed in table 9.6; the observations used are from the satellites listed in table 9.7. The distribution of these satellites (inclination versus height) is plotted in figure 9.7. Satellite arcs were chosen from satellites whose orbits were relatively uncorrupted by errors. Specifically, we eliminated satellites with drag model errors (large area-to-mass ratio and low perigee height) particular sensitivity to gravity-field model errors (resonances), or poor orbital distribution (less than six stations observing the satellite). The data were kept in two parts. Before 1970 most of the observations were directions. A number of laser system ranges were made, and where it was possible to do so, they were included in the orbits. In 1971, the International Satellite Geodesy Experiment, ISAGEX, a cooperative tracking program with 10 laser stations, was carried out and provided for

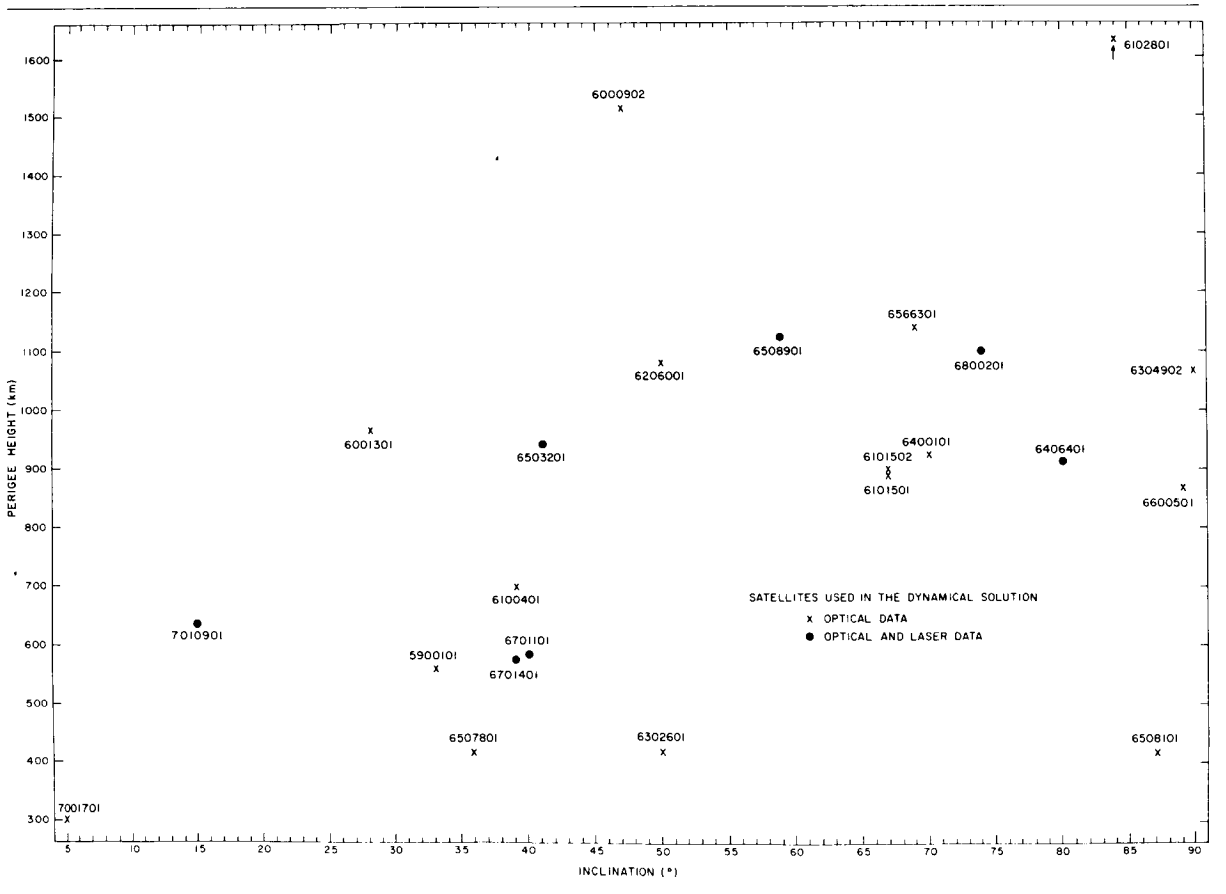

FIGURE 9.7.—Distribution of satellites used in SE III.

the first time relatively complete orbital and geographical coverage with laser data. From these ISAGEX data, 15 orbits were selected and used in the dynamical determination of station coordinates.

The assumed accuracies of the instruments are given in table 9.8. Camera data were given an assumed accuracy of 4″. When five or more observations were made within a few minutes, e.g., of GEOS flashes, a smoothed or synthetic observation was determined. The same calculation was used to generate simultaneous observations, since in general one cannot make exactly simultaneous observations. These synthetic observations were given an accuracy determined from the polynomial fit. If the computed uncertainty was less than 2″, then 2″ was used. In the reduction of camera data, annual aberration and parallactic refraction which were determined from mean nighttime temperature and pressure for each station, in addition to precession and nutation, were applied.

The distance measurement in range data used in this analysis has a precision of 1 to 2 m. The accuracy, including timing errors, will not be so good. In addition, other errors, e.g., those due to the gravitational field, are that large. Therefore, the assumed accuracy of the laser system data was taken to be 5 m. Some laser system data taken in 1967 appear to have errors in timing of a millisecond, and these data were given an assumed accuracy of 10 m. Furthermore, certain laser systems provide a larger volume of data than is useful here (e.g., more than 400 points per pass). Therefore, for passes containing more than 25 points, approximately 25 evenly distributed observations were selected. Numerical experiments indicated no improvement in the results by smoothing the points or calculating synthetic observation.

The laser system data were corrected for tropospheric refraction with the use of observed values of pressure, temperature, and relative humidity. In addition, the observations were reduced to the center of mass of the satellite by means of the formulas presented in table 9.9. These formulas relate the range correction Δ in meters to the angle ϕ in degrees between the satellite's axis of symmetry and the line of sight to the observing station. The corrections made in this manner are relatively small but systematic. The tropospheric correction is 2.1 m at zenith, and the reduction to the center of gravity is 80 cm for GEOS–1.

Table 9.8 summarizes the adopted uncertainties. Table 9.10 gives the number of observations selected from the data.

The dynamical solution used data taken between 1962 and 1969 on 140 arcs of 15 satellites and ISAGEX data taken in 1970 on 15 arcs of 3 satellites. These two sources of data were kept separate, and several solutions were made.

Since the ISAGEX data are of a new type, we examined the origin of the node and the relative weighting in order to find the best treatment. Two iterations were performed as part of the larger computation of station coordinates. The pre-ISAGEX data were in arcs from 4 to 30 days, as appropriate, and the ISAGEX data were in 10-day arcs.

The length scale in a dynamical solution is, for all practical purposes, fixed by the value of GM, which directly enters the calculations of radius vector through

$$r=\left(\frac{GM}{n^2}\right)^{1/3}(1-\cos E)\,(1+\text{perturbations})$$

With camera directions, no further information in scale is available. With range data, both scale and GM can, in principle, be determined. The unit of distance then is defined by the speed of light and becomes the "light second." In this analysis, GM was assumed to be the value given in table 9.11. Our dynamical scale is therefore defined by GM. If this value of GM is far from the true value, some deterioration of the coordinate will result. We return to this question in the discussion and evaluation of results.

Table 9.11 gives the values adopted, in this computation, for GM, c, and k_2.

9.3.1.3 Data Combined With Both Methods

9.3.1.3.1 INFORMATION FROM DEEP-SPACE PROBES

JPL operates the Deep Space Net (DSN), eight stations for tracking deep-space probes. Data from the DSN have been used to obtain, among other parameters, the longitudes (relative and absolute) of each station and the distance of its antennas to the Earth's instantaneous axis of rotation (Vegos and Trask, 1967; Trask and Vegos, 1968). The DSN data are particularly interesting because (1) they constitute a unique, complementary, and independent determination of geocentric locations, and (2) they provide a very strong determination of scale.

Comparisons of the JPL and SAO results were made by Veis (1966a) and Vegos and Trask (1967) from data from the Ranger missions and from SE I (Lundquist and Veis, 1966). More refined JPL solutions were combined with satellite-tracking data in the determination of SE II. The combination was made with Location Set (LS) 25, as determined by Mottinger (1969), by using data from the Mariner 4 and 5 missions. Continued refinement of the DSN data has provided LS 37, which is used in the present analysis.

Each DSN site is located near other stations whose coordinates were determined in the analysis presented here. Surface-triangulation data, in the form of geodetic coordinates, can be used to relate the DSN coordinates to the SAO coordinates.

The ephemeris r of a deep-space probe is assumed known. For a distant spacecraft, the observed range rate $\dot{\rho}$ can be expressed approximately as

$$\dot{\rho}=\dot{r}+\omega r_s \cos\delta \sin(\alpha_s-\alpha_0)$$

where ω is the earth's rotation rate, r_s is the spin-axis distance of the observer, δ and α_0 are the declination and right ascension of the spacecraft, and α_s is the right ascension of the observer. Each station observes a diurnal variation in $\dot{\rho}$, the amplitude and phase depending on r_s and α_s, respectively.

Generally, any data can be analyzed. However, cruise data seem less reliable than close-encounter data for determining α_s and they are used only for the determination of r_s. In any case, refraction (tropospheric and ionospheric) and orbit computation must be done with great care, and recent improvements come from refinements in the treatment of refraction. The ephemeris r, (δ, α_0) will be determined in the system of the JPL planetary ephemeris. We can expect to find a systematic difference in the definition of longitude between the planetary ephemeris and the astronomical reference system (FK4) used for analysis of close-earth satellites. The DSN data reduction used numerical values for pole position and UT1 from BIH, as was done for the close-Earth-satellite analyses.

The data for LS 37 are summarized in table 9.12. The main improvements over LS 25 are as follows: (1) better treatment of refraction, particularly ionospheric; (2) inclusion of more data because of (1); (3) inclusion of Mariner–6 encounter data; (4) revision of the planetary ephemeris; and (5) use of BIH polar motion and UT1. Realistic estimates of accuracy are 2 m for r_s, 4 m for absolute longitude, and 2 m for relative longitude (Mottinger, private communication, 1972).

Mottinger provided a solution and covariance matrix for r_s, λ, in addition to the masses of Venus, Mars, and the Moon and the oblateness of Mars. This system was transformed by SAO for corrections in coordinates X, Y of the station. These converted equations were then added to the larger system of normal equations, which included the other stations sought.

The LS 37 coordinates for the DSN stations are given in table 9.13. In LS 37, the relative coordinates of DSS 11, DSS 12, and DSS 14 and of DSS 61 and DSS 62 were constrained to agree with the survey data.

9.3.1.3.2 INFORMATION FROM SURFACE TRIANGULATION

Extensive surface-triangulation data exist that relate station positions. These data are generally given in terms of datum coordinates and occasionally in terms of interstation vectors for collocated stations. We have used this information in four ways:

(1) For stations in the same datum, the geodetic coordinates are used as observations relating the positions of the stations in the general combination adjustment.

(2) For collocated instruments, these datum coordinates are used as a constraint relating the two sites. These cases could be treated as in (1) above.

(3) The geodetic coordinates are utilized as a check on the accuracy of the final coordinates.

(4) The geodetic coordinates are employed to determine the relation of each datum to a geocentric reference system.

Evaluating geodetic coordinates is the most difficult aspect of this analysis. When reliable, they are very accurate; but problems often exist in relating the local survey at the station to the datum.

In (1), (2), and (3) above, care must be taken to ensure that datum tilts, distortions, and scale differences do not corrupt the results. For most uses, limiting the application of geodetic coordinates to lengths of 100 km or less is satisfactory. Otherwise, the datum orientation must be determined and applied before the geodetic coordinates can be used with geocentric satellite-based coordinates.

The use of datum coordinates as observations of relative station positions assumes no correlation between X, Y, and Z. If we have datum coordinates for station i, X_i^d, Y_i^d, Z_i^d, and initial values for the geocentric coordinates that are to be corrected, X_i^g, Y_i^g, Z_i^g, we can write observation equations for each component of the vector between two stations:

$$X_i^d - X_j^d = X_i^g - X_j^g + \Delta X_i - \Delta X_j$$

with similar expressions for Y and Z. If these are given weights W_{ij}, we can immediately write the normal system as

$$\begin{bmatrix} \sum_i \sigma_{ij} & \cdots & -\sigma_{ij} \\ \vdots & & \vdots \\ -\sigma_{ij} & \cdots & \sum_j \sigma_{ij} \end{bmatrix} \begin{bmatrix} \Delta X_i \\ \vdots \\ \Delta X_j \end{bmatrix} = \begin{bmatrix} \sum_i \sigma_{ij}[(X_i^d - X_j^d) - (X_i^g - X_j^g)] \\ \vdots \\ \sum_j \sigma_{ij}[(X_j^d - X_i^d) - (X_j^g - X_i^g)] \end{bmatrix}$$

where $\sigma_{ij} = (1/W_{ij})^2$. This system can augment a normal system for determining ΔX, ΔY, ΔZ.

The weight W_{ij} of the geodetic ties chosen is given in table 9.14. Table 9.15 presents the geodetic coordinates for all the stations used in the 1973 Smithsonian Standard Earth (SE III).

9.3.2 Data Used for Potential

(E. M. Gaposchkin, M. R. Williamson, Y. Kozai, and G. Mendes)

The potential was divided into two parts: one expressed by zonal harmonics and the other by tesseral (sec. 9.4.3). The data used for the two parts were different. In the determination of the zonal coefficients, secular changes in the Keplerian elements were expressed as functions of the zonal coefficients. (The "observed" quantities in secs. 9.3.2.1, 9.4.3, and 9.5.2 are not observations but values of $\dot{\omega}$, $\dot{\Omega}$, etc., computed from observations.)

9.3.2.1 Data Used in Determining Coefficients of Zonal Harmonics

Table 9.16 gives the orbital elements for the 14 satellites of this analysis. Gaps still exist in inclinations around 20° and 40°. The

values of $(O\text{-}C)$ for the secular motions and the amplitudes of $\begin{matrix}\sin\\\cos\end{matrix}\Big\}\omega$ terms based on 1964 values (Kozai, 1964) follow:

	$\dot{\omega}$ day^{-1}	$\dot{\Omega}$ day^{-1}	A_ω
DIAL	$-0^\circ.01806$	$0^\circ.01012$	$-0^\circ.070$
	± 9	± 7	± 5
PEOLE	-0.0022	0.00516	0.045
	± 8	± 10	± 30

	A_Ω	A_I	A_e
DIAL	$-0^\circ.019$	$0^\circ.0043$	-9.1×10^{-5}
	± 3	± 3	± 6
PEOLE	-0.002	-0.0017	2.8×10^{-5}
	± 5	± 30	± 2.0

The large values of $(O\text{-}C)$ for these two satellites show that the previous sets of zonal-harmonic coefficients were inadequate.

The data for DIAL were derived from orbital elements from March 18 to July 16, 1970; during that period, the argument of perigee made four revolutions. The orbital elements for PEOLE were obtained for January 9 to March 13, 1971, and for March 28 to August 30, 1971. These data are not so accurate as those for DIAL, since there were not enough observations and there was a period during which no orbital elements were available.

In this new determination, the $(O\text{-}C)$ values for satellite 6000902 are a revision by Gaposchkin for February 10, 1961, to April 21, 1963.

The other satellites included in this determination are 6001301, 5900101, 6202901, 6302601, 6206001, 6508901, 6101501, 6400101, 6406401, 6508101, and 6102801. The data for these satellites are the same as those given by Kozai (1964). The $(O\text{-}C)$ values were computed from the 1964 values of coefficients as given in table 9.17.

The following values have been used for the geocentric gravitational constant and the equatorial radius of the Earth:

$$GM = 3.986\,01\times10^{20}\ \text{cm}^2\ \text{sec}^{-2}$$

$$a_e = 6.378\,16\times10^{8}\ \text{cm} \qquad (9.1)$$

Table 9.18 lists the values of $(O\text{-}C)$, based on the coefficients from Kozai (1964), for the secular motions of the 14 satellites and their standard deviations. The latter are used to compute weights assigned to the data. The columns headed I and II represent the differences computed by 12 unknowns and 11 unknowns, respectively, and the dates refer to previous Kozai solutions. Kozai (1969) intentionally increased some of the standard deviations, since he thought that neglect of higher order terms would cause errors larger than the standard deviations of the observed values. For the same reason, we have increased the standard deviation (10^{-6} degree per day) to $3^\circ\times10^{-6}$ day^{-1} for $\dot{\omega}$ of satellite 5900101 and $\dot{\Omega}$ of satellites 5900101, 6000902, 6302601, 6206001, 6101501, and 6508101. The standard deviation assigned to the secular motions of 6508901 was erroneously given in the previous paper.

In the determination of even-order harmonic coefficients, we have used the secular motions and the amplitudes of $\begin{matrix}\cos\\\sin\end{matrix}2\omega$ terms for selected orbital elements of those satellites for which the eccentricities are small. We could not use data from the other satellites, since the orbital elements available for them were not of sufficient accuracy. The $(O\text{-}C)$ values and their standard deviations for the amplitudes of the long-periodic terms are given in tables 9.19 and 9.20. The longitude of the ascending node and the inclination have been omitted for some of the satellites in tables 9.19 and 9.20 because their amplitudes are extremely small. The differences for ω of 6508901 and 6101501 and for e of 6400101 computed after the determination were found to be much larger than their standard deviations computed from observations. Also, since the inclinations of these satellites are near the critical inclination, higher degree interaction terms neglected in the computations—such as C_3^2/C_2 and $C_2^2\,C_3/C_4$—might have affected the data reduction. For these reasons, we increased the standard deviations assigned to these data from 1.5, 2, and 1 to 4, 5, and 3, respectively; the increased values are given

in table 9.20. One misprint appeared in table 2b of Kozai (1969): $(O\text{-}C)$ for ω of 6508901 should be $(6\pm2)\times10^{-3}$ instead of $(6\pm2)\times10^{-4}$.

9.3.2.2 Data Used in Determining Coefficients of Tesseral Harmonics

9.3.2.2.1. SATELLITE TRACKING DATA

Laser data from ISAGEX provided global coverage with 2-m data for the first time. Table 9.7 lists all the satellites used in the analysis, including those from which ISAGEX and earlier observing programs obtained laser data, and figure 9.7 shows their distribution in inclination and height. Separation of the station-coordinate and the gravity-field determinations allowed a better selection of satellite data. For the former, high satellites less affected by the anomalous gravity field were emphasized, while for the latter, lower satellites, with a better distribution, were stressed. Certain satellites with unmanageable, long-period resonances (e.g., 5900701) were used only for the determination of station coordinates; they have such a rich body of data that relatively short-arc orbits (4 days) could be derived for this purpose.

Each observation was given an a priori weight (detailed in table 9.21 so that when the normal equations were combined, each type of data could be scaled. The scale factor for surface-gravity data was arrived at by experiment. The scale factors for the 550 km$\times$550 km anomalies and for the zero anomalies were chosen so that the resulting solution improved the satellite orbit, the surface-gravity residuals, and the errors in the surface-gravity comparison and did not introduce spurious short-wavelength detail where no surface-gravity data were available.

All available optical data were used for the orbital arcs chosen. For each pass of laser data containing more than 30 points, approximately 30 uniformly distributed observations were selected.

9.3.2.2.2 TERRESTRIAL GRAVITY DATA

The primary objective of the analysis of terrestrial gravity data was to obtain mean anomalies for regions 550 km $\times$ 550 km. When these data are combined with the satellite-perturbation analysis, the spherical harmonics representing the geopotential can be determined. A set of gravity data with known (and preferably simple) statistical properties is needed. Our approach is based on covariance analysis, following the ideas of Wiener (1966) and Kolmogoroff. When this technique is used in communications engineering, it is sometimes known as filtering theory. The ideas here are an extension of a one-dimensional time series to the two-dimensional surface of a sphere (Kaula, 1967d).

Estimation of gravity by covariance methods hinges on the stationarity of gravity data; that is, the statistical properties of the data are independent of location. There is some evidence that gravity data are not stationary; however, if some subsets of the total gravity population are stationary, then gravity covariance functions between sets and within each set can be defined.

The $1°\times1°$ Data Available.—A set of $1°\times1°$ mean free-air anomalies, containing 19 115 measured means, was obtained from ACIC (1971), and another set, of 1454 $1°\times1°$ means for Australia, from Mather (1970). The two sets were combined, with the Mather data being used for all areas they covered. Figure 9.8 shows the geographical coverage of all the data. The combined data set contained 19 328 means. A complete set of $1°\times1°$ mean topographic heights, used to define oceanic and continental areas, was obtained from Kaula (Kaula and Lee, 1967). The distribution of $1°\times1°$ mean gravity data is summarized below:

Depth of boundary (km)	Ocean		Continent	
	Measured	Total	Measured	Total
0	9213	42 918	10 115	21 882
−1	7015	36 199	12 313	28 601

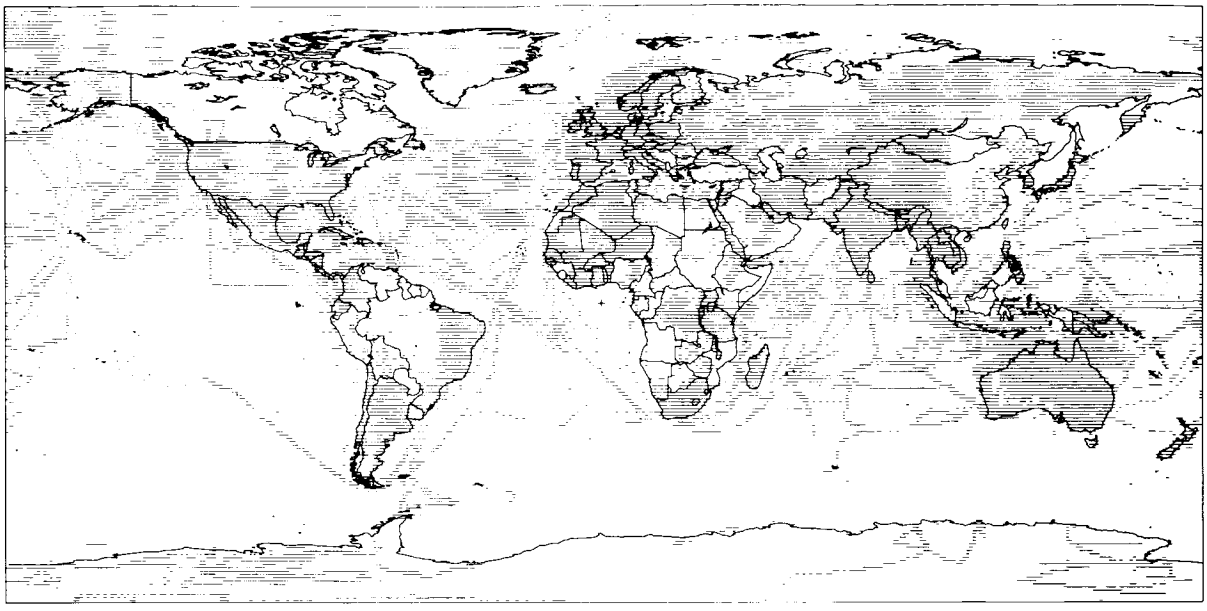

FIGURE 9.8.—Distribution of $1° \times 1°$ surface gravity data.

The estimated uncertainty given with each gravity anomaly for 99.9 percent of the data is less than 25 mGal. Comparing the Mather data with the ACIC data at the 1241 common points, we find that the average difference is 1.7 mGal and the root-mean-square difference is 20 mGal. At a number of points, the discrepancy between the two sets exceeds 100 mGal.

The Estimation Procedure.—Kaula (1967d) has developed a procedure that greatly simplifies the calculation of covariance function which is called the block covariance function, and the gravity estimates. This method has both advantages and disadvantages. The disadvantages are (1) the estimate of gravity does not make use of all the gravity information (i.e., the estimates are not as good as possible); and (2) the covariance function must be determined by using only the combinations of anomalies within blocs and therefore is not determined with all possible combinations of the data.

The advantages of Kaula's method are as follows: (1) it greatly simplifies calculation of the covariance function and the gravity estimates; (2) it produces mean anomalies 550 km $\times$ 550 km with uncorrelated errors; and (3) the statistical properties of data within a block may be closer to stationarity since the method involves primarily the short-distance covariance.

If gravity were a stationary process, then it would have the same statistical properties everywhere. Possible nonstationarity was investigated by determining the covariance function for subsets of gravity data. A separation of oceanic from continental gravity was used. A 0– and a 1–km depth were used to define the ocean-continent boundary, which was determined from topographic data. The boundary was also expanded to a width of 400 km for the 1–km depth, and the covariance functions were computed without the gravity data in that region. Finally, gravity data were divided into an equatorial set, $|\phi| < \pi/4$, and a polar set, $|\phi| > \pi/4$. The covariance functions for all the gravity data and the four sets of split data and the block covariance function are plotted in figure 9.9.

Since the differences between the covariance functions are significant, we conclude that gravity is not stationary. Any estimation procedure that makes that assumption must be carefully examined.

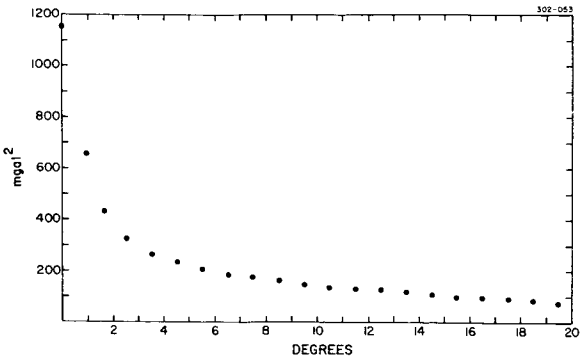

FIGURE 9.9a.—The covariance function of mean 1°×1° gravity anomalies.

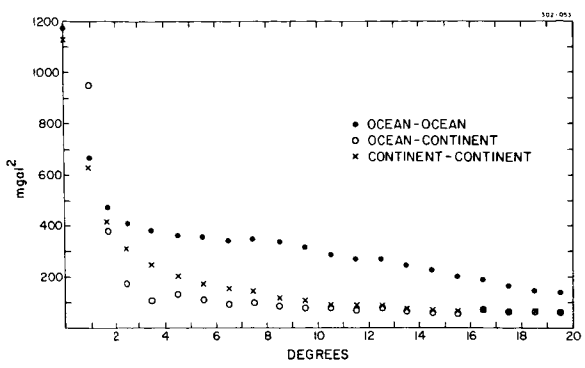

FIGURE 9.9b.—The covariance function of mean 1°×1° gravity anomalies for a 1-km ocean-continent boundary.

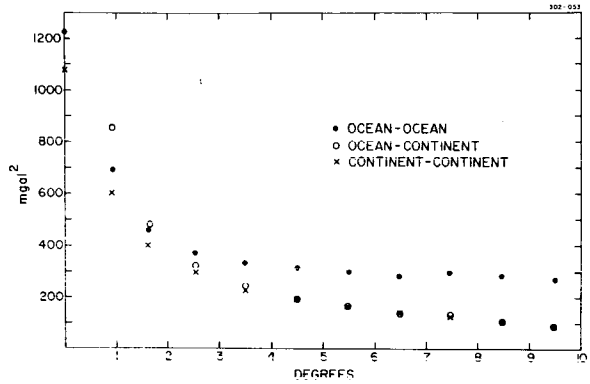

FIGURE 9.9c.—The covariance functions of mean 1°×1° gravity anomalies for a 0-km ocean-continent boundary.

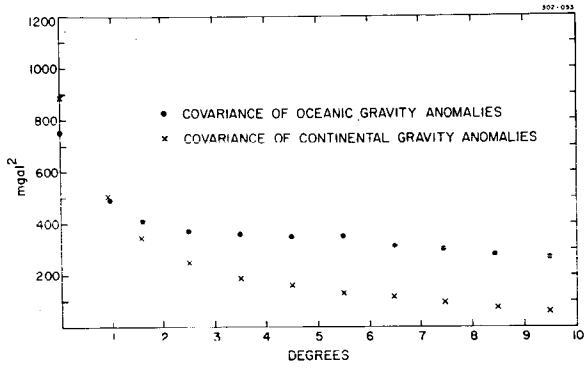

FIGURE 9.9d.—The covariance functions of mean 1°×1° gravity anomalies for a 1-km ocean-continent boundary 400 km wide.

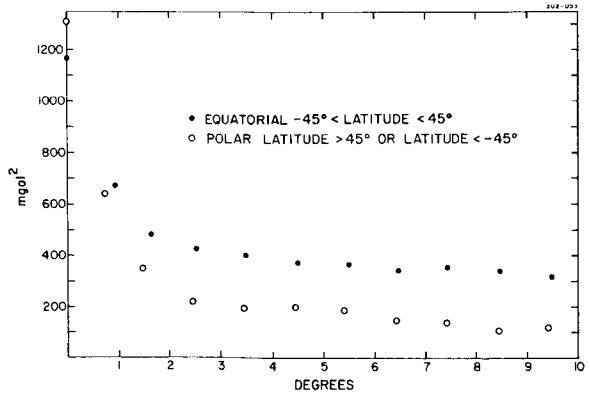

FIGURE 9.9e.—The covariance functions of mean 1°×1° oceanic gravity anomalies for polar and equatorial regions.

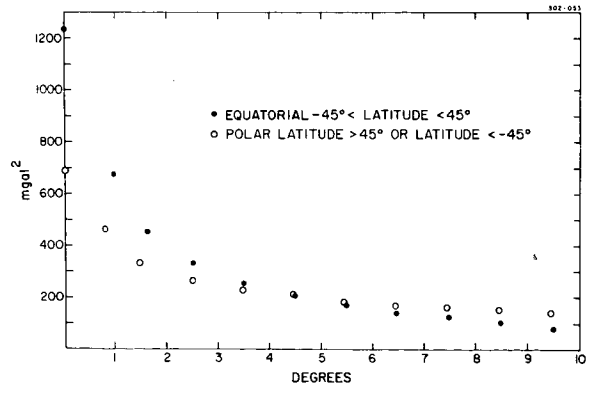

FIGURE 9.9f.—The covariance functions of mean 1°×1° continental gravity anomalies for polar and equatorial regions.

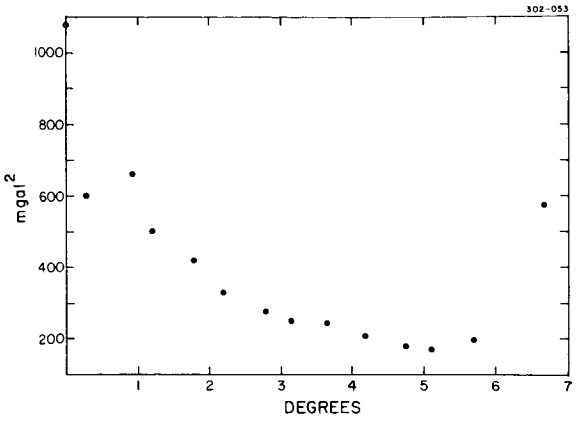

FIGURE 9.9g.—The block covariance function of unit gravity anomalies.

The different estimates of gravity from the global covariance estimator, from the split covariance estimators with a 0- and a −1-km ocean-continent boundary, and from the Kaula estimator were obtained and compared. At the equator, the Kaula-type units and the $1°\times1°$ areas coincide, so that the four estimates can be compared directly. Figure 9.10 shows a few blocks at the equator. Large differences are in blocks with few observed points. In the combination with satellite data, these points will have a small effect due to the weighting, which is proportional to the number of units contributing to the average. Therefore, by using the block covariance estimator of Kaula, we obtained a statistically independent set of 550 km × 550 km averages with no loss of accuracy. Block covariance provides the optimum set of gravity anomalies to be used in combination with satellite observations. Of course, of all the methods used here, the split covariance estimator is preferable for the prediction of $1°\times1°$ mean gravity anomalies.

The gravity anomalies are given with respect to the International Gravity Formula (Heiskanen and Moritz, 1967, p. 79) and must be corrected to refer to the best-fitting ellipsoid defined by C_2 and the adopted values of a_e, GM, and ω_e. We must also include the Potsdam correction of −14 mGal. Using the following initial values:

$$\bar{C}_2 = -484.170\times10^{-6}$$
$$a_e = 6.378\ 140\times10^{8}\ \text{cm}$$
$$GM = 3.986\ 013\times10^{20}\ \text{cm}^3\ \text{sec}^{-2}$$
$$\omega_e = 7.292\ 115\ 085\times10^{-5}\ \text{sec}^{-1}$$

we have

$$1/f = 298.256$$

and the correction

$$\delta g_{\text{SAO}} - \delta g_{\text{int}} = 1.3 - 13.8\ \sin^2\phi\ \text{mGal}$$

9.3.3 Preprocessing

(M. R. Pearlman, J. M. Thorp, C. R. H. Tsiang, D. A. Arnold, C. G. Lehr, and J. Wohn)

9.3.3.1 Baker-Nunn Camera Data

9.3.3.1.1 STAR CATALOG

The stellar reference system used for the Baker-Nunn reductions is defined by the SAO Star Catalog (Staff, Smithsonian Astrophysical Observatory, 1966) which contains approximately 260 000 stars. The average standard deviation of the positions in the SAO catalog is of the order 0″.5 for the current epoch, although individual values may range from 0 to 2″.5. The SAO catalog is in the FK4 system, which has possible systematic errors of 0″.2; further, in the compilation of the other star catalogs into this fundamental system, substantial systematic differences may have resulted for some regions of the sky. Until more observational data become available from new catalogs, there is no means of determining the magnitudes of these errors; and as these discrepancies will be systematic over large parts of the sky, they cannot be detected from the film reduction. The best safeguard against systematic errors is to observe the satellite in as many regions of the sky as possible. This means that more observations are required for a specific problem than would be indicated by a simple theory based on random errors.

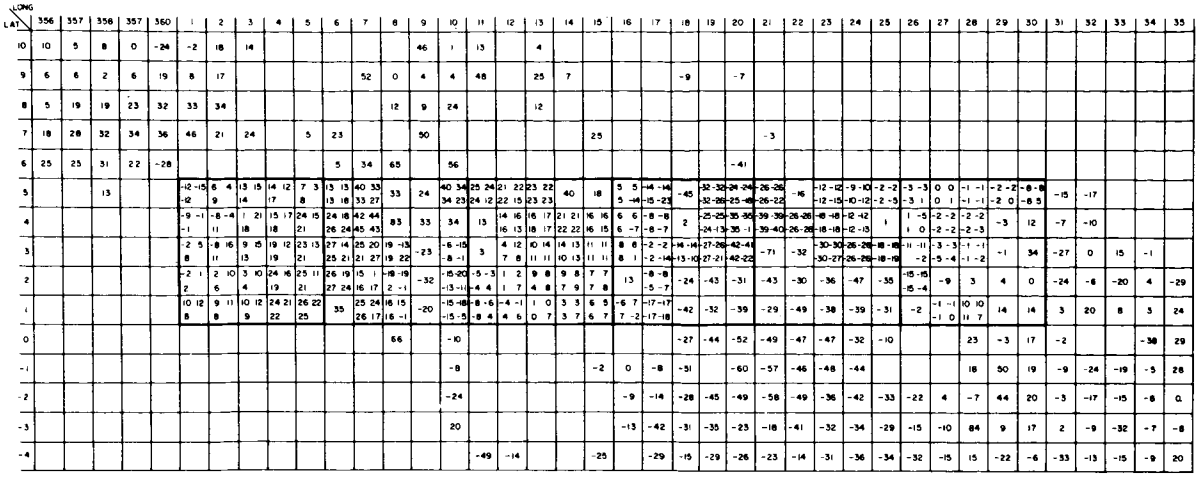

FIGURE 9.10.—Comparison of the four estimate procedures. $1° \times 1°$ squares with single numbers represent the measured mean free-air gravity anomalies. $1° \times 1°$ squares with four numbers represent estimates as follows: upper left, the split covariance estimator with a 0-km ocean-continent boundary; lower left, the global covariance estimate; upper right, the split covariance estimator with a 1-km ocean-continent boundary; lower right, the Kaula estimator.

9.3.3.1.2 PRECISE REDUCTIONS

Methods and Rationale.—The reduction procedure of SAO's Baker-Nunn observations has been discussed by Haefner (1967) and Haefner and Martin (1966); the latter presents, with some minor modifications, the standard reduction procedures now in use at SAO. Our reduction procedure is based on astrometric principles, which differ significantly from the photogrammetric methods widely used in conjunction with ballistic cameras.

Because of the differences in the data-acquisition and reduction techniques, a direct comparison of the astrometric and photogrammetric methods is not valid. A brief generalization, however, can be made: Astrometric methods are most suitable where narrow fields ($<5°$) are used; the photogrammetric methods are most applicable to wide fields (20° to 30°); and in the intervening range, a compromise between the two methods will often provide the most practical solution. The reduction procedure to be employed is the one that is most economical yet commensurate with the physical characteristics of the camera and with the external phenomena affecting the observations. This economic requirement is particularly important because a total of over 200 000 Baker-Nunn observations have been reduced during the program.

The chief advantage of the astrometric (Turner's) method is that a variety of phenomena affecting the relative positions of the satellite and the star images need not be corrected for explicitly. The method describes an affine transformation between the standard coordinates and the plate coordinates. It assumes that (1) the two coordinate planes are parallel and (2) a small field is used. This first requirement is adequately satisfied by the design of the camera, the principal ray at any point being normal to the backup plate. The second requirement is met by using only those reference stars that lie within 2° to 2°.5 of the satellite image. The reductions are valid for any small area away from the physical film center, although residual distortions at the outer parts of the field mean that the satellite image should lie within about 10° of the center.

Transformations.—The relationship between the stellar coordinates and the standard coordinates is expressed by the azimuthal equidistant projection. Let D_0 and A_0, respectively, denote the declination and right ascension of the adopted film center, and δ and α, the declination and right ascension of the satellite position. Then

$$\begin{pmatrix} v_1 \\ v_2 \\ v_3 \end{pmatrix} = \begin{pmatrix} 1 & 0 & 0 \\ 0 & \sin D_0 & \cos D_0 \\ 0 & -\cos D_0 & \sin D_0 \end{pmatrix} \begin{pmatrix} -\sin A_0 & \cos A_0 & 0 \\ -\cos A_0 & -\sin A_0 & 0 \\ 0 & 0 & 1 \end{pmatrix} \begin{pmatrix} \cos\alpha\cos\delta \\ \sin\alpha\cos\delta \\ \sin\delta \end{pmatrix}$$

and the standard coordinates (ζ, η) of a reference point become

$$\zeta = \frac{v_1}{v_2} \cdot \frac{\theta}{D} \cdot f$$

$$\eta = \frac{v_2}{v_3} \cdot \frac{\theta}{D} \cdot f$$

where f is the camera focal length and θ is the angle between the plate center and the star; that is,

$$\theta = \tan^{-1}\left(\frac{\sqrt{v_1^2 + v_2^2}}{v_3}\right)$$

$$\mathrm{D} = \tan\theta$$

Such a projection is valid for any region of the film. The adopted choice for the film "center" is the geometric center of the selected images of reference stars. With well-distributed reference points, the separation between this center and the satellite image is less than 0°.5. The projection preserves the azimuth and scale in the radial direction from the adopted film center, but distortions in other directions will occur. These distortions, however, are small, and the average distortion over the small field used is less than 0.5 μ.

Corrections.—In the process of precise reductions, a number of corrections must be applied to the data.

(1) Shutter corrections: During the exposure of the Baker-Nunn film, the satellite image and the star images trail along the film. These trails are periodically broken into six segments by the two diametrically opposite staves of a rotating barrel shutter. The third break corresponds to the satellite position to be measured, and its time is not directly recorded; the other breaks are not currently used. At some instant during the stave passage, its position and time are recorded on the film. The time of the image and the time of the stave passage are related by the shutter-sweep correction. Thus, if β is the angle of rotation of the shutter about its axis between the two events, the sweep correction Δt is given in the first instance by

$$\Delta t = \frac{\beta}{\omega}$$

ω being the angular velocity of the shutter.

The situation is somewhat complicated because the time is not necessarily displayed when the stave passes over the film center. However, if the stave displacement $\Delta\beta$ is not excessive, the camera has a device for measuring $\Delta\beta$, and the total sweep correction becomes

$$\Delta t = \frac{\beta - \Delta\beta}{\omega}$$

Zadunaisky (1960) gives the equations necessary to compute the angles β and $\Delta\beta$. These formulations are based on a number of simplifying assumptions whose effects on the accuracy of the time determination can be investigated.

(2) Aberration corrections: The film reduction is carried out for the epoch of 1950.0, and the only aberration correction applied at this stage is for annual aberration. Owing to the small field, the correction is applied to the satellite position, rather than to each star position individually. The formulas used are the closed expressions:

$$\Delta\alpha = -\frac{20''.47 \sin\alpha \sin\odot + 18''.87 \cos\alpha \cos\odot}{\cos\delta}$$

$$\Delta\delta = -[20''.47 \sin\delta \cos\alpha \sin\odot + 18''.87 (0.433\,666\,1 \cos\delta - \sin\delta \sin\alpha) \cos\odot]$$

where $\odot$ is the geocentric longitude of the sun. Though not rigorous, these expressions will always be correct to better than 0".1 (Scott, 1964).

(3) Atmospheric-refraction corrections: In the film-reduction process, atmospheric-refraction corrections are not applied to individual star positions, since it is assumed that the atmospheric-refraction correction varies linearly over the 4° to 5° field used in the reduction. This condition is nearly always satisfied since observations are seldom made at zenith distances of greater than 70°. At this zenith distance, the average departure of the differential refraction from linearity is about 1", and with eight well-distributed stars, the uncertainty in the satellite position (all other factors being ignored) will be at most 0".4.

A parallactic-refraction correction is applied to the satellite position during analysis. The value for the refractivity constant in this correction is based not on the atmospheric conditions at the time of observation, but rather on the average year-round, nighttime conditions for the station from which the observations are made. For the present Baker-Nunn camera locations, the error in the refraction correction is less than 20 percent of the value of the correction itself. As this correction is always small, the error is minimal.

Of greater importance than uncertainties in the parallactic-refraction correction is the random-image displacement caused by microturbulence in the atmosphere. When the Baker-Nunn camera is used in the stationary mode, this image motion will exist in both the along-track and the across-track directions, with the greater deviations occurring in the former because of the different time-integration effects. The satellite position will not be seriously affected when the camera is used in the tracking mode, but each star image may be displaced. The average one-dimensional deviation from the mean, σ_ψ, can be approximately formulated (Lambeck, 1968) as follows:

$$\sigma_\psi = \left\{(0.03)^2 + \left[\frac{4.5\ \sec^{1/2}\zeta}{\sqrt{D}}(1 - 0.35 \log \Delta t)\right]^2\right\}^{1/2}$$

$$\Delta t < 1000 \text{ msec}$$

where D is the aperture in centimeters and Δt, the exposure time in milliseconds.

(4) GEOS flash corrections: The star and satellite images of Baker-Nunn films of passive objects refer to the same instant of time. This is not the case for observations of flashing satellites, so a correction must be applied to the observed position to ensure that both the star images and the satellite image refer to the same time instant. For operational reasons, the star-trail exposure is offset by $\approx$0.1 sec from the flash time. The correction is computed by precessing the satellite position to the date of observation, adding the correction

$\Delta\alpha = 1.0027 \times$ (time difference between satellite and star exposure)

and precessing the corrected position back to the epoch of 1950.0. Because of the small time interval between the star exposures and the flash observation, nutation need not be considered.

9.3.3.1.3 SYNTHETIC OBSERVATIONS

The arcs formed by several successive observations can be used to create synthetic observations at some intermediate time by interpolation. Simultaneous observations used in the geometrical satellite solution rely almost entirely on such synthetic observations, and they are also used in the dynamical solution whenever four or more successive frames are available.

Since it is virtually impossible to observe a passive satellite at exactly the same

instant from two or more distant stations, the only practical way of obtaining simultaneous observations is to observe the satellite from the participating stations for approximately the same time interval and to interpolate for a fictitious simultaneous instant. In orbital analysis, use of synthetic observations reduces the amount of data to be handled without any significant loss of accuracy and resolution. But probably the most cogent reason for using synthetic observations is that a better accuracy or reliability estimate can be associated with the synthetic observation than with a single observation. Only average values can be assigned to the errors in a single observation. Some of these errors vary more or less randomly from exposure to exposure and will be reflected in the residuals resulting from a least-squares interpolation procedure for a synthetic observation.

A second-degree polynomial is adequate for the majority of observations. Since a seven-frame arc generally subtends less than 10° of arc, the object's orbit can be adequately approximated by quadratic functions. When there are more than seven or eight frames in a sequence, a third-degree polynomial may be required, but proper constraints must be placed on the coefficients to ensure that the curve approximates the orbit and does not reflect characteristics of the image-forming process for the points in the sequence. If higher degree polynomials are used without such constraints, the accuracy estimates of the interpolated positions become optimistic, although the mean position of the satellite is not seriously affected.

The interpolation procedure is based on several assumptions: (1) that the errors in successive positions in the arc are uncorrelated, (2) that the along- and across-track errors for each position are uncorrelated, (3) that the along-track uncertainties are equal for all frames, and (4) that the across-track uncertainties are equal for all frames. Since systematic errors in timing would destroy the first assumption, timing uncertainties are not included in the uncertainty of each position. Other correlations between successive Baker-Nunn images are much smaller than with ballistic cameras, where images lie on a single frame. For the Baker-Nunn, plate constants are derived independently for each frame, so that the influence of such factors as measuring uncertainties, nonlinear lens and film distortions, and short-period atmospheric effects (on each satellite position) will be random from frame to frame. Since the same reference stars may be used in two or even three successive frames, errors in stellar coordinates could introduce some correlated errors between successive frames.

Synthetic simultaneous directions are corrected for parallactic refraction, diurnal aberration, and light travel time between the station and the satellite (see Haefner and Martin (1966) for the corrections used) and refer to the terrestrial system defined by the mean pole of 1900 to 1905 and by the meridian plane at 75°03′55″.94 east of the mean meridian of the USNO. The time of the observations is expressed in Smithsonian Atomic Time as defined in table 9.22. The directions are given as direction cosines, and their standard deviations are given in the along- and across-track components. Timing uncertainties have been introduced in the former. The angle the satellite trail makes with the right-ascension axis is also computed so that the accuracy of the direction in the right-ascension and declination components can be determined.

9.3.3.1.4 ACCURACY AND ERROR BUDGET FOR DATA FROM BAKER-NUNN CAMERA

A summary of the principal error sources in the determination of star positions and an estimate of the total influence are given below (Lambeck, 1968) :

Measuring errors	1″.2 (6 measurements)
Calibration of comparator	0″.2
Film and emulsion distortion	0″.8

Atmospheric refraction	1″.1 (image motion for tracking camera)
	0″.8 (differential refraction)
	0″.3 (wandering)
Approximations in reduction method	0″.2
Star positions from SAO catalog	0″.5 (random)
	0″.2 (systematic)
Total standard deviation of each star position	1″.8 (stationary mode)
	2″.1 (tracking mode)

The principal error sources in the determination of satellite position and an estimate of the total influence are summarized below (Lambeck, 1968) :

Measuring errors	0″.8 (12 measurements)
Calibration of comparator	0″.2
Film and emulsion distortion	0″.8
Atmospheric refraction	1″.1 (image motion along track, or flash images)
	0″.5 (image motion across track)
	0″.3 (wandering)
	0″.1 (parallactic refraction)
Contribution of standard deviation of 8 stars	0″.8 (stationary)
	0″.9 (tracking)
Total standard deviation of satellite position	1″.8 (stationary, along track)
	1″.5 (stationary, across track)
	1″.6 (tracking)

Before 1965, time was maintained at the stations by the Norrman clock and by the monitoring of WWV broadcasts at HF and VHF. The root-mean-square (rms) accuracy of an observation epoch was about 1 msec, with excursions of several milliseconds in some cases.

Installation of the EECo clock system in 1964 and use of frequency broadcasts on VLF and of portable clocks improved the timing situation. All the stations had ± 100-μsec clock accuracies by 1967.

A summary of the overall accuracy of a single Baker-Nunn observation for different topocentric velocities of a satellite is given in table 9.23.

Before the installation of the EECo clocks, the average accuracy of the synthetic observations was about 1″.1 in each component. Now, with the improved timekeeping procedures, the average accuracy of the synthetic observation is about 0″.9 along track and 0″.7 across track.

9.3.3.2 Data From a Laser System

9.3.3.2.1 CALIBRATION

The laser systems are calibrated by ranging on a fixed land-based target situated at a known distance from the laser. The system delay or system-calibration constant is the difference between the raw target range time measured by the system, τ_m, and the range time to the target, τ_s, computed from the surveyed distance between the laser and the target and corrected for local atmospheric refraction. The targets, which are 8 ft $\times$ 8 ft wooden surfaces painted flat white, are 0.5 to 2.0 km distant from the laser system. The exact placement is usually dictated by local terrain.

The routine calibration of the system is performed nightly and consists of 20 measurements on the target. For these measurements, the return-pulse intensity is controlled by use of neutral-density filters to produce signal levels similar to satellite echoes.

Computation of a calibration correction factor τ_c, which must be added (algebraically) to all satellite range-time observations, is obtained from

$$\tau_c = \tau_s - \tau_m$$

where τ_m is the average of the 20 range-time measurements. The computed range time to the target is given by

$$\tau_s = \frac{d_s}{0.15}\left[1 + (N \times 10^{-6}) \div (6.917 \times 10^{-1})\right]$$

where d_s is the surveyed distance to the target and N is the local atmospheric refractivity

$$N = 80.29\frac{P}{T} - 11.9\frac{e}{T}$$

in which P is the measured barometric pressure in millibars, e is the partial pressure of water vapor, and T is the temperature in degrees Kelvin.

The effect of local variations in barometric pressure on the value of τ_s for distances of less than 1 km was found to be small enough so that a constant value of the atmospheric refractivity could be defined for each station. This value was taken from a chart prepared to give a direct conversion from station altitude in kilometers to values of N (Gaposchkin, 1972, unpublished).

During individual nightly (or daily) calibration sequences, the range scatter from one measurement to the next is seldom more than a few nanoseconds. The variation in the target-range averages is rarely more than a few tenths of a nanosecond from calibration to calibration, giving a stability of better than 10 cm. The target surveys at the stations currently have an estimated accuracy of about 10 cm.

9.3.3.2.2 ATMOSPHERIC CORRECTIONS

Ranges determined by using the vacuum velocity of light must be corrected for the fact that the laser pulse travels at a lower velocity in the earth's atmosphere. We used the following correction during this program (G. Thayer, 1967, private communication):

$$r_m = r_v - \frac{2.238 + 0.0414\,PT^{-1} - 0.238\,h_s}{\sin\alpha + 10^{-3}\cot\alpha}$$

where r_v is the uncorected range in meters, r_m is the corrected range in meters, P is the atmospheric pressure at the laser station, T is the temperature at the laser station, h_s is the laser's height above mean sea level in kilometers, and α is the elevation angle of the satellite. The formula holds for a ruby laser, which operates at 694 nm.

The formula was derived from a regression analysis based on a large sample of radiosonde balloon flights from a number of locations that were chosen to give a reasonable sampling of anticipated atmospheric conditions. The error in range correction is estimated to be about 2 to 3 cm at zenith.

9.3.3.2.3 TRANSFER FUNCTIONS OF A SATELLITE-RETROREFLECTOR ARRAY

Range erors now present in routine tracking by laser systems are actually smaller than the satellite dimensions. Since we must relate all observations to the satellite center of mass (both for dynamic and for purely geometric analyses), it is necessary to derive some means for reducing each range observation to the distance from the ground-based laser to the satellite center of mass, which, in all cases, is displaced from the reflecting elements. For this purpose, we have developed and applied in our geodetic analyses a set of retroreflector-array transfer functions for each of the United States satellites with cube corners now in orbit. These transfer functions are computed from the geometric and optical parameters of each retroreflector array and take into account the satellite geometry and position. The functions for 6508901 (GEOS–1), GEOS–2, 6406401 (BE–B), 6503201 (BE–C), 6701101 (D1C), 6701401 (D1D), and 7010901 (PEOLE) were computed.

The computer model includes both incoherent and coherent return signals for arrays of retroreflectors whose faces are cut in the form of a circle, triangle, or even-sided polygon (such as a hexagon). Diffraction, including changes in amplitude and polariza-

tion of the reflected laser beam, and influences of dihedral-angle errors can also be accounted for. The model accommodates obscuration of retroreflectors by satellite and subsystem structure, a particular problem with the two GEOS spacecraft and with PEOLE. When the position of each reflector is being computed, the model accounts for the dielectric properties of the retroreflectors in terms of ray bending and propagation velocity. Once the return signal has been constructed, the relationship of the centroid of the signal to the satellite center of mass is determined and then applied as a range correction to the laser data used in the geodetic analyses.

The major limitation on the accuracy with which transfer functions can be determined for the existing satellites with retroreflectors is the lack of precise information on the beam patterns of the retroreflectors in relation to the large size of the arrays. With the existing uncertainties in retroreflector optical characteristics, geometric placement, and satellite attitude, we estimate that the range corrections for these satellites have an accuracy of about 10 cm. It should be noted that this error is quite systematic.

9.3.3.3 Network Time Base

9.3.3.3.1 STATION-CLOCK SYNCHRONIZATION

Synchronization of the station clocks throughout the network is achieved by relating all the time and frequency references to UTC as maintained by USNO. The field stations steer their clock frequencies with VLF transmissions from stations NAA and NLK, and in some cases, WWVL or WWVB. Crude epoch checks are made at many of the stations by monitoring HF/VHF time signals. The USNO and the National Bureau of Standards (NBS) timing bulletins, which give the relative phase values of VLF stations and time intercomparisons with other timing services, are used to relate all field timing values to UTC(USNO).

Use of a portable clock is the principal method of synchronizing with a source of reliable timing. The comparison of the portable clock with the clock at the station gives a correction relating the station time to the source time, and published comparison values relate the source time to UTC (USNO). Therefore, each field-station clock is referred to a common time scale with an accuracy dependent on the reliability of the portable-clock comparison and on the accuracy of the published comparison value.

The trips to the field stations have been conducted with a Sulzer A5 portable crystal clock that carries time related to UTC (USNO). These trips have been run by SAO or, in some instances, by other agencies (such as NASA, USNO, Naval Research Laboratory, and NBS) who have either carried an SAO clock or been in the vicinity of an SAO field station with a clock of their own. Portable-clock comparisons are made with each station on a biennial basis. However, to maintain higher levels of accuracy and reliability, a portable-clock comparison is made at least once a year at the laser stations. Time corrections, determined to be necessary by portable-clock comparisons or intercomparison between station-clock and VLF-monitor readings, are documented and applied directly to the station clocks. Corrections for the difference between the VLF stations and USNO are applied in Cambridge during data preprocessing.

9.3.3.3.2 ACCURACY AND ERROR BUDGET

The accuracy of station timing depends on (1) the success of the portable-clock trips, (2) the ability to trace the relationship of the time references back to USNO, (3) the ability of the station to maintain the time setting with the aid of the VLF tracking receiver, and (4) the uncontrollable variations in propagation path of the VLF signal. The requirements for system timing originally called for the station clocks to be within ± 1 msec of WWV (rms of net devia-

tion from UTC(NBS) over a month). This requirement was tightened to ±100 μsec UTC (USNO) for the camera stations and ±50 μsec for the laser stations. This improvement was made possible by the installation of the EECo timing systems in the mid-1960's and was realized by 1967. In practice, many of the camera stations have been operating within ±50 μsec of UTC(USNO).

The synchronization accuracy by use of a portable clock depends on the amount of unpredictable time drift experienced during the period spent traveling to and from the field station. Most of the trips to the field stations use a crystal clock and provide a time set accurately to within 5 to 25 μsec of USNO. The least reliable results have been in India and South America, where the stations are fairly remote and long travel times are involved.

USNO publishes a weekly bulletin, "Daily Phase Values, Series 4," giving the emitted phase values of the major VLF transmitting stations to 1 μsec. The time differences between UTC as maintained by USNO, NBS, and the Bureau International de l'Heure (BIH) are well documented by each agency to microsecond accuracy. The relationships between the HF time broadcasts of foreign countries and UTC(USNO) are generally less precisely known.

Timing accuracy at the field station is maintained by controlling the clock drift with the aid of VLF monitoring equipment. In cases of minor clock failures, time has often been recovered with fair accuracy by referring to backup clocks and to VLF and HF monitor references. The clock-time drift is a product of oscillator frequency offset and is generally controlled to keep the station epoch within 50 μsec of the VLF reference position.

The accuracy of VLF-derived time is a function of receiver and propagation-path stability. The uncertainties of the day-to-day and seasonal path variations added to the error contribution of the receiver amount to less than 5 μsec in epoch uncertainty. The system timing accuracy is a composite figure encompassing setting accuracy, uncorrected drift of the clock, and inaccuracy of the VLF monitor.

The degree of accuracy in setting a portable clock gives the initial accuracy of the station epoch, and VLF monitoring permits the clock to maintain time. When subsequent incidents of minor clock failure that affect time and frequency increase the epoch uncertainty to ±50 μsec, another portable-clock comparison is considered. When requirements are stringent, additional efforts are made to obtain more accurate time comparisons, to reduce the oscillator drift, and to minimize the acccrual of uncertainty due to repeated clock resets. This extra effort is the key to maintaining station epochs at the ±50–μsec level with a minimum of clock trips.

9.4 THEORY

The following three sections provide the theory used for determining (1) coordinates of ground tracking systems and (2) the gravitational potential of the Earth. The coordinates were determined both by a purely geometric method (sec. 9.4.2.1) and by the dynamic method (sec. 9.4.2.2), which uses the equations of motion of satellites, together with the geometric. The gravitational potential can be determined with the help of the equations of motion alone, the gravimetric theory alone, or the two together. The zonal harmonics of the gravitational potential of Standard Earth III were determined by using the equations of motion alone (sec. 9.4.3.2); the tesseral harmonics were determined by using both the equations of motion and the gravimetric theory (sec. 9.4.3.3). Because the equations of motion have been used for determining both coordinates and the potential, their theory is discussed first.

9.4.1 Orbital Theory

(E. M. Gaposchkin)

The theory used to connect the position of a satellite to the time of observation at a single station is the dynamics of a particle

in an approximately central field of force. The theory is presented in this section. It is used to find both the coordinates of the tracking station and the constants that determine the field of force. The coordinates, the constants, or both may be determined at the same time as the six constants of integration that, together with the time, determine the orbit.

The symbolism used in this chapter differs from that used throughout the rest of this volume. The major deviations are as follows:

J_n	for	$-C_n$
$\bar{P}_{lm}, \bar{C}_{lm}, \bar{S}_{lm}$	for	P_n^m, C_n^m, S_n^m
I	for	i
μ	for	GM
ϕ	for	ψ

9.4.1.1 Transformation and Coordinate Systems

Consider the coordinate system x_1, y_1, z_1, a point

$$[P]=\begin{bmatrix} p_x \\ p_y \\ p_z \end{bmatrix}$$

and a second coordinate system rotated about the z axis by an angle Ω. The coordinates of p in the x_2, y_2, z_2 system can be expressed with the matrix operation

$$[P_2]=R_3(\Omega)\,[P_1]$$

where

$$R_3=\begin{bmatrix} \cos\Omega & \sin\Omega & 0 \\ -\sin\Omega & \cos\Omega & 0 \\ 0 & 0 & 1 \end{bmatrix} \qquad (9.2)$$

In an analogous way, we can define rotation around any axis with

$$R_1=\begin{bmatrix} 1 & 0 & 0 \\ 0 & \cos I & -\sin I \\ 0 & \sin I & \cos I \end{bmatrix} \qquad (9.3)$$

about the x axis and

$$R_2=\begin{bmatrix} \cos\phi & 0 & -\sin\phi \\ 0 & 1 & 0 \\ \sin\phi & 0 & \cos\phi \end{bmatrix} \qquad (9.4)$$

about the y axis. Here, R_1, R_2, and R_3 are matrices, and their mathematical properties are the subject of linear algebra. We need know only that these quantities have the following properties:

(1) The length of a vector is unchanged by rotation.

(2) Multiplication of matrices does not commute; that is,

$$R_i(\phi)\,R_j(\lambda)\neq R_j(\lambda)\,R_i(\phi)$$

(3) Multiplication does satisfy the associative rule; that is,

$$R_i(R_jR_k)=(R_iR_j)\,R_k$$

(4) Rotation about the same axis is additive; that is,

$$R_i(\phi)\,R_i(\lambda)=R_i(\phi+\lambda)$$

(5) For rotation matrices, the inverse and transpose are related by

$$R_i^{-1}(\phi)=R_i^T(\phi)=R_i(-\phi)$$

(6) We also have

$$(R_iR_j)^{-1}=R_j^{-1}R_i^{-1}$$

(7) Differentiation and integration are performed on each element.

Although multiplication does not commute, for small rotations around the x, y, and z axes—that is, ϵ_x, ϵ_y, ϵ_z—we can define the infinitesimal rotation matrix

$$R(\epsilon_x, \epsilon_y, \epsilon_z)=\begin{bmatrix} 1 & \epsilon_z & -\epsilon_y \\ -\epsilon_z & 1 & \epsilon_x \\ \epsilon_y & -\epsilon_x & 1 \end{bmatrix} \qquad (9.5)$$

which does commute.

In satellite geodesy, dynamical astronomy, and astrometry, we are concerned with four reference frames: (1) the terrestrial system,

(2) the inertial system, (3) the celestial (sidereal) system, and (4) the orbital system. Since a systematic account of these systems and their relationships to one another can be found in Veis (1960, 1963) and elsewhere, we confine ourselves to a descriptive summary.

The terrestrial system is fixed to the Earth. Positions on the surface can be considered invariant in time if we ignore tides and crustal motions for the moment. The representation of the terrestrial system can be in terms of geocentric coordinates or datum coordinates. The datum can be defined in a geocentric system with the following seven parameters: the three datum origin coordinates, the three orientation parameters, and a scale factor. Datum coordinates can be determined from precise knowledge of the geocentric coordinates. One of the objectives of satellite geodesy is to determine coordinates in a geocentric system. Through coordinates common to geocentric and datum systems, the relation of the datum to the geocentric system is determined.

The inertial system is fundamental to dynamics, and all orbit theory is ultimately developed in this system. We hope to materialize the inertial through the celestial system. The latter is defined by the stars and, it is hoped, with respect to the distant galaxies. The distant galaxies define an inertial reference frame.

The celestial system is represented by coordinates of stars insofar as we can treat proper motion accurately. Individual star catalogs are similar to compilations of geodetic coordinates in that the positions are relative. Positions can be combined into a uniform system by use of stars common to any two catalogs. This technique was used to compile the SAO Star Catalog (Staff, Smithsonian Astrophysical Observatory, 1966), which is in computer-accessible form, covers the whole sky, and contains about 250 000 stars with their positions and proper motions reduced to the FK4 system.

The equations of motion are most easily given in an inertial reference frame. However, in this system, the Earth is moving in an irregular manner, and the gravitational field, assumed static in an Earth-fixed system, has an irregular time dependence. This irregular temporal variation will give rise to perturbations.

For this reason, we have adopted an intermediate, quasi-inertial reference frame. This orbital system has a fixed equinox (the mean equinox of 1950.0) and a moving equator (the instantaneous equator of date), and the gravitational field is rotating about the z axis at a constant rate. This orbital system has been shown by Kozai (1960) and Kozai and Kinoshita (1973) to be optimum for our work. That is to say, short-period terms are unaffected by the change, and the effects of being noninertial and those of variations of the gravity field are minimized. We can then proceed with the theory for periodic perturbations as if we had an inertial reference frame and make some corrections (section 9.4.1.7). A further result of this choice is that the Earth is rotating uniformly in this system, thus giving a particularly simple expression for the sidereal angle.

The relation between the celestial system and the terrestrial is established in two steps. A general theory of precession and nutation deals with the secular and periodic parts, respectively, of the forced motion due to the gravitational attraction of the Sun and Moon. A general reference for these effects is chapter 2 of the *Explanatory Supplement to the Astronomical Ephemeris and the American Ephemeris and Nautical Almanac* (hereafter called ESAENA). The instantaneous orientation of the Earth is described to 2×10^{-6} rad with these formulas. The irregular fluctuations of the Earth's orientation with respect to this computed orientation are routinely measured as three angles and published by the Bureau International de l'Heure. The free nutation of the Earth is the motion of the adopted reference point of the z axis about the spin axis in the terrestrial system. The spin axis, of course, moves owing to precession and nutation, and that axis defines the astronomical equator. The rotation rate has small fluctuations, resulting in irregular fluctuations in the true

sidereal angle. The coordinates of the reference pole (x,y) and the change in the sidereal angle (ΔUT1) are observed quantities and provide the relationship between the celestial and the terrestrial systems.

The variations of pole position are not strictly periodic. There is considerable uncertainty about the actual properties of the polar motion. As a result, an arbitrary reference point was adopted by the International Union of Geodesy in 1967. This point was the mean pole for the time 1900.0 to 1905.0, and all pole coordinates are now given with respect to it. The mean pole today is about 10 m west of the adopted pole.

In summary, we now give the relations between the orbital system and the others. If X_0 is the position of a station in an Earth-fixed system, then X is the position in the orbital system:

$$X = R_3(-\theta) R(y, x, 0) X_0 \qquad (9.6)$$

where θ is the sidereal angle computed from

$$\theta = 0.277\,987\,616 + 1.002\,737\,811\,91 \\ (T - 33\,282.0) + \Delta\text{UT1}\,(\text{rev}) \qquad (9.7)$$

and x and y are the observed coordinates of the pole.

In general, camera observations provide directions in a celestial system at some epoch T_0. To express this direction in the adopted orbital system, we must apply precession κ, ω, ν from T_0 to 1950.0, and then apply κ, ω, ν to the motion of the equator, thus preserving the origin of 1950.0. If $\kappa(b,a)$ is the amount of precession in right ascension from dates a to b, and if similar expressions are given for ω and ν, then

$$[\hat{l}] = R(-\Delta\epsilon, \psi \sin \epsilon, 0) R_3[\kappa(T, 1950)] \\ R_2[\nu(T, 1950)] R_3[-\kappa(T, 1950)] \\ R_3[-\omega(1950, T_0)] R_2[-\nu(1950, T_0)] \\ R_3[-\kappa(1950, T_0)] [\hat{l}_0] \qquad (9.8)$$

expresses the direction in the orbital system. The nutation $(\Delta\epsilon, \psi \sin \epsilon)$ must also be applied to the original direction if the true coordinates are given. The reader is referred to the ESAENA for numerical values. It has been found satisfactory to use the quadratic expressions for precession and to retain all terms in nutation such that the total neglected part is less than 0.5 m.

9.4.1.2 Two-Body Motion

The first approximation for satellite motion is two-body motion, which forms the reference for all subsequent analysis. Two-body motion can be completely solved in closed form by simple methods. (See, e.g., Brouwer and Clemence, 1961.)

If the origin of coordinates is taken at the center of mass of the system, then the paths of both bodies lie in a common plane through that point and the path of each body is an ellipse with one focus at that point. When the mass of one body is immensely greater than that of the other, only the mass M of the larger body need be considered. The equation for the motion of a point with unit mass moving in the gravitational field of such a large body is

$$r = \frac{a(1 \quad e^2)}{1 + e \cos v} = a(1 - e \cos E) \qquad (9.9)$$

with

$$r \sin v = a(1-e^2)^{1/2} \sin E \\ r \cos v = a(\cos E - e)$$

The angles are defined in figure 9.11. By comparing the constants, we find that

$$e = \left(1 + 2\mathcal{H}\frac{N^2}{\mu^2}\right)^{1/2} \\ a = -\frac{\mu}{2\mathcal{H}} = \frac{N^2}{\mu(1-e^2)} \qquad (9.10)$$

where $\mathcal{H}$ is the Hamiltonian of the system, N is a constant of integration, and $\mu \equiv GM$. From these equations, it is easy to derive the relation between mean motion n and semi-major axes a:

$$n^2 a^3 = \mu \qquad (9.11)$$

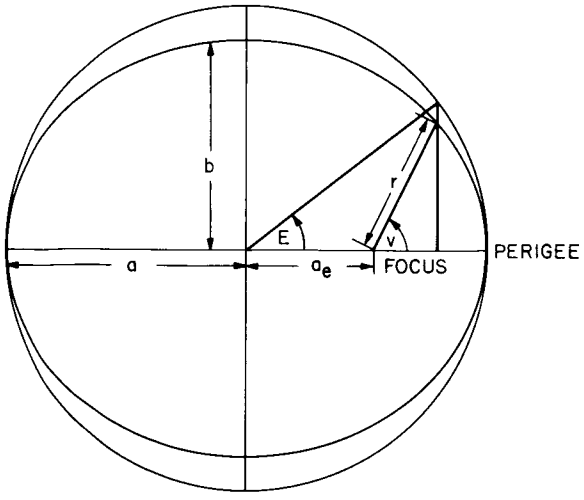

FIGURE 9.11.—Geometry of ellipse.

which is equivalent to Kepler's third law.

We proceed to find $v(t)$ by differentiating (9.9):

$$\frac{dr}{dt}=ae\sin E\frac{dE}{dt}=\frac{a(1-e^2)e\sin v}{1+e\cos v}\frac{dv}{dt} \tag{9.12}$$

This equation reduces to

$$\frac{dE}{dt}=\left(\frac{\mu}{a}\right)^{1/2}\frac{1}{r}=\frac{\mu^{1/2}}{a^{3/2}(1-e\cos E)} \tag{9.13}$$

which integrates to

$$E-e\sin E=n(t-t_0)\equiv M \tag{9.14}$$

which is Kepler's equation.

Given a time, (9.14) must be solved by iteration. Using (9.9), we obtain the true anomaly v and the radius vector r. The position is calculated from

$$\begin{bmatrix}x\\y\\z\end{bmatrix}=r\begin{bmatrix}\cos v\\\sin v\\0\end{bmatrix}=a\begin{bmatrix}\cos E-e\\(1-e^2)^{1/2}\sin E\\0\end{bmatrix} \tag{9.15}$$

The velocity is obtained directly,

$$\begin{bmatrix}\dot{x}\\\dot{y}\\\dot{z}\end{bmatrix}=\frac{na}{(1-e^2)^{1/2}}\begin{bmatrix}-\sin v\\e+\cos v\\0\end{bmatrix}=\frac{na}{1-e\cos E}\begin{bmatrix}-\sin E\\(1-e^2)^{1/2}\cos E\\0\end{bmatrix} \tag{9.16}$$

We have given the analysis of two-body Keplerian motion in a plane. To refer the position $\begin{bmatrix}x\\y\\0\end{bmatrix}$ to the orbital system, we perform the coordinate transformation

$$[X]=R_3(-\Omega)R_1(-I)R_3(-\omega)\begin{bmatrix}x\\y\\0\end{bmatrix} \tag{9.17}$$

The angle ω corresponds to v_0. The angles Ω and I specify the orientation of the orbital plane.

Given the position and velocity, we use the constancy of the angular momentum to determine the angles Ω, I, ω. The direction of the angular momentum is computed from

$$[\hat{L}]=[X]\times[\dot{X}]/|X||\dot{X}| \tag{9.18}$$

and the inclination is obtained from

$$\cos I=\left|[\hat{L}]\times\begin{bmatrix}0\\0\\1\end{bmatrix}\right| \tag{9.19}$$

If $\hat{L}_z$ is negative, the convention is to take $\pi-I$ for the inclination. The node is defined by a unit vector in the direction of the node:

$$\hat{e}_\Omega=\begin{bmatrix}\cos\Omega\\\sin\Omega\\0\end{bmatrix}=\begin{bmatrix}0\\0\\1\end{bmatrix}\times[\hat{L}] \tag{9.20}$$

To find ω, we must determine the satellite position in the orbital plane referred to the node. Using

$$[X']=R_1(I)R_3(\Omega)[X]$$

we have

$$\cos(v+\omega) = X'_x/r$$

$$\sin(v+\omega) = X'_y/r$$

which determine $v+\omega$. With v from (9.9), we immediately have ω.

We give here the equations for a hyperbolic orbit. The position is

$$x = r\cos v = -a(e-\cosh F)$$

$$y = r\sin v = -a(e^2-1)^{1/2}\sinh F$$

$$r = \frac{-a(e^2-1)}{1+e\cos v} = a(e\cosh F - 1)$$

where $a<0$. We still have

$$n^2(-a)^3 = \mu$$

Kepler's equation becomes

$$n(t-t_0) = e\sinh F - F$$

and $r^2v - N$ is still a constant of the motion.

The final question in the discussion of two-body motion concerns the development of (9.9) and its generalization in series. Kepler's equation, (9.14), is transcendental, and closed expressions are not possible. However, rapidly converging series are available. They are needed for the development of perturbations, a topic that will be treated by itself in a later section.

9.4.1.3 Equations of Motion

For conservative forces, rectangular coordinates are canonical, and the Poisson brackets have the values

$$[\dot{x}_i,\dot{x}_j] = 0$$

$$[x_i,x_j] = 0 \qquad (9.21)$$

$$[x_i,\dot{x}_j] = \delta_{ij}$$

The equations of motion can be written in any set of variables $\{\mathcal{E}_i\}$ by using Poisson brackets:

$$d\mathcal{E}_i/dt = -\sum_k [\mathcal{E}_i,\mathcal{E}_k]\,\partial\mathcal{H}/\partial\mathcal{E}_k \qquad (9.22)$$

where $\mathcal{H}$ is the Hamiltonian for the system.

In addition, if $\mathcal{H} = \mathcal{H}_0 + \mathcal{H}_1$ and if we can obtain a solution

$$x_i^0 = x_i^0(\alpha_i,t)$$

$$\dot{x}_i^0 = \dot{x}_i^0(\alpha_i,t)$$

(α_i being constant) for $\mathcal{H}_0$, then by selecting $\mathcal{E}_i$ to be α_i, we can write

$$d\mathcal{E}_i/dt = -\sum_k [\mathcal{E}_i,\mathcal{E}_k]_{x^0,\dot{x}^0}\,\partial\mathcal{H}_1/\partial\mathcal{E}_k \qquad (9.23)$$

where $[\mathcal{E}_i,\mathcal{E}_k]_{x^0,\dot{x}^0}$ are evaluated for the solvable problem. In what follows, we will use only variables that are the solution of the two-body problem (section 9.4.1.2). This choice is not unique, for one could select any combination of $\mathcal{H}$ that had a solution; e.g., there is a separable solution for a potential:

$$\mathcal{U} = -\frac{\mu}{r}\left[1 + \sum_{n=1}^{\infty}\left(\frac{a_e}{r}\right)^n (-J_2)^n P_{2n}(\sin\phi)\right] \qquad (9.24)$$

which is due to Vinti (1959) and has been explored by Izsak (1963b).

The Kepler elements a, e, I, M, ω, Ω are the most commonly used. Using (9.17) in the expression for the Lagrange brackets and employing the time independence of $\{\mathcal{E}_i, \mathcal{E}_j\}_{x^0,\dot{x}^0}$, we obtain for the Lagrange brackets

$$\{\Omega,I\} = -\{I,\Omega\} = -(\mu a)^{1/2}(1-e^2)^{1/2}\sin I$$

$$\{\Omega,a\} = -\{a,\Omega\} = (1-e^2)^{1/2}[\cos(I/2)]\,(\mu/a)^{1/2}$$

$$\{\Omega,e\} = -\{e,\Omega\} = [-(\mu a)^{1/2}\cos I]/(1-e^2)^{1/2}$$

$$\{\omega,a\} = -\{a,\omega\} = [(1-e^2)^{1/2}/2]\,(\mu/a)^{1/2}$$

$$\{\omega,e\} = -\{e,\omega\} = -(\mu a)^{1/2}e/(1-e^2)^{1/2}$$

$$\{a,M\} = -\{M,a\} = -\tfrac{1}{2}(\mu/a)^{1/2} \qquad (9.25)$$

the other combinations being zero. By inverting the matrix implied by (9.25), we obtain for the Poisson brackets

$$
\begin{aligned}
&[a,M] = -[M,a] = 2(a/\mu)^{1/2} \\
&[e,\omega] = -[\omega,e] = -(1-e^2)^{1/2}/(\mu a)^{1/2}e \\
&[I,\Omega] = -[\Omega,I] = -1/[\mu a)^{1/2}(1-e^2)^{1/2}\sin I] \\
&[e,M] = -[M,e] = (1-e^2)/(\mu a)^{1/2}e \\
&[I,\omega] = -[\omega,I] = (\cos I)/(\mu a)^{1/2} \\
&\qquad (1-e^2)^{1/2}\sin I
\end{aligned}
\tag{9.26}
$$

Equations (9.26) inserted into (9.23) can be integrated numerically. They remain a set of coupled differential equations. Analytical solutions are obtained by approximate methods. A particular difficulty arises if these equations are used in a straightforward manner.

It is customary to express the Hamiltonian

$$
\mathcal{H} = \frac{1}{2}V^2 + u = \frac{1}{2}V^2 - \frac{\mu}{r} - R \tag{9.27}
$$

where $R < \mu/a$ and is called the disturbing function. Then R is expressed in a trigonometric series of the form

$$
\sum A(a,e,I) \begin{matrix}\sin \\ \cos\end{matrix} [\alpha M + \beta\omega + \gamma\Omega + \phi(t)]
$$

with $M = M_0 + nt$, where n is the mean motion. Straightforward use of (9.26) introduces

$$
\frac{\partial}{\partial a} A(a,e,I) \begin{matrix}\sin \\ \cos\end{matrix} [\alpha M + \beta\omega + \gamma\Omega + \phi(t)]
$$

giving

$$
\frac{\partial A}{\partial a} \begin{matrix}\sin \\ \cos\end{matrix} [\alpha M + \beta\omega + \gamma\Omega + \phi(t)] + A \begin{matrix}\cos \\ \sin\end{matrix} [\alpha M + \beta\omega + \gamma\Omega + \phi(t)] \alpha \frac{\partial n}{\partial a} t
$$

since n^2a^3 is a constant. The occurrence of t outside a trigonometric argument leads to terms that are not periodic.

If we consider all occurrences of a in coefficients of trigonometric terms and all occurrences of n in the trigonometric argument, then the differential equation for M becomes

$$
M = 2\left(\frac{a}{\mu}\right)^{1/2} \left\{ \left.\frac{\partial \mathcal{H}}{\partial a}\right|_{n=\text{const}} + \frac{\partial \mathcal{H}}{\partial M}\frac{dM}{dn}\frac{dn}{da} \right\} + \frac{1-e^2}{(\mu a)^{1/2}e}\frac{\partial \mathcal{H}}{\partial e}
$$

Now

$$
\frac{da}{dt} = -2\left(\frac{a}{\mu}\right)^{1/2}\frac{\partial \mathcal{H}}{\partial M}
$$

and

$$
\frac{dM}{dn} = t
$$

giving

$$
\begin{aligned}
\frac{\partial \mathcal{H}}{\partial a} &= \frac{\mu}{2a} - \left.\frac{\partial R}{\partial a}\right|_{n=\text{const}} \\
\frac{\partial \mathcal{H}}{\partial e} &= -\frac{\partial R}{\partial e} \\
\frac{\partial \mathcal{H}}{\partial M} &= -\frac{\partial R}{\partial M}
\end{aligned}
$$

that is,

$$
M = n - t\frac{dn}{dt} - 2\left(\frac{a}{\mu}\right)^{1/2}\left.\frac{\partial R}{\partial a}\right|_{n=\text{const}} - \frac{1-e^2}{(\mu a)^{1/2}e}\frac{\partial R}{\partial e}
$$

where $n = (\mu)^{1/2}/a^{3/2}$ and is not constant.

With the previously described separation of a and n, we can write the Lagrange planetary equations (LPE) in their usual form.

$$
\frac{da}{dt} = \frac{2}{na}\frac{\partial R}{\partial M}
$$

$$
\frac{de}{dt} = \frac{1-e^2}{na^2e}\frac{\partial R}{\partial M} - \frac{(1-e^2)^{1/2}}{na^2e}\frac{\partial R}{\partial \omega}
$$

$$
\frac{d\omega}{dt} = -\frac{\cos I}{na^2(1-e^2)^{1/2}\sin I}\frac{\partial R}{\partial I} - \frac{(1-e^2)^{1/2}}{na^2e}\frac{\partial R}{\partial e}
$$

$$\frac{dI}{dt}=\frac{\cos I}{na^2(1-e^2)^{1/2}\sin I}\frac{\partial R}{\partial \omega}-\frac{1}{na^2(1-e^2)^{1/2}\sin I}\frac{\partial R}{\partial \Omega}$$

$$\frac{d\Omega}{dt}=\frac{1}{na^2(1-e^2)^{1/2}\sin I}\frac{\partial R}{\partial I}$$

$$\frac{dM}{dt}=n-\frac{(1-e^2)^{1/2}}{na^2e}\frac{\partial R}{\partial e}-\frac{2}{na}\frac{\partial R}{\partial a}$$

$$n^2a^3=\mu \tag{9.28}$$

Kepler elements are used extensively. They have the advantage over Cartesian coordinates in that five of the elements are constant for two-body motion and the sixth (M) increases linearly with time. In addition, each element has a geometrical interpretation. However, any five constants could be chosen, as long as they lead to a unique calculation of position and velocity.

As $e\to 0$, the element ω ceases to have any geometrical meaning. Since the position of the satellite depends on $v+\omega$, we can consider the new variables

$$\begin{array}{ll}\lambda=M+\tilde{\omega} & e=e\\ \tilde{\omega}=\omega+\Omega & \Omega=\Omega\\ a=a & I=I\end{array} \tag{9.29}$$

with the Poisson brackets

$$[a,\lambda]=-[\lambda,a]=\frac{2}{na}$$

$$[\lambda,e]=-[e,\lambda]=\frac{(1-e^2)^{1/2}[1-(1-e^2)^{1/2}]}{na^2e}$$

$$[\lambda,I]=-[I,\lambda]=\frac{\tan(I/2)}{na^2(1-e^2)^{1/2}}$$

$$[e,\tilde{\omega}]=-[\tilde{\omega},e]=-\frac{(1-e^2)^{1/2}}{na^2e} \tag{9.30}$$

$$[\Omega,I]=-[I,\Omega]=\frac{1}{na^2(1-e^2)^{1/2}\sin I}$$

$$[I,\tilde{\omega}]=-[\tilde{\omega},I]=[I,\lambda]$$

It has also been found useful to eliminate e and $\tilde{\omega}$ by use of the variables

$$\begin{array}{ll}h=e\sin\tilde{\omega} & a=a\\ k=e\cos\tilde{\omega} & \Omega=\Omega\\ \lambda=\lambda & I=I\end{array} \tag{9.31}$$

These variables have the following Poisson brackets, written for convenience in terms of e:

$$[h,k]=-[k,h]=\frac{(1-e^2)^{1/2}}{na^2}$$

$$[h,\lambda]=-[\lambda,h]=\frac{-h(1-e^2)^{1/2}}{na^2[1+(1-e^2)^{1/2}]}$$

$$[h,I]=-[I,h]=\frac{k\tan(I/2)}{na^2(1-e^2)^{1/2}} \tag{9.32}$$

$$[k,\lambda]=-[\lambda,k]=\frac{-k(1-e^2)^{1/2}}{na^2[1+(1-e^2)^{1/2}]}$$

$$[k,I]=-[I,k]=\frac{-h\tan(I/2)}{na^2(1-e^2)^{1/2}}$$

with $[a,\lambda]$, $[\lambda,I]$, $[\Omega,I]$ as given in (9.30). Of course, these equations hold for all eccentricities.

A further modification would be to use the variables

$$\begin{array}{ll}p=\tan I\sin\Omega & k=k\\ q=\tan I\cos\Omega & \lambda=\lambda\\ h=h & a=a\end{array} \tag{9.33}$$

These have the following Poisson brackets, written for convenience in terms of e and I:

$$[p,q]=-[q,p]=\frac{\cos I}{na^2(1-e^2)^{1/2}}$$

$$\begin{aligned}[p,\lambda]=-[\lambda,p]&=\frac{1}{k}[p,h]=-\frac{1}{k}[h,p]\\ &=-\frac{1}{h}[p,k]=\frac{1}{h}[k,p]\\ &=-\frac{p\cos I}{2na^2(1-e^2)^{1/2}\cos^2(I/2)}\end{aligned} \tag{9.34}$$

$$\begin{aligned}[q,\lambda]=-[\lambda,q]&=\frac{1}{k}[q,h]=-\frac{1}{k}[h,q]\\ &=-\frac{1}{h}[q,k]=\frac{1}{h}[k,q]\\ &=-\frac{q\cos I}{2na^2(1-e^2)^{1/2}\cos^2(I/2)}\end{aligned}$$

$$[q, p] = -\frac{\cos I}{na^2(1-e^2)^{1/2}}$$

where $[h, k]$, $[h, \lambda]$, $[k, \lambda]$ are the same as (9.32) and where we take $[a, \lambda]$ from (9.30). The variables p and q should not be confused with generalized coordinates. These expressions are valid for all e and I but are especially valuable for small e and I—for example, in the planetary theory.

It is possible to construct other combinations. For example, one could use

$$\begin{array}{ll} \chi = M + \omega & a = a \\ \xi = e \sin \omega & \Omega = \Omega \\ \eta = e \cos \omega & I = I \end{array} \tag{9.35}$$

We now turn to sets of canonical variables that have the simplest form of Poisson brackets. We have observed that Cartesian coordinates are canonical. We give two other sets, the Delaunay and the Hill.

The combination of coordinates and conjugate momenta for Delaunay variables are the following:

Coordinates	*Momenta*
$l = M$	$L = (\mu a)^{1/2}$
$g = \omega$	$G = [\mu a(1-e^2)]^{1/2}$
$h = \Omega$	$H = [\mu a(1-e^2)]^{1/2} \cos I$

(9.36)

Now, l, g, h are new labels for three familiar Kepler elements, in order to provide a symmetric notation. We see that G is the angular-momentum constant N in the two-body motion given by (9.10) and that H is the projection of the angular momentum on the z axis.

Another set of canonical variables introduced into satellite theory by Izsak (1962) and used to great advantage by Aksnes (1970) consists of the Hill variables, as follows:

Coordinates	*Momenta*
$r = a(1 - e \sin E)$	$\dot{r} = (e/r) L \sin E$
$u = v + \omega$	$G = G$
$h = \Omega$	$H = H$

(9.37)

These are natural coordinates, with the important advantage that there is no singularity for small eccentricity—in contrast to the situation with Delaunay variables, which complicates their use.

Finally, we consider the equations of LPE type, which contain the forces explicitly. Consider the forces with components S, T, and W, which are, respectively, along the radius vector, in the orbital plane normal to the radius vector (along track), and perpendicular to the orbital plane (cross track). The direction cosines of satellite position are

$$\hat{l}_S = R_3(-\Omega) R_1(-I) R_3(-u) \begin{bmatrix} 1 \\ 0 \\ 0 \end{bmatrix} \tag{9.38}$$

We can define the direction cosines along track and cross track with

$$\hat{l}_T = R_3(-\Omega) R_1(-I) \times R_3(-\Omega) \begin{bmatrix} \dot{x} \\ \dot{y} \\ 0 \end{bmatrix} \Big/ (\dot{x}^2 + \dot{y}^2)^{1/2} \tag{9.39}$$

$$\hat{l}_W = \hat{l}_T \times \hat{l}_S \tag{9.40}$$

where $\dot{x}$, $\dot{y}$ are obtained from (9.16). If we let $\mathcal{E}_i$ be any variable, then

$$\frac{\partial R}{\partial \mathcal{E}_i} = \frac{\partial R}{\partial x}\frac{\partial x}{\partial \mathcal{E}_i} + \frac{\partial R}{\partial y}\frac{\partial y}{\partial \mathcal{E}_i} + \frac{\partial R}{\partial z}\frac{\partial z}{\partial \mathcal{E}_i}$$

But $\frac{\partial R}{\partial x}, \frac{\partial R}{\partial y}, \frac{\partial R}{\partial z}$ are the components of force along x, y, z given by

$$\begin{bmatrix} \frac{\partial R}{\partial x} \\ \frac{\partial R}{\partial y} \\ \frac{\partial R}{\partial z} \end{bmatrix} = \begin{bmatrix} & & \\ \hat{e}_S & \hat{e}_T & \hat{e}_W \\ & & \end{bmatrix} \begin{bmatrix} S \\ T \\ W \end{bmatrix} \tag{9.41}$$

With expressions $\bar{x} = \bar{x}(\mathcal{E}_i)$, say, (9.17), we can form $\partial x/\partial \mathcal{E}$ and substitute the result in

(9.23). This could be done for any set of variables. We give here the results for the Kepler elements, since they are widely used. We have

$$\frac{da}{dt}=\frac{2}{n(1-e^2)^{1/2}}\left[S\,e\sin v+T\frac{p}{r}\right]$$

$$\frac{de}{dt}=\frac{(1-e^2)^{1/2}}{na}\times\left\{S\sin v+T\left[\cos v+\frac{1}{e}\left(1-\frac{r}{a}\right)\right]\right\}$$

$$\frac{dI}{dt}=\frac{1}{na(1-e^2)^{1/2}}W\frac{r}{a}\cos\,(v+\omega)$$

$$\frac{d\Omega}{dt}=\frac{1}{na(1-e^2)^{1/2}\sin I}W\frac{r}{a}\sin\,(v+\omega)$$

$$\frac{d\omega}{dt}=-\cos I\frac{d\Omega}{dt}+\frac{1}{na}\frac{(1-e^2)^{1/2}}{e}\times\left[-S\cos v+T\left(1+\frac{r}{p}\right)\sin v\right]$$

$$\frac{dM}{dt}=n-\frac{2}{na}S\frac{r}{a}-(1-e^2)^{1/2}\left(\frac{d\omega}{dt}+\cos I\frac{d\Omega}{dt}\right)$$

$$p=a(1-e^2) \qquad (9.42)$$

These expressions are known as the LPE in Gaussian form. They have been calculated by using a force derived from a potential. However, the equations would have the same form for any force, and they can be so used. These expressions are especially useful in numerical integration and with nonconservative forces such as air drag and radiation pressure.

9.4.1.4 Spherical Harmonics

Legendre functions and associated Legendre functions arise naturally in the solution of Laplace's equations in spherical coordinates. They also constitute a set of orthogonal base functions for mapping arbitrary functions in spherical coordinates. In dynamical astronomy and satellite geodesy, spherical coordinates are the natural ones. We find that much of the subsequent analysis is facilitated by use of these functions, and we give here a short summary of their properties. Hobson (1955) is an excellent reference for mathematical proofs, and texts on mathematical physics (e.g., Jeffreys and Jeffreys, 1956; Morse and Feshback, 1953) provide many useful formulas. Legendre functions are extensively used in quantum mechanics, and its literature is recommended for the transformation properties.

For numerical computation, an expansion of P_{lm} in power series in z can be used. This expression can have large roundoff errors, and direct use may require multiple-precision computation. One alternative device is to employ the recurrence relationship

$$P_{l,m+2}(z)+2(m+1)\,[z/(1-z^2)^{1/2}]\,P_{l,m+1}(z)+(l-m)\,(l+m+1)P_{lm}(z)=0 \qquad (9.43)$$

where $z=\sin\phi$, and use

$$P_{ll}(z)=[(2l)!/2^l l!]\cos^l\phi$$
$$P_{l,l-1}(z)=z\,P_{ll}(z)$$

For each degree l, we compute all the $P_{lm}(z)$ from (9.43). In general, we require all the $P_{lm}(z)$, and this device will be efficient as well as accurate. We will need to find the expression for $P_{lm}(z)\,e^{im\lambda}$ in a coordinate system rotated by the Euler angles I, Ω, ω. The results given here are taken from Jeffreys (1965). We can write

$$\bar{P}_{lm}(\sin\phi)\;e^{im\lambda}=\sum_{s=-l}^{l}(i)^{s-m}E_{lms}(I)\,\bar{P}_{ls}(\sin\phi')\,e^{i[s(\lambda'+\omega')+m\Omega]} \qquad (9.44)$$

with

$$E_{lms}(I)=N_{lms}\sum_{r=\max\left|\begin{smallmatrix}0\\-(m+s)\end{smallmatrix}\right.}^{\min\left|\begin{smallmatrix}l-s\\l-m\end{smallmatrix}\right.}(-1)^{l-m-r}\binom{l+m}{m+s+r}\binom{l+m}{r}\gamma^{2r+m+s}\sigma^{2(l-r)-m-s} \qquad (9.45)$$

where

$$\gamma = \cos\ (I/2)$$

$$\sigma = \sin\ (I/2)$$

$$N^2_{lms} = \frac{(l-s)\,!\,(l+s)\,!\,\epsilon_m}{(l-m)\,!\,(l+m)\,!\,\epsilon_s}$$

Further, if $\phi' = 0$, we can write this in a more compact form as

$$\bar{P}_{lm}(\sin\phi)\, e^{im\lambda} = \sum_{p=0}^{l} (i)^{l-m} D_{lmp}(I)\, e^{i[(l-2p)(\lambda'+\omega')+m\Omega]} \tag{9.46}$$

for $l \geq m \geq l$, where

$$D_{lmp}(I) = \frac{1}{N_{lm}} \frac{(l+m)\,!}{2^l l!} \sum_{r=\max\left|\begin{smallmatrix} 0 \\ 2p-l-m \end{smallmatrix}\right.}^{\min\left|\begin{smallmatrix} l-m \\ 2p \end{smallmatrix}\right.} (-1)^{l-m-r} \binom{l}{p} \binom{2p}{r} \binom{2l-2p}{l-m-r} \gamma^{l+m+2r-2p} \sigma^{l-m-2r+2p} \tag{9.47}$$

where

$$r = \cos\ (I/2)$$

$$\sigma = \sin\ (I/2)$$

$$N^2_{lm} = \frac{(l+m)\,!}{\epsilon_m (2l+1)\,(l-m)\,!}$$

We note that

$$\bar{P}_{l,m}(z) = (-1)^m \bar{P}_{l,|m|} z \tag{9.48}$$

If we make the association $v = \lambda$, we see that (9.46) is a natural expression of spherical harmonics in Kepler elements. The development has been carried out by Kaula (1966b) on other considerations for conventional harmonics. The $D_{lmp}(I)$ here are related to the inclination functions of Kaula by

$$D_{lmp}(I) = [(-1)^{\{(l-m)/2\}}/N_{lm}] F_{lmp}(I) \tag{9.49}$$

The two developments are equivalent. We give here the expressions for calculating $F_{lmp}(I)$ as derived by Kaula, since they are extensively used:

$$F_{lmp}(I) = \sum_{t=0}^{\min\left|\begin{smallmatrix} \{(l-m)/2\} \\ p \end{smallmatrix}\right.} \frac{(2l-2t)\,!}{t!\,(l-t)\,!\,(l-m-2t)\,!\,2^{2l-2t}} S^{l-m-2t} \times \sum_{s=0}^{m} \binom{m}{s} C^s \sum_{c} \binom{l-m-2t+s}{c} \binom{m-s}{p-t-c} (-1)^{c-k} \tag{9.50}$$

where $S = \sin I$ and $C = \cos I$. Kaula gives tables of $F_{lmp}(I)$ through 4,4,4. Since (9.50) has three summations, whereas (9.47) has only one, the latter is somewhat more economical for computing numerical values.

9.4.1.5 Elliptic Expansions

In section 9.4.1.2, we found the relation between the mean anomaly M, the eccentric anomaly E, and the true anomaly v. Whereas E and v have geometric significance and are related by

$$\tan\ (v/2) = [(1+e)/(1-e)]^{1/2} \tan\ (E/2) \tag{9.51}$$

the mean anomaly has dynamical significance, increasing proportionally with time; that is,

$$M = M_0 + nt \tag{9.52}$$

The connection between M and E and hence v is made through Kepler's equation (9.14):

$$M = n(t-t_0) = E - e \sin E \tag{9.53}$$

Equations (9.51) to (9.53) are sufficient for all computations in two-body motion. Equation (9.53) is transcendental for E in terms of M and can easily be solved numerically by iteration. The obvious iteration is

$$E_0 = M$$

$$E_{n+1} = M + e \sin E_n \tag{9.54}$$

which converges very quicky for small eccentricity. Typical geodetic satellites have $e > 0.1$, for which (9.54) is quite sufficient. There are numerical methods to speed con-

vergence, and in cases where efficiency is important, methods like Newton's have been successful.

In developing complete solutions by use of, for example, LPE, we are faced with integrals of the following forms:

$$\int f(v)\,dt \qquad \int f(E)\,dt \tag{9.55}$$

It is therefore useful to be able to express functions of v and E in terms of t or M. These expressions generally involve infinite series in powers of eccentricity.

A particularly useful device for transforming (9.55) is to use

$$dv=(a/r)^2(1-e^2)^{1/2}dM=(a/r)^2(1-e^2)^{1/2}ndt \tag{9.56}$$

$$dE=(a/r)\,dM=(a/r)\,ndt$$

(See Gaposchkin, 1973.)

By use of (9.56), integrals in t can be converted to integrals in v or E. Where necessary, a/r can be expressed in v or E by (9.9), repeated here for convenience:

$$a/r=(1+e\cos v)/a(1-e^2)=1/(1-e\cos E) \tag{9.57}$$

Transformation (9.56) is useful when M is absent from the integral. Generally, this is not the case, and we must explicitly make the conversion. More general expressions are used, complete developments being carried out on computers either numerically or algebraically. In the following, we develop some of these formulas.

If, following many authors (e.g., Plummer, 1918), we define the variable $\beta(e)$ by

$$(1+\beta)/(1-\beta)=[(1+e)/(1-e)]^{1/2} \tag{9.58}$$

we have

$$e=2\beta/(1+\beta^2) \tag{9.59}$$

$$\beta=e/[1+(1-e^2)^{1/2}] \tag{9.60}$$

We see that $\beta\approx e/2$.

By using the Bessel function $J_n(x)$, we can write

$$E-M=2\sum_{s=1}^{\infty}\frac{1}{s}J_s(se)\sin sM \tag{9.61}$$

$$v-M=2\sum_{s=1}^{\infty}\frac{1}{s}\Big\{J_s(se)+\sum_{p=1}^{\infty}\beta^p[J_{s-p}(se)+J_{s+p}(se)]\Big\}\sin sM \tag{9.62}$$

The first few terms of (9.61) and (9.62) are

$$E-M=\Big(e-\frac{1}{8}e^3+\ldots\Big)\sin M+\Big(\frac{e^2}{2}+\ldots\Big)\sin 2M+\frac{3}{8}\Big(e^3+\ldots\Big)\sin 3M \tag{9.63}$$

$$v-M=\Big(2e-\frac{1}{4}e^3+\qquad\Big)\sin M+\Big(\frac{5}{4}e^2+\ldots\Big)\sin 2M+\Big(\frac{13}{12}e^3+\ldots\Big)\sin 3M \tag{9.64}$$

Brouwer and Clemence (1961) give these expressions to seventh order in eccentricity.

We have need of similar expressions when v or E occurs in the argument of a trigonometric function. There are several methods to obtain such expressions. We give two here. The first is due to Kaula (1966b) and taken from Tisserand (1960). Kaula investigates the conversion of

$$\Big(\frac{a}{r}\Big)^{l+1}\begin{pmatrix}\cos\\ \sin\end{pmatrix}[(l-2p)v+\psi]$$

where ψ does not depend on v, and gives it in the form

$$\Big(\frac{a}{r}\Big)^{l+1}\begin{pmatrix}\cos\\ \sin\end{pmatrix}[(l-2p)v+\psi]=\sum_{q=-\infty}^{\infty}G_{lpq}(e)\begin{pmatrix}\cos\\ \sin\end{pmatrix}[(l-2p+q)m+\psi] \tag{9.65}$$

This form is natural for the computation of perturbations due to tesseral harmonics. The

formulas have two forms. The first is for "long-term" terms, i.e., those terms in (9.65) independent of M—that is, $q=2p-l$. These can be obtained by integrating (9.65) with respect to M from 0 to 2π. Using the transformation (9.56), we obtain

$$G_{lp,\,2p-l}(e)=\frac{1}{(1-e^2)^{l-(1/2)}}\sum_{d=0}^{p'-1}\binom{l-1}{2d+l-2p'}\binom{2d+l-2p'}{d}\left(\frac{e}{2}\right)^{2d+l-2p'} \tag{9.66}$$

in which

$$p'=l-p \quad \text{for } p\geq l/2$$
$$p'=p \quad \text{for } p\leq l/2$$

For the short-period terms, $l-2p+q\neq 0$, we have

$$G_{lpq}(e)=(-1)^{|q|}(1+\beta^2)^{l}\beta^{|q|}\sum_{k=0}^{\infty}P_{lpqk}Q_{lpqk}\beta^{2k} \tag{9.67}$$

where

$$\beta=e/[1+(1-e^2)^{1/2}]$$

$$P_{lpqk}=\sum_{r=0}^{h}\binom{2p'-2l}{h-r}\frac{(-1)^r}{r!}\left[\frac{(l-2p'+q')\,e}{2\beta}\right]^r \tag{9.68}$$

$$h=k+q \quad \text{for } q'>0$$
$$h=k \quad \text{for } q'<0$$

and

$$Q_{lpqk}=\sum_{r=0}^{h}\binom{-2p'}{h-r}\frac{1}{r!}\left[\frac{(l-2p'+q')\,e}{2\beta}\right]^r \tag{9.69}$$

where

$$h=k \quad \text{for } q'>0$$
$$h=k-q' \quad \text{for } q<0$$
$$\left.\begin{aligned}p'&=p\\q'&=q\end{aligned}\right\} \text{ for } p\leq l/2$$
$$\left.\begin{aligned}p'&=l-p\\q'&=-q\end{aligned}\right\} \text{ for } p>l/2$$

The transformation (9.65) is a doubly infinite sum over q. However, it is important to note that

$$G_{lpq}(e)\propto\beta^{|q|}\approx(e/2)^{|q|}$$

We can choose a desired accuracy and select a finite number of terms. For small e, the number can be very limited. This selection can be made numerically or analytically.

A second and more general method for this development, given in Plummer (1918, p. 44), involves the Hansen coefficients X_q^{nm}, defined by

$$(r/a)^n e^{imv}=\sum_{q=-\infty}^{\infty}X_q^{nm}(e)\,e^{iqM} \tag{9.70}$$

where the $X_q^{nm}(e)$ are polynomials in eccentricity. We have

$$X_q^{mn}(e)=(1+\beta^2)^{-(n+1)}\sum_p J_p(qe)\,X_{qp}^{mn} \tag{9.71}$$

and

$$\left.\begin{aligned}
X_{qp}^{nm}&=(-\beta)^{q-p-m}\binom{n+1-m}{q-p-m}F(q-p-n-1,-m-n-1,q-p-m+1,\beta^2) && \text{for } q-p-m>0\\
X_{qp}^{nm}&=(-\beta)^{-q+p+m}\binom{n+1+m}{-q+p+m}F(-q+p-n-1,m-n-1,-q+p+m+1,\beta^2) && \text{for } q-p-m<0\\
X_{qp}^{nm}&=F(m-n-1,-m-n-1,1,\beta^2) && \text{for } q-p-m=0
\end{aligned}\right\} \tag{9.72}$$

We have the Bessel function

$$J_n(z) = (z/2)^n \sum_{k=0}^{\infty} \left(-\frac{1}{4}z^2\right)^k \Big/ [k!(n+k)!] \tag{9.73}$$

and the hypergeometric function

$$F(a,b,c,z) = \sum_{n=0}^{\infty} [(a)_n (b)_n / (c)_n] (z^n/n!) \tag{9.74}$$

where Pochhammer's symbol is

$$\left.\begin{aligned} (a)_n &= a(a+1)(a+2)\cdots(a+n-1) \\ (a)_0 &= 1 \end{aligned}\right\} \tag{9.75}$$

We see by comparing coefficients that

$$G_{lpq}(e) = X^{-(l+1),l-2p}_{l-2p+q}(e) \tag{9.76}$$

However, formulas (9.67) to (9.69) are valid only for $l+1>0$, whereas (9.70) to (9.76) are valid for any $n=-(l+1)$. Both forms have been used. With recent developments in the computing of elementary functions, the latter seems more economical for numerical calculation. For use with computer algebra, one would prefer to obtain polynomials in eccentricity with rational fractions as coefficients. This has been done through a recurrence relation originated by Andoyer (1903) and introduced into satellite work by Izsak *et al.* (1964). The method starts with the observation that

$$(r/a)^{\pm n} e^{i(\pm mv)} = X^{\pm n,\pm m} = (X^{\pm 1,0})^n (X^{0,\pm 1})^m$$

We compute $X^{\pm 1,0}$, $X^{0,\pm 1}$ by any method, and all other combinations are determined by simple polynomial multiplication. Cherniack (1972) gives these polynomials to 12th order in e. Kaula (1966b) gives a table through 4,4,2. Cayley (1961) gives more extensive tables.

9.4.1.6 First-Order Perturbations Due to the Potential

We have seen that the potential can be expressed in terms of associated Legendre functions (sec. 9.4.1.4) and a set of numerical constants,

$$\mathcal{U} = \mathcal{R}e\left(\frac{GM}{r}\right) \times \left[1 + \sum_{l=2}^{\infty}\sum_{m=0}^{l} \overline{\mathcal{C}}_{lm}\left(\frac{a_e}{r}\right)^l \bar{P}_{lm}(\sin\phi)\, e^{im\lambda}\right] \tag{9.77}$$

where ϕ, λ, r are the coordinates of a point in the terrestrial or Earth-fixed system. The terms $\overline{\mathcal{C}}_{1,0}$, $\overline{\mathcal{C}}_{1,1}$, $\overline{\mathcal{C}}_{2,1}$ are missing owing to the orientation and origin of the system chosen. In fact, the elastic Earth introduces the terms $\overline{\mathcal{C}}_{2,1}$, which will be discussed along with other questions relating to the Earth's elasticity in section 9.4.1.7. Selecting Kepler elements, we now use (9.77) in (9.28) for the disturbing function r, omitting, of course, GM/r.

The conversion of $R(r,\phi,\lambda)$ to $R(a,e,I,v,\omega, \Omega-\theta)$ is accomplished as follows. We express $R(r,\phi,\lambda)$ in the orbital system by rotating by $-\theta$. This introduces $\lambda-\theta$ in place of λ in (9.77). From the formula (9.46), we have

$$R = \mathcal{R}e\left(\frac{GM}{r}\right)\sum_{l=2}^{\infty}\sum_{m=0}^{l}\overline{\mathcal{C}}_{lm}\left(\frac{a_e}{r}\right)^l (i)^{l-m} \sum_{p=0}^{l} D_{lmp}(I)\, e^{i[(l-2p)(v+\omega)+m(\Omega-\theta)]} \tag{9.78}$$

where $i=\sqrt{-1}$ and $D_{lmp}(I)$ are polynomials in $\cos(I/2)$, $\sin(I/2)$. This is further converted to the mean anomaly with (9.67) or (9.70), giving

$$R = \mathcal{R}eGM\sum_{l=2}^{\infty}\sum_{m=0}^{l}\sum_{p=0}^{l}\sum_{q=-\infty}^{\infty}\left(\frac{1}{a}\right)\left(\frac{a_e}{a}\right)^l (i)^{l-m} D_{lmp}(I)\, G_{lpq}(e)\, e^{i\psi} \tag{9.79}$$

where

$$\psi = (l-2p)\omega + (l-2p+q)M + m(\Omega-\theta)$$

Equation (9.79) can also be written in terms of Hansen coefficients with (9.76).

The first-order secular rates can be determined by selecting terms in R independent of $\omega,\Omega,M,\vartheta$. These arise for $m=0$—that is, only zonal harmonics and $l-2p=q=0$. By use of algebra, we find secular terms only in ω, Ω, M.

A corollary is that the size a of the orbit, its shape e, and its orientation can have only periodic perturbations. We have shown it to first order only, but it is true for any order (Kozai, 1959c). We obtain for the first-order secular rates

$$\dot{\omega} = n(3\sqrt{5}/4)\,[\bar{C}_{2,0}/(1-e^2)^2]\,(a_e/a)^2\,(1-5\cos^2 I)$$

$$\dot{\Omega} = n(3\sqrt{5}/2)\,[\bar{C}_{2,0}/(1-e^2)^2]\,(a_e/a)^2\cos I$$

$$M = n\{1-(3\sqrt{5}/4)\,[\bar{C}_{2,0}/(1-e^2)^{3/2}]\,(a_e/a)^2(3\cos^2 I-1)\} \tag{9.80}$$

First-order periodic perturbations are easily obtained by assuming that a, e, I are relatively constant on the right-hand side of (9.28) and that ω, Ω, M, θ have linear rates; that is,

$$\begin{aligned} \omega &= \omega_0 + \dot{\omega}t \\ \Omega &= \Omega_0 + \dot{\Omega}t \\ M &= M_0 + nt \\ \theta &= \theta_0 + \dot{\theta}t \end{aligned} \tag{9.81}$$

The equations are integrated as a linear harmonic oscillator for those terms containing any of the variables in (9.81). In actual computation, we would use the values of $\dot{\omega}$, $\dot{\Omega}$, n, $\dot{\theta}$ derived from observations.

Letting $\mathcal{E}_i$ be a generic element, we have the following:

$$\Delta\mathcal{E}_i = \sum_{l=2}^{\infty}\sum_{m=0}^{l}\sum_{p=0}^{l}\sum_{q=-\infty}^{\infty}\Delta\mathcal{E}_{lmpq}$$

$$\Delta a_{lmpq} = \mathcal{R}e\frac{GMa_e^l(i)^{l-m}}{na^{l+2}}\frac{2}{\dot{\psi}_{lmpq}}D_{lmp}(I)\,G_{lpq}(e)\,(l-2p+q)\,\bar{C}_{lm}e^{i\psi_{lmpq}}$$

$$\Delta e_{lmpq} = \mathcal{R}e\frac{GMa_e^l(i)^{l-m}}{na^{l+3}e\dot{\psi}_{lmpq}}D_{lmp}G_{lpq}(1-e^2)^{1/2}[(1-e^2)^{1/2}(l-2p+q)-(l-2p)]\,\bar{C}_{lm}e^{i\psi_{lmpq}}$$

$$\Delta I_{lmpq} = \mathcal{R}e\frac{GMa_e^l(i)^{l-m}}{na^{l+3}(1-e^2)^{1/2}\dot{\psi}_{lmpq}}D_{lmp}G_{lpq}[(l-2p)\cos I-m]\,\bar{C}_{lm}e^{i\psi_{lmpq}} \tag{9.82}$$

$$\Delta\omega_{lmpq} = \mathcal{R}e\frac{GMa_e^l(i)^{l-m-1}}{na^{l+3}(1-e^2)^{1/2}\sin I\,\dot{\psi}_{lmpq}}\left[\frac{(1-e^2)^{1/2}}{e}D_{lmp}\frac{\partial G_{lm}}{\partial e}\frac{\cos I}{\sin I}\frac{G_{lmp}}{(1-e^2)^{1/2}}\frac{\partial D_{lmp}}{\partial I}\right]\bar{C}_{lm}e^{i\psi_{lmpq}}$$

$$\Delta\Omega_{lmpq} = \mathcal{R}e\frac{GMa_e^l(i)^{l-m-1}G_{lpq}}{na^{l+3}(1-e^2)^{1/2}\sin I\,\dot{\psi}_{lmpq}}\frac{\partial D_{lmp}}{\partial I}\bar{C}_{lm}e^{i\psi_{lmpq}}$$

$$\Delta M_{lmpq} = \mathcal{R}e\frac{GMa_e^l(i)^{l-m-1}}{na^{l+3}\dot{\psi}_{lmpq}}\left[-\frac{(1-e^2)^{1/2}}{e}\frac{\partial G_{lpq}}{\partial e}+2(l+1)\,G_{lpq}\right]D_{lmp}\bar{C}_{lm}e^{i\psi_{lmpq}}$$

where

$$\dot{\psi}_{lmpq} = (l-2p)\,\dot{\omega}+(l-2p+q)\,n+m(\dot{\Omega}-\dot{\theta})$$

After the substitution of (9.44), these formulas agree with Kaula (1966b).

The final calculation necessary is to determine $\int n\,dt$ for the perturbation in M according to (9.28). We see that for $l-2p+q\neq 0$, we have a perturbation in a from the first equation of (9.82). From $n^2a^3=GM$, we have

$$\Delta n_{lmpq} = -(3/2)\,(n/a)\,\Delta a_{lmpq} \tag{9.83}$$

Therefore, to the last equation of (9.82), we must add the term

$$\begin{aligned}\Delta M_{lmpq} &= \int \Delta n_{lmpq}\,dt \\ &= \mathcal{R}e\left[\frac{-3GMa_e^l(i)^{l-m-1}}{a^{l+3}(\dot{\psi}_{lmpq})^2}\right] \\ &\quad\times D_{lmp}G_{lpq}(l-2p+q)\,\bar{C}_{lm}e^{i\psi_{lmpq}}\end{aligned} \tag{9.84}$$

We can combine both parts and obtain

$$\begin{aligned}\Delta M_{lmpq} = \mathcal{R}e\,\frac{GMa_e^lD_{lmp}}{a^{l+3}}\Bigg[&-\frac{(1-e^2)^{1/2}}{ne\dot{\psi}_{lmpq}}\frac{\partial G_{lpq}}{\partial e} \\ &+\frac{2(l+1)}{n\dot{\psi}_{lmpq}}G_{lpq}-\frac{3G_{lpq}(l-2p+q)}{(\dot{\psi}_{lmpq})^2}\Bigg] \\ &\times i^{l-m-1}\bar{C}_{lm}e^{i\psi_{lmpq}}\end{aligned}$$

This completes the first-order theory. If we take as our goal an accuracy of 10^{-7}, then it is quite satisfactory unless $|\bar{C}_{lm}|$ is larger than 10^{-4} or $\dot{\psi}_{lmpq}$ is very small. From observations, we find that $\bar{C}_{2,0} \approx 10^{-3}$ and that all the remaining $|\bar{C}_{lm}| \approx 10^{-6}$. Therefore, this theory is inadequate for the effects of $\bar{C}_{2,0} = -J_2/\sqrt{5}$, and so other methods are used, as described in section 9.4.1.8. The discussion of small ψ_{lmpq} goes by the name of resonance, which will be dealt with shortly.

If we consider the rate

$$\dot{\psi}_{lmpq} = (l-2p)\,\dot{\omega} + (l-2p+q)\,n + m(\dot{\Omega}-\dot{\theta}) \qquad (9.85)$$

and $\dot{\omega}$, $\dot{\Omega}$ from (9.80), we see that $(\dot{\omega}, \dot{\Omega}) \propto 10^{-3}\, n$. The rotation rate of the Earth, $\dot{\theta}$, is once per day, and n for geodetic satellites is 12 ± 2 revolutions per day. Therefore, the period of a perturbation is primarily determined by

$$2\pi/P = (l-2p+q)\,n - m\dot{\theta} \qquad (9.86)$$

We see that in general the largest perturbations—that is, the smallest divisors—are for $l-2p+q=0$, and we have periodic terms with frequency $m\dot{\theta}$. Resonance occurs with the near-commensurability of $(l-2p+q)n$ and $m\dot{\theta}$. That means that when the mean motion of the satellite is approximately equal to the order of the tesseral harmonics, we can have arbitrary long periods and large amplitudes. When analyzing terms with small divisors, we must include the effects of $\dot{\omega}$ and $\dot{\Omega}$ to obtain meaningful results. Resonance has yet to be treated completely. For a single resonant term, a solution in terms of elliptic functions can be obtained, and these have played an important role in the study of synchronous satellites. For close-Earth satellites, the problems are more difficult, since the satellite will be resonant with the whole set of harmonics of order m. In addition, if the drag changes n appreciably during one resonant oscillation, the theory is not even approximately correct. Fortunately, geodetic satellites have had relatively short resonant periods (≈ 10 days), and the linear theory seems to work well enough.

A second class of long-period perturbations is due to the zonal harmonics ($m=0$, $l-2p+q=0$). These have the principal period of the rotation of perigee, as given by (9.80). The period of these terms can go to zero for the so-called critical inclination—that is, when $(1-5\cos^2 I)=0$ or $I \cong 63^\circ.4$. The theory given here is not valid near that region of inclination. It has variously been viewed as a resonant phenomenon and as a physically important effect. Izsak (1963*c*), Garfinkle (1963), and others have discussed this question.

Table 9.24 gives here for a typical geodetic satellite a short table of amplitudes of the perturbations due to the Earth's field.

9.4.1.7 Third-Body Perturbations, Elasticity, and Tides

There is an extensive literature on third-body perturbations. The principal effect of the Moon is a perturbation ≈ 120 m, and that of the Sun, about 6 times that amount. Continuous analysis has been necessary because of three factors:

(1) The Moon's motion is itself complicated, making integration of the equations of motion difficult. The inclination of the Moon's orbit is not constant in the adopted orbital system. There is a rich spectrum of periodic terms in the lunar longitude.

(2) The Moon and Sun deform the elastic Earth. This variation in mass distribution has significant orbital effects. Improved geophysical information is needed in order to account for them.

(3) The Sun and Moon cause precession and nutation. These motions are the reason for our adopting a quasi-inertial reference system. We must include in the theory terms to compensate for the noninertialness. These terms can be viewed as an indirect effect of the lunisolar perturbations.

There are two avenues to be taken. The first is to eliminate periodic perturbations with periods commensurate with the length

of orbit we wish to determine—that is, periods <20 days. We take an analytical approach by assuming linear variation of the orbital elements of the disturbing body. The second avenue is for long-period analysis, in which we obtain averaged equations—that is, ones not depending on the mean anomaly of the satellite. These can be integrated numerically and are used for study of all long-period effects.

In the following, we develop the disturbing function for the Moon; that for the Sun has the same form. We assume that the semimajor axis of the satellite is small with respect to that of the Sun or the Moon. This disturbing function can be averaged and then numerically integrated with (9.28), or if a, e, I' of the Moon are assumed constant, it can be integrated approximately.

We introduce the elastic deformation of the Earth at this point, as it is most easily incorporated into the theory from the beginning. Following A. E. H. Love (Munk and MacDonald, 1960, ch. 5), the additional potential $\mathcal{U}_n$ due to the deformation from a potential of degree n is

$$\mathcal{U}_n' = k_n (a_e/r)^{2n+1} \mathcal{U}_n \tag{9.87}$$

where k_n are numerical constants depending on the elastic properties of the Earth. The total potential acting on the satellite is then

$$[1 + k_n (a_e/r)^{2n+1}] \mathcal{U}_n \tag{9.88}$$

Now the direct potential acting on the satellite due to the Moon (or Sun) can be written

$$\mathcal{U} = GM' \left[(1/\Delta) - (\bar{r} \cdot \bar{r}'/|r'|^3) \right] \tag{9.89}$$

where $\bar{r}$ and $\bar{r}'$ are the positions of the satellite and of the disturbing body, respectively, M' is the mass of the disturbing body, and Δ is the distance between r and r'. As is well known, we can write $1/\Delta$ in spherical harmonics. To calculate orbital perturbations, we use the gradient of $\mathcal{U}$ with respect to the satellite position, and we can drop the $l=0$ term in $1/\Delta$. The $l=1$ term just cancels $\bar{r} \cdot \bar{r}'/|r'|^3$. Thus, we have for the third-body potential, including the tidal deformation,

$$\mathcal{U} = GM' \mathcal{R}e \sum_{l=2}^{\infty} \sum_{m=0}^{l} \frac{1}{2l+1} \left[\frac{r^l}{r'^{l+1}} + \frac{k_l a_e^{2l+1}}{(r'r)^{l+1}} \right] \bar{P}_{lm} (\sin \phi) \, \bar{P}_{lm} (\sin \phi') \, e^{im(\lambda - \lambda')} \tag{9.90}$$

To include the effects of tidal phase lag, we introduce a fictitious Moon lagging the real Moon by Δt and separate (9.90) into two parts. In this case, the disturbing potential cannot be written in such a compact form. We proceed by assuming $\Delta t = 0$, the revision of the theory being straightforward if the effect of lag is desired.

By introducing the rotation operation (9.45) and Hansen coefficients (9.70), we can write the disturbing function as

$$R = \mathcal{R}e \sum_{l=2}^{\infty} \sum_{m=0}^{l} \sum_{p=0}^{l} \sum_{p'=0}^{l} \sum_{q=-\infty}^{\infty} \sum_{q'=-\infty}^{\infty} R_{lmpp'qq'} \tag{9.91}$$

where

$$R_{lmpp'qq'} = \frac{GM' (-l)^{l+m}}{2l+1} D_{lmp}(I) D_{l,-m,p'}(I') \times \left[\frac{a^l}{a'^{l+1}} X_q^{lm}(e) X_{q'}^{-l-1,m}(e') + \frac{k_l a_e^{2l+1}}{(a'a)^{l+1}} X^{-l-1,m}(e) X_{q'}^{-l-1,m}(e') \right] e^{i\psi} \tag{9.92}$$

in which

$$\psi = qM + q'M' + (l-2p)\omega + (l-2p')\omega' + m(\Omega - \Omega')$$

We can integrate the LPE (9.28) by utilizing the disturbing function (9.91) and the same techniques used for the tesseral harmonics. Considerable simplification is achieved by the following steps:

(1) We delete all terms containing M—that is, $q=0$. These short-period effects are about 1 m and can be ignored for some problems. A consequence is that $\Delta a = 0$.

(2) For the second-degree terms, we can use, for the Moon,

$$GM_\oplus = n_\leftmoon^2 a_\leftmoon^3 \tag{9.93a}$$

and

$$GM' = GM_\oplus (M_\leftmoon/M_\oplus) = (M_\leftmoon/M_\oplus) n_\leftmoon^2 a_\leftmoon^3 \tag{9.93b}$$

where $M_\leftmoon/M_\oplus = 1/81.53$ and, for the Sun,

$$GM' = n_\odot^2 a_\odot^3 \tag{9.93c}$$

(3) The third-degree terms from the Sun are negligible, and those from the Moon are $\approx$1 m and can be ignored for some problems. However, the third-degree terms and the short-period terms in the second-degree development must be included for future work. The interaction between J_2 and the lunar perturbations is the same size and must also be added, that is, the contributions to $\dot{\omega}$ and $\dot{\Omega}$ from

$$\begin{aligned} &\frac{d\dot{\omega}}{de}\Delta e + \frac{\partial \dot{\omega}}{\partial I}\Delta I \\ &\frac{d\dot{\Omega}}{de}\Delta e + \frac{d\dot{\Omega}}{dI}\Delta I \\ &\frac{d\dot{M}}{de}\Delta e + \frac{d\dot{M}}{dI}\Delta I \end{aligned} \tag{9.94}$$

where $\dot{\omega}$, $\dot{\Omega}$, and $\dot{M}$ are given by (9.80).

A number of formulas have been used (e.g., Kozai, 1973; Gaposchkin, 1966a). We give here just the secular rates in ω, Ω, and M and a representative periodic term. The complete expressions for lunar perturbations are developed by computer algebra and are described in section 9.4.1.11. We have

$$\begin{aligned} \dot{\omega}_{L\text{-}S} = &\frac{3}{4}\frac{n'^2}{n} m' \frac{1}{(1-e^2)^{1/2}} \\ &\times \left(2 - \frac{5}{2}\sin^2 I + \frac{1}{2}e^2\right)\left(1 - \frac{3}{2}\sin^2 I'\right) \\ &\times \left(1 + \frac{3}{2}e'^2\right)\left[1 + k_2\left(\frac{a_e}{a}\right)^2\right] \\ \dot{\Omega}_{L\text{-}S} = &-\frac{3}{4}\frac{n'^2}{n} m' \frac{\cos I}{(1-e^2)^{1/2}} \\ &\times \left(1 + \frac{3}{2}e^2\right)\left(1 - \frac{3}{2}\sin^2 I'\right) \\ &\times \left(1 + \frac{3}{2}e'^2\right)\left[1 + k_2\left(\frac{a_e}{a}\right)^2\right] \end{aligned} \tag{9.95}$$

$$\begin{aligned} \dot{M}_{L\text{-}S} = &-\frac{1}{4}\frac{n'^2}{n} m' \left(1 - \frac{3}{2}\sin^2 I'\right) \\ &\times \left(1 - \frac{3}{2}\sin^2 I\right)\left(1 + \frac{3}{2}e'^2\right) \\ &\times \left[7 + 3e^2 - 3(1+4e^2) k_2 \left(\frac{a_e}{a}\right)^2\right] \end{aligned}$$

where, for the Moon, $m' = M_\leftmoon/M_\oplus = 1/81.53$, and, for the Sun, $m' = 1$, and where

$$\begin{aligned} \sin^2 I' = &\frac{1}{2}\sin^2 J (1 + \cos^2 \epsilon) + \sin^2 \epsilon \cos^2 J \\ &+ \frac{1}{2}\sin 2\epsilon \sin 2J \cos N \\ &- \frac{1}{2}\sin^2 J \sin^2 \epsilon \cos 2N \end{aligned} \tag{9.96}$$

Here, J is the lunar inclination, N is the lunar longitude referred to the ecliptic, and ϵ is the obliquity. Although I is not constant, it is a reasonable approximation for a year or so. We note that $J = 5''.145\,396$. The other dements can be taken from the ESAENA. For the Sun, of course, $m' = J = 0$. For the periodic perturbation, we give as an example, for the second degree,

$$\begin{aligned} \Delta I_{2,m,p,q',q'} = &\frac{n'^2 (-1)^m}{\partial \psi} D_{2,m,p}(I) D_{2,-m,q'}(I') \\ &\times \left[X_q^{2,m}(e) X_{q'}^{-3,m}(e') \right. \\ &\left. + k_2 \left(\frac{a_e}{a}\right)^5 X_q^{-3,m}(e) X_{q'}^{-3,m}(e') \right] \\ &\times [2(1-p)\cos I - m] \cos \psi \end{aligned} \tag{9.97}$$

where

$$\begin{aligned} \dot{\psi} = &2(1-p)\dot{\omega} + 2(1-p')\dot{\omega}' + qn + q'n' \\ &+ m(\dot{\Omega} - \dot{\Omega}') \end{aligned}$$

We note that the secular rates depend on k_2, which corresponds to that part of the oblateness resulting from the permanent tidal deformation. Conventionally, this term is omitted from the lunar theory and is effectively included in the numerical value of J_2. A slight error will arise since, in the lunar theory, k_2 occurs multiplied by a_e/a^5, whereas J_2 is multiplied by a_e/a^3. Furthermore, the

secular term in M must be included in the definition of the semimajor axis.

The adopted reference system for orbit computation is the equinox of 1950.0 and the equator of date. The equations of motion must be modified to include the motion of the reference system. There is no need to modify the short-period perturbations in the linear theory described above. However, for the complete set of LPE with (9.92) for long-period perturbations or in terms of coordinates (Kozai and Kinoshita, 1973), we can include the following factors:

$$\left.\begin{aligned} di/dt &= \cdots \partial i/\partial t \\ d\omega/dt &= \cdots \partial \omega/\partial t \\ d\Omega/dt &= \cdots \partial \Omega/\partial t \end{aligned}\right\}$$

where

$$\left.\begin{aligned} \frac{\partial i}{\partial t} &= -\frac{d(\theta\cos\alpha)}{dt}\cos\Omega - \frac{d(\theta\sin\alpha)}{dt}\sin\Omega \\ \frac{\partial \omega}{\partial t} &= \operatorname{cosec} i\left[\frac{d(\theta\sin\alpha)}{dt}\cos\Omega - \frac{d(\theta\cos\alpha)}{dt}\sin\Omega\right] \\ \frac{\partial \Omega}{\partial t} &= -\cot i\left[\frac{d(\theta\sin\alpha)}{dt}\cos\Omega - \frac{d(\theta\cos\alpha)}{dt}\sin\Omega\right] \\ &\quad + \frac{1}{2}\left[\frac{d(\theta\sin\alpha)}{dt}\theta\cos\alpha - \frac{d(\theta\cos\alpha)}{dt}\theta\sin\alpha\right] \end{aligned}\right\} \quad (9.98)$$

$$\left.\begin{aligned} \theta\sin\alpha &= (0.3979 + \epsilon_1 - \epsilon_0)\sin\psi \\ \theta\cos\alpha &= 0.3651\ (1-\cos\psi) - \epsilon_1 + \epsilon_0 \end{aligned}\right\} \quad (9.99)$$

$$\begin{aligned} \psi = &-17''.24\sin N + 0''.21\sin 2N \\ &-1''.27\sin 2L_\odot + 0''.13\sin l_\odot \\ &-0''.20\sin 2L_\mathbb{C} + 0''.07\sin l_\mathbb{C} \\ &+0''.137\,914\,6\,t \\ \epsilon_1 - \epsilon_0 = &\ 9''.21\cos N - 0''.09\cos 2N \\ &+0''.55\cos 2L_\odot + 0''.09\cos 2L_\mathbb{C} \\ &-0''.001\,281\,t \end{aligned}$$

where $l_\odot$, $l_\mathbb{C}$, $L_\odot$, and $L_\mathbb{C}$ are the mean anomalies and mean longitudes of the Sun and the Moon, respectively; t is the number of days from 1950.0; and N is the lunar ascending node referred to the ecliptic. We have

$$\left.\begin{aligned} \frac{d(\theta\sin\alpha)}{dt} &= 0.9175\sin\psi\frac{d(\epsilon_1-\epsilon_0)}{dt} + 0.3979\cos\psi\frac{d\psi}{dt} \\ \frac{d(\theta\cos\alpha)}{dt} &= -(0.1583 + 0.8418\cos\psi)\frac{d(\epsilon_1-\epsilon_0)}{dt} + 0.3651\sin\psi\frac{d\psi}{dt} \end{aligned}\right\} \quad (9.100)$$

$$\left.\begin{aligned} \frac{d\psi}{dt} &= -17''.24\,\dot{N}\cos N + 0''.42\,\dot{N}\cos 2N - 2''.54\,n_\odot\cos 2L_\odot + 0''.13\,n_\odot\cos l_\odot \\ &\quad - 0''.40\,n_\mathbb{C}\cos 2L_\mathbb{C} + 0''.07\,n_\mathbb{C}\cos l_\mathbb{C} + 0''.137\,914\,6 \\ \frac{d(\epsilon_1-\epsilon_0)}{dt} &= -9''.21\,\dot{N}\sin N + 0''.18\,\dot{N}\sin 2N - 1''.10\,n_\odot\sin 2L_\odot \\ &\quad - 0''.18\,n_\mathbb{C}\sin 2L_\mathbb{C} - 0''.001\,281 \end{aligned}\right\} \quad (9.101)$$

where $\dot{N} = dN/dt$, $n_\odot$ is the mean motion of the Sun, and $n_\mathbb{C}$ is the mean motion of the Moon.

We have incorporated the effects of body tides on satellite motion. There remain to be included ocean and atmospheric tides. The former, expressed in spherical harmonics, is not yet very well known and so we give only a qualitative analysis. The M_2 tide has been studied by Pekeris and Accad (1969) and by Hendershott (1972) and we will examine it. If we develop the tide in an Earth-fixed system as

$$\zeta = \mathcal{R}e\sum_{lm}\bar{C}_{lm}\bar{P}_{lm}(\sin\phi)\ e^{i(m\lambda+\theta t)} \quad (9.102)$$

then the tide will appear static in the inertial reference frame of the satellite. The external potential due to this tide, including the loading effect, is

$$\mathcal{U}=\mathcal{R}e\sum_{lm}\frac{(1+k_l')\,4\pi G\rho_w a_e^{l+2}}{(2l+1)\,r^{l+1}}\bar{C}_{lm}\bar{P}_{lm}(\sin\phi)\,e^{im\lambda}) \tag{9.103}$$

where k is the loading Love number (Munk and MacDonald, 1960) and ρ_w is the density of ocean water. This can be developed in terms of orbital elements along the lines of the tesseral harmonics; we have

$$\mathcal{U}=\sum_{lmp}\mathcal{U}_{lmp}$$

in which

$$\mathcal{U}_{lmp}=\Gamma_{lm}(a_e^{l+2}/r^{l+1})\,D_{lmp}(I)\,e^{i[(l-2p)(v+\omega)+m(\Omega-v'-\omega'-\Omega')]} \tag{9.104}$$

where

$$\Gamma_{lm}=4\pi G\rho_w(1+k_l')\,\bar{C}_{lm}/(2l+1) \tag{9.105}$$

We can develop equation (9.104) into perturbations, giving, for example,

$$\Delta\omega_{lmpqq'}=\mathcal{R}e\,(i)^{l-m}\,\Gamma_{lm}(a_e^{l+2}/na^{l+2})\,[D_{lmp}(I)/\dot{\psi}]\,X_q^{-l-1}(e)^{l-2p}X_{q'}^{q,m}(e')\times[(l-2p)\cos I-m]e^{i\psi} \tag{9.106}$$

where

$$\psi=qM+q'M'+(l-2p)\,\omega+m(\Omega-\Omega'-\omega')$$
$$\psi=qn+q'n'+(l-2p)\,\dot{\omega}'+m(\dot{\Omega}-\dot{\Omega}'-\dot{\omega}')$$

It is useful to note characteristics of lunar and solar perturbations in addition to the secular terms given in (9.95). The principal periodic terms from the Moon have a 14-day period and an amplitude of about 120 m. The principal solar term is of 6-month period and about 800 m. The tidal effects are of the order of 10 percent of the direct effect, or about 15 m for the lunar tides. Therefore, it is essential to compute lunar effects when orbits are being determined for more than a few days. The solar effects can be absorbed in the orbital elements. There are also very important long-period perturbations from the Moon. Of greater difficulty in the treatment of long-period perturbations is the solar radiation pressure, which is yet to be satisfactorily computed (section 9.4.1.9).

It is instructive to determine the ocean-tide equivalent of the body tide. We can do this only approximately. The correspondence is made by comparing the potentials in (9.92) and (9.106) for a particular lmp combination. We have

$$\mathcal{U}_{lmp}^{\text{body}}=\frac{GM'(-1)^{l+m}}{2l+1}\frac{k_l a_e^{l+1}}{r'^{l+1}r^{l+1}}D_{lmp}(I)\sum_{p'=0}^{l}D_{l(-m)p'}(I')\,e^{i\phi} \tag{9.107}$$

where $\phi=(l-2p)(v+\omega)+(l-2p')(v'+\omega')+m(\Omega-\Omega')$; and

$$\mathcal{U}_{lmp}^{M_2}=\frac{4\pi G\rho_\omega(1+k_l')}{2l+1}\frac{a_e^{l+2}}{r^{l+1}}\bar{C}_{lm}(i)^{l-m}D_{lmp}(I')\,e^{i\psi} \tag{9.108}$$

where $\psi=(l-2p)(v+\omega)-m(v'+\omega'+\Omega'-\Omega)$. We note that the lunar inclination is $I'=23°\pm5°$ and that $D_{2,-2,0}\cong0.925$, $D_{2,-2,1}\cong0.160$, and $D_{2,-2,2}\cong0.0036$. So, for the principal semidiurnal term, we can take $l=2$, $m=2$, $l-2p=2$, $p=0$, and $p'=0$, giving

$$\frac{k_2}{1+k_2'}=\frac{4\pi G\rho_\omega\bar{C}_{2,2}}{\mu n'^2a_cD_{2,-2,0}(I')} \tag{9.109}$$

$$\bar{C}_{2,2}=\frac{k_2}{1+k_2'}\frac{\mu n'^2a_cD_{2,-2,0}(I')}{4\pi G\rho_\omega} \tag{9.110}$$

where k_2 would have a complex value. Using nominal values, we have

$$k_2=0.0114\bar{C}_{lm}/D_{2,-2,0}(I') \tag{9.111}$$

From K. Lambeck (1972, private communication), the Pekeris and Accad (1969) solution with dissipation gives (in cm)

$$\bar{C}_{2,2}=4.4e^{-i330\pi/180}=-2.19-3.81i$$

We then have $k_2^{\text{ocean}}=-0.026-0.047\text{i}$. Adding this to the body tide, we obtain the effective

Love number that a satellite would sense. Choosing $k_2^{\text{body}}=0.29$ with no dissipation, we have

$$k_2^{\text{effective}}=k_2^{\text{body}}+k_2^{\text{ocean}}=0.264-0.047\,i$$

Therefore, a satellite would sense a Love number of 0.268 with a phase lag of 10°.09 or 40 m. Conversely, by adopting a value for k_2^{body} and determining $k_2^{\text{effective}}$ from satellite observations, the height of the ocean tide could be calculated.

We have analyzed perturbations due to the $\bar{P}_{2,2}$ component of the ocean tide and note that they have the same dependence on the satellite inclination as does the body tide. Therefore, it is not possible to separate the second-degree body and ocean tide with satellite perturbation analysis. The ocean tides have a much richer spectrum in spherical harmonics than do the body tides (Hendershott, 1973). Selected terms of equation (9.102) are important, principally, $\bar{P}_{4,2}$ and $\bar{P}_{6,2}$. Although they result in orbital perturbations with the same frequency spectrum as does $\bar{P}_{2,2}$, the inclination dependence allows the determination of these coefficients by use of several satellites, in an analogous way to the geopotential.

Finally, we consider another effect of the Earth's elasticity. The orbital system we have adopted is not precisely a system of the principal axis of inertia. Rather, we use a mean pole. There is a free nutation of the Earth called polar motion, which introduces the tesseral harmonics $\bar{C}_{lm}=\bar{C}_{lm}-i\,\bar{S}_{lm}$. There are two effects that to some extent cancel each other: The first is the motion of the axis of the principal moment of inertia; the second, the deformation due to the rotation about a moving axis. If we let ξ, η be the coordinates of the principal moments with respect to the mean pole and let l_1, l_2 be the coordinates of the instantaneous rotation axis, then we can write

$$\begin{aligned}\bar{C}_{2,1}=&-\bar{C}_{2,0}\sqrt{3}\,(\xi-i\eta)\\&-k_2(\omega_e^2a_e^3/\sqrt{15}\,GM)\;(l-il_2)\end{aligned}$$

where $\omega_e=\dot{\theta}$. This harmonic is a slowly varying function of time with a 14-month period. If we assume $\xi=l_1$, $\eta=l_2$—that is, that we know where the principal axes are—then we have

$$\bar{C}_{2,1}=-\bar{C}_{2,0}\sqrt{3}-k_2(\omega_e^2a_e^3/\sqrt{15}\,GM)\,]\;(\xi-i\eta)$$

Using these values, we know

$$\bar{C}_{2,1}=(0.838-k_2x0.893)\;(\xi-i\eta)$$

the elasticity reducing the effect by about one-third. The perturbations for the seven retroreflector satellites are all about 1 m.

9.4.1.8 Higher Order Perturbations Due to Oblateness; Methods of Von Zeipel and Lie-Hori

Although a linear first-order approximation to the equations of motion proved adequate to obtain 1–m accuracy for the tesseral harmonics and the zonal harmonics excluding J_2 and J_3, we must have a more thorough treatment for the oblateness perturbations. Various solutions and formulas have been used (Brouwer, 1959; Kozai, 1959c, 1962b, 1966c; Izsak, 1963b; Aksnes, 1970), but only the last has proved completely satisfactory. Except for Kozai's (1959c), the methods depend on a canonical transformation. We sketch the basic ideas here. There are two equivalent approaches. The first, based on a device employed by Von Zeipel (1916) and known by his name, utilizes expansions in the form of Taylor series. It was introduced into the satellite problem by Brouwer (1959). The second, from a transformation due to Hori (1966), is based on expansions in Lie series and is known as the Lie-Hori method.

In both developments, we use canonical variables,

$$\left.\begin{array}{ll}l=M & L=(\mu a)^{1/2}\\ g=\omega & G=L(1-e^2)^{1/2}\\ h=\Omega & H=G\cos I\end{array}\right\}\qquad(9.112)$$

In the Aksnes theory, use is also made of the Hill variables introduced into satellite theory by Izsak (1963d):

$$r,\ v+\omega,\ h,\ \dot{r},\ G,\ H \qquad (9.113)$$

In the mathematical problem we are discussing, the Hamiltonian is

$$\mathcal{H}=\frac{\mu^2}{2L^2}-\frac{\mu^4 J_2 a_e^2}{L^6}\left\{\left[-\frac{1}{2}+\frac{3}{2}\left(\frac{H}{G}\right)^2\right]\left(\frac{a}{r}\right)^3+\left[\frac{3}{2}-\frac{3}{2}\left(\frac{H}{G}\right)^2\right]\left(\frac{a}{r}\right)^3\cos\,(2g+2v)\right\} \qquad (9.114)$$

Since t and h are both absent from $\mathcal{H}$, we therefore have immediately

$$H=G\cos I=\text{const} \qquad (9.115)$$

and $\mathcal{H}=\text{const}$. We have limited this discussion to J_2, and all the developments mentioned above have carried the analysis to higher orders.

The method of Von Zeipel (1916) was proposed by Poincaré (1893). The latter showed that a transformation was always possible, but he was not convinced that the expansion would converge; Barrar (1970) has discussed this question further. We look for a determining function $S(L',G',H',l,g,h) = F_2$ relating the new momenta and old coordinates, such that the new Hamiltonian $\mathcal{H}^*$ does not depend on l; that is,

$$\mathcal{H}(L,G,H,l,g)=\mathcal{H}^*(L,G,H,g) \qquad (9.116)$$

We then have

$$\left.\begin{array}{ll} l'=\partial S/\partial L' & L=\partial S/\partial l \\ g'=\partial S/\partial G' & G=\partial S/\partial g \\ h'=\partial S/\partial H' & H=\partial S/\partial h \end{array}\right\} \qquad (9.117)$$

Since this is a canonical transformation, we have

$$\left.\begin{array}{l} dL'/dt=\partial\mathcal{H}^*/\partial l' \\ dl'/dt=-\partial\mathcal{H}^*/\partial L' \end{array}\right\} \qquad (9.118)$$

and four similar equations. Having solved this problem, we can perform a second transformation to eliminate g' and obtain a third set of variables, L'',G'',H'',l'',g'',h'', where the Hamiltonian is

$$\mathcal{H}^{**}(L'',G'',H'')=\mathcal{H}^*(L',G',H',g)$$

We proceed by expressing $\mathcal{H}$ and S in a Taylor series in terms of a small parameter α, which will be proportional to J_2:

$$\left.\begin{array}{l} \mathcal{H}=\mathcal{H}_0+\alpha\mathcal{H}_1 \\ S=S_0+\alpha S_1+\alpha^2 S_2+\cdots \\ \mathcal{H}^*=\mathcal{H}_2^*+\alpha\mathcal{H}_1^*+\alpha^2\mathcal{H}_2^*+\cdots \end{array}\right\} \qquad (9.119)$$

We want an identity transformation for $\alpha=0$; therefore,

$$S_0=L'l+G'g+H'h \qquad (9.120)$$

We proceed by using expression (9.117) in (9.116) to give

$$\mathcal{H}_0\left(\frac{\partial S}{\partial L}\right)+\mathcal{H}_1\left(\frac{\partial S}{\partial l},\frac{\partial S}{\partial g},\frac{\partial S}{\partial h},l,g\right) \equiv \mathcal{H}_0^*+\mathcal{H}_1^*\left(L',G',H',\frac{\partial S}{\partial G'}\right) \qquad (9.121)$$

If we expand (9.121) into a Taylor series and equate equal powers of α, we have

$$\left.\begin{array}{l} \mathcal{H}_0(L')=\mathcal{H}_0^*(L')=\dfrac{\mu^2}{2L'^2} \\ \dfrac{\partial\mathcal{H}_0}{\partial L'}\dfrac{\partial S_1}{\partial l}+\mathcal{H}_1=\mathcal{H}_1^* \\ \dfrac{\partial\mathcal{H}_0}{\partial L'}\dfrac{\partial S_2}{\partial l}+\dfrac{1}{2}\dfrac{\partial^2\mathcal{H}_0}{\partial L'^2}\left(\dfrac{\partial S_1}{\partial l}\right)^2 \\ \quad+\dfrac{\partial\mathcal{H}_1}{\partial L'}\dfrac{\partial S_1}{\partial l}+\dfrac{\partial\mathcal{H}_1}{\partial G'}\dfrac{\partial S_1}{\partial g}=\mathcal{H}_2^*\dfrac{\partial\mathcal{H}_1^*}{\partial g}\dfrac{\partial S_1}{\partial G} \end{array}\right\} \qquad (9.122)$$

Kozai (1962b) correctly gives the third-order expression.

We now separate $\mathcal{H}_1$ into a part independent of l (called $\mathcal{H}_{1sec}$) and a part dependent on l (called $\mathcal{H}_{1p}$) and then make the association

$$\left.\begin{array}{l} \dfrac{\partial\mathcal{H}_0}{\partial L'}\dfrac{\partial S_1}{\partial l}+\mathcal{H}_{1p}=0 \\ \mathcal{H}_{1sec}=\mathcal{H}_1^* \end{array}\right\} \qquad (9.123)$$

The expression for S_1 obtained from (9.123) can be used in the last line of equation (9.122), again separating the parts dependent on l or not. We obtain a solution for S_2, and so on. Through equations (9.117), we obtain

$$\begin{aligned} l' &= l'(L',G',H',l,g) \\ L &= L(L',G',H',l,g) \end{aligned}$$

and four similar expressions for g',h',L,H. These expressions must be inverted to obtain

$$\left.\begin{aligned} l &= l(L',G',H',l',g') \\ L &= L(L',G',H',l',g') \end{aligned}\right\} \quad (9.124)$$

which is accomplished by Taylor expansion to the desired order and is very tedious.

The Lie-Hori method is developed along somewhat different lines. Hori (1966) considered a transformation from p,q to P,Q given by

$$\left.\begin{aligned} p_i &= P_i + \frac{\partial S}{\partial Q_i} + \frac{1}{2}\left[\frac{\partial S}{\partial Q_i}, S\right] + \cdots \\ q_i &= Q_i - \frac{\partial S}{\partial P_i} - \frac{1}{2}\left[\frac{\partial S}{\partial P_i}, S\right] + \cdots \end{aligned}\right\} \quad (9.125)$$

where $[a,b]$ are Poisson brackets. In this notation, any function can be written

$$f(p,q) = f(P,Q) + [f,S] + \frac{1}{2}\left[[f,S],S\right] + \cdots \quad (9.126)$$

The canonical equations are

$$\left.\begin{aligned} dP_i/dt &= \partial\mathcal{H}^*/\partial Q_i \\ dQ_i/dt &= -\partial\mathcal{H}^*/\partial P_i \end{aligned}\right\} \quad (9.127)$$

We further assume that S and $\mathcal{H}$ can be written in terms of a small parameter

$$\left.\begin{aligned} S &= S_1 + S_2 + \cdots \\ \mathcal{H}^* &= \mathcal{H}_1^* + \mathcal{H}_2^* + \cdots \end{aligned}\right\} \quad (9.128)$$

If a parameter τ defined by

$$\left.\begin{aligned} dP_i/d\tau &= \partial\mathcal{H}_0/\partial Q_i \\ dQ_i/d\tau &= -\partial\mathcal{H}_0/\partial P_i \end{aligned}\right\} \quad (9.129)$$

is eliminated from $\mathcal{H}^*$, we have

$$\left.\begin{aligned} \mathcal{H}_0^* &= \text{const} \\ \mathcal{H} &= \text{const} \end{aligned}\right\} \quad (9.130)$$

This development led Hori to the following formulas:

$$\left.\begin{aligned} \mathcal{H}_0^* &= \mathcal{H}_0 \\ \mathcal{H}_1^* &= \mathcal{H}_{1\text{sec}} \\ S_1 &= \int \mathcal{H}_{1p}\, d\tau \\ \mathcal{H}_2^* &= \mathcal{H}_{2\text{sec}} + \frac{1}{2}[\mathcal{H}_1 + \mathcal{H}_1^*, S_1]_{\text{sec}} \\ S_2 &= \int\left(\mathcal{H}_{2p} + \frac{1}{2}[\mathcal{H}_1 + \mathcal{H}_1^*, S_1]_p\right) d\tau \end{aligned}\right\} \quad (9.131)$$

Here we designate the subscripts sec and p to mean the parts independent of and dependent on l, respectively, as in the Von Zeipel method. These formulas are given by Aksnes (1970).

The Lie-Hori method has a number of advantages. The transformation is completely in terms of the new variables, and no inversion of series is necessary. The formulas are all canonically invariant, so they hold for any canonical variables. Aksnes could then make two fundamental advances in the treatment of oblateness perturbations. First, he chose as an intermediate orbit a precessing ellipse that incorporated all the first-order secular terms and most of the periodic terms. That is to say, in the analogous process of finding $\partial\mathcal{H}/\partial q_i$, he discovered another solution, q^0, p^0, that included a part of the disturbing function instead of a Kepler ellipse. Second, with a canonically invariant formulation, he employed appropriate variables. For long-period and secular effects, Delaunay variables were used. The results agree with the Von Zeipel method. For short-period perturbations, Hill variables were used, a procedure that eliminates the difficulty with small eccentricities.

The first-order determining functions for the Lie-Hori and the Von Zeipel methods are the same, as can be seen by comparing the defining equations or the results (Kozai, 1962b; Aksnes, 1970). In fact, this must be

so because both formulations work for Delaunay variables and have been shown to be equivalent. Therefore, the first-order perturbations are the same.

Space does not permit us to give a more detailed account of this beautiful theory or the detailed formulas, for which we refer the reader to Aksnes (1970).

We summarize the status of oblateness perturbations:

(1) Two complete second-order developments, one by the Von Zeipel method (Kozai, 1962b) and the other by the Lie-Hori method, have been compared. For short-periodic perturbations, the agreement is 10 cm. The secular rates predicted by the two theories can be reconciled to within their given accuracy (Aksnes, 1972).

(2) The second-order development of Aksnes has the advantages of compactness and efficiency of computation, and no singularity for small eccentricity. The small-eccentricity problem is avoided by the use of Hill variables.

(3) For long-period and secular perturbations to 10 cm, further work is necessary. Terms in J_2J_3, J_2J_4, etc. must be included, as well as interaction with all other forces—lunar and solar effects, tesseral harmonics, drag, and radiation pressure.

We cannot give the complete set of formulas, but we present the first-order periodic and second-order secular perturbations as developed by Aksnes (1970), although we have dropped the primes:

$$\Delta\dot{r} = (-\gamma G^3/2\mu r^2)\left[s^2 \sin 2u - \frac{1}{8} D\, s^2 e \sin (2u-v) \right]$$

$$\Delta r = (\gamma G^2/4\mu)\left[1-3c^2+s^2\cos 2u - \frac{1}{4} D\, s^2 e \cos (2u-v) \right]$$

$$\Delta G = (\gamma G/4)\left[3s^2 e \cos (2u-v) + s^2 e \cos (2u+v) - \frac{1}{4} D\, s^2 e^2 \cos (2u-2v) \right]$$

$$\Delta u = (-\gamma/4)\left\{ (2-12c^2)\, e \sin v - \frac{1}{8}(4+D\,e^2)\, s^2 \sin 2u - (2-5c^2 + \frac{1}{2} D s^2)\, e \sin (2u-v) + c^2 e \sin (2u+v) - \frac{1}{4}[D - D^{(1)} s^2]\, c^2 e^2 \sin (2u-2v) \right\}$$

$$\Delta h = (-\gamma c/4)\left\{ 6e \sin v - 3e \sin (2u-v) - e \sin (2u+v) + \frac{1}{4}[D - D^{(1)} s^2] e^2 \sin (2u-v) \right\}$$

where

$$D = (1-15c^2)/(1-5c^2)$$

$$D^{(1)} = \partial D/\partial c^2$$

$$c = \cos I$$

$$s = \sin I$$

$$\gamma = J_2/a^2\eta^4$$

$$\eta^2 = 1-e^2$$

The secular rates can be obtained from letting

$$g_{21} = -\frac{3}{4}\gamma(1-5c^2) - \frac{1}{64}\gamma^2 (41+30c^2-135c^4)$$

$$g_{32} = -\frac{3}{16} c[8\gamma + \gamma^2 (7-33c^2)]$$

with

$$\gamma_4 = J_4/J_2^2$$

$$\dot{M} = n + \frac{3}{128} n\gamma^2\eta[8(1-6c^2+5c^4) - 5(5-18c^2+5c^4)\, e^2 - 15\,\gamma_4 (3-30c^2+35c^4)\, e^2]$$

$$\dot{\omega} = \dot{g} + g_{21}(\dot{g}+\dot{M}) = -\frac{1}{128} n\gamma^2[44-300c^4 + (75-378c^2+135c^4)\, e^2 + 60\,\gamma_4 (3-36c^2+49c^4) + 135\,\gamma_4 (1-14c^2+21c^4)\, e^2]$$

$$\dot{\Omega} = \dot{h} + g_{32}(\dot{\omega}+\dot{M})$$

$$h = \frac{3}{32} nc\gamma^2[2-10c^2-(9-5c^2)\, e^2 - 5\gamma_4 (3-7c^2)\,(2+3e^2)]$$

As was discussed in section 9.4.1.5, periodic perturbations for J_2 were developed by using computer algebra. The expressions were employed in orbit computation, and the orbital fits were identical. This agreement validates both sets of formulas since they are based on quite different methods. The mean elements in the two developments are different by factors of order J_2. Aksnes (1970) has given the formulas relating the two theories and a numerical verification. If we let a subscript 0 designate the Von Zeipel element, then the elements of a, e, I are related by

$$
\begin{aligned}
1/a &= (1/a_0)\left\{1-\frac{1}{2}\eta_0\gamma_0(1-3\cos^2 I_0)\right. \\
&\quad +\frac{1}{32}\eta_0\gamma_0^2[1+6\eta_0-(6+36\eta_0)\cos^2 I_0 \\
&\quad \left.+(45+54\eta_0)\cos^4 I_0]+\cdots\right\} \\
G &= G_0\left[1+\frac{1}{4}\gamma_0(1-3\cos^2 I_0)\right]+\cdots \\
\cos I &= \cos I_0=\left[1+\frac{3}{4}\gamma_0(1-\cos^2 I_0)\right]+\cdots \\
\eta^2 &= 1-e^2 \\
G^2 &= \eta^2\,\mu a \\
\gamma &= J_2/a^2\,\eta^4
\end{aligned}
$$

9.4.1.9 Atmospheric Drag and Radiation Pressure

For several reasons, atmospheric drag and radiation pressure are treated by different methods than are gravitational perturbations. First, they are not conservative forces derivable from a potential function. Second, they involve considerably more unknowns. Whereas the geopotential may be considered unknown and require improvement, we can assume that the main field is constant in time, that tidal variations are known, and that the geopotential has a known mathematical and physical form. Similarly, for lunar and solar perturbations, we assume sufficient knowledge of the mass and position of the Moon and the Sun. With drag and radiation pressure, we are in a much less favorable position. In drag perturbations, the atmospheric density is critical; it has been studied extensively from its orbital effects. The parameters controlling density variations are becoming known, and one can probably predict a posteriori the mean-density structure to within a factor of 2. However, the satellite aspect and the drag coefficient must also be known. Radiation-pressure effects involve similar problems: What is the value of the solar constant and is it constant? How much is diffuse and how much specular reflection? How do the reflective properties change with time? How variable is the albedo radiation? How does the satellite aspect change? And how is the boundary of the Earth's shadow defined? For some satellites, this information is available, though difficult to obtain. Some of these questions are subjects of current research.

The following treatment of radiation pressure developed by Kozai (1963c) and extended by Lála (1968, 1971) and Lála and Sehnal (1969) assumes, for one revolution, the following: (1) the satellite is spherical, with constant reflective properties; (2) the solar parallax can be neglected; (3) the solar flux is constant; and (4) there is no albedo radiation.

The natural vehicle for treating forces directly is the Lagrange planetary equations in Gaussian form (9.42). The forces are expressed as

$$
\left.
\begin{aligned}
S &= n^2a^3\,F\,S(v) \\
T &= n^2a^3\,F\,T(v) \\
W &= n^2a^3\,F\,W
\end{aligned}
\right\} \qquad (9.132)
$$

where

$$F=(A/M)\,(K/GM)\approx 0.5\times 10^{-4}\,(A/M)$$

with A (area)/M (mass) in $\mathrm{cm^2\,g^{-1}}$. We have

$$
\begin{aligned}
S(v) = &-\cos^2(I/2)\cos^2(\epsilon/2)\cos(\lambda_\odot-L-\Omega) \\
&-\sin^2(I/2)\sin^2(\epsilon/2)\cos(\lambda_\odot+\Omega-L) \\
&-\frac{1}{2}\sin I\sin\epsilon\,[\cos(\lambda_\odot-L) \\
&-\cos(-\lambda_\odot-L)\,] \\
&-\sin^2(I/2)\cos^2(\epsilon/2)\cos(\Omega-\lambda_\odot-L) \\
&-\cos^2(I/2)\sin^2(\epsilon/2)\cos(-\lambda_\odot-L-\Omega)
\end{aligned}
\qquad (9.133)
$$

$$\begin{aligned}\Gamma(v) = &-\cos^2(I/2)\cos^2(\epsilon/2)\sin(\lambda_\odot - L - \Omega) - \sin^2(I/2)\cos^2(\epsilon/2)\sin(\lambda_\odot + \Omega - L)\\ &-\frac{1}{2}\sin I \sin\epsilon[\sin(\lambda_\odot - L) - \sin(-\lambda_\odot - L)]\\ &-\sin^2(I/2)\cos^2(\epsilon/2)\sin(\Omega - \lambda_\odot - L) - \cos^2(I/2)\sin^2(\epsilon/2)\sin(-\lambda_\odot - L - \Omega) \qquad (9.134)\end{aligned}$$

$$W = \sin I\cos^2(\epsilon/2)\sin(\lambda_\odot - \Omega) - \sin I\sin^2(\epsilon/2)\sin(\lambda_\odot + \Omega) - \cos I\sin\epsilon\sin\lambda_\odot \qquad (9.135)$$

where $L = v + \omega$, $\lambda_\odot$ = the longitude of the Sun, and ϵ = the obliquity. We have the LPE

$$\left.\begin{aligned}&\frac{da}{dt} = \frac{2na^3}{(1-e^2)^{1/2}}F\left[S(v)\,e\sin v + T(v)\frac{p}{r}\right] \qquad p = a(1-e^2)\\ &\sin I\frac{d\Omega}{dt} = \frac{na^2}{(1-e^2)^{1/2}}WF\frac{r}{a}\sin L \qquad \frac{dI}{dt} = \frac{na^2}{(1-e^2)^{1/2}}WF\frac{a}{r}\cos L\\ &\frac{de}{dt} = na^2(1-e^2)^{1/2}F\left\{S(v)\sin v + T(v)\left[\cos v + \frac{1}{e}\left(1 - \frac{r}{a}\right)\right]\right\}\\ &\frac{d\omega}{dt} = -\cos I\frac{d\Omega}{dt} + na^2\frac{(1-e^2)^{1/2}}{e}F\left[-S(v)\cos v + T(v)\left(1 + \frac{r}{p}\right)\sin v\right]\\ &\frac{dM}{dt} = n - 2a^2FS(v)\frac{r}{a}n - (1-e^2)^{1/2}\left(\frac{d\omega}{dt} + \cos I\frac{d\Omega}{dt}\right)\end{aligned}\right\} \qquad (9.136)$$

Since radiation pressure is a discontinuous force, it is difficult to obtain analytical solutions for it. Two approaches have been used successfully. The first, by Kozai (1963c), is to determine numerically the time of shadow exit E_1 and shadow entry E_2 in terms of the eccentric anomaly. Then, by assuming everything else constant for one revolution, Kozai obtains the following first-order perturbations after one revolution, where $S = S(0)$, $T = T(0)$ are written for their values at $L = \omega$:

$$\left.\begin{aligned}&\delta a = 2a^2F\Big|[S\cos E - T(1-e^2)^{1/2}\sin E]\Big|_{E_1}^{E_2}\\ &\delta e = a^2F(1-e^2)^{1/2}\left[\left|\frac{1}{4}S(1-e^2)^{1/2}\cos 2E + T\left(-2e\sin E + \frac{1}{4}\sin 2E\right)\right|_{E_1}^{E_2} + \frac{3}{2}\int T\,dE\right]\\ &\delta I = a^2F\frac{W}{(1-e^2)^{1/2}}\left\{\left|\left[(1+e^2)\sin E - \frac{e}{4}\sin 2E\right]\cos\omega\right.\right.\\ &\qquad\left.\left. + (1-e^2)^{1/2}\left(\cos E - \frac{e}{4}\cos 2E\right)\sin\omega\right|_{E_1}^{E_2} - \frac{3}{2}e\int\cos\omega\,dE\right\}\\ &\sin I\,\delta\Omega = a^2F\frac{W}{(1-e^2)^{1/2}}\left\{\left|\left[(1+e^2)\sin E - \frac{e}{4}\sin 2E\right]\sin\omega\right.\right.\\ &\qquad\left.\left. - (1-e^2)^{1/2}\left(\cos E - \frac{e}{4}\cos 2E\right)\cos\omega\right|_{E_1}^{E_2} - \frac{3}{2}e\int\sin\omega\,dE\right\}\\ &\delta\omega = -\cos I\,\delta\Omega + a^2F\frac{(1-e^2)^{1/2}}{e}\left[\left|S\left(e\sin E + \frac{1}{4}\sin 2E\right)\right.\right.\\ &\qquad\left.\left. + \frac{T}{(1-e^2)^{1/2}}\left(e\cos E - \frac{1}{4}\cos 2E\right)\right|_{E_1}^{E_2} - \frac{3}{2}\int S\,dE\right]\\ &\delta M = -\frac{3}{2}\int_0^{2\pi}\frac{\delta a}{a}dM - (1-e^2)^{1/2}\,\delta\omega - (1-e^2)^{1/2}\cos I\,\delta\Omega - 2a^2F\\ &\qquad\left\{\left|S\left[(1+e^2)\sin E - \frac{e}{4}\sin 2E\right]\right.\right.\\ &\qquad\left.\left. - T(1-e^2)^{1/2}\left(\cos E - \frac{e}{4}\cos 2E\right)\right|_{E_1}^{E_2} - \frac{3}{2}e\int S\,dE\right\}\end{aligned}\right\} \qquad (9.137)$$

If the satellite does not enter the shadow, then the terms evaluated at E_1 and E_2 vanish. How the perturbations after part of a revolution can be computed is obvious. These expressions provide the differential equations to be integrated for mean elements—that is, $d\bar{a}/dt = \delta a/\delta t = n\delta a$, and so on. This is the method used to calculate the long-term effects due to radiation pressure in the determination of zonal harmonics and tidal parameters. In addition, one can determine quite reasonable mean reflectivities for the satellites.

An alternative approach was taken by Lála (1968, 1971) and Lála and Sehnal (1969). They developed the shadow function in Fourier series in E and found solutions for the periodic perturbations. They required 36 terms in the development to obtain agreement with the above special perturbation formulas. These periodic perturbations were formally integrated. For further details, the reader is referred to the Lála and Sehnal papers.

The development of drag perturbations by Sterne (1959) follows the same lines. Assuming a rotating atmosphere with an oblate planet, he considers the drag force per unit mass

$$\frac{1}{2}C_D\frac{A}{M}\rho V^2 \tag{9.138}$$

where C_D is a drag coefficient, A/M is the area-to-mass ratio, ρ is the atmospheric density, and V is the satellite velocity with respect to the atmosphere. Now, C_D, A/M, and ρ are all difficult to know. Sterne adopts $C_D \approx 2.2$. If precise values of A/M are not known, then the average A is taken as one-fourth the total surface area. He then gives the forces acting on the satellite as

$$\begin{bmatrix} S \\ T \\ W \end{bmatrix} = \begin{bmatrix} \dot{r} \\ r\dot{v} - \dot{\theta} r \cos I \\ \dot{\theta} r \sin I \cos (v+\omega) \end{bmatrix} \tag{9.139}$$

and after calculation, the velocity as

$$V = \left(\frac{\mu}{a}\right)^{1/2}\left(\frac{1+e\cos E}{1-e\cos E}\right)^{1/2}\left(1 - d\frac{1-e\cos E}{1+e\cos E}\right) \tag{9.140}$$

where

$$d = \frac{\dot{\theta}}{n}(1-e^2)^{1/2}\cos I \tag{9.141}$$

and the forces per unit mass are

$$\begin{bmatrix} S \\ T \\ W \end{bmatrix} = \frac{1}{2}C_D\frac{A}{M}\rho\, aV \begin{bmatrix} e\sin E\,\dot{E} \\ -(1-e^2)^{1/2}\left[1 - d\frac{(1-e\cos E)^2}{1-e^2}\right]\dot{E} \\ -\frac{\dot{\theta}}{n}(1-e\cos E)^2 \sin I \cos (v+\omega)\dot{E} \end{bmatrix} \tag{9.142}$$

With these equations, the LPE can be integrated numerically. Alternatively, if we can specify how C_D, A/M, and ρ vary, we could attempt a formal solution. We make the analogous solution to that for radiation pressure, assuming C_D and A/M constant, and obtain formal quadrature formulas for the perturbations after one revolution. These formulas are given in the inset on page 855. We see from the last two expressions of (9.143) that the direct perturbation in $M+\omega$ is quite small, the major change in M coming from

$$\delta n = (-3n/2a)\ \delta a$$

These expressions are used with numerical quadrature to obtain the evolution of mean elements. The implementation is done by Slowey (1974) for studying drag. Alternatively, taking Jacchia's (1960, 1964) density model, Sehnal and Mills (1966) have developed ρ in harmonic functions and obtained formulas for the periodic terms. These are sometimes used in analyses of satellite orbits. However, since for geodetic satellites the short-period drag terms are always less than 1 m, we can ignore them. The secular part is more conveniently absorbed in some constants of our orbital model. Therefore, the principal use of these formulas is in the

$$
\begin{aligned}
\delta a &= -C_D \frac{A}{M} a^2 \int_0^{2\pi} \rho(E) \frac{(1+e\cos E)^{3/2}}{(1-e\cos E)^{1/2}} \left(1 - d\frac{1-e\cos E}{1+e\cos E}\right)^2 dE \\
\delta e &= -C_D \frac{A}{M} \frac{(1-e^2)^{1/2} a}{2\pi} \int_0^{2\pi} \rho(E) \left(\frac{1+e\cos E}{1-e\cos E}\right)^{1/2} \left(1 - d\frac{1-e\cos E}{1+e\cos E}\right) \\
&\quad \left[\cos E - \frac{d}{2(1-e^2)}(1-e\cos E)(2\cos E - e - e\cos^2 E)\right] dE \\
\delta I &= \frac{1}{8\pi} C_D \frac{A}{M} \frac{a}{n} \dot{\theta} \sin I \frac{1}{(1-e^2)^{1/2}} \int_0^{2\pi} \rho(E)\,(1-e\cos E)^{1/2}\,(1+e\cos E)^{1/2} \\
&\quad \times \left(1 - d\frac{1-e\cos E}{1+e\cos E}\right)\left[1 + \cos 2\omega \frac{(2-e^2)\cos^2 E - 1 + 2e^2 - 2e - 2e\cos E}{(1-e\cos E)^2}\right] dE \\
\delta\Omega &= -\frac{1}{8\pi} C_D \frac{A}{M} \frac{a}{n} \frac{\dot{\theta} \sin 2\omega}{(1-e^2)^{1/2}} \int_0^{2\pi} \rho(E)\,(\mathrm{v} - e^2\cos^2 E)^{1/2} \\
&\quad \left(1 - d\frac{1-e\cos E}{1+e\cos E}\right)[2e^2 - 1 - 2e\cos E + (2-e^2)\cos^2 E] dE \\
\delta\omega &= -\cos I\, \delta\Omega \\
\delta M &= -(1-e^2)^{1/2}\, d\omega + \int \delta n\, dt
\end{aligned}
\qquad (9.143)
$$

analysis of long-period effects by numerical integration of these mean elements, along the same lines as those used for radiation pressure. In this case, we are able to make a reliable determination of drag factors, which could be systematic errors in the density model, or an estimate of C_D or A/M. These factors are generally between 0.5 and 1.5, which is less than the uncertainty of these parameters.

9.4.1.10 Computer Algebra

A great deal of the analysis used for satellite-perturbation theory involves considerable tedious algebra. One is led to do some of this work on a computer. A major support of the development of analytical theories has been the computer program Smithsonian Package for Algebra and Symbolic Manipulation (SPASM), described by Hall and Cherniack (1969), and Cherniack (1973) has contrasted it with other algebra systems. Since the subject of computer algebra is beyond the scope of this discussion, we confine ourselves to a few remarks and the description of two problems in satellite theory.

Algebra programs perform the elementary operations of addition, multiplication, subtraction, division, differentiation, and integration of a certain class of functions. We can define functions, make substitutions, and truncate on powers of designated parameters. We can examine expressions term by term and parenthesize and expand them. Numerical coefficients are kept as rational numbers where possible. One can read expressions in, print them out, or punch them as FORTRAN cards for subsequent numerical computation. We have two forms of internal representation—expressions and Poisson series. Each has its advantages. An expression may be

$$(ETA**2 - R)/E$$

The Poisson series are of the form

$$\sum A_i \begin{pmatrix} \sin \\ \cos \end{pmatrix} B_i$$

where A_i and B_i are any expressions. All the operations described apply to both expressions and Poisson series.

Poisson series have three advantages: (1) all trigonometric identities are automatically applied; (2) because of the highly structured nature of Poisson series, multi-

plication and addition can be optimized, and further, secondary computer storage can be used for long Poisson series; and (3) the bulk of problems in celestial mechanics is solved by developing the disturbing function in Poisson series and integrating term by term.

In addition to the operations described above, we can convert from expressions to Poisson series, and then back. Great efficiency is gained by judiciously choosing the form. Consider

$$(\cos^{20}x)^{30}-(\cos^{30}x)^{20}$$

As a trigonometric polynomial, this operation is trivial; as a Poisson series, it is not. We have here two very important features of computer algebra: the noncommutativity of operations with respect to time, and intermediate swell. The above expression is obviously zero, but one has two 50-term Poisson series along the way. Neither of these problems occurs in numerical work.

SPASM is 99 percent in FORTRAN; storage management is accomplished with SLIP, which is accessible from FORTRAN programs. We are concerned with the efficiency of SPASM and with the size and speed of the FORTRAN code generated. These are part of the more general problem of expression simplification.

Although general simplification seems to be very difficult, we have had some success with the following approach. We assume that the coefficients of Poisson series can be factored as the product of polynomials. Further, we want to consider the choice of variables. In developing perturbation theories, we convert to Poisson series all angle variables except the inclination. Therefore, we have the side relations

$$\eta^2+e^2=1$$

$$SI^2+CI^2=SIP^2+CIP^2=1$$

where we have substituted SI for sin (I), CI for cos (I), SIP for sin (IP), and CIP for cos (IP). The P designates the primed variables—in this case, the elements of the disturbing body (see sec. 9.4.1.7). We try each substitution, as indicated. It would be more direct to convert each coefficient of the Poisson series to a Poisson series, using $e=\sin\phi$, $\eta=\cos\phi$, in order to obtain all simplifications, and then to convert back to an expression. However, the substitution and the test for length of expression are easily done. We retain the expression that has the fewest terms and remove all common factors. Next, we assume that the remaining expression can be written

$$f\begin{pmatrix} e & SI & eP & SIP \\ \eta & CI & \eta P & CIP \end{pmatrix} = P_e\begin{pmatrix} e \\ \eta \end{pmatrix} P_I\begin{pmatrix} SI \\ CI \end{pmatrix} P_{e'}\begin{pmatrix} eP \\ \eta P \end{pmatrix} P_{I'}\begin{pmatrix} SIP \\ CIP \end{pmatrix}$$

where P_i is just a polynomial. In turn, by setting all the variables but one equal to zero, we obtain each polynomial. The results of factorization are then verified by expanding and subtracting. We have found that in this way we obtain all the simplifications that would have been obtained by hand.

SPASM has been used for a wide variety of problems. We describe here two of particular relevance to satellite theory: development of oblateness perturbations in Delaunay variables by the method of Von Zeipel, and third-body perturbations in Kepler elements by use of LPE.

Von Zeipel's method is described in section 9.4.1.8. Two features can be pointed out. First, once the determining function S is known, the perturbations are obtained by differentiation. Second, the first- and second-order determining functions can be obtained in closed form, as was done by Kozai (1962b) by a change of variable using

$$dv=(1/\eta^3)\ (a/r)^3\,dl$$

Both these operations are within the scope of SPASM, and the problem proved tractable.

The necessity of an accurate theory for J_2 was discussed in section 9.4.1.8. The development by Kozai (1962b) had been used, but

with such a complicated development that further verification was necessary. The details of the work are recounted by Gaposchkin *et al.* (1971, unpublished). The important results are the following:

(1) The problem proved tractable with an algebra program.

(2) The determining function of Kozai (1962b) has been verified, and the problem solved to second order.

(3) The accuracy of the theory and the inversion have been verified against numerical integration. The inversion was checked by use of the numerical inverse from (9.124).

(4) The difficulty with the small eccentricity remains. The third-order periodic perturbations were developed and were shown to contain $1/e$ terms. Numerical tests indicate $1/e^2$ terms in the fourth order. We conclude that this is due to the Delaunay variables we had selected.

(5) The development of computer algebra enabled us to obtain the third-order perturbations in 3 weeks; we would probably not have attempted it by hand.

(6) The perturbation theory was used in the orbit-computation program. The theory of Aksnes (1970) (see sec. 9.4.1.8) was also used; it gave identical results for orbital position, thus verifying both developments.

The second problem attempted is the perturbation due to a third body. In this case, we start with equation (9.89) (sec. 9.4.1.7 analytically develops that expression). Using the algebra program, we now determine $1/\Delta$ by analytical inversion. The basic idea, due to Broucke (1971), allows the inversion of invertible expressions; that is,

$$(E)^{-a/b}=Z$$

An iterative scheme is developed, with each iterant

$$Z_{n+1}-Z_n=\Delta Z_n=-\frac{a}{b}(EZ_n^{b/a}-1)\,Z_n$$

This is enormously powerful. Since we can invert any expression without division, it is applicable to computers without a divide instruction. In the case of lunar perturbations, we have $a/b=\frac{1}{2}$, where

$$E=(\bar{X}-Y)\cdot(\bar{X}-\bar{Y})$$

Here, $\bar{X}$ is the position of the satellite, and Y is the position of the Moon. We have

$$\bar{X}=r\begin{bmatrix}\cos u\cos\Omega-\sin u\sin\Omega\cos I\\ \cos u\sin\Omega+\sin u\cos\Omega\cos I\\ \sin u\sin I\end{bmatrix}$$

A similar expression for Y uses r', u', Ω', I'. With this expression, we perform the analytical inversion, starting with Z_0-1/r' and truncating on r^3. We have a simple check: The r/r'^2 are all canceled by the $(X\cdot Y)/|Y|^3$ term. The effects of body tides are easily introduced at this point by the substitution

$$r^n\rightarrow r^n+k_n\frac{a_e^{2n+1}}{r^{n+1}}$$

Next, the expressions are expanded with use of Hansen coefficients as described in section 9.4.1.5. The resulting expressions are then put in the LPE and integrated on the assumption that the angular variables, except the inclinations, have a linear change with time. The resulting expressions are simplified as described above.

In conclusion, we can say that computer algebra has been a successful tool for satellite-dynamics problems. It balances efficiency and expediency. The lunar perturbations were being used in the orbit computation program a month after the work started with SPASM, and we developed the third-order perturbation due to J_2 in 3 weeks. We can develop even more efficient programs by careful analysis (cf. formulas of Kozai (1962b) and Aksnes (1970)).

9.4.1.11 Orbit Determination and Parameter Estimation

The elaboration of an orbital theory, the main objective of the preceding sections, is but one of the four aspects of using satellite-tracking data to obtain ephemerides and

other information. We also have the data reduction, the relation between the observations and the parameters sought, and the estimation procedure.

We adopt Kepler elements as the orbital parameters to be determined. However, we choose to determine n, the mean motion, rather than a, as n is the best known of the orbital parameters. In addition, we recognize that the coefficients of the gravitational field and the nongravitational forces are imperfectly known, thus introducing model errors. We can reduce these errors to some extent by determining secular rates for each of the elements. Therefore, the uncertainty in the orbital model will be limited to the short-period perturbations.

The polynomial representations of the elements account for the bulk of the nongravitational forces, including the long-period effect of gravitational perturbations. The polynomials (mean elements) can be analyzed to obtain the zonal harmonics of the gravity field, some long-term resonant terms, and the reflective and drag properties of the satellites.

The basic relation used here is

$$\left.\begin{aligned} \bar{\rho} &= \bar{r} - R \\ \dot{\bar{\rho}} &= \frac{d}{dt}\bar{\rho} = \dot{\bar{r}} - \dot{R} \end{aligned}\right\} \quad (9.144)$$

where $\bar{\rho}$ is the topocentric station-to-statellite vector, $\bar{r}$ is the satellite position, and R is the station position. It is convenient to use this equation in the orbital system; therefore, R is given by (9.7) and $\bar{r}$ by (9.17). We generally observe $A\bar{\rho}$, where A is a transformation matrix. So we have

$$\mathcal{O} = \text{observation} = A\bar{\rho} = A\bar{r} - AR \quad (9.145)$$

In principle, any parameter that enters (9.145) can be determined from the observations, but it may not be unique.

There are basically four distinct types of observation to be considered: (1) optical directions given in a celestial reference frame (e.g., Baker-Nunn data); (2) direction observations in a topocentric reference frame (e.g., MINITRACK); (3) range observations (e.g., laser); and (4) range-rate observations (e.g., TRANET Doppler). The transformations for each type are as follows:

(1) Right ascension and declination:

$$\begin{bmatrix} \Delta\delta \\ \cos\delta\,\Delta\alpha \end{bmatrix} = \begin{bmatrix} -\cos\alpha\sin\delta & -\sin\alpha\sin\delta & \cos\delta \\ -\sin\alpha & \cos\alpha & 0 \end{bmatrix} \overline{\Delta\rho}$$

(2) Altitude (a), azimuth (A_z), range (ρ) are given in the inset below with ϕ, λ as the latitude and longitude of the observer, and ρ_x, ρ_y, ρ_z as the components of $\bar{\rho}$.

(3) Range:

$$\Delta\rho = \hat{\rho}\cdot\overline{\Delta\rho} = (\bar{\rho}/|\bar{\rho}|)\,\overline{\Delta\rho}$$

(4) Range rate:

$$\Delta\dot{\rho} = \hat{\rho}\cdot\overline{\Delta\dot{\rho}}$$

The domain of parameters to be determined can be expanded to include gravitational coefficients, station coordinates, GM, a scale factor for all stations, and the position of the Earth's pole of rotation. For unique

$$\begin{bmatrix} da \\ -\cos a\; d(A_z) \\ \dfrac{d\rho}{\rho} \end{bmatrix} = \left\{ \begin{bmatrix} -\sin A_z \sin a & -\cos A_z \sin a & \cos a \\ \cos A_z & \sin A_z & 0 \\ \rho_x/\rho & \rho_y/\rho & \rho_z/\rho \end{bmatrix} \begin{bmatrix} -\sin(\lambda+0) & \cos(\lambda+0) & 0 \\ -\cos(\lambda+0)\sin\phi & -\sin(\lambda+0)\sin\phi & \cos\phi \\ \sin(\lambda+0)\cos\phi & \sin(\lambda+0)\cos\phi & \sin\phi \end{bmatrix} \right\} \overline{\Delta\rho}$$

and meaningful results to be obtained, several orbits may have to be combined. This is most conveniently done by dealing with normal equations, which will be discussed later.

If we wish to determine any parameter p_i from observations, we use our elaborated theory for $\bar{r}$ and our initial estimate for p, p_i^0 and compute

$$C = A\bar{\rho} \qquad (9.146)$$

In general, the dependence of C on p_i is nonlinear and we must linearize. We want to find a correction to p_i that will reduce the difference between O and C; that is,

$$O - C = (\partial/\partial p_i) A\bar{\rho}\Delta p_i \qquad (9.147)$$

Now if A can be determined from the observation, we need only $\partial\bar{\rho}/\partial p_i$. For range rate, A depends on p_i, and the expressions are more involved. For those parameters influencing C through the orbit, we obtain

$$\frac{\partial\bar{r}}{\partial p_i} = \frac{\partial\bar{r}}{\partial\omega}\frac{\partial\omega}{\partial p_i} + \frac{\partial\bar{r}}{\partial\Omega}\frac{\partial\Omega}{\partial p_i} + \frac{\partial\bar{r}}{\partial I}\frac{\partial I}{\partial p_i} + \frac{\partial\bar{r}}{\partial e}\frac{\partial e}{\partial p_i} + \frac{\partial\bar{r}}{\partial M}\frac{\partial M}{\partial p_i} - \frac{2}{3}\frac{a}{n}\frac{\partial\bar{r}}{\partial a}\frac{\partial n}{\partial p_i}$$

Now, from Izsak (1962) and Gaposchkin (1966*a*, p. 107), we have

$$\partial\bar{r}/\partial\omega = \hat{e}_n \times \bar{r}$$

$$\partial\bar{r}/\partial\Omega = \hat{e}_z \times \bar{r}$$

$$\partial\bar{r}/\partial I = r \sin u \hat{e}_n$$

$$\partial\bar{r}/\partial e = (\hat{e}_n \times \bar{r})\ (a/r)\ [\sin E/(1-e^2)^{1/2}] - \bar{a}$$

$$\partial\bar{r}/\partial M = 2\pi\bar{r}/n$$

$$\partial\bar{r}/\partial a = \bar{r}/a$$

where

$$u = v + \omega$$

$$\hat{e}_n = \begin{bmatrix} \sin I \sin\Omega \\ -\sin I \cos\Omega \\ \cos I \end{bmatrix}$$

$$\hat{e}_z = \begin{bmatrix} 0 \\ 0 \\ 1 \end{bmatrix}$$

expressed in the orbital system. For example, if $p_i = \omega_0$, the constant of perigee is then $\partial\omega/\partial p_i = 1$, the other being zero. If $p_i = \bar{C}_{lm}$, then with $C_{lm} = 1$

$$\partial\omega/\partial C_{lm} = \sum_p \sum_q \Delta\omega_{lmpq}$$

$$\partial\Omega/\partial C_{lm} = \sum_p \sum_q \Delta\Omega_{lmpq}$$

and so on. If $p_i = GM$, then

$$\partial\bar{r}/\partial(GM) = \frac{1}{3}\bar{r}/GM$$

If we want to determine station coordinates, we have

$$R = R_3(-\theta)\, R(y,x,0)\, X_0$$

giving

$$\left[\left[\frac{\partial\bar{\rho}}{\partial X}\right], \left[\frac{\partial\bar{\rho}}{\partial Y}\right], \left[\frac{\partial\bar{\rho}}{\partial Z}\right]\right] = -R_3(-\theta)\, R(y,x,0) \begin{bmatrix} 1 & 0 & 0 \\ 0 & 1 & 0 \\ 0 & 0 & 1 \end{bmatrix}$$

If we want a scale factor α for all stations—that is, $\overline{\Delta R} = \alpha\bar{R}_0$—we have

$$\partial\bar{\rho}/\partial\alpha = -R_3(-\theta)\, R(y,0)\, X_0$$

To determine the polar motion, we have

$$\frac{\partial\bar{\rho}}{\partial y}\begin{bmatrix} \sin\theta Z_0 \\ -\cos\theta Z_0 \\ Y_0 \end{bmatrix}$$

$$\frac{\partial\bar{\rho}}{\partial x}\begin{bmatrix} \cos\theta Z_0 \\ \sin\theta Z_0 \\ -X_0 \end{bmatrix}$$

If we have the instantaneous coordinate

$$R=\begin{bmatrix} X \\ Y \\ Z \end{bmatrix}$$

of the station, then

$$X_0 = X\cos\theta + Y\sin\theta$$

$$Y_0 = -X\sin\theta + Y\cos\theta$$

$$Z_0 \approx Z$$

The data reduction falls into two parts: those reductions necessary for all data, and those related to particular data types.

All data must be expressed in the same time system. For orbital computation, we need a uniform time system, and so we have chosen AS, an atomic time system, as a standard. The differences between AS and A3 and between AS and A1 are

$$\text{AS} - \text{A1} = 0.8983 \text{ msec}$$

$$\text{AS} - \text{A3} = 35.4 \text{ msec}$$

Although these values change slowly, the adopted constants are sufficient for data taken between 1965 and 1971. Numerical values of AS−UTC are given in the form of polynomials and are published (e.g., Gaposchkin, 1972).

We must also know the physical point to be associated with each time. For optical data, the time detected is that of receiving the light. The orbital position corresponds to an earlier time, the difference being the travel time of light. For a flashing-light satellite, the flash times are given at the satellite. Nominal values of range are sufficient for correcting the time associated with the satellite position. With ranging data, we often have the time of firing of the laser—that is, the time of transmission—and therefore the satellite time is later by the travel time. In all cases, we must know precisely what the satellite position time is.

We have a similar situation with the station position. The position of the Earth is a measured quantity given in terms of UT1. We must use the actual value of UT1 to compute the sidereal angle in (9.7). The time associated with the station is the received time for optical observations, but it is the satellite time for range observations. The satellite time corresponds to the average position of the station during the round trip of the signal.

Data from cameras must be reduced to the adopted reference system by use of (9.8). In addition, we must apply annual aberration and parallactic refraction. The first is usually applied during film reduction, and parallactic refraction is computed from

$$\Delta R = [(0.435\times 0.484813\times 10^{-5})/\rho]\,(\tan z/\cos z)\,[1-\exp(-138.5\,\rho\cos z)]$$

where ρ is the topocentric range in megameters, z is the zenith angle, and ΔR is the correction in radians. Now we have

$$\Delta\delta = -\Delta R\cos q$$

$$\Delta\alpha = -\Delta R\sin q/\cos\delta$$

where q is the parallactic angle measured in a positive (clockwise direction) from the object to the great circle through the pole (Veis, 1960, p. 119). This correction is based on standard pressure and temperature. If measured values are available, a better value can be obtained by taking mean nighttime data. A table of corrections is given in Gaposchkin (1972).

For laser range observations, we make a correction for the tropospheric refraction and for the geometry of the satellite. The refraction correction becomes (Lehr, 1972)

$$\Delta r = -\frac{2.238+0.0414\,(P/T)-0.238\,h_s}{\sin\alpha+10^{-3}\cot\alpha}$$

where P is the atmospheric pressure (mb) at the laser station, T is the temperature (K), h_s is the elevation above mean sea level (km), and α is the elevation angle of the satellite. This formula holds true for light

from a ruby laser at 694 nm when the apparent elevation angle is greater than 5°.

The accuracy of data from laser systems is connected with the physical size of the satellite equipped with corner reflectors. Arnold (1972) (unpublished) gives in tabular form a correction to reduce the observed range to the center of mass of the satellite as a function of angle of incidence. By use of these data, all observations by laser systems can be reduced to the center of mass.

Equation (9.147) will, in general, be overdetermined, and so we use the method of least squares to obtain an estimate of the unknowns. The general references are Arley and Buch (1950) and Linnik (1961). By collecting normal equations, we can merge the observations from many orbital arcs.

In the least-squares estimate, the weight or accuracy of each observation must be established a priori. For the estimation process, only the relative accuracy is important; however, one can have greater confidence if the standard error of unit weight comes to be unity.

For the weighting, we assume that the errors are uncorrelated, probably not a bad assumption with data taken over several years. We have given each observation an individual weight, as described in table 9.10.

In addition, where there were more than 30 points in a pass of laser data, 30 points were chosen, evenly distributed through the pass. Some numerical tests indicate this was no worse than if we had averaged the points.

Finally, the process of parameter estimation must be iterative, for two reasons: The model is nonlinear, and gross observation errors must be discarded. On each iteration, the computation discards data on a 3σ criterion; that is, a point is discarded if

$$(O-C)\sqrt{w}>3\sigma \quad .$$

where w is the weight, and σ is the standard deviation at the last iteration. The process is said to converge or stabilize when

$$|(\sigma_n-\sigma_{n-1})/\sigma_n|<0.01$$

9.4.2 Coordinates

(E. M. Gaposchkin, J. Latimer, and G. Veis)

A number of approaches can be used to determine the position of points on the Earth's surface. Of these, we have chosen tracking of close-Earth satellites, deep-space probes, and surface-triangulation measurements for this analysis. The data and the method of analysis have been selected to optimize the results for a global network of reference points.

The satellite methods separate nicely into two distinct types of analysis: geometrical and dynamical. The former hinges on making simultaneous observations of a satellite from two or more points on the earth's surface. When these are camera observations, the vector connecting the two stations must lie in the plane defined by the two observed directions. A number of independent simultaneous observations will define the direction between the two stations. The Smithsonian Astrophysical Observatory (SAO) has obtained a sufficient number of simultaneous observations to determine a network for its stations. The National Ocean Survey (NOS) of the National Oceanic and Atmospheric Administration (NOAA) has carried out a program of observations with the BC–4 camera to establish a global geometrical network.

Alternatively, the dynamical analysis assumes that the satellite's orbit is known, and computes the location of the observing station from individual observations. In practice, the orbit is determined from the same observations. The orbital mode has been used by SAO to analyze tracking data on close-Earth satellites and by the Jet Propulsion Laboratory (JPL) to analyze tracking data on deep-space probes.

Surface-triangulation measurements are reduced by organizations such as the U. S. Coast and Geodetic Survey (now NOS) and the Army Map Service (now DMA/TC), who publish coordinates of given points referred to a datum that, in general, has an arbitrary origin, orientation, and scale. The relative positions of stations are determined from these data.

The main objectives of this analysis were the following:

(1) To improve the accuracy of the fundamental stations. Heretofore (SE II), the accuracy was estimated as 5 to 10 m.

(2) To improve the distribution of reference points or tracking sites. In SE II, coordinates were obtained for 39 independent sites.

(3) To use the latest available data. New data included the complete BC–4 network and all the laser tracking data taken during the International Satellite Geodesy Experiment (ISAGEX) program. Surface-triangulation data were used as observations rather than as constraints.

The analysis assumes that the stations form a fixed system (i.e., there is no relative motion), that the pole position and the instantaneous position of the Earth are known without error from numerical values published by the International Polar Motion Service (IPMS) and the Bureau International de l'Heure (BIH), that the error in observing time is random, and that Atomic Time is a satisfactory system for ephemeris calculations.

9.4.2.1 Geometrical Solution

In deriving a geometrical solution, the objective was to produce a system of normal equations for use in combination with other data. The data consisted of direction observations only, and there is no scale information in the geometric net. Nor is there any information to locate the origin of a geometrical network. Hence, any purely geometrical solution with these data would require an arbitrary scale and origin. The combination of normal systems avoids this problem, as other data sets contain scale and origin information. The result of an unscaled, purely geometrical solution is a set of interstation directions, independent of the arbitrary scale and origin introduced.

The computation was divided into two stages. First, all data between pairs of stations were used to determine, by least squares, the interstation direction and its covariance matrix for each pair. The mathematical model for determining this direction uses the condition that the interstation direction (u_3) and the two directions from the stations to the satellite (u_1, u_2) must be coplanar:

$$\hat{u}_1 \cdot \hat{u}_2 \times \hat{u}_3 = 0 \qquad (9.148)$$

A system of first-order Taylor expansion approximations to equation (9.148) is solved by least squares to determine u_3 and its 2×2 covariance matrix. In order for truly simultaneous directions (u_1, u_2) to be obtained, synthetic observations were computed by interpolation from a series of observations overlapping in time from two stations (Aardoom *et al.*, 1966).

The synthetic observations (u_1, u_2) were weighted according to the quadratic fit of the individual observations used to determine the synthetic ones. The weight was modified according to SE II to account for the possibility of systematic errors, principally in station timing. Separate synthetic observations were considered to be uncorrelated. For BC–4 data, the NOS has derived seven simultaneous observations from each photographic plate (event) with the associated 14×14 covariance matrix for each set of directions. These were the data provided and used to determine u_3.

The data were then screened. When the adjustments to u_1 and u_2 (corrections to the observations) were judged to be too large with respect to the remaining data for that interstation direction, those points were deleted and the direction redetermined. For the SAO block, 68 directions were determined, and for the BC–4 group, 152.

The second stage consisted of a network adjustment for each data block. The mathematical model for stage two is that of variation of coordinates:

$$\mathbf{u}_1 - \mathbf{u}_2 - \mathbf{u}_3 = 0$$

where $\mathbf{u}_1$ is the vector from station 1 to the satellite, $\mathbf{u}_2$, is that from station 2 to the satellite, and $\mathbf{u}_3$ is the interstation vector.

Satellite positions are eliminated, and we obtain a solution for station coordinates, thus deriving adjusted interstation directions. This is equivalent to adjusting the directions directly by using the coplanarity condition for each triangle formed by observed directions between three stations. The advantage of this normal system is that it refers to coordinates, not directions, and can be readily combined with other normal systems for station coordinates. These directions are given in table 9.25.

We had available for comparison the interstation directions and their accuracy estimates σ_1^2 resulting from simultaneous-observation data and also the new directions and accuracy estimates σ_2^2 resulting from the network adjustment. Table 9.26b lists σ_1^2, σ_2^2, and the square of the difference δ^2 between the two estimates of the interstation direction.

We expected that, on the average, for the interstation direction adjustment δ,

$$\delta^2 \leq (\sigma_1^2+\sigma_2^2)/2$$

To satisfy this condition, we must multiply the variance estimates by a factor

$$k^2 = \frac{\delta^2}{(\sigma_1^2+\sigma_2^2)/2}$$

From table 9.26b the average value for k^2 is 2.65, and the accuracy estimates for the geometrical solution are scaled by this number. A similar analysis of the BC–4 network (see table 9.26a) gives an average value for k^2 of 2.60.

9.4.2.2 Dynamical Solution

An observation θ of direction, right ascension and declination, or range can be related to the satellite position $\bar{r}(t)$ and to the station position X by

$$\theta = [A]\,[\bar{r}(t) - R(\theta,x,y)\,X] \quad (9.149)$$

In general, A is an easily computed transformation matrix. Further, the orbit $\bar{r}(t)$ depends on the orbital elements, the gravitational field, the atmospheric density, solar and lunar gravitational attraction, and radiation pressure. Finally, equation (9.149) depends on UT1—i.e., the sidereal angle θ—and on the pole position x and y. None of these quantities is known without error and each, in itself, provides a number of difficult problems. For a certain class of satellites, the Earth's gravitational field presents the major source of error but is improved as part of the analysis described above.

Two types of data have been used in the dynamical solution. Observations of direction are made by photographing the satellite against a star background. The star positions then define the direction from the observing station to the satellite in the coordinates of right ascension and declination. The star positions are taken from a catalog and refer to its epoch. Precession and nutation are therefore applied to refer the observation to the reference system desired. For reasons related to the orbital theory for $\bar{r}(t)$, we have chosen to work in the quasi-inertial reference system defined by the equinox of 1950.0 and the equator of date. In addition, UT1 and pole positions are applied to bring the terrestrial reference frame, defined by the Conventional International Origin and the zero meridian of the BIH, into this system. Therefore, orbital elements and station positions are expressed in this quasi-inertial reference system when determined with direction observations. Specifically, the right ascension of the ascending node of the satellite (hereafter called the node) is unambiguously defined.

Observations of range relate the relative position of the satellite to the observer and not to the reference system; i.e., the observation is unchanged if the reference system is transformed by translation or rotation. Specifically, the node is defined only relative to the adopted value of +UT1. Therefore, when only observations of range (and velocity) are used, a correction for the longitude must be allowed for in each orbit. This is accomplished with the following device. In gen-

eral, the normal system for each orbit has the form

$$\begin{Bmatrix} N & B \\ B^T & C \end{Bmatrix} \begin{Bmatrix} \overline{\Delta X} \\ \overline{\Delta p} \end{Bmatrix} = \begin{Bmatrix} \bar{a} \\ \bar{b} \end{Bmatrix} \quad (9.150)$$

where $\overline{\Delta X}$ are the corrections to the station coordinates, and $\overline{\Delta p}$ are the corrections to the orbital elements.

It has been observed that with direction observations, $B \approx 0$, and so the interactions between orbital elements and station coordinates can be ignored. For observations of range, we form the set of reduced normal equations

$$[N - BCB^T]\overline{\Delta X} = \bar{a} - BC\bar{b} \quad (9.151)$$

These equations eliminate the correction $\overline{\Delta p}$ while preserving the interactions between $\overline{\Delta p}$ and $\overline{\Delta X}$. This set of reduced normal equations can be added to another set, and the solution for $\overline{\Delta X}$ can be used to determine $\overline{\Delta p}$ if so desired. The complete set of $\overline{\Delta p}$ was computed and found to be very small. The same device is used in processing simultaneous observations to eliminate the satellite position from each simultaneous observation. In summary, orbits determined by direction observations were processed directly by assuming $B = 0$. Those orbits based primarily on range data were reduced by means of equation (9.151).

9.4.3 Gravitational Field

9.4.3.1 Analysis of Satellite Orbital Data

(E. M. Gaposchkin, M. R. Williamson, Y. Kozai, and G. Mendes)

The external potential of the Earth is represented by a set of orthogonal functions:

$$\mathcal{U} = \mathcal{R}e \frac{GM}{r} \sum_{l=0}^{\infty} \sum_{m=0}^{l} \left(\frac{a_e}{r}\right)^l \bar{C}_{lm} \bar{P}_{lm}(\sin\phi)\, e^{im\lambda} \quad (9.152)$$

where M is the mass of the Earth, including the atmosphere; G is the universal constant of gravitation; $C_{lm} = C_{lm} - iS_{lm}$; $\bar{C}_{l0} = -J_l/\sqrt{2l+1}$; $\mathcal{R}e\ \{\ \}$ designates the real part of $\{\ \}$; $\bar{P}_{lm}(\sin\phi)$ are fully normalized associated Legendre polynomials; and r, ϕ, λ are the coordinates of the test particle. It is possible to choose a coordinate system such that

$$\bar{C}_{2,0} = \bar{C}_{1,1} = \bar{C}_{2,1} = 0 + i0$$

and we assume that the instantaneous spin axis as defined by the International Polar Motion Service and the center of gravity of the Earth are that system. This assumption is not strictly true, but the departures are small and are ignored in this analysis.

It is observed that for the Earth the amplitude of $E(|\bar{C}_{lm}|)$ decreases uniformly according to

$$E(|\bar{C}_{lm}|) = \frac{10^5}{l^2} \quad (9.153)$$

Although for theoretical reasons $E(|\bar{C}_{lm}|)$ must decrease more rapidly than equation (9.153) at some point, and individual coefficients can be arbitrarily large, this rule seems valid throughout the range of l used in this investigation.

We use two types of data on the Earth's gravity field: those derived from gravimeters and those obtained from the motion of artificial satellites. The gravity calculated from the gradient of equation (9.152) is

$$\Delta g = \gamma \mathcal{R}e \sum_{l=2}^{\infty} \sum_{m=0}^{l} (l-1)\left(\frac{a_e}{r}\right)^l \bar{C}'_{lm} \bar{P}_{lm}(\sin\phi)\, e^{im\lambda} \quad (9.154)$$

where $\gamma = GM/r^2$ and $\bar{C}'_{lm}$ are $\bar{C}_{lm}$ modified to accommodate those effects of the reference ellipsoid (or gravity formula) that change the definition of $\bar{C}_{2,0}$, $\bar{C}_{4,0}$, and $\bar{C}_{6,0}$. Comparing equations (9.152) and (9.154) makes it apparent that Δg is more influenced by $\bar{C}_{lm}$ of high degree and order than is $\mathcal{U}$ and that measurements of Δg are more useful for

determining these high-degree and high-order coefficients.

Determination of $\bar{C}_{lm}$ from analysis of satellite observations requires a theory for satellite motion. General solutions for the motion in an arbitrary potential field have not yet been found. We must therefore restrict ourselves to approximate solutions, which are quite sufficient for the following reasons. It is observed that for the Earth, the second-degree zonal harmonic $\bar{C}_{2,0}$ makes the largest contribution to the anomalous potential and is 10^{-3} of the main term. The remaining anomalous potential is 10^{-3} of $\bar{C}_{2,0}$, or 10^{-6} of the main term. Therefore, to calculate the trajectory to 10^{-6} (our objective), we require at least a second-order theory for $\bar{C}_{2,0}$ (i.e., one including $\bar{C}_{2,0}$), but only a first-order linear theory for the remaining $\bar{C}_{lm}$. Although there are notable exceptions—resonances and some zonal harmonics—these considerations provide a workable base.

The Earth's motion is complicated because of precession, nutation, polar motion, and rotation. A convenient reference frame is defined by the stars and, in practice, is defined (imperfectly) in terms of a star catalog at some epoch. On the other hand, in an inertial frame, the Earth's gravity field has a temporal variation that significantly complicates the construction of an analytical theory. For this reason, a compromise quasi-inertial reference frame referred to an equinox (epoch 1950.0) and an equator (epoch of date) has been adopted. Veis (1960a) knew, Kozai (1960) proved, and we have used the fact that this coordinate system minimizes the additional effects required to account for the temporal variations of the gravity field and the noninertial property of the coordinate system.

Accordingly, the determination of $\bar{C}_{lm}$ from analysis of satellite observations uses the elaboration of a satellite perturbation theory. This elaboration is too lengthy to detail here, so we confine ourselves to a few remarks. The perturbation theory is developed by expressing equation (9.152) in terms of satellite coordinates (a, the semimajor axis; e, the eccentricity; I, the inclination; ω, the argument of perigee; Ω, the right ascension of the ascending node; and M, the mean anomaly). If we express equation (9.152) as

$$\mathcal{U}=\sum_{l=0}^{\infty}\sum_{m=0}^{l}\mathcal{U}_{lm} \tag{9.155}$$

we can write

$$\mathcal{U}_{lm}=\mathcal{R}e\sum_{p=0}^{l}\sum_{q=-\infty}^{\infty}\bar{C}_{lm}A_{lmpq}(a,e,I)\,e^{i\psi} \tag{9.156a}$$

where

$$A_{lmpq}(a,e,I)=\frac{GM}{a}\left(\frac{a_e}{a}\right)^l D_{lmp}(I)\,G_{lpq}(e) \tag{9.156b}$$

and

$$\psi=(l-2p)\,\omega+(l-2p+q)\,M+m\,(\Omega-\theta)+(l-m)\,\frac{\pi}{2} \tag{9.156c}$$

These four equations are the exact equivalent of equation (9.152). Expressed in this way, the variables with large secular change (ω, Ω, M) are separated from those with only periodic changes (a, e, I). Therefore, the functions $A_{lmpq}(a,e,I)$ can, with sufficient accuracy, be considered constant. In addition, $G_{lpq}(e)\approx 0(e^{|q|})$. Since satellites of interest have small or modest eccentricity, only a few terms in the sum over q are necessary. The number of terms is selected automatically for each satellite by means of a numerical test; typically, $|q|<5$ is sufficient.

The differential equations relating the disturbing potential and the changes in orbital elements are known as the Lagrange planetary equations, a set of simultaneous ordinary differential equations of the form

$$\frac{d}{dt}\mathcal{E}^k=\mathcal{L}^k(a,e,I)\,\mathcal{U} \tag{9.157}$$

where $\mathcal{E}^k$ is a generic element, $\mathcal{L}^k(a,e,I)$ is a linear differential operator, and $\mathcal{U}$ is the disturbing potential. If we assume that the

interaction of perturbations can be ignored, then we can write

$$\mathcal{E}^k = \mathcal{E}_0^k + \sum_{l=2}^{\infty} \sum_{m=0}^{l} \delta\mathcal{E}_{lm}^k \qquad (9.158)$$

where $\mathcal{E}_0^k$ is the unperturbed element. This is an excellent assumption except for $\bar{C}_{2,0}$. The secular changes in ω, Ω, and M due to $\bar{C}_{2,0}$ interact significantly with all the perturbations, and so for these angles variables, we use

$$\mathcal{E}^k = \mathcal{E}_0^k + \dot{\mathcal{E}}^k t + \sum_{l=2}^{\infty} \sum_{m=0}^{l} \delta\mathcal{E}_{lm}^k \qquad (9.159)$$

Substituting (9.155), (9.156), (9.158), and (9.159) into (9.157), formally expanding the resulting equation, and discarding all interactions on the right-hand side, we obtain

$$\frac{d}{dt}\delta\mathcal{E}_{lm}^k = \mathcal{R}e\, \mathcal{L}^k(a_0,e_0,I_0) \times \sum_{p=0}^{l} \sum_{q=-\infty}^{\infty} \bar{C}_{lm} A_{lmpq}(a_0,e_0,I_0)\, e^{i\psi_0} \qquad (9.160a)$$

where

$$\psi_0 = (l-2p)(\omega_0+\dot{\omega}t) + (l-2p+q)(M_0+nt) + m(\Omega_0+\dot{\Omega}t-\theta) + (l-m)\frac{\pi}{2} \qquad (9.160b)$$

Here, $\dot{\omega}$, n, and $\dot{\Omega}$ are the secular rates of ω, M, and Ω. The rotation of the Earth is sufficiently uniform so that we can write

$$\theta = \theta_0 + \dot{\theta}t \qquad (9.161)$$

Finally, $\delta\mathcal{E}_{lm}^k$ is the perturbation in element $\mathcal{E}^k$ due to the potential coefficient $\bar{C}_{lm}$. Equations (9.160) are now uncoupled differential equations, which can be integrated immediately to

$$\delta\mathcal{E}_{lm}^k = \mathcal{R}e\, \mathcal{L}^k(a_0,e_0,I_0) \sum_{p=0}^{l} \sum_{q=-\infty}^{\infty} \bar{C}_{lm} A_{lmpq}(a_0,e_0,I_0) \frac{e^{i[\psi_0-(\pi/2)]}}{\dot{\psi}_0} \qquad (9.162a)$$

$$\dot{\psi}_0 = (l-2p)\dot{\omega} + (l-2p+q)n + m(\dot{\Omega}-\dot{\theta}) \qquad (9.162b)$$

The general properties of the solution are now apparent. We see that $\dot{\psi}$ can be exactly zero only when $m=0$. Therefore, only even zonal harmonics $\bar{C}_{l0}$ can cause secular perturbations. The period of the periodic terms is given by equation (9.162b), and we see from equation (9.162a) that the longer the period is, the larger the perturbation. Thus, when $m=0$, long-period terms with argument ω, 2ω, 3ω, . . . occur when $q=-1, -2, -3, \ldots$. For nonzonal harmonics, long-period, large-amplitude perturbations arise when $\dot{\psi} \approx 0$. Since $n(\approx 13 \text{ rev day}^{-1}) > \dot{\theta}(\approx 1 \text{ rev day}^{-1}) \gg \dot{\omega}, \dot{\Omega} \propto \bar{C}_{2,0}\, n = 10^{-3}n$, this resonance condition occurs when $n \approx m\dot{\theta}$—that is, when the mean motion n is approximately an integral number (the order m) of revolutions per day. In fact, resonant conditions always exist to some extent. Resonant terms occur in both satellite theory and planetary theory, and there is extensive literature on the subject (e.g., Kaula, 1966b; Hagihara, 1961a), but as yet there is no completely satisfactory treatment. It is true, for example, that a solution such as that employed here by using linearized equations can be invalid for some cases, since the series are not uniformly convergent; fortunately, this does not occur here. The occurrence of resonances between the field of the Earth and a satellite has been viewed as an opportunity to determine particular harmonics to high precision. In fact, some of the low-degree harmonics have been studied extensively with synchronous satellites, and many harmonics of orders 12, 13, and 14 have been determined by SAO and others. Long-period terms in ω, 2ω, 3ω, . . . from the zonal harmonics are resonant perturbations in the sense of the term as discussed here. Satellites with strong resonances interact with the field to $l=35$ and higher. Finally, we have seen that the largest perturbations result when equation (9.162b) is smallest. With $m=0$, the largest terms are for $l-2p+q=0$—that is, there is no dependence on M. Therefore,

long-period terms can be analyzed. For $m \neq 0$, the largest effects are also without M. In this case, the frequency is m oscillations per day, and the first-order term will be the largest. Terms for $m = 8$—that is, eight oscillations per day—become very difficult to determine, and reliable values for $m \geq 10$ can be obtained only by the study of resonances or from terrestrial gravimetry.

The formal theory, equation (9.162), accounts for both resonances and short-period terms. For example, the resonant perturbation in mean anomaly for satellite 5900701 is

$$\delta M = \bar{C}_{11,11}\left\{-1.387\times 10^{2}\cos\left[\frac{2\pi}{35.8}(t-t_0)\right] - 1.798\times 10^{5}\cos\left[\frac{2\pi}{1124.8}(t-t_0)\right]+\cdots\right\} \tag{9.163}$$

with similar terms for $\bar{S}_{11,11}$, $\bar{C}_{12,11}$, ... The 1124-day term is much longer than any span of data for one orbit. Because we have imperfect knowledge of the coefficient $\bar{C}_{11,11}$, the empirically determined orbit will absorb the residual 1124-day term into the mean elements. The mean elements can be analyzed for improvements to the field in the same way as is done for zonal harmonics.

Because most of the zonal harmonics give rise to short-period perturbations, the residuals of individual observations are analyzed to determine these field coefficients. Since we are dealing with instantaneous observations of position, the observation equation is of the form

$$\Delta X = \left(\frac{\partial \bar{r}}{\partial M}\frac{\partial \delta M}{\partial \bar{C}_{lm}} + \frac{\partial \bar{r}}{\partial \omega}\frac{\partial \delta \omega}{\partial \bar{C}_{lm}} + \cdots\right)\Delta \bar{C}_{lm} \tag{9.164}$$

As an example, the perturbations in M for satellite D1D are given on page 868 for only the principal terms, with $m = 1,2$; $l = 3,4,5,6,7,8$. For this satellite, $a = 7614$ km, $e = 0.0843$, and $I = 39°.455$.

Even if we assume the satellite to be a perfect filter, uncontaminated by other model errors, and the tracking data and analysis process to be perfect, we see that with one satellite, we can determine only spectral components that are linear combinations of the gravity field ($\bar{C}_{lm}$) and functions of orbital elements [$A_{lmpq}(a,e,I)$]. From each satellite, we obtain one or two linear combinations of harmonics for l odd and for l even. With additional data, we can only refine the numerical value of these linear combinations. The coefficients of the relations will depend on the orbital elements, so that other linear combinations can be determined only from additional distinct orbits. Generally, this is achieved by selecting satellites with different inclinations, but independent linear relations can also be obtained with changes in eccentricity or semimajor axis.

As the degree increases, the perturbations become negligible, and so the linear relation does not involve an infinite number of parameters. Of course, the spectrum analysis gives both amplitude and phase, or, as generally written, $\bar{C}_{lm}$.

From equation (9.166), we see that one linear combination of $\bar{C}_{3,1}$, $\bar{C}_{5,1}$, $\bar{C}_{7,1}$, . . . can be determined from the -1.001-day period term and another of equal size from the -0.971-day term. The third term is a factor of 10 smaller and will not contribute significantly as an observation equation; there are also many smaller terms. The linear combination of $\bar{C}_{3,2}$, $\bar{C}_{5,2}$, $\bar{C}_{7,2}$, . . . has only one significant spectral component for the -0.327-day period.

The linear relations are not determined with equal accuracy; for example, the resonant harmonics have a very large effect and the spectral component is strongly determined. However, the resonant period is commensurate with the arc length, which will cover only a small number of cycles. This makes it difficult to separate nearly commensurate periods.

If we consider equations (9.162) as expressing the spectral decomposition of the perturbation, we see that each harmonic $\bar{C}_{lm}$ of order m causes the same spectrum of perturbations. Further, the spectrum has several lines close together. With a short

$$
\begin{aligned}
\delta M = {} & \bar{C}_{3,1}[-7.1\sin(\omega+\Omega-\theta)+0.8\sin(\omega+2M+\Omega-\theta)-63.3\sin(-\omega+\Omega-\theta)+\cdots] \\
& +\bar{C}_{3,2}\{-42.5\cos[\omega+2(\Omega-\theta)]+10.5\cos[\omega+2M+2(\Omega-\theta)]-13.6\cos[-\omega+2(\Omega-\theta)]+\cdots\} \\
& +\bar{C}_{4,1}[7.0\cos(-M+\Omega-\theta)-8.2\cos(M+\Omega-\theta)+5.1\cos(-2\omega+\Omega-\theta)+\cdots] \\
& +\bar{C}_{4,2}\{-10.3\sin[-M+2(\Omega-\theta)]+14.2\sin[M+2(\Omega-\theta)]+\cdots\} \\
& +\bar{C}_{5,1}[-87.4\sin(\omega+\Omega-\theta)+6.9\sin(\omega+2M+\Omega-\theta)+87.9\sin(-\omega+\Omega-\theta)+\cdots] \\
& +\bar{C}_{5,2}\{8.6\cos[\omega+2(\Omega-\theta)]-1.4\cos[\omega+2M+2(\Omega-\theta)]+43.9\cos[-\omega+2(\Omega-\theta)]+\cdots\} \\
& +\bar{C}_{6,1}[5.1\cos(-M+\Omega-\theta)-6.0\cos(M+\Omega-\theta)-16.2\cos(-2\omega+\Omega-\theta)+\cdots] \\
& +\bar{C}_{6,2}\{5.4\sin[-M+2(\Omega-\theta)]-7.4\sin[M+2(\Omega-\theta)]+\cdots\} \\
& +\bar{C}_{7,1}[33.1\sin(\omega+\Omega-\theta)+0.0\sin(\omega+2M+\Omega-\theta)+1.4\sin(-\omega+\Omega-\theta)+\cdots] \\
& +\bar{C}_{7,2}\{40.0\cos[\omega+2(\Omega-\theta)]-5.5\cos[\omega+2M+2(\Omega-\theta)]-40.3\cos[-\omega+2(\Omega-\theta)]+\cdots\} \\
& +\bar{C}_{8,1}[-6.8\cos(-M+\Omega-\theta)+7.9\cos(M+\Omega-\theta)+19.1\cos(-2\omega+\Omega-\theta)+\cdots] \\
& +\bar{C}_{8,2}\{4.1\sin[-M+2(\Omega-\theta)]-5.7\sin[M+2(\Omega-\theta)]+\cdots\}
\end{aligned}
\tag{9.165}
$$

We can rearrange this expression in terms of the same frequency (with the period P of each term in days given in parentheses):

$$
\begin{aligned}
\delta M = {} & (-7.1\bar{C}_{3,1}-87.4\bar{C}_{5,1}+33.1\bar{C}_{7,1}+\cdots)\sin(\omega+\Omega-\theta) && (-1.001\text{ day}) \\
& +(0.8\bar{C}_{3,1}+6.9\bar{C}_{5,1}+0.0\bar{C}_{7,1}+\cdots)\sin(\omega+2M+\Omega-\theta) && (0.040) \\
& +(-63.3\bar{C}_{3,1}+87.9\bar{C}_{5,1}+1.4\bar{C}_{7,1}+\cdots)\sin(-\omega+\Omega-\theta) && (-0.971) \\
& +(7.0\bar{C}_{4,1}+5.1\bar{C}_{6,1}-6.8\bar{C}_{8,1}+\cdots)\cos(-M+\Omega-\theta) && (-0.071) \\
& +(-8.2\bar{C}_{4,1}-6.0\bar{C}_{6,1}+7.9\bar{C}_{8,1}+\cdots)\cos(M+\Omega-\theta) && (0.083) \\
& +(5.1\bar{C}_{4,1}-16.2\bar{C}_{6,1}+19.1\bar{C}_{8,1}+\cdots)\cos(-2\omega+\Omega-\theta) && (-0.958) \\
& +(-42.5\bar{C}_{3,2}+8.6\bar{C}_{5,2}+40.0\bar{C}_{7,2}+\cdots)\cos[\omega+2(\Omega-\theta)] && (-0.497) \\
& +(10.5\bar{C}_{3,2}-1.4\bar{C}_{5,2}-5.5\bar{C}_{7,2}+\cdots)\cos[\omega+2M+2(\Omega-\theta)] && (0.041) \\
& +(-13.6\bar{C}_{3,2}+43.9\bar{C}_{5,2}-40.3\bar{C}_{7,2}+\cdots)\cos[-\omega+2(\Omega-\theta)] && (-0.327) \\
& +(-10.3\bar{C}_{4,2}+5.4\bar{C}_{6,2}+4.1\bar{C}_{8,2}+\cdots)\sin[-M+2(\Omega-\theta)] && (-0.066) \\
& +(14.2\bar{C}_{4,2}-7.4\bar{C}_{6,2}-5.7\bar{C}_{8,2}+\cdots)\sin[M+2(\Omega-\theta)] && (0.091) \\
& +\cdots
\end{aligned}
\tag{9.166}
$$

span of data, these spectral components are difficult to separate.

The large number of harmonics affecting a satellite is related by a linear equation similar to equation (9.166). For one satellite, only a linear combination of coefficients can be determined. In those cases where an insufficient number of satellites is observed, additional assumptions are necessary in order to obtain independent equations. The usual assumption is to set some of the higher degree terms to zero, leading to lumped coefficients that are useful for orbit determination but that may be unrelated to the actual field.

In summary, the process of field determination begins with the evaluation of the secular and long-period perturbations to determine the J_n. The perturbations accumulate for weeks and months, and the effects are very large. The mean orbital elements, determined from overlapping 4-day arcs, constitute the basic data used in the analysis. Data and reference orbits of moderate accuracy are adequate for the J_n determination. The unbiased recovery of the J_n requires painstaking evaluation of the long-period and secular perturbations from other sources, principally solar radiation pressure, atmospheric drag, and lunar and solar attraction.

This phase of the analysis is accomplished first. The tesseral harmonics are determined from the short-period (1 revolution to 1 day) changes in the orbit. The detailed structure of the orbit must be observed, and each observation provides an observation equation. Data of the highest possible precision are needed. The unbiased recovery of $\bar{C}_{lm}$ requires the evaluation of the periodic terms from other sources that have periods similar to those arising from the potential coefficients. The most important are the short-period terms due to J_n and the lunar attraction. Because they are smaller than 1 m for the satellites used in this analysis, the periodic effects of air drag and radiation pressure can be ignored. The nonperiodic terms are empirically determined and hence accounted for. The short-period terms due to J_2 must be carried to second order.

9.4.3.2 Coefficients of Zonal Spherical Harmonics in the Potential

9.4.3.2.1 INTRODUCTION

Coefficients of zonal spherical harmonics in the potential determined from secular variations of angular variables and from amplitudes of long-periodic terms with the argument of perigee ω in the orbits of artificial satellites are more accurate than are coefficients derived by classical terrestrial methods. The reason is that the component of geoid height represented by the zonal harmonics is amplified by a factor of 1000 when they appear as secular and long-periodic perturbations of satellites. However, because these perturbations are averaged effects, contributions from the harmonics in each are not very different from one satellite to another unless their orbital elements are quite different. Also, few satellites with inclinations below 30° have been employed in the determination of the coefficients, since accurate observations of such satellites have been scarce. It was also found that many more terms than expected were necessary to represent the potential. Therefore, it has usually been very difficult to separate the contributions from each harmonic in the observed values of the secular motion and of the amplitudes of the long-periodic terms. In other words, different sets of coefficients could represent these observations within observed accuracies for satellites with inclinations larger than 30°.

9.4.3.2.2 EQUATIONS OF CONDITION

A computer program has been developed to calculate coefficients of $J_n (n \leq 55)$ in expressions of secular motion and of the amplitudes of $\begin{matrix}\cos \\ \sin\end{matrix} 2\omega$ and $\begin{matrix}\cos \\ \sin\end{matrix} \omega$ terms. Numerical values for $n \leq 37$ are given in tables 9.27 to 9.29 for 14 satellites. Since secondary effects due to the interaction with the J_2 secular terms were not included, the values here for the coefficients of the amplitudes of the long-periodic terms in the argument of perigee and the longitude of the ascending node are slightly different from those we gave previously.

For the two angular variables ω and Ω, the secular and long-periodic perturbations have been derived from

$$\frac{d(\omega,\Omega)}{dt} - (\dot{\omega},\dot{\Omega}) + A \sin \omega + B \cos 2\omega \qquad (9.167)$$

where $\dot{\omega}$ and $\dot{\Omega}$, the secular parts, are functions of the semimajor axis, inclination, and eccentricity, which are not constant and, except for the semimajor axis, have long-periodic terms. The inclination and the eccentricity cannot be assumed constant in expressions for $\dot{\omega}$, $\dot{\Omega}$ in equation (9.167) but must include long-period terms. The effects of these long-period terms are of the same order as A and B and produce secondary effects. Therefore, if constant values for secular motions are adopted in order to analyze the data, the secondary effects in expressions for the long-period terms must be included in equation (9.167). In earlier papers by Kozai, the secular motions were determined from observation by assuming they were constant. Corrections to the secu-

lar motions and the amplitudes of the long-periodic terms were derived in recent papers by fitting the observed orbital elements with the integrated results of equation (9.167) by using assumed values of J_n and the instantaneous observed mean values of the semimajor axis, inclination, and eccentricity. Thus, it is not necessary to incorporate the interaction terms, as they have already been included numerically and subtracted from the observed data.

As tables 9.27 to 9.29 show, the decrease of the coefficients with degree of the harmonics is slow, particularly for low-altitude and for low-inclination satellites. For DIAL and PEOLE, the coefficients of the secular motions for lower harmonics are not independent, as $\dot{\omega}$ is almost twice as large as $-\dot{\Omega}$.

For low-inclination satellites, the signs of the coefficients change continually as the degree of the harmonics is increased, while for high-inclination satellites, they change only rarely. Therefore, to reduce correlations between the coefficients in the determination of zonal spherical harmonics, it is necessary to use data for satellites with well-distributed orbital elements. However, such data are usually not available.

9.4.3.3 Determination of Tesseral Harmonics

Tesseral harmonics were computed by combining satellite perturbations and terrestrial gravimetry. In the computation of the normal system, terms with small contributions have been omitted. Therefore, the normal system determined from orbit analysis is complete through $l=m=12$. In each higher order, terms have been omitted—for example, 13,6 through 13,9 and 14,5 through 14,11. Resonance harmonics through 23,14 have been incorporated. Of course, all terms were included in the computation of the residuals. In the same way, for surface gravity all available potential coefficients have been used, but no partial derivatives for the zonal harmonics or tesseral harmonics less than ninth degree were computed, since they are negligibly small.

For each orbital arc, a set of six mean elements, $\bar{c}_i$, is determined. The linear rates are derived empirically, as is the mean anomaly. In addition, higher polynomials in the mean anomaly are employed, where appropriate, to account for the nonperiodic, yet nonsecular, effects of air drag and radiation pressure. Twelve or more orbital elements are determined for each arc, and the arcs range in length from 4 to 30 days. Therefore, with the more than 100 orbital arcs used in this solution, over 1500 additional parameters need to be determined. By use of a device described in section 9.4.2.2 for reducing the normal equations, this can be accomplished without dealing with 2000×2000 matrices. For systems of 2000 unknowns, the time required to compute reduced normal equations is much greater than that for the adopted method, which is a block Gauss-Seidel iteration. Reduced normal equations are used with more limited problems—e.g., in a solution for resonant harmonics—because they rigorously account for the interaction of the elements and unknowns.

The determination of orbital elements and of geodetic parameters (potential and station coordinates) was done separately and iterations were performed alternately; this method improves first one set and then the other. As the iterations proceed, the choice of unknowns is modified: Satellite data were either deleted or augmented, depending on whether coefficients (and station coordinates) appeared to be ill-determined or significant.

Equations (9.162) lead us to the method of selecting those coefficients that affect the orbit and that therefore can be determined from observing the orbit. We know that $\bar{C}_{lm}$, a, e, and I determine the size of $\delta\bar{C}^k_{lmpq}$, which can be computed by using an estimate of $|\bar{C}_{lm}|$ and the value of the mean elements. We estimate $|\bar{C}_{lm}|=\alpha l^{-\beta}$ to test for significance, and only terms greater than $\alpha l^{-\beta}$ are retained. All the $\delta\bar{C}^k$ are calculated and combined into a shift of position $\sqrt{d\bar{\rho}\cdot d\bar{\rho}}$; they

are given in table 9.24 for satellite 6701401 with $l=11,12,...,20$. The units are adjusted so that with $\bar{C}_{lm}$ expressed in units of 10^{-6} (e.g., $\bar{C}_{2,2}=2.4$), the perturbation in position is in meters. Conservative values for α and β are used, and more terms are carried than are perhaps necessary. For example, for $l=11$, $m=5$, and $C_{lm}=10^{-5}/l^2=0.083$, the perturbation is $0.083\times 38\approx 3$ m. From such tabulations for each satellite, we can choose the coefficients that affect the motion of the satellite and ascertain how many satellites contribute to the determination of a coefficient. In addition, the accuracy of the available data controls the size of the effect that can be detected. The choice of coefficients is made by balancing the amount and precision of the data available for a particular satellite against the sensitivity of that satellite to particular coefficients. Further, it is apparent that the surface-gravity data are stronger than the satellite information for some coefficients, and for that reason some higher coefficients have been dropped from the satellite solution.

Table 9.24 illustrates two points referred to earlier. The amplitudes for $m=13$ are quite large because of the resonance; the large size of the effects continues well into the 20th-degree terms. The $m-12$ and $m=14$ harmonics also have sizable effects because they are adjacent to a resonant harmonic.

Apart from the resonant harmonics, terms higher than $l=12$, $m=12$ are weakly determined by the satellite data, but it had been demonstrated in earlier iterations that the surface gravity could determine these higher harmonics. The satellite solution was limited to those harmonics that have an effect greater than 3 to 4 m on the orbit. The resulting terms were complete through $l=12$, $m=12$. The higher order terms selected were $C/S(l,1)$ $13\leq l\leq 16$; $C/S(l,2)$ $13\leq l\leq 15$; $C/S(14,3)$; $C/S(l,12)$ $13\leq l\leq 19$; $C/S(l,13)$ $13\leq l\leq 23$; and $C/S(l,14)$ $14\leq l\leq 24$.

The $m=9$, 12, 13, 14 terms are resonant with some satellites, which are listed in table 9.30 along with their resonant periods. Several satellites are resonant with more than one order. For example, 6701101 has a 1.6-day period with the 13th order and a 2.6-day period with the 14th, the latter being the principal effect. Other resonances have several periods, as illustrated by equation (9.163) for 5900701 (which was not used in the final solution) and in table 9.30 for 6701401. The multiple periods are due to the nonzero eccentricity, which causes the frequency splitting.

9.5 RESULTS

As was explained in section 9.4, the process used by SAO in solving for station coordinates and the gravitational potential is such that station coordinates and the potential are determined both independently and in combination. These quantities are therefore easily discussed and analyzed separately. The station coordinates are discussed in section 9.5.1. The potential, in terms of coefficients $\bar{C}_{lm}$, $\bar{S}_{lm}$, is given and discussed in section 9.5.2. The geoid derived from this potential is discussed in section 9.5.3.

The analysis was divided into two parts because of the initial high accuracy of the geodetic parameters, the good coverage of all types of observational material, and the result from Gaposchkin and Lambeck (1970) indicating that the interaction between the potential and the station coordinates is relatively small. The determinations of the potential and of station coordinates were carried out in parallel. In an iterative process, the improved coordinates were used in the next iteration for the potential, and then the improved potential was used in the subsequent iteration for the station coordinates. This process, known as the block Gauss-Seidel iteration, will rigorously converge.

9.5.1 Coordinates

(E. M. Gaposchkin, J. Latimer, and G. Veis)

Each subset of data was treated to provide a system of normal equations and residuals. These systems are combined

with their relative weights. In addition, each system *may* have a different origin, orientation, and scale, but these differences should *not* occur if each system had been referred to the defined system without error. In the combination, additional parameters as necessary were introduced into the combined normal system to account for possible systematic errors. The SAO dynamical, pre-ISAGEX data were taken as the reference. Since the geometrical networks have no scale, only translation and rotation parameters were introduced. For practical purposes, the SAO geometrical network covers only one hemisphere in an east-west orientation, so only the rotation about the z axis (ϵ_z) may be meaningful. This corresponds to a correction to UT1. The polar orientation (ϵ_x, ϵ_y) for the SAO geometrical network turned out to be smaller than the formal uncertainty. The JPL net had only a scale and ϵ_z parameter as it is not sensitive to ϵ_x, ϵ_y or to the origin. Experiments with determining corrections ($\Delta\Omega$) to the node for each arc of ISAGEX data indicated that (1) the corrections were small, generally less than 1 μrad, and (2) they were satisfactorily included through the reduced normal equations. Therefore, formally, the combination solution contained 14 additional parameters. The final values of these parameters are given in table 9.31. The translation of the two geometrical networks is the correction to the station used as the origin. Excellent agreement occurs between these translations and the coordinates determined from an a posteriori geometric adjustment. The formal uncertainty for the translation of the SAO geometrical network is not given, because the origin, station 9051, has very few observations and is not determined very well.

Two iterations were completed, the first starting with the coordinates given in Gaposchkin and Lambeck (1970). Examination of the solutions indicated problem stations; in particular, the geodetic coordinates were sometimes seriously in error.

The strategy used to determine the relative weights and the formal uncertainty was based on the geometrical solutions, and all other solutions were referred to them. Geometrical solutions are relatively uncomplicated and free from assumptions. Furthermore, the statistics are straightforward.

The accuracy of each station-to-station direction was computed. This estimate can be verified by comparison with the direction determined in the network adjustment. The adjustment essentially enforces the coplanarity condition for any three directions that connect three stations. By comparing these estimates of the direction, we can compute a scale factor that is a measure of the agreement between the formal statistics of the adjustment and the actual errors. This scale factor turned out to be $k^2=2.65$ for the SAO geometrical network and $k^2=2.60$ for the BC–4. Since the difference between these estimates of k^2 is not significant, we adopted an overall scale factor of $k^2=2.625$ for the geometrical networks. It is interesting to note that when only the 12 SAO Baker-Nunn cameras are used, the scale factor becomes $k^2=1.03$, indicating excellent control of systematic errors.

In the combination of the six types of data, the geometrical networks, the JPL network, and the geodetic survey data were used with a priori variances. The pre-ISAGEX dynamical data were given a weight of 0.25 for the combination of the normal equations, which effectively doubles the assumed accuracy. In addition, the assumed accuracy of the pre-ISAGEX laser data was further multiplied by a factor of $1/\sqrt{10}$, and thus the assumed accuracy of the laser data was multiplied by 6. The ISAGEX data were given an overall weight of 0.0625; i.e., the assumed accuracy was multiplied by 4. Thus, the reference orbits were computed by using the assumed accuracy in table 9.8, but the normal system was scaled by these factors. These adjustments were necessary in order to accommodate the enormous volume of data used for the dynamical solutions. Large volumes of well-distributed data lead to cancellation of errors, which is desirable, but give optimistic estimates of variance. The balance of weights presented here leads to an internally consistent solution, which has

acceptable agreement with independent determinations.

Table 9.32 lists the geocentric coordinates for the stations determined in SE III together with their uncertainties scaled by $k^2=2.625$. Station 8820, Dakar, Senegal, is not given, the poor agreement and paucity of data precluding reliable results.

The solution for coordinates from the combination scaled by $k^2=2.625$ gave estimates of variance of 2 m for the best stations. Since no comparison exists that can verify this accuracy for geocentric coordinates, we are limited to consistency checks. The coordinates should agree with the standard at least as well as the accuracy of the standard. A number of internal checks (e.g., between geometrical and dynamical solutions) can be performed. Comparisons can be made with surface data, but they test only the relative position and not the geocentric position of the coordinates. Nevertheless, these comparisons are instructive and indicate that the computed variances (uncertainties) are realistic estimates. Further, the general agreement internally in the satellite data—and externally with the terrestrial data—indicates that, as a rule, discrepancies are within the expected uncertainties. The large discrepancies are probably due to errors in the survey data, and further analysis is needed.

Comparisons with satellite orbits are inconclusive at best, because of the large number of error sources. In section 9.5.2.3 numerical results are given for orbit computations with laser data by using the latest potential and station coordinates. This comparison indicates that the orbit computing system (data, theory, physical parameters, and station coordinates) has an accuracy of 5 to 10 m, which is not consistent with a 2- to 5-m accuracy for the station coordinates.

The typical direction is determined with an accuracy of 5 μrad, equivalent to a relative position of 10 m. For selected sets of stations, figure 9.12 compares the determined direction (both before and after the coplanarity condition is applied), the dynamical solution, and the combination solution. In some cases, a direction from the SAO geometrical net and another from the BC–4 geometrical net are available. These comparisons are perhaps unfavorable in that the errors of both stations are reflected in the figures. The error ellipses for all the directions are scaled by the factor $k^2=2.625$. In order to express all the directions in the same coordinate system, the plotted directions are rotated by the parameters given in table 9.35.

When the origin and scale are provided, the BC–4 network of 48 stations gives a geometric solution that can be compared with the combination solution. Table 9.33 gives the results of such a comparison, with differences in X, Y, and Z and North, East, and height. The geometrical solution has an average uncertainty of 5 m for each coordinate, while the combined solution has the uncertainty given in table 9.32. The adjustment uses a weight computed from the two solutions. The root mean square of 12 m and the standard error of unit weight $\sigma_0=0.8$ indicate the excellent agreement in the coordinates and the estimated uncertainties. A number of the individual coordinates are too large. The North-South difference of -25 m for station 6068, which is tied geodetically to 7092 and 4751, is the most troublesome.

The JPL coordinates given by the LS 37 solutions, rotated and scaled by the results in table 9.31 are compared in table 9.34 with the coordinates determined in the combination solution.

Comparisons within each datum are possible. The four major datums where this was done are North American datum (NAD 1927), South American datum (SAD 1969), Australian datum (AGD), and European datum (EU50).

As described earlier, the use of datum coordinates in the combination solution has been restricted to nearby stations, primarily in order to relate different types of observations. Therefore, datum coordinates constitute a relatively independent set of data. However, each datum has an arbitrary origin, orientation, and scale, and the relation between each datum and the geocentric

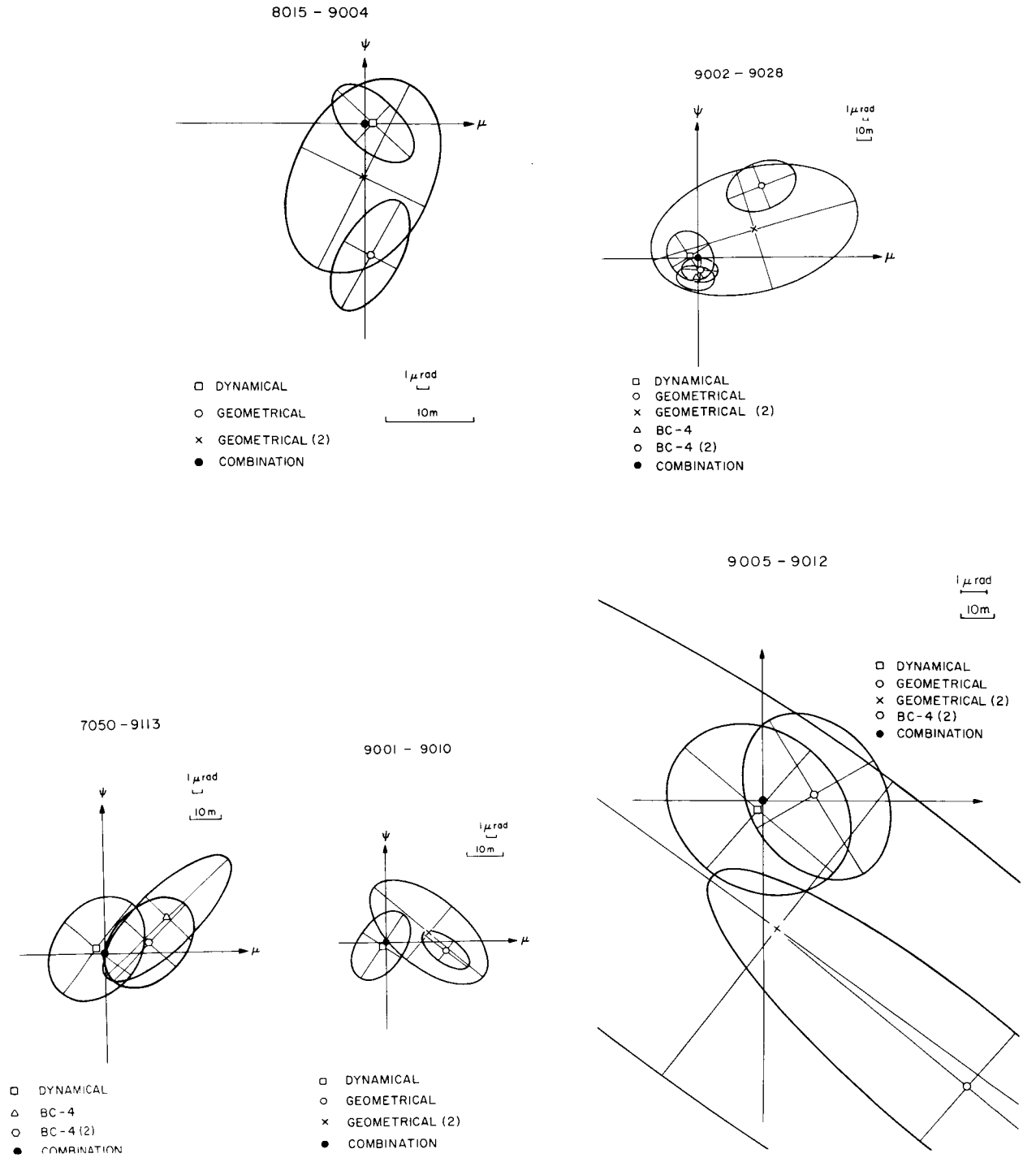

FIGURE 9.12.—Comparison of interstation directions from the combination, dynamical, and geometrical solutions. Each of the two geometrical solutions yields two directions. BC-4 (2) and geometrical (2) are the directions obtained from the network adjustment. ψ is in the direction of increasing declination, and μ is in the direction of increasing right ascension.

system must be determined. One can therefore determine up to seven parameters, but depending on the size of the datum and the distribution of stations on the datum, some of these transformation parameters may not be significant. The seven transformation parameters are three translations, three rotations, and one scale. We have elected to express the rotations as rotations of the datum origin about the normal to the ellipsoid and around two axes in the tangent plane oriented north-south and east-west. These rotations have a physical interpretation since they express an error in the azimuth of orientation of the datum and a tilt of the ellipsoid. Accordingly, the transformation will be given by

$$\bar{X}_{sat}=\bar{X}_{dat}+\bar{T}+(1+K)\bar{R}(\bar{X}_{dat}-\bar{X}_0)$$

where $\bar{X}_{sat}$ and $\bar{X}_{dat}$ are the coordinates from the satellite solution and the datum, respectively, $\bar{T}$ is the vector of the three translation parameters, K is the scale correction, $\bar{X}_0$ are the coordinates of the datum origin, and $\bar{R}$ is a rotation matrix depending on the three rotational parameters and the latitude and longitude of the datum origin.

Table 9.35 gives the translation, rotation and scale parameters for four major datums as computed from the adjustment of the datum coordinates to the satellite solution. A positive scale here means that the datum scale has to be increased in order to agree with the satellite scale. The table also gives the number of stations used in each datum. In the computation of datum shifts, each station was assigned a weight computed from the standard deviation of the satellite solution and the standard deviation of the datum coordinates, which was taken as $\sigma(m)=5\times(S\times10^{-6})^{3/4}(m)$, where S is the distance of the station from the datum origin in meters. In all cases, the standard deviation of unit weight σ_0 (given in table 9.35) after the adjustment is smaller than 1, which means that the weights are somewhat pessimistic. The rms, $\sigma(m)$, of the final differences for each datum in table 9.36 is between 5 and 16 m. It is apparent that the European and the South American datum coordinates do not agree very well with the satellite solution. The European datum is rather inhomogeneous and its extension into Africa and Asia, which we used, makes it rather weak.

Further checks with datum information can be obtained with station heights. The height above the reference ellipsoid (h_{ell}) should be equal to the mean height above sea level (H_{msl}), which is approximately the height above the geoid plus the geoid height N; i.e., the disagreement between these two estimates, Δh, is

$$\Delta h=h_{ell}-H_{msl}-N-\overline{H}_{\text{datum mean}}$$

If we use the satellite geoid to calculate N, we can make this comparison for all stations but we lose the detailed variation in geoid height. The computation does provide a value for the semimajor axis of the best-fitting ellipsoid used to calculate h_{ell}. We get

$$a_e=6\ 378\ 140.4\pm1.2\ \text{m}$$

To employ the detailed geoid-height information given for each datum in table 9.15, we must refer the coordinates to the datum origin by using the datum shifts in table 9.35. Table 9.36 lists the standard deviations of the heights calculated for each datum. The average of 3.98 must be considered excellent in view of all the uncertainties in calculating Δh. Figure 9.13 shows these heights residuals as a function of latitude.

The results by Gaposchkin and Lambeck (1970) were derived in the same manner, by combining several types of data, establishing relative weights, and verifying the accuracy by intercomparison. Their accuracy was 7 to 10 m for the fundamental stations. In table 9.37 we give the corrections derived in this analysis for selected stations. The overall agreement of $\sigma=10$ m and a standard error of unit weight $\sigma_0=0.662$ indicate excellent agreement in the derived coordinates and the accuracy estimates; if any-

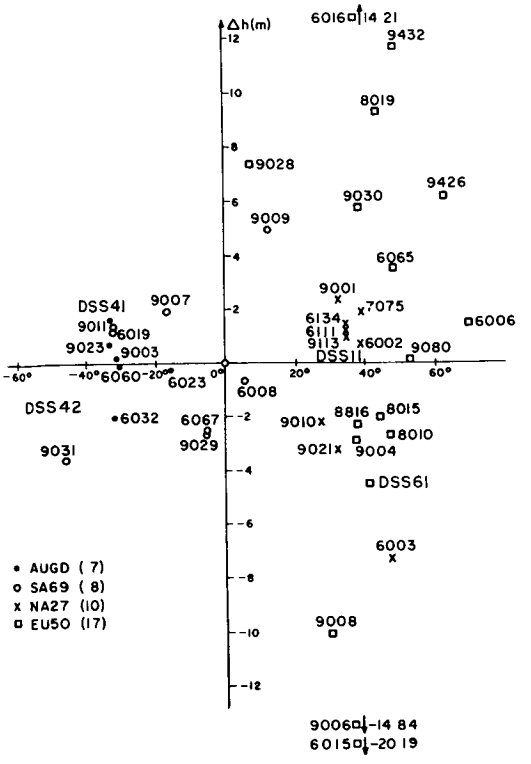

FIGURE 9.13.—Geoid height comparison as a function of latitude $\Delta h = h_{ell} - H_{msl} - N_{datum\ geoid} - h_{datum\ mean}$, where h_{ell} is transformed by the appropriate datum shift parameters $\sigma_{\Delta h} = 3.98$ m.

thing, the accuracy estimates are pessimistic. The very small shift in origin indicates that the whole reference system has not changed.

Williams *et al.* (1972) have determined the spin-axis distance of McDonald Observatory from lunar-laser observations. Table 9.38 compares this distance with that deduced by means of the coordinates of station 9001 from survey data. The agreement of -3.51 m must be considered acceptable.

The scale of the combination solution is defined by the value of GM adopted in the dynamical solution, given in table 9.11. We found a scale difference of 0.18 ± 0.55 ppm between the JPL and the SAO coordinates, the JPL ones being slightly larger. If the discrepancy with lunar laser is attributed to scale, the scale difference would be 0.7 ppm.

The scale obtained for the four major datums is given in table 9.35. It appears from the NAD 1927, EU50, and AGD datums that the datum scale is smaller than the satellite scale by approximately 2 ± 1 ppm, while from the SAD 1969 datum, it is larger by 1 ± 1 ppm. Since the survey scales are not expected to be established to better than a few ppm, the weighted mean of 1.6 ± 1 ppm is not considered to be significantly different from zero.

Each geometrical network has an arbitrary origin specified by the intial coordinates of one station, a station not explicitly determined in the combination solution. The translation parameters in table 9.33 correspond to the correction to the origin of the network, i.e., the correction to the initial coordinates of the reference station.

In principle, the orientation of the two geometrical systems and that of the dynamical system should be identical. Orientation parameters (ϵ_x, ϵ_y, ϵ_z) are determined to accommodate possible systematic differences in the actual representation of the three systems. Since the SAO geometrical network covers only one hemisphere in an east-west orientation, the orientation of its pole (ϵ_x, ϵ_y) may be poorly determined.

The polar orientation of the BC–4 system with respect to the SAO dynamical system is $1.88 = \sqrt{1.76^2 + 0.65^2} \pm 1.16$ μrad. This systematic difference is obtained by comparing the observed BC–4 directions with directions determined from eleven stations in the combination solution with characteristic interstation distances of 2 to 3 Mm. In metric terms, the orientation difference is $1.88 \times 10^{-6} \times 2 \times 10^6 \approx 4$ m. The accuracy of the mean station for the 11 stations is approximately 4 m. It is assumed that the value of 1.88 μrad results from differences in pole-position data or in processing methods.

The rotation in longitude (ϵ_z) corresponds to a correction in UT1. Figure 9.14 indicates the relative position of the zero meridian of each system. We note almost the same relation between SAO and the JPL systems that we found in SE II, which was 4.0 μrad. The difference between the SAO geometrical and the SAO dynamical systems is -0.40 ± 1.43, and that between BC–4 and the SAO dynamical is -2.20 ± 0.82. The relative rotation in

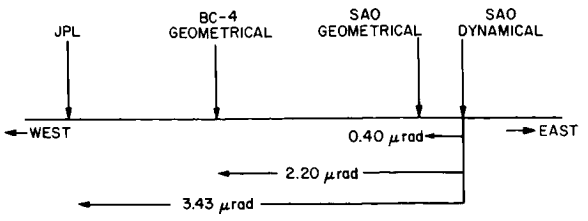

FIGURE 9.14.—The relative zero meridians of the different systems.

longitude between the JPL and the SAO systems is probably due to a difference between the JPL's planetary ephemeris and the FK4 system used by SAO, while that between the geometrical and dynamical nets most likely results from differences in the UT1 data or in the processing methods.

The results described above, the procedures, the tests and comparisons, and the experience of carrying out the work have led to the following conclusions about the use of artificial satellites for the determination of station coordinates:

(1) Observations of close-Earth satellites have been successfully combined with observations of deep-space probes and surface triangulation enabling us to determine the coordinates of 90 satellite-tracking sites in a uniform homogeneous system.

(2) The combination of these data provides a better solution than we can obtain from each set of data separately, because more complete coverage results and because the combination enables us to overcome weaknesses in each system.

(3) The methods of processing each type of data are sufficiently understood to make a rational combination.

(4) Successive solutions have resulted in improvements. When compared with the previous solution, each new one has agreed to within the estimated uncertainty, and that uncertainty has steadily decreased from 10 to 20 m in 1966, to 5 to 10 m in 1969, to 2 to 8 m in 1973.

(5) Formal statistics are generally optimistic, and therefore the uncertainty in coordinates is established by intercomparison, a method that has proved reliable.

(6) A comparison between coordinates indicates an accuracy of 2 to 4 m for fundamental stations and 5 to 10 m for most others.

(7) The body of data available from laser systems, though small, has made a significant contribution. The laser data dominate the solution through the relatively great weight assigned and thereby essentially establish the reference frame for the station's coordinates.

(8) The use of a variety of orbits spanning a considerable period of time is very important. Data from such orbits average over error sources with a slow variation such as UT1 or epoch timing and eliminate poor orbital geometry. The laser data suffered from both problems.

(9) Geometrical data require a minimum of assumptions, and geometrical solutions have relatively straightforward statistics. Geometrical data are more difficult to obtain owing to the necessity of simultaneous observations. Dynamical data are more plentiful, but their processing requires an elaborate orbit-computation program that may introduce model errors. The well-behaved statistical properties of the geometrical data allowed the use of the geometrical networks to establish the uncertainties.

(10) Small but significant systematic differences in scale and orientation are found between satellite coordinate systems. These differences may result from variations in data-processing methods or from fundamental and obscure differences in the definition of reference systems, e.g., the FK4 system and the JPL planetary ephemeris.

(11) Satellite determinations of site location are now sufficiently accurate to verify terrestrial survey data. The most troublesome part of the analysis was finding the erroneous survey coordinates. Considerable effort remains in providing global geodetic coordinates with sufficient reliability.

(12) Scale obtained for the four major datums is systematically smaller than the satellite results by 1.6 ± 1 ppm. Since survey scales are not expected to be established to better than a few ppm, this result is not significantly different from zero.

9.5.2 Potential

(E. M. Gaposchkin, M. R. Williamson, Y. Kozai, and G. Mendes)

The Smithsonian Astrophysical Observatory has published a series of Standard Earth models based on satellite-tracking and other data (Kozai, 1964, 1969; Gaposchkin, 1967, 1970a; Köhnlein, 1967; Veis, 1967a,b; Whipple, 1967; Lundquist and Veis, 1966; Lambeck, 1970; Gaposchkin and Lambeck, 1970). There has been a steady advance in the accuracy of the analytical treatment, in both the accuracy as well as the completeness of the data, and in the significance of the results.

Each Standard Earth model consists of (1) a set of geocentric coordinates for stations observing satellites and (2) a set of spherical harmonics representing the potential. These two sets of unknowns can be correlated, and both sets of parameters have been determined in the same computation. This led, for example in Gaposchkin and Lambeck (1970), to solving a system with 428 unknowns—i.e., for 39 stations and potential coefficients complete through degree and order 16. Evaluation of the Gaposchkin and Lambeck (1970) results indicated that the remaining errors in these parameters were small; that is, the corrections to the parameters would be small. Therefore, the effect of errors in the adopted station coordinates on the determination of the potential, and vice versa, would be small. Because these effects are small the two sets of parameters could be computed separately.

A general revision of the parameters for SE III was undertaken because of new and improved data for almost all types of observations. Observations by cameras have been augmented by a considerable number of data from laser DME with global coverage from ISAGEX. Two satellites with inclinations significantly lower (5° and 15°) than previously available have been launched since 1970. Available surface-gravity data have been significantly improved by the distribution of a compilation of gravity anomalies by the Aeronautical Chart and Information Center (ACIC). Determinations of station coordinates have been improved by data from the worldwide BC–4 geometrical network. Finally, among these improved data is the information on site locations from JPL's DSN which has been revised with the addition of new data and improved processing techniques.

Gaposchkin (1970a) has shown that, except for isolated harmonics, the terms beyond 18th or 20th degree have a negligible effect on a satellite. The only exceptions are some zonal harmonics that give rise to secular and long-period effects, and the resonant harmonics. Therefore, one cannot hope to obtain from analysis of satellite perturbations much more detail beyond 16th degree and order than is already available. Greater detail will have to come from other methods, such as terrestrial gravimetry. Many of the harmonics between 10th and 18th degree are not very well determined from satellite-perturbation analysis, but terrestrial gravimetry provides a good determination of the coefficients when combined with satellite data. So, our objectives are to improve the low-degree and low-order harmonics from satellite data and the higher harmonics from terrestrial data that best represent the gravity field.

Since the terms beyond 18th degree do not give rise to an observable change in satellite position, the satellite observations could be modeled with the use of a potential complete through degree and order 18, including, of course, some additional resonant and zonal harmonics. Therefore, there is no model error due to neglected higher harmonics. However, the surface-gravity data are given in area-means of 550 km $\times$ 550 km squares. This surface distribution of gravity would require a spherical harmonic development to $l=m-36$. Therefore, using a potential through degree and order 18 will have a significant model error that must be taken into account in establishing weights and making comparisons with surface-gravity data.

9.5.2.1 Coefficients of Zonal Harmonics [2]

The equations of condition were solved by least squares for both the even-degree and the odd-degree harmonics. They were solved first with 11 unknowns, $J_n (n \leqq 23)$, and then with 12, the 12th being $J_n (24 \leqq n \leqq 49)$. Eight solutions were obtained. The solutions, given in tables 9.39 and 9.40, include the sums of the squared differences from the assumed values. The values for coefficients of degrees lower than 14 express corrections to those in table 9.16.

Tables 9.39 and 9.40 show that the solutions are quite stable, especially for lower degree coefficients, and that the data can be expressed quite nicely by including J_{35} and J_{36}. The sum of the squared differences drops from 114 to 39 when J_{36} is included for the even degree and from 53.7 to 40.6 when J_{35} is incorporated for the odd degree. Although there is some uncertainty as to whether J_{35} and J_{36} can have such large values, the 12-unknown solutions that include them are regarded as the best. The sum of squared residuals cannot be reduced much further even if the number of unknowns were increased beyond 12.

In tables 9.41, 9.42, and 9.43, the differences computed for the 12 unknowns and for the 11 unknowns are given under the headings I and II, respectively. Solution I for even orders can express the secular motions of all the satellites except 7010901 and 6202901. Since only in table 9.43 is the difference between difference I and difference II much larger than the standard deviation for the data on 7001701, 6508901, and 6508101, it can be said that J_{36} is determined essentially from the data on these three satellites. If more accurate data become available for 7010901, so that the standard deviations for this satellite become smaller than the differences, a more definite conclusion regarding J_{36} can be obtained. Table 9.43 shows no essential difference between differences I and II; for odd degrees, the 12-unknown solution is not yet much better than the 11-unknown one.

[2] Note that $J_n = -C_n$.

For comparison, five previous solutions (Kozai, 1959b, 1961a, 1963a, 1964, 1969) are given in table 9.44. These solutions were derived from the following numbers of satellites with inclinations ranging from 28° to 96°:

Date	*Number of satellites*	*Inclination range (deg)*
1959	1	34
1961	3	33 to 50
1963	13	32 to 65
1964	9	33 to 96
1969	12	28 to 96

Except for some from the 1963 determination, the standard deviations in the first three determinations are more than 10 times larger than the present ones; therefore, the differences computed by these solutions are very large even for satellites within the indicated inclination ranges. The differences from the 1964 solution are listed as $(O-C)$ in tables 9.41, 9.43, and 9.44. Both the 1964 and the 1969 solutions give very large differences for PEOLE and DIAL. Table 9.44 also includes a solution by Cazenave, Forestier, Nouel, and Pieplu (1971, unpublished), who incorporated data for PEOLE, DIAL, and SAS (7010701; $I=3°$) in addition to the satellites used by Kozai (1969). Their solution agrees quite well with ours except for the odd higher degree coefficients.

9.5.2.2 Tesserals

The results of the dynamical solution must be discussed in the context of the combination solutions. A summary of the data is given in table 9.7. The selection of data and unknowns evolved through the analysis. The number of satellites used ranged from 21 to 25, and the number of arcs in the largest solution was 203. Arcs were added or rejected on the basis of their contribution to the normal equations, the number of observations for a particular station, the improvement of distribution for a resonant harmonic, and the quality of the orbital fit.

Two iterations were performed to find the potential. The first employed the potential and station coordinates determined by Gaposchkin and Lambeck (1970) as initial values; and the second used the results of the first iteration for the potential and the station coordinates determined earlier in this chapter.

For each iteration, several solutions were obtained. Orbital arcs were added or deleted to improve the satellite distribution and the variance-covariance matrix.

Several weights for the surface gravity were used. For areas without surface-gravity data, we had four choices of treatment:

(1) We could make no assumptions about unobserved areas.

(2) We could use a zero anomaly with a very large variance; that is, the expected value of gravity would be zero.

(3) We could use a reference gravity field with a very large variance; that is, only the higher harmonics would have an expected value of zero.

(4) We could use a model anomaly, for example, one determined from topography.

Adoption of method (1) would introduce very large short-wavelength features into those regions where no gravity is measured. In addition, the statistical comparisons discussed later are very poor, although the $(O-C)$ values and the satellite orbits are good. Therefore, (1) had to be discarded. Gaposchkin and Lambeck tried methods (2) and (4) and found them equivalent. Choice (3) is an improvement over (2) because the low-degree and low-order terms are well determined by means of satellite data. Therefore, (3) was adopted, with the weight given in table 9.21. Comparing the results of choices (1) and (3), we found that satellite comparisons are identical, the $(O-C)$ for the surface gravity is marginally improved, and the statistical comparisons of the surface gravity are quite acceptable.

The fully normalized spherical-harmonic coefficients of the adopted solution are given in table 9.45. Figure 9.15 shows the mean potential coefficient by degree, extended by numerical quadrature.

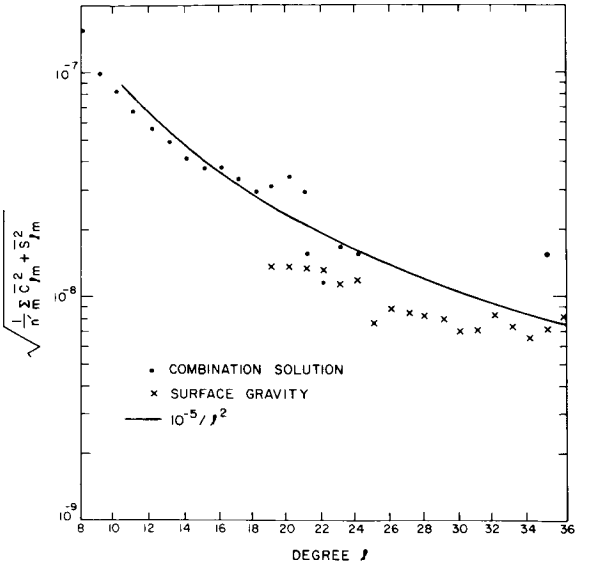

FIGURE 9.15.—Mean potential coefficient by degree.

9.5.2.3 Results of Comparison

9.5.2.3.1 ORBIT DETERMINATION BY USE OF SE III

A detailed evaluation of SE III results with satellite orbits is difficult. Although other effects—such as lunar and solar perturbations, body tides, radiation pressure, and air drag—are all included in the orbit computation, none of these is known without error, and each, in itself, provides a number of problems. Also, the coordinates of the tracking stations are not known without error. Furthermore, incomplete orbital coverage can result in overoptimistic estimates of orbital accuracy from formal statistics. Finally, the tracking data contain errors. A few comparisons are given here to indicate approximately the accuracy of the total orbit-computation system. The potential is certainly one of the larger contributors to the error budget.

From ISAGEX data, consecutive orbits were computed every 2 days, by using 4 days of data (except for 6800201, where 6 days of data were employed). This type of analysis is especially valuable for (1) detection of bad observations, since each observation is

used in two orbits, and (2) evaluation of the reliability of the orbital elements by comparison of adjacent orbits.

Results for 6508901, 6800201, and 6701401 are given in table 9.46, together with the number of observed points used in the final iteration. All calculations were performed by using the final station coordinates and the tidal parameter $k_2=0.30$; radiation-pressure perturbations were calculated with a fixed area-to-mass ratio.

We see that with good orbital coverage, we can expect to have rms residuals of between 4 and 10 m.

Satellite 6701401 has a relatively low perigee, and the poorer orbits from MJD 41072 to 41078 coincide with increased solar activity resulting in increased drag.

Of the 4– to 10–m rms residuals, 2 to 3 m come from station coordinates and 1 to 4 m could be attributed to the orbital theory. Therefore, the accuracy of the gravity field for orbit computation may actually be somewhat better than indicated by table 9.46.

9.5.2.3.2 COMPARISON WITH GRAVITY

To compare a model (g_s) with observed values of surface gravity (g_t), the following quantities defined by Kaula (1966b) can be computed:

- $\langle g_t^2 \rangle$ the mean value of g_t^2, where g_t is the mean free-air gravity anomaly based on surface gravity, indicating the amount of information contained in the surface-gravity anomalies
- $\langle g_s^2 \rangle$ the mean value of g_s^2, where g_s is the mean free-air gravity anomaly computed from the potential model, indicating the amount of information in the computed gravity anomalies
- $\langle g_t g_s \rangle$ an estimate of g_h—i.e., the true value of the contribution to the average gravity anomaly of the potential model and the amount of information common to both g_t and g_s
- $\langle (g_t-g_s)^2 \rangle$ the mean-square difference of g_t and g_s
- $E(\epsilon_s^2)$ the mean-square error in the gravity anomalies
- $E(\epsilon_t^2)$ the mean-square error of the observed gravity
- $E(\delta g^2)$ the mean square of the error of omission—that is, the difference between true gravity and g_h; this term is then the model error

If the potential model were perfect, then $\langle g_s^2 \rangle = \langle g_h^2 \rangle$, which in turn would equal $\langle g_t g_s \rangle$ if g_t were free from error and known everywhere. Then, ϵ_s^2 would be zero even though g_s would not contain all the information necessary to describe the total field. The information not contained in the model field—i.e., the error of omission, δg—then consists of the higher order coefficients. The quantity $\langle (g_t-g_s)^2 \rangle$ is a measure of the agreement between the two estimates g_t and g_s and is equal to

$$\langle (g_t-g_s)^2 \rangle = E(\epsilon_s^2) + E(\epsilon_t^2) + E(\delta g^2)$$

Another estimate of g_h can be obtained from the gravimetric estimates of degree variance σ_l^2 (Kaula, 1966b):

$$E(g_h^2) = D = \sum_l \frac{n_l}{2l+1} \sigma_l^2$$

where n_l is the number of coefficients of degree l included in g_h, and

$$\sigma_l^2 = \gamma^2 (l-1)^2 \sum_m (\bar{C}_{lm}^2 + \bar{S}_{lm}^2)$$

We also have

$$E(\epsilon_s^2) = \langle g_s^2 \rangle - \langle g_s g_t \rangle$$

and

$$E(\epsilon_t^2) = \langle g_t^2 \rangle / \langle n \rangle$$

Table 9.47 summarizes the above quantities for SE III. The improvement over SE II in the coverage of surface-gravity data is evident. The more limited gravity coverage

used for SE II resulted in accuracy estimates that were consistently optimistic. The revised set of average gravity anomalies has greater coverage and is more independent of the model used for the potential. Even so, line 2 represents an estimate of the accuracy, $E(\epsilon_s^2) = 52$ mGal^2, that is more optimistic than that based on independent gravity data for SE II, which was 99 mGal^2 (Gaposchkin and Lambeck, 1970).

We used the 306 average gravity anomalies with more than 19 observed units in each average for the comparison. There is very good agreement between $\langle g_t g_s \rangle$, $\langle g_s^2 \rangle$, and D, which would be equal for a perfect solution. In $E(\delta g^2)$, we have a measure of the information remaining in the higher harmonics. The formal statistics give an error in the combination reference field of $E(\epsilon_s^2) = 15$ mGal^2.

An alternative is to eliminate δg by use of

$$\begin{bmatrix} \Delta\bar{C}_{lm} \\ \Delta\bar{S}_{lm} \end{bmatrix} = \frac{1}{4\pi\gamma(l-1)} \int_{\text{sphere}} (g_t - g_{ref}) \left\langle \bar{P}_{lm}(\sin\phi) \begin{bmatrix} \cos m\lambda \\ \sin m\lambda \end{bmatrix}_\sigma \right\rangle d\sigma$$

where

$$\left\langle \bar{P}_{lm}(\sin\phi) \begin{bmatrix} \cos m\lambda \\ \sin m\lambda \end{bmatrix} \right\rangle$$

is the mean of

$$\bar{P}_{lm}(\sin\phi) \begin{bmatrix} \cos m\lambda \\ \sin m\lambda \end{bmatrix}$$

over the area defined for the gravity anomaly. We can compute any harmonic with respect to a reference gravity field, but care must be used in treating areas where no observed gravity is available. A gravity field defined by g_{ref} and the $\Delta\bar{C}_{lm}$, $\Delta\bar{S}_{lm}$ will have an error of

$$\langle (g_t - g)^2 \rangle = E(\epsilon_s^2) + E(\epsilon_t^2) + E(\delta g^2) + E(\epsilon_{\text{quad}}^2)$$

where $E(\epsilon_s^2)$ is the error in the composite field and $E(\epsilon_{\text{quad}}^2)$ is the error due to the inexact quadrature and imperfect distribution of the data.

Table 9.48 gives the results of this numerical quadrature with reference fields defined by the first l degrees of SE III. Computing all the potential coefficients to $l = m = 36$, i.e., the null reference field, we get $E(\epsilon_s^2) \equiv 0$, and

$$E(\epsilon_t^2) + E(\delta g^2) + E(\epsilon_{\text{quad}}^2) = 29 \text{ mGal}^2$$

Using an increasingly detailed reference field, we obtain an estimate of $E(\epsilon_s^2)$ as a function of degree. As expected, the mean-square error for the low-degree and low-order harmonics estimated from a comparison with terrestrial gravimetry is quite small. The satellite data provide accurate values, and the low harmonics have a smaller effect on gravity anomalies. The mean-square error for the 8th to 18th degrees is relatively constant, as expected, since these harmonics are determined largely by surface-gravity data. The mean-square error $E(\epsilon_s^2)$ estimated from the quadrature is in good agreement with that obtained from statistical analysis. For comparison, the values are given in table 9.49.

The estimate of $E(\epsilon_s^2)$ assumes that g_s and g_t are independent; i.e., they have uncorrelated errors. Since the terrestrial gravity (g_t) was used to determine the combination solution (g_s), this assumption is certainly incorrect, and therefore, the estimate of $E(\epsilon_s^2) = 15$ mGal^2 is definitely optimistic. A better test could be made with independent data for g_t. Since the mean gravity anomalies used in the combination solution were computed, two compilations of $1° \times 1°$ anomalies have been published: the North America and the North Atlantic (Talwani *et al.*, 1972) and for the Indian Ocean (Kahle and Talwani, 1973). These compilations were published after the set of mean anomalies used here became available, but some basic data are probably common to both. The processing methods used by Talwani and his coworkers were different from those of ACIC, and additional data were included. It is true that these two new compilations may not be completely independent of the data used in the combination solution.

Two comparisons are nevertheless instructive. A simple $5° \times 5°$ average was computed

for these data since all $1° \times 1°$ areas had values given in the region of interest. These $5° \times 5°$ averages, with the mean of the whole region subtracted, were used to compute the same statistical quantities given in table 9.49. The number n is the number of points, centered in a $1° \times 1°$ area, for which a $5° \times 5°$ mean was computed. Therefore, we have a moving $5° \times 5°$ mean calculated every 1°. Most of the gravity data in these ancillary compilations were taken at sea, and the estimate $E(\epsilon_t^2)$ of their variance may be optimistic. The weighted mean of $E(\epsilon_s^2)$ is 65 mGal^2, equivalent to 3.1 m in geoid height. The remaining gravity information in the higher harmonics, δg, equals 68 mGal^2. We notice that δg for the Indian Ocean is larger than δg for North America and the Atlantic and is probably due to the very sharp low below the Indian subcontinent, which cannot be modeled very well by the generalized geoid. Further, $\langle (g_t - g_s)^2 \rangle$, $\langle g_s^2 \rangle$, $\langle g_t^2 \rangle$, and $\langle g_t g_s \rangle$, which are all in good agreement with the global values from Table 9.47. Therefore, we feel reasonably certain that for comparison purposes, both the North America and North Atlantic region and the Indian Ocean region are typical. Thus, we conclude that the generalized geoid has an accuracy of ± 3 m in geoid height and ± 8 mGal for the whole earth. Figures 9.16 to 9.19 give north-south and east-west profiles for both North America and the Indian Ocean.

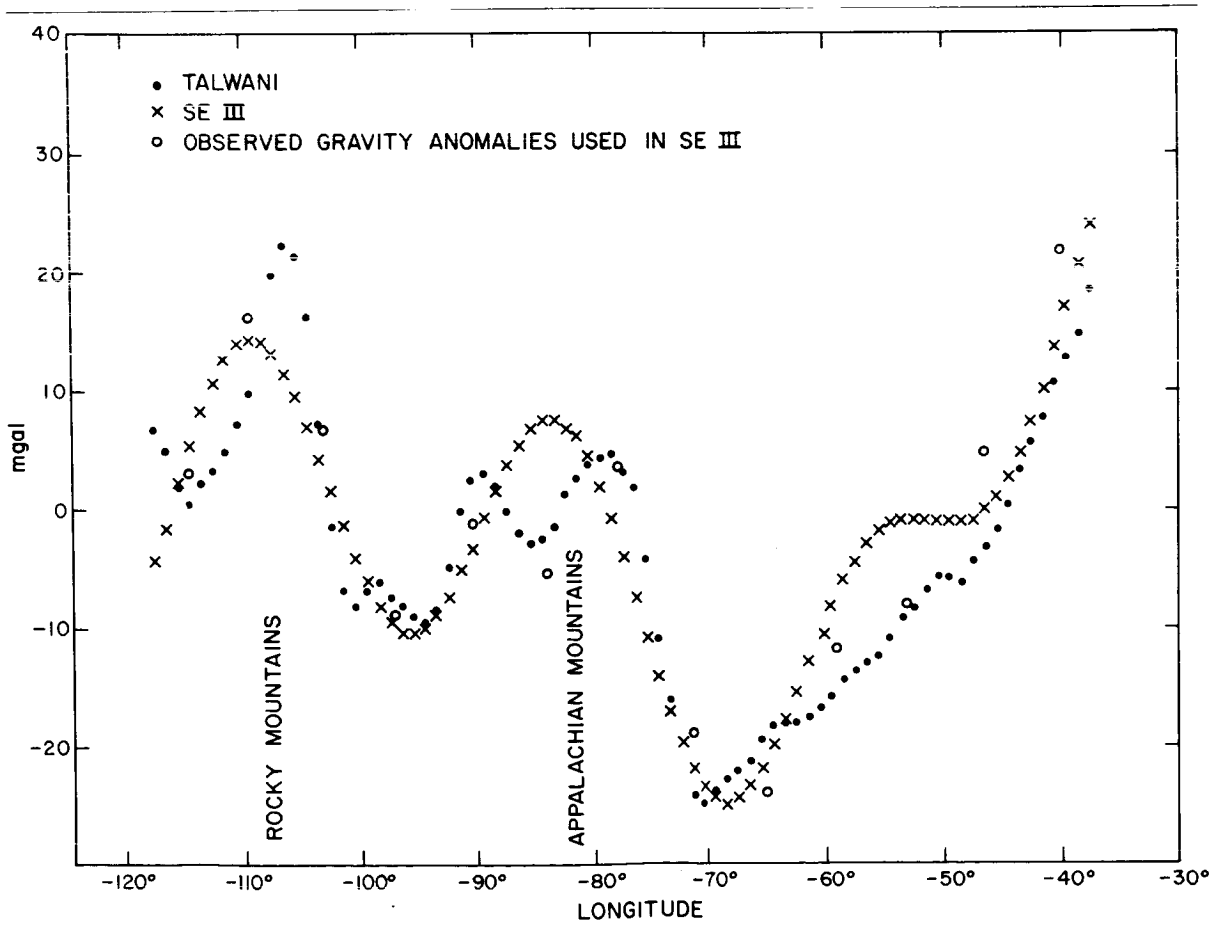

FIGURE 9.16.—Free-air mean gravity anomalies for North America at latitude 37°.5.

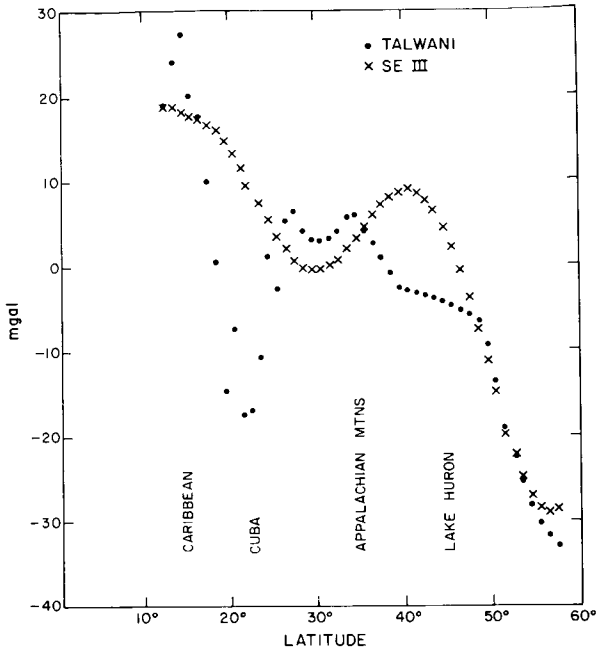

FIGURE 9.17.—Free-air mean gravity anomalies for North America at longitude −82°.5.

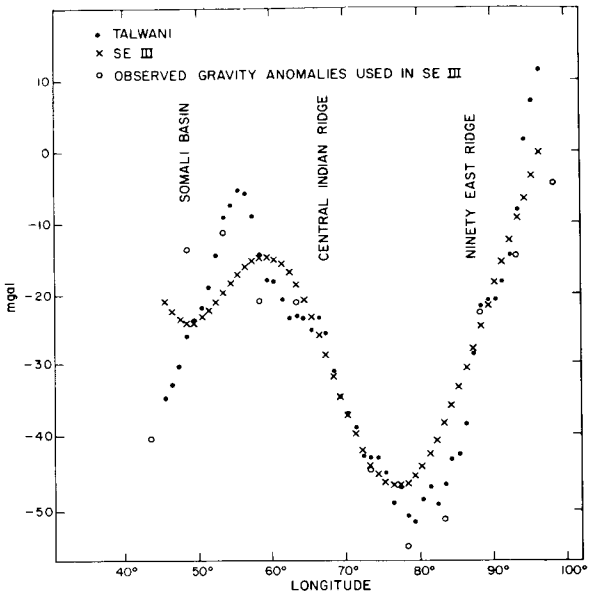

FIGURE 9.18.—Free-air mean gravity anomalies for the Indian Ocean at latitude −2°.5.

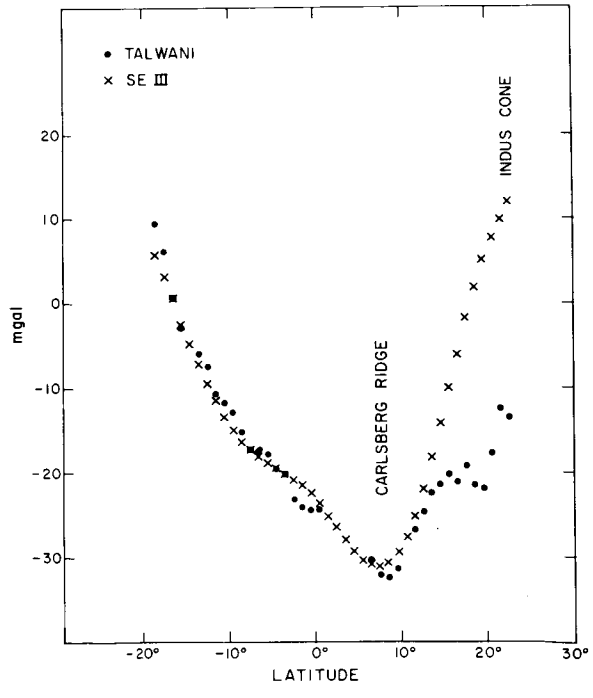

FIGURE 9.19.—Free-air mean gravity anomalies for the Indian Ocean at longitude 64°.5.

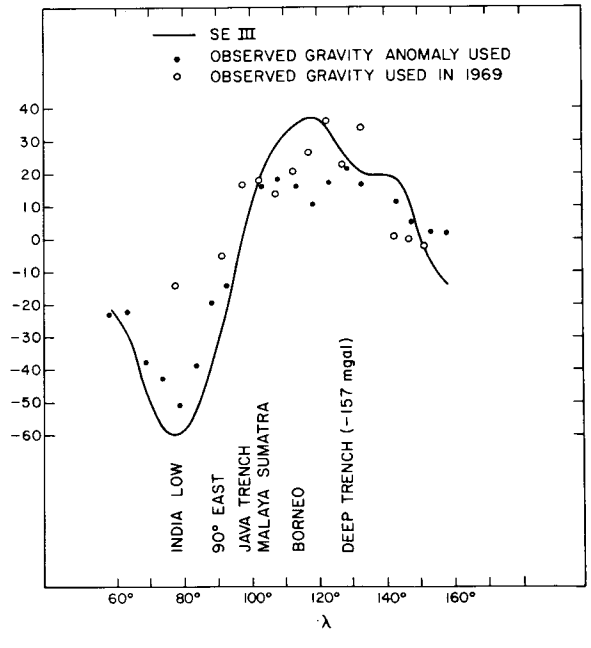

FIGURE 9.20.—Free-air mean anomalies; profile at $\phi = 2°.5$.

Figure 9.20 was selected because of the large change in the values at the India low from those given in SE II. However, the terrestrial gravity and the combination solution are in good agreement there. A further point is the disagreement, east of Borneo, between the observed gravity from the ACIC compilation and the anomalies used in 1969.

The results described above, the procedures, the tests and comparisons, and the experience of carrying out the work have led to the following conclusions about the use of artificial satellites for the determination of the geopotential:

(1) Satellite-tracking data from 25 satellites have been combined with terrestrial gravity data to determine the spherical-harmonic representation of the potential complete through degree and order 18, plus several higher harmonics to which satellite orbits are sensitive.

(2) The zonal harmonics are successfully determined from analysis of long-period and secular perturbations; the tesseral and sectorial harmonics are obtained from short-periodic satellite perturbations and terrestrial gravimetry. Low-degree and low-order $l,m \leq 8$ are primarily determined from satellite perturbations, and the short-wavelength $l,m \geq 8$, primarily from terrestrial gravity data.

(3) The principal improvements over Gaposchkin and Lambeck (1970) are due to the addition of two low-inclination satellites for the determination of the zonal harmonics, the use of a sizable number of precise laser observations, and the use of an improved set of terrestrial gravity anomalies.

(4) In the combination of satellite and surface-gravity measurements, some attention must be given to the unobserved areas.

(5) The unobserved areas were treated by using anomalies computed from a satellite-determined reference field and by taking the expected value of this residual field as zero, with a large variance.

(6) The accuracy of the solution is established by comparison with satellite orbits and with terrestrial gravity data not used in the solution.

(7) The lower harmonics have been improved such that the total orbit-computing system has an rms error of between 5 and 10 m for 4-day arcs.

(8) The accuracy of the generalized geoid is ≈ 64 mGal[2], or 3 m.

(9) The geoid is very similar to that found by Gaposchkin and Lambeck (1970); no new features have been found, and none has disappeared. Therefore, geophysical analyses from these results remain valid (see, e.g., Kaula, 1970, 1972; Gaposchkin *et al.*, 1970, unpublished).

9.5.3 The Geoid

Figure 9.21 shows the geoid computed from the $\{C_{lm}, S_{lm}\}$ given in section 9.5.2. The geoid in figure 9.21 is with respect to a best fitting ellipsoid of flattening 1/298.256; the geoid in fig. 9.21b is with respect to a hydrostatic ellipsoid of flattening 1/299.67; and the geoid in figure 9.21c is with respect to a surface computed from only those coefficients (found for the potential) which have l,m less than or equal to 5. In figure 9.22 are plotted the "gravity anomalies" calculated from the potential and with respect to the same ellipsoids as in figure 9.21.

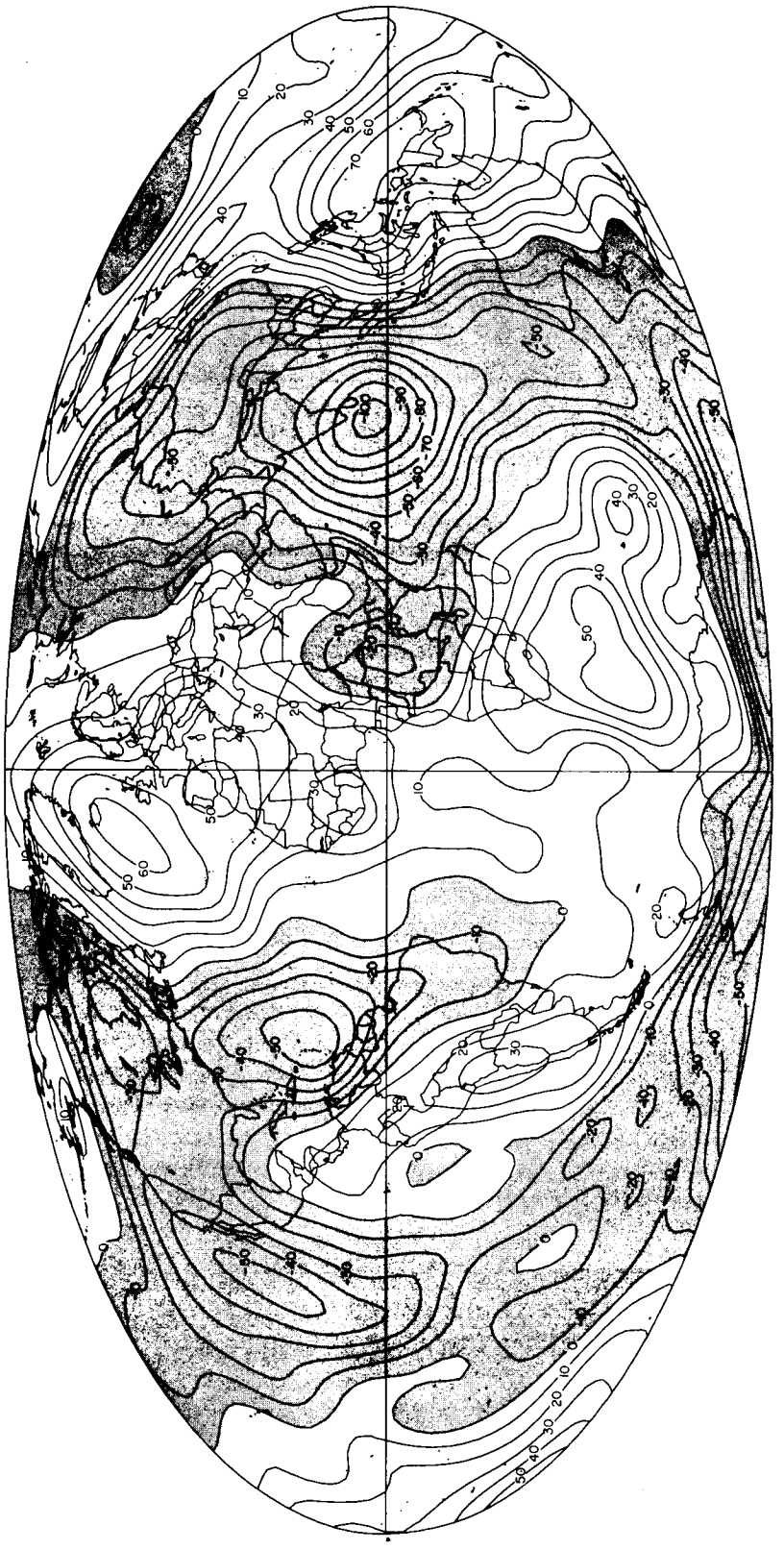

FIGURE 9.21a.—Standard Earth III, geoid heights in meters with respect to the best fitting ellipsoid, $f=1/298.256$.

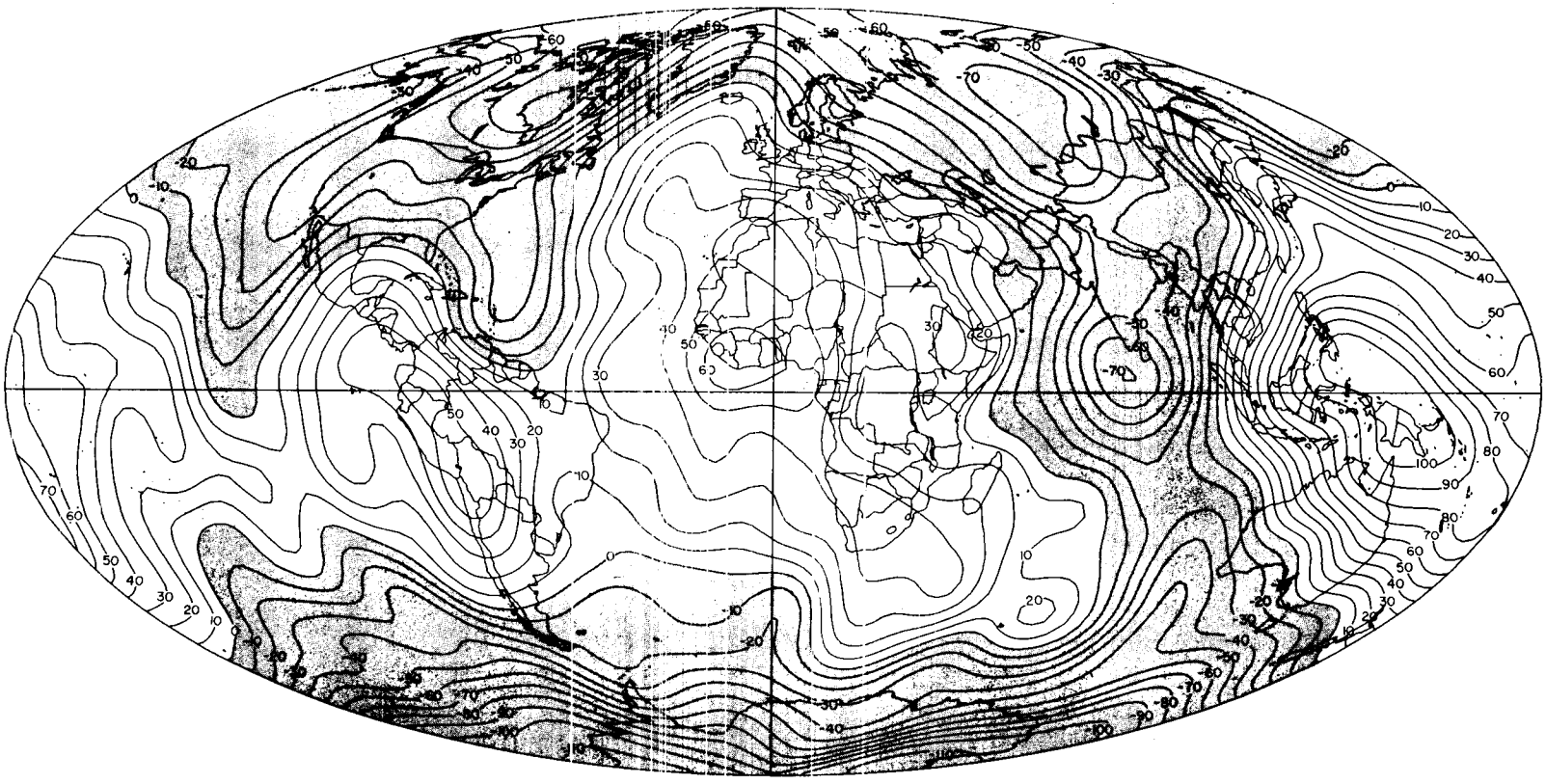

FIGURE 9.21b.—Standard Earth III, geoid heights in meters with respect to the hydrostatic ellipsoid, $f=1/299.67$.

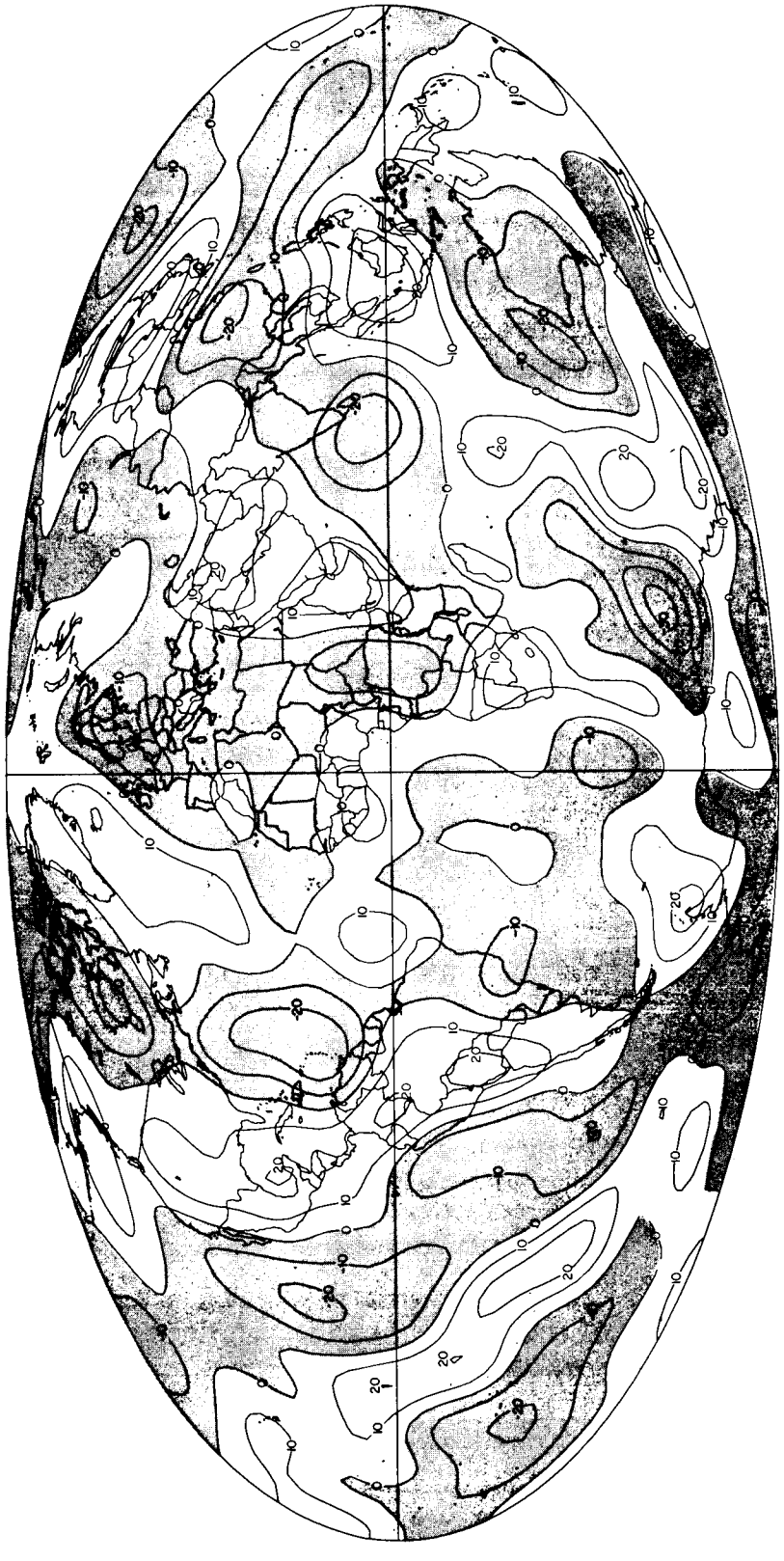

FIGURE 9.21c.—Standard Earth III, geoid heights in meters with respect to the fifth degree and order reference surface, $C_{lm}=S_{lm}=0$; $l,m\leq 5$.

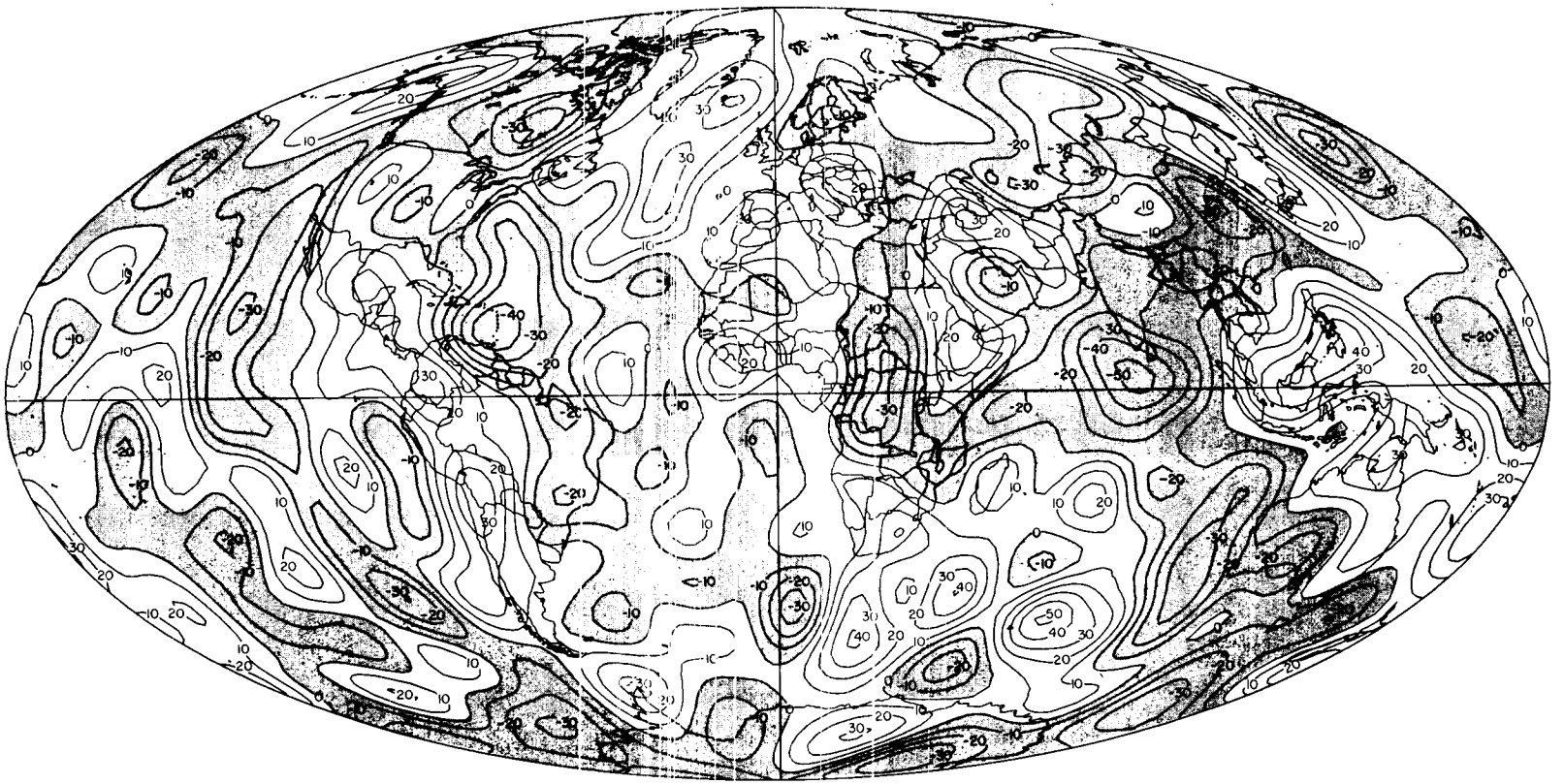

FIGURE 9.22a.—Standard Earth III, gravity anomalies in milligals with respect to the best fitting ellipsoid, $f=1/298.256$.

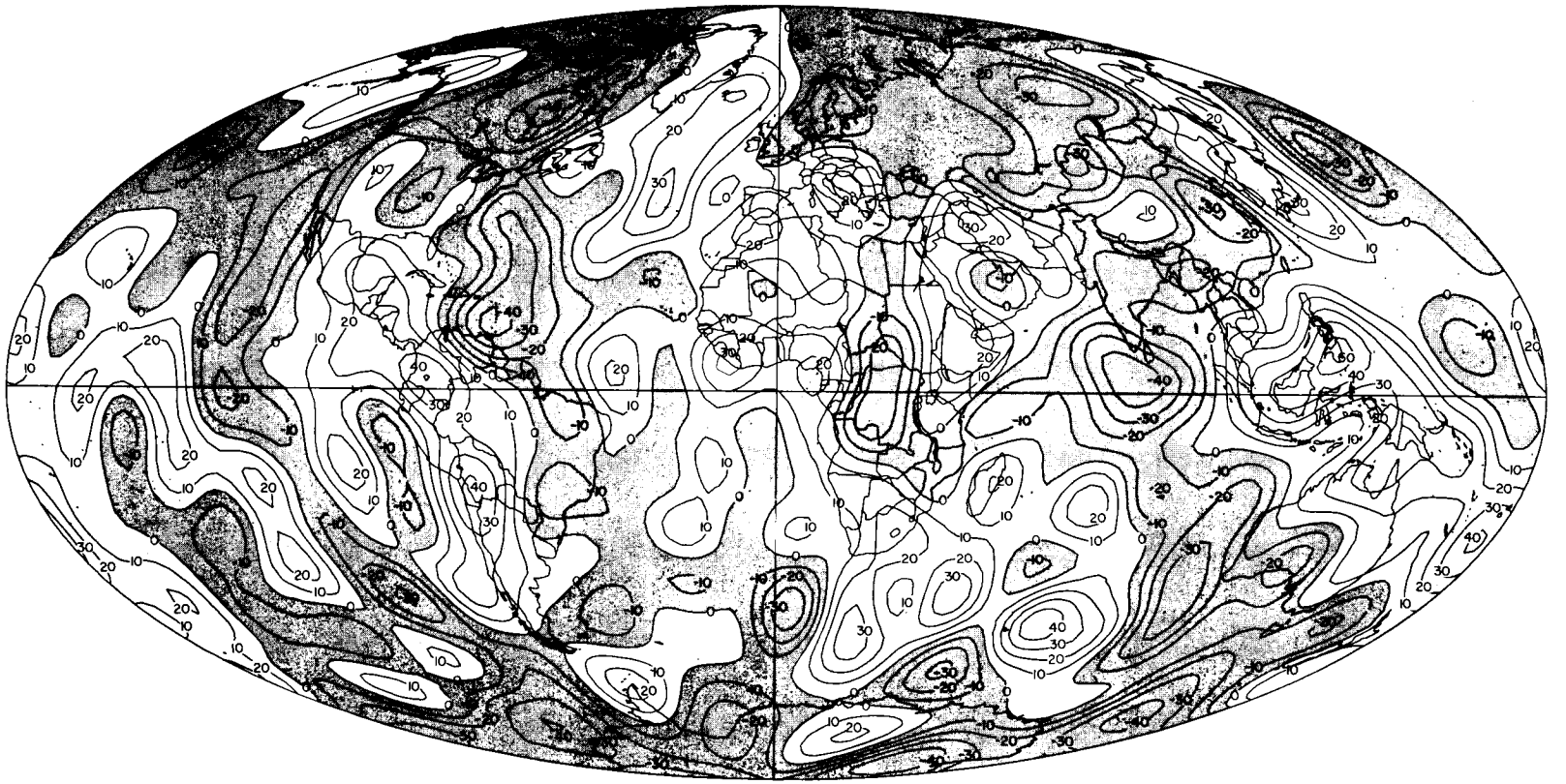

FIGURE 9.22b.—Standard Earth III, gravity anomalies in milligals with respect to the hydrostatic ellipsoid, $f=1/299.67$.

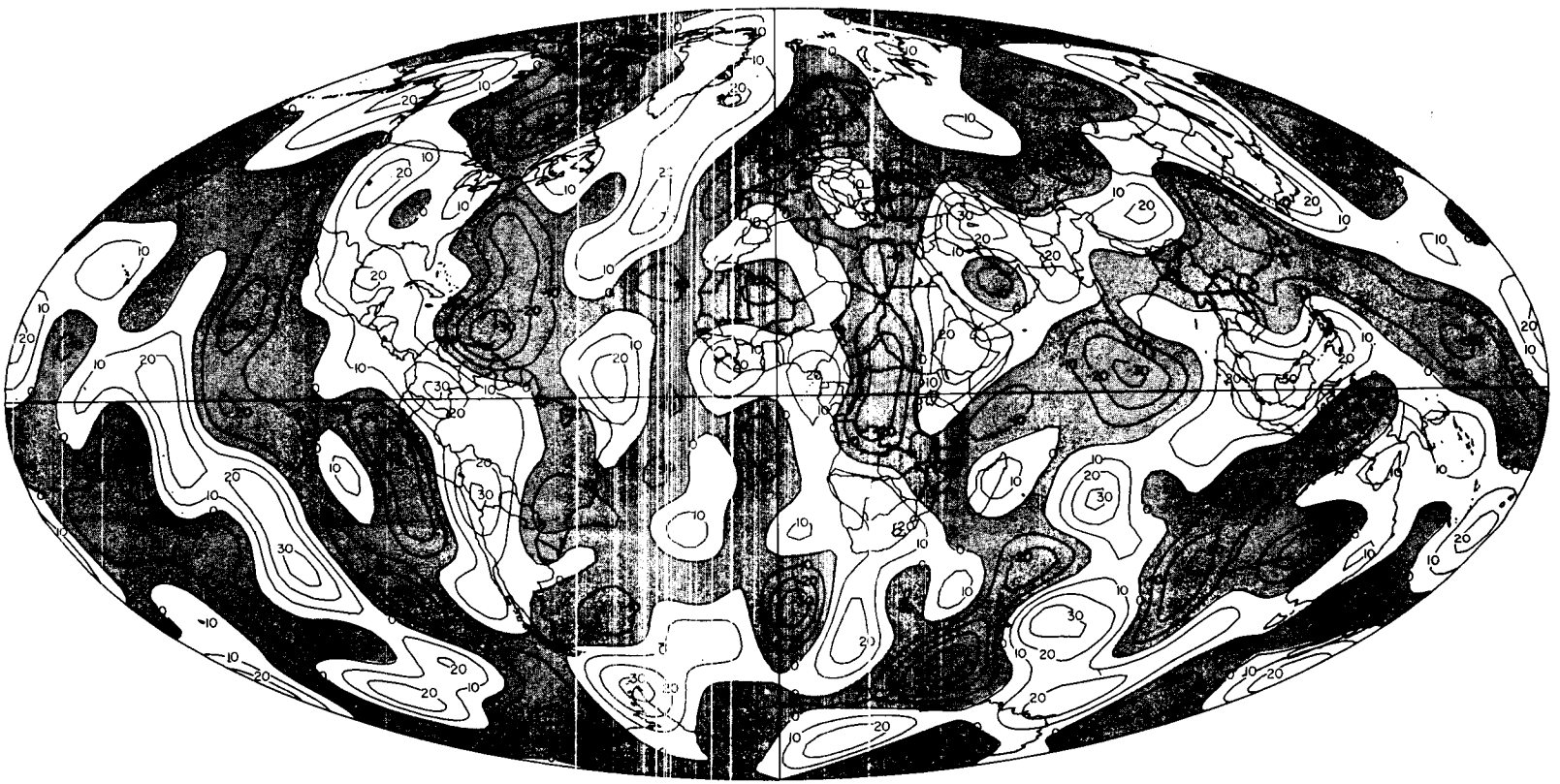

FIGURE 9.22c.—Standard Earth III, gravity anomalies in milligals with respect to the fifth degree and order reference surface, $\bar{C}_{lm}=\bar{S}_{lm}=0$; $l,m\leq 5$.

APPENDIX

TABLE 9.1.—*History of the SAO*

Satellite camera number	COSPAR number and station location	First successful observation	Last successful observation	Transferred to number and station
SC–1	9001 Organ Pass, New Mexico	November 26, 1957	March 18, 1968	9021 Mt. Hopkins, Arizona
SC–2	9002 Olifantsfontein, South Africa	March 18, 1958	December 17, 1970	9022 Olifantsfontein, South Africa (new building)
SC–3	9003 Woomera, Australia	March 11, 1968	June 1964	9023 Island Lagoon, Australia
SC–4	9004 San Fernando, Spain	March 18, 1958	----------	----------
SC–5	9005 Tokyo, Japan	April 5, 1958	May 24, 1968	9025 Dodaira, Japan
SC–6	9006 Naini Tal, India	August 29, 1958	----------	----------
SC–7	9007 Arequipa, Peru	July 4, 1958	May 30, 1970	9027 Arequipa, Peru (new building)
SC–8	9008 Shiraz, Iran	May 20, 1958	July 15, 1966	9088 Addis Ababa, Ethiopia
SC–9	9009 Curaçao, Netherlands Antilles	June 22, 1958	July 10, 1966	9029 Natal, Brazil
SC–10	9010 Jupiter, Florida	June 10, 1958	October 12, 1967	9091 Dionysos, Greece
SC–11	9011 Villa Dolores, Argentina	July 10, 1958	October 28, 1966	9031 Comodoro Rivadavia, Argentina
SC–11a[a]	9040 Dakar, Senegal	December 1970	September 1971	9040 Ouagadougou, Upper Volta
SC–12	9012 Maui, Hawaii	July 4, 1958	----------	----------

[a] On loan to CNES.

Baker-Nunn Satellite-Tracking Cameras

First successful observation	Last successful observation	Transferred to number and station	First successful observation	Last successful observation
March 31, 1968	----------	----------	----------	----------
January 5, 1971	----------	----------	----------	----------
July 1964	April 13, 1973	9043 Orroral Valley, Australia	January 1974 (est)	----------
----------	----------	----------	----------	----------
May 24, 1968	----------	----------	----------	----------
----------	----------	----------	----------	----------
June 1, 1970	----------	----------	----------	----------
August 15, 1966	----------	----------	----------	----------
September 27, 1966	May 5, 1970	9039 Natal, Brazil (new building)	May 7, 1970	----------
December 7, 1967	June 25, 1969	9030 Dionysos, Greece (new building)	July 3, 1969	----------
November 14, 1966	January 1970	See SC 11a	----------	----------
May 1972	----------	----------	----------	----------
----------	----------	----------	----------	----------

TABLE 9.2.—*Laser Sites*

Station number NGSP	SAO	Station location	Period of operation
9901	7901	Organ Pass, New Mexico	March 1966 to July 1967
9912	7912	Maui, Hawaii	May 24, 1968 to March 27, 1969
9902	7902	Olifantsfontein, South Africa	February 1971 to present
9907	7907	Arequipa, Peru	December 1970 to present
9921	7921	Mt. Hopkins, Arizona (prototype)	December 1967 to June 20, 1972
9921	7921	Mt. Hopkins, Arizona (rebuilt system)	November 1972 to present
9929	7929	Natal, Brazil	November 1970 to present
9991	7991	Athens, Greece	September 1968 to June 1969
9930	7930	Dionysos, Greece	July 1969 to present
9925	7925	Tokyo, Japan	November 1972 to present

TABLE 9.3.—*Air Force Baker-Nunn Sites*

Station number NGSP	SAO	Station location	Period of operation
9425	9113	Edwards AFB, California (Rosamund)	December 1960 to present
9424	9114	Cold Lake, Canada (I)	January 1963 to June 1971
9426	9115	Harestua, Norway	December 1959 to July 1967
	9116	Santiago, Chile	September 1960 to May 1964
9427	9117	Sand Island (Johnston Island), Pacific	September 1963 to present
	9118	Kwajalein Island	Not operational for satellite photography
9119	9119	Mt. John, New Zealand	October 1969 to present
9120	9120	San Vito, Italy	March 1971 to present
	9124	Cold Lake, Canada (II)	July 1971 to present
	9010[a]	Jupiter, Florida (AF)	June 1968 to July 1971

[a] Site previously occupied by SAO Baker-Nunn camera (see figure 9.10).

TABLE 9.4.—*Sources of Data Used in the Orbit-Generation Program*

Agency	Instrument
SAO	Baker-Nunn cameras
	Lasers
	MOONWATCH
NASA/GSFC	PRIME MINITRACK
	Lasers
U.S. Air Force	Baker-Nunn cameras
CNES	CNES cameras
	Lasers

TABLE 9.5.—*Number of Observations*

Line	n	Line	n
8015–8019	29	9006–9091	10
8015–9004	122	9006–9426	19
8015–8010	133	9007–9009	263
8015–9431	25	9007–9010	86
8015–8011	67	9007–9011	437
8015–9091	30	9007–9029	74
8019–9004	301	9007–9031	32
8019–9091	61	9008–9028	25
9001–9009	183	9008–8011	8
9001–9010	154	9008–9426	38
9001–9012	187	9009–9010	248
9001–9425	20	9009–9011	201
9001–9424	74	9009–9424	13
9001–9427	16	9010–9029	6
9002–9008	7	9010–9424	38
9002–9028	25	9011–9029	7
9004–9006	14	9011–9031	9
9004–9008	139	9012–9021	29
9004–9009	43	9012–9425	14
9004–9010	41	9012–9424	24
9004–9028	35	9012–9427	216
9004–9029	42	9021–9425	57
9004–8010	192	9021–9427	8
9004–9431	65	9028–9091	37
9004–8011	164	9029–9031	26
9008–9091	442	8010–9431	13
9004–9426	60	8010–8011	27
9005–9006	61	9431–9432	42
9005–9012	25	9431–9091	43
9005–9427	16	9432–9091	30
9006–9008	172	8425–9424	30

TABLE 9.6.—*Stations Whose Coordinates Were Determined by Orbital Theory*

Orbital theory alone		Orbital plus geometric theory		
				9021
8818	9003	1021	9001	9028
	9020	1030	9002	9029
	9023	1042	9004	9031
			9006	9050
		7050	9007	9091
		8815	9009	
		8816	9010	9113
			9011	9114
		8015	9012	9115
		8019		9117

TABLE 9.7.—*Dynamical Data Used in SE III*

Satellite										
Number	Name	Inclination	Eccentricity	a (km)	Perigee (km)	Laser observations	Station coordinates	Zonal harmonics	Tesseral harmonics	Number of files
7001701	DIAL	5°	0.088	7344	301			x		
7010901	PEOLE	15	0.017	7070	635	x		x	x	4
6001301	COURIER 1B 1970ν1	28	0.016	7465	965		x	x	x	7
5900101	VANGUARD 2 1959 α1	33	0.165	8300	557		x	x	x	7
5900701	1959 η1	33	0.188	8483	515		x			18
6100401	1961 δ1	39	0.119	7960	700				x	4
6701401	D1D	39	0.053	7337	569	x	x		x	10
6701101	D1C	40	0.052	7336	579	x	x		x	9
6503201	Explorer 24 BE-C	41	0.026	7311	941	x	x		x	13
6202901	TELSTAR 1 1962 $\alpha\epsilon$1	44	0.241	9672	962			x		4
6000902	1960 ι2	47	0.011	7971	1512		x	x	x	10
6206001	ANNA-1B 1962 $\beta\mu$1	50	0.007	7508	1077		x	x	x	12
6302601	Geophysical Research	50	0.062	7237	424			x		6
6508901	Explorer 29 GEOS-1	59	0.073	8074	1121	x	x	x	x	56
6101501	TRANSIT 4A 6101	67	0.008	7318	885			x	x	10
6101502	INJUN-1 6102	67	0.008	7316	896				x	9
6506301	SECOR-5	69	0.079	8159	1137		x		x	2
6400101		70	0.002	7301	921			x	x	4
6406401	Explorer 22 BE-B	80	0.012	7362	912	x	x	x	x	6
6508101	OGO-2	87	0.075	7344	420			x	x	5
6600501	OSCAR-07	89	0.023	7417	868		x		x	1
6304902	5BN-2	90	0.005	7473	1070		x		x	5
6102801	MIDAS-4 1961 $\alpha\delta$1	96	0.013	10005	3503		x	x	x	6
6800201	Explorer 36 GEOS-2	106	0.031	7709	1101	x	x		x	13
6507801	OV1-2	144	0.182	8306	416		x		x	4

TABLE 9.8.—*Assumed Accuracy for Data Used in SE III*

Data	Weight	Remarks
Baker-Nunn	4″	
Smoothed Baker-Nunn	2″	
SAO laser	5 m	Observed before 1970
CNES laser	10 m	Observed before 1970
GSFC laser	5 m	Observed before 1970
ISAGEX laser	5 m	1971 International Campaign

TABLE 9.9.—*Satellite Center of Mass*[a]

BE–B and BE–C	$\Delta = 0.3493 - 1.09183 \times 10^{-3} \times \phi + 2.9222 \times 10^{-6} \times \phi^2 - 1.5338 \times 10^{-7} \times \phi^3$ ($\Delta = 0$ for $\phi > 120°$)
D1C and D1D	$\Delta = 0.164612 - 2.824 \times 10^{-3} \times \phi + 2.0639 \times 10^{-5} \times \phi^2 + 8.1214 \times 10^{-7} \times \phi^3 - 5.81302 \times 10^{-9} \times \phi^4$ ($\Delta = 0$ for $\phi > 120°$)
GEOS–1	$\Delta = 0.3972 \cos \phi$
GEOS–2	$\Delta = 0.4298 \cos \phi$
PEOLE	$\Delta = 0.48 - 1.108 \times 10^{-2} \times \phi + 4.19267 \times 10^{-4} \times \phi^2 - 3.619 \times 10^{-6} \times \phi^3 + 8.12555 \times 10^{-9} \times \phi^4$ ($\Delta = 0.768$ for $\phi > 96°$)

[a] From D. Arnold and J. Latimer.

TABLE 9.10.—*Number of Observations Used in the Dynamical Solution*

Station no.	No. of observations
Pre-ISAGEX Data (15 satellites, 140 arcs)	
7050	274
8818	1223
8015	612
8815	1970
9001	4357
9002	2120
9003	349
9023	2630
9004	3343
9005	945
9006	3170
9007	1646
9008	2301
9009	1825
9010	2424
9011	1637
9012	3088
9028	525
9029	261
9031	467
9021	81
9066	809
9025	9
9080	47
9091	143
9921	9
8816	2382
8804	200
9901	761
ISAGEX Data (3 satellites, 15 arcs)	
7050	1425
7060	1514
8804	625
8809	1178
8820	296
9902	1484
9907	746
9921	225
9929	213
9930	89
9030	172
9021	29

TABLE 9.11.—*Adopted Constants*

$GM = 3.986\,013 \times 10^{20}$ cm^3 sec^{-2}	
$c = 2.997\,925 \times 10^{10}$ cm sec^{-1}	(velocity of light)
$k_2 = 0.30$	(Love number)

TABLE 9.12.—*DSN Data Used in LS 37*

Flight	Tracking time period	δ (deg)
Mariner 4 encounter	July 10–21, 1965	−3
Mariner 5 cruise	July 28–September 16, 1967	−8 to +8
Mariner 5 encounter	October 14–25, 1967	6
Mariner 5 post encounter	October 28–November 21, 1967	+2 to −2
Mariner 6	July 26–31, 1969	−24

TABLE 9.13.—*LS 37 Coordinates, From Mottinger (1973)*

Station	r (Mm)	λ	X (Mm)	Y (Mm)
DSS 11	5.206 340 9	243°15059	−2.351 428 8	−4.645 080 0
DSS 12	5.212 052 5	243°19452	−2.350 442 4	−4.651 979 4
DSS 14	5.203 997 8	243°11047	−2.353 621 1	−4.641 342 5
DSS 41	5.450 201 9	136°88749	−3.978 718 6	3.724 848 8
DSS 42	5.205 349 4	148°98126	−4.460 978 2	2.682 412 4
DSS 51	5.742 939 9	27°68542	5.085 441 5	2.668 265 9
DSS 61	4.862 608 3	355°75097	4.849 243 1	−0.360 278 5
DSS 62	4.860 818 1	355°63217	4.846 700 7	−0.370 196 0

TABLE 9.14.—*The Stations Related by the Survey*

Location	Station pairs	$1/\sigma^2$ (m^{-2})
Maryland	7050–6002	1.0
Hawaii	9012–6011	1.0
Argentina	9011–6019	1.0
Japan	9005–6013	0.1
Spain	DSS 61–DSS 62	5.0
	9004–DSS 61	0.20
Central Europe	9066–8015	0.25
	9066–6065	0.0025
	8816–9030	0.01
Brazil	9029–6067	1.0
California	DSS 14–DSS 12	5.0
	DSS 14–DSS 11	5.0
	9113–DSS 14	0.7
	9113–6111	2.0
	6111–6134	5.0
Ethiopia	9028–6042	2.0
Australia	6060–DSS 41	1.0
	9003–DSS 41	1.0
	9003–9023	1.0
	DSS 41–DSS 42	0.04
South Africa	9002–6068	1.0
	9002–DSS 51	0.1

TABLE 9.15.—*Geodetic Coordinates Used in SE–III*

Agency	Sta. no.	Latitude	Longitude	H_{msl} (m)	H_{ell} (m)	Datum	GH (m)	Name	X	Y (megameters)	Z
									a = 6 378 388.0 m		$1/f$ = 297.0000
JPL	DSS61	+40 25 47.717	355 45 06.178	788.4	766.4	EU50	−22.0	MADRI1	4.849 332 01	−.360 171 92	4.115 005 79
JPL	DSS62	+40 27 15.273	355 38 00.572	738.3	716.3	EU50	−22.0	MADRI2	4.846 789 68	−.370 090 30	4.117 028 98
NOAA	6006	+69 39 44.2698	018 56 31.9076	106.0	119.0	EU50	+13.0	TROMSO	2.103 040 80	.721 762 62	5.958 301 35
NOAA	6012	+19 17 23.227	166 36 39.780	3.5	3.5	ASTR	0.	WAKEIS	−5.858 825 61	1.394 575 85	2.093 679 89
NOAA	6015	+36 14 29.527	059 37 42.729	991.0	959.0	EU50	−32.0	MASMAD	2.604 467 55	4.444 277 33	3.750 465 44
NOAA	6016	+37 26 42.628	015 02 47.308	9.24	−6.8	EU50	−16.0	SICILY	4.896 494 12	1.316 269 43	3.856 792 86
NOAA	6020	−27 10 39.213	250 34 37.495	230.8	230.8	EI67	0.0	EASTER	−1.888 796 16	−5.355 031 80	−2.895 877 21
NOAA	6031	−46 25 03.491	168 19 31.155	0.9	.	NZ49	.	INVERC	−4.313 886 56	.891 374 93	−4.597 458 23
NOAA	6039	−25 04 07.146	229 53 11.882	339.4	339.4	PITC	0.0	PITCAN	−3.724 932 90	−4.421 406 20	−2.686 144 64
NOAA	6043	−52 46 52.468	290 46 29.573	80.7	.	CH63	.	SOMBRO	1.371 375 97	−3.614 945 94	−5.056 020 37
NOAA	6044	−53 01 12.031	073 23 27.415	3.8	3.8	HR69	0.0	HERDIS	1.099 079 48	3.684 662 62	−5.071 987 40
NOAA	6050	−64 46 33.98	295 56 37.04	16.44	.	PLMR	.	PALMER	1.192 460 38	−2.451 024 27	−5.747 260 40
NOAA	6053	−77 50 46.2487	166 38 07.5845	19.0	.	CA62	.	MCMURD	−1.310 740 80	.311 405 86	−6.213 514 12
NOAA	6055	−07 58 16.634	345 35 32.764	70.94	.	AS58	.	ASCENS	6.118 561 51	−1.571 840 78	−.878 654 81
NOAA	6065	+47 48 07.011	011 01 29.378	943.2	942.4	EU50	−0.8	PEISEN	4.213 664 69	.820 948 44	4.702 898 97
NOAA	6069	−37 03 26.2572	347 40 53.5548	24.8	24.8	TR68	0.0	DACUNA	4.979 075 44	−1.087 294 30	−3.822 545 43
NOAA	6073	−07 20 58.5270	072 28 32.1556	3.9	.	GRAC	.	CHAGOS	1.904 935 20	6.032 722 80	−.810 502 73
NOAA	6078	−17 41 46.956	168 17 57.921	15.2	.	EFAT	.	NWHBRD	−5.952 163 90	1.232 696 45	−1.926 425 29
CNES	8804	+36 27 50.1191	353 47 41.2862	25.40	−9.6	EU50	−35.0	SFRLAS	5.105 702 63	−.555 125 50	3.769 769 71
CNES	8809	+43 56 00.190	005 42 48.788	657.82	649.4	EU50	−8.4	HTPRVL	4.578 434 82	.458 082 30	4.403 291 78
CNES	8809	+43 56 00.190	005 42 48.788	657.82	647.8	EU50	−10.0	HTPRVL	4.578 435 96	.458 082 42	4.403 292 89
CNES	8815	+43 55 59.183	005 42 48.382	657.83	649.4	EU50	−8.4	HTPRVL	4.578 458 32	.458 075 55	4.403 270 50
CNES	8816	+37 45 17.043	022 49 43.313	803.11	788.7	EU50	−14.4	STPHNL	4.654 421 39	1.959 282 40	3.884 501 87
CNES	8818	+31 43 19.25	357 34 54.06	855.65	813.7	EU50	−42.0	BECHRL	5.426 419 14	−.229 172 16	3.334 728 56
SAO	9930	+38 04 46.147	023 55 59.991	473.02	466.62	EU50	−6.4	DIOSLS	4.595 303 76	2.039 557 34	3.912 743 97
CNES	8015	+43 56 01.142	005 42 49.277	658.85	650.4	EU50	−8.4	HTPROV	4.578 415 31	.458 091 32	4.403 314 74
CNES	8019	+43 43 36.496	007 18 03.309	377.42	369.4	EU50	−8.	NICEFR	4.579 557 55	.586 729 53	4.386 538 88
SAO	9004	+36 27 51.3666	353 47 42.0891	26.00	−9.0	EU50	−35.0	S.FERN	5.105 682 54	−.555 103 20	3.769 801 00
SAO	9006	+29 21 38.97	079 27 25.51	1927.	1827.	EU50	−100.	NA.TAL	1.018 269 70	5.471 218 80	3.109 759 10
SAO	9008	+29 38 18.112	052 31 11.445	1597.4	1549.4	EU50	−48.0	SHIRAZ	3.376 963 53	4.404 102 29	3.136 405 45
SAO	9028	+08 44 56.39	038 57 33.61	1923.2	1820.2	EU50	−105.	ETHIOP	4.903 855 04	3.965 304 21	.964 021 18
SAO	9030	+38 04 46.564	023 56 00.130	472.64	466.24	EU50	−6.4	DIOSBN	4.595 294 86	2.039 557 10	3.912 753 85
SAO	9051	+37 58 40.31	023 46 42.89	187.9	180.9	EU50	−7.0	ATHENG	4.606 949 19	2.029 849 75	3.903 882 23
INT.	8010	+46 52 40.318	007 27 58.238	903.44	900.3	EU50	−3.1	ZIMMWL	4.331 391 50	.567 637 49	4.633 236 85
INT.	9431	+56 56 54.98	024 03 37.81	8.0	2.4	EU50	−5.6	RIGALT	3.183 998 49	1.421 638 06	5.322 893 86
INT.	9432	+48 38 04.56	022 17 57.88	189.0	187.5	EU50	−1.5	UZGROD	3.907 492 64	1.602 532 61	4.764 032 96
INT.	8011	+52 08 39.116	358 01 59.492	113.19	108.6	EU50	−4.6	MALVRN	3.920 249 42	−.134 624 34	5.012 850 24
SAO	9091	+38 04 48.215	023 56 01.587	466.25	460.85	EU50	−6.4	DIONBN	4.595 247 88	2.039 575 10	3.912 790 60
AF	9426	+60 12 40.38	010 45 08.74	575.92	581.7	EU50	+5.8	HAREST	3.121 368 36	.592 747 33	5.512 829 59
AF	9427	+16 44 45.39	190 29 05.59	5.0	5.0	JI61	0.0	JOHNST	−6.007 589 42	−1.111 801 81	1.825 951 15

TABLE 9.15.—*(Cont'd)*

Agency	Sta. no.	Latitude	Longitude	H_{msl} (m)	H_{ell} (m)	Datum	GH (m)	Name	X	Y (megameters)	Z
									a = 6 377 397.2 m		$1/f$ = 299.1528
NOAA	6013	+31 23 30.1397	130 52 24.8595	65.9	46.9	TKYO	−19.	KANOYA	−3.565 710 19	4.120 207 06	3.302 741 97
SAO	9005	+35 40 11.078	139 32 28.222	59.77	59.8	TKYO	+0.0	TOKYOJ	−3.946 555 04	3.365 774 71	3.698 152 01
SAO	9025	+36 00 08.606	139 11 43.159	855.89	855.4	TKYO	−0.5	DODRAJ	−3.910 298 61	3.375 836 40	3.728 538 81
									a = 6 378 206.4 m		$1/f$ = 294.9787
GSFC	1021	+38 25 49.628	282 54 48.225	5.76	6.7	NA27	+0.9	IBPOIN	1.118 061 22	−4.876 472 15	3.942 793 54
JPL	DSS11	+35 23 22.346	243 09 05.262	1036.3	1014.3	NA27	−22.0	GOLDS1	−2.351 415 01	−4.645 228 10	3.673 582 42
JPL	DSS12	+35 17 59.854	243 11 43.414	988.9	966.9	NA27	−22.0	GOLDS2	−2.350 428 27	−4.652 127 55	3.665 447 06
JPL	DSS14	+35 25 33.340	243 06 40.850	1031.8	1009.8	NA27	−22.0	GOLDS4	−2.353 607 04	−4.641 490 95	3.676 870 68
NOAA	6001	+76 30 03.4106	291 27 51.8867	206.0	238.	NA27	+32.	THULEG	.546 580 65	−1.390 107 20	6.180 059 57
NOAA	6002	+39 01 39.003	283 10 26.942	44.3	43.9	NA27	−0.4	BELTVL	1.130 798 67	−4.830 987 41	3.994 520 58
NOAA	6003	+47 11 07.132	240 39 48.118	368.74	356.2	NA27	−12.5	MOSELK	−2.127 796 49	−3.786 014 63	4.655 848 03
NOAA	6004	+52 42 54.89	174 07 37.87	36.8	−9.2	NA27	−46.0	SHEMYA	−3.851 745 00	.396 192 09	5.051 199 36
NOAA	6011	+20 42 38.561	203 44 28.529	3049.27	3041.3	OHAW	−8.	HAVAII	−5.466 062 54	−2.404 129 70	2.242 407 61
NOAA	6022	−14 20 12.216	189 17 13.242	5.34	5.3	AS62	0.0	PAGOGO	−6.099 842 41	−.997 467 71	−1.569 008 83
NOAA	6038	+18 43 44.93	249 02 39.28	23.2	23.2	ISOC	0.0	GIGEDO	−2.161 114 55	−5.642 916 48	2.034 864 29
NOAA	6047	+06 55 26.132	122 04 04.838	9.39	10.1	LZ11	+0.7	ZAMBOA	−3.361 826 92	5.365 864 13	.763 735 96
NOAA	6111	+34 22 54.537	242 19 09.484	2284.41	2258.11	NA27	−26.3	WRWDBA	−2.448 815 18	−4.688 125 78	3.582 568 64
NOAA	6123	+71 18 49.882	203 21 20.720	8.3	−6.	NA27	+1.3	PTBRRW	−1.881 756 24	−.812 583 99	6.019 403 56
NOAA	6134	+34 22 44.444	242 19 09.259	2198.37	2172.07	NA27	−26.3	WRWDBB	−2.448 868 89	−4.668 215 79	3.582 263 30
GSFC	7050	+39 01 13.676	283 10 18.035	54.812	56.1	NA27	+1.2	GODLAS	1.130 704 28	−4.831 524 29	3.993 921 50
GSFC	7060	+13 18 28.6136	144 44 05.3744	85.873	85.9	GUAM	0.	GUAMLS	−5.068 867 06	3.584 334 33	1.458 509 59
SAO	9901	+32 25 24.56	253 26 51.17	1651.33	1648.93	NA27	−2.4	ORGN L	−1.535 725 37	−5.167 146 55	3.400 867 41
SAO	9912	+20 42 37.23	203 44 24.03	3034.14	3026.1	OHAW	−8.	MAUIHL	−5.466 115 22	−2.404 010 58	2.242 363 93
SAO	9921	+31 41 02.87	249 07 21.35	2383.14	2370.4	NA27	−12.7	MHSAOL	−1.936 750 26	−5.077 855 96	3.331 744 02
SAO	9001	+32 25 25.56	253 26 51.17	1651.3	1648.9	NA27	2.4	ORGN P	−1.535 725 37	−5.167 146 55	3.400 867 41
SAO	9010	+27 01 12.882	279 53 13.008	15.13	26.5	NA27	+11.4	JUPITE	.976 312 16	−5.601 550 92	2.880 064 23
SAO	9012	+20 42 37.50	203 44 24.08	3034.14	3026.1	OHAW	−8.	MAUI,H	−5.466 111 95	−2.404 010 72	2.242 371 70
SAO	9021	+31 41 02.67	249 07 21.35	2383.12	2370.4	NA27	−12.7	MTHPBN	−1.936 751 41	−5.077 858 98	3.331 738 78
AF	9425	+34 57 50.742	242 05 11.584	784.231	760.4	NA27	−23.8	ROSMND	−2.449 975 02	−4.624 572 36	3.634 851 19
AF	9424	+54 44 33.858	249 57 26.389	704.6	701.7	NA27	−2.9	CLALBC	−1.264 825 81	−3.467 044 42	5.185 275 10

TABLE 9.15.—*(Cont'd)*

Agency	Sta. no.	Latitude	Longitude	H_{msl} (m)	H_{ell} (m)	Datum	GH (m)	Name	X	Y (megameters)	Z
									a = 6 378 249.145 m		$1/f$ = 293.465
JPL	DSS51	−25 53 21.15	027 41 08.53	1391.0	1399.0	ARCC	+8.	JOHANG	5.085 580 65	2.668 370 93	−2.768 408 99
NOAA	6042	+08 46 08.501	038 34 49.164	1886.46	1857.5	ADDN	−29.0	ADDABA	4.900 912 36	3.968 254 30	.966 118 39
NOAA	6063	+14 44 44.228	342 30 55.594	26.3	26.3	YO67	0.	SENGAL	5.884 522 66	−1.853 639 29	1.612 760 05
NOAA	6064	+12 07 51.750	015 02 06.151	295.4	316.4	ADDN	+21.0	FTLAMY	6.023 554 50	1.617 955 70	1.331 525 26
NOAA	6068	−25 52 56.98	027 42 25.17	1523.8	1531.8	ARCC	+8.	JOHANS	5.084 982 16	2.670 466 91	−2.767 797 68
NOAA	6075	−04 40 07.23	035 28 50.38	588.98	.	SEIL	.	MAHEIS	3.602 875 32	5.238 427 44	−.515 676 27
CNES	8820	+14 46 04.878	342 35 22.462	28.48	28.5	YO67	0.0	DAKARL	5.886 315 60	−1.845 836 00	1.615 157 50
SAO	9902	−25 57 33.851	028 14 53.909	1543.88	1551.9	ARCC	+8.	OLIFTL	5.056 260 03	2.716 634 10	−2.775 471 14
SAO	9002	−25 57 33.85	028 14 53.91	1544.1	1552.1	ARCC	+8.	OLFSFT	5.056 260 19	2.716 634 22	−2.775 471 20
CNES	9020	+14 46 05.975	342 35 22.936	24.59	24.6	YO67	0.0	DAKARS	5.886 308 05	−1.845 818 78	1.615 189 11
SAO	9022	−25 57 33.815	028 14 54.351	1543.34	1551.3	ARCC	+8.	OLIFTS	5.056 254 16	2.716 644 91	−2.775 469 88
SAO	9028	+08 44 47.23	038 57 30.48	1925.2	1896.2	ADDN	−29.	ETHIOP	4.903 904 76	3.965 221 35	.963 656 06
									a = 6 378 160.0 m		$1/f$ = 298.25
JPL	DSS41	−31 22 59.4305	136 53 10.1244	148.28	147.3	AUGD	−1.0	WOOMAU	−3.978 581 94	3.724 896 03	−3.302 323 84
JPL	DSS42	−35 24 08.0381	148 58 48.2057	656.08	664.5	AUGD	+8.4	TIDBIN	−4.460 848 00	2.682 461 57	−3.674 729 47
NOAA	6008	+05 26 55.325	304 47 42.832	18.38	+8.7	SA69	−9.7	SURNAM	3.623 335 39	−5.214 222 41	.601 599 57
NOAA	6009	−00 05 50.468	281 34 49.212	2682.1	2706.7	SA69	+24.6	ECUADR	1.280 904 38	−6.250 970 09	−.010 769 28
NOAA	6019	−31 56 33.9540	294 53 41.3415	608.18	621.2	SA69	+13.0	DLORES	2.280 712 97	−4.914 539 50	−3.355 387 84
NOAA	6023	−10 35 08.0374	142 12 35.4955	60.5	61.7	AUGD	+1.2	THURIS	−4.955 236 08	3.842 309 46	−1.163 990 61
NOAA	6032	−31 50 28.992	115 58 26.618	26.30	32.5	AUGD	+6.2	PERTHA	−2.375 257 20	4.875 599 99	−3.345 531 90
NOAA	6060	−30 18 39.4182	149 33 36.8921	211.08	211.8	AUGD	+0.7	CULGOR	−4.751 500 46	2.792 121 93	−3.200 296 97
NOAA	6067	−05 55 37.414	324 50 06.200	40.63	66.7	SA69	+26.1	BRAZIL	5.186 494 84	−3.653 919 32	−.654 244 53
SAO	9907	−16 27 55.085	288 30 26.814	2452.274	2486.5	SA69	+34.2	ARQUPL	1.942 859 44	−5.804 087 19	−1.796 876 89
SAO	9929	−05 55 38.616	324 50 08.660	45.6	71.7	SA69	+26.1	NATALL	5.186 539 40	−3.653 858 15	−.654 281 78
SAO	9003	−31 06 07.2608	136 46 58.6988	159.21	158.1	AUGD	−1.1	WOOMER	−3.983 657 92	3.743 132 37	−3.275 676 47
SAO	9007	−16 27 55.085	288 30 26.814	2451.86	2486.1	SA69	+34.2	AREQUI	1.942 859 32	−5.804 086 83	−1.796 876 77
SAO	9009	+12 05 25.912	291 09 46.078	7.44	−3.4	SA69	−10.8	CURACA	2.251 890 08	−5.816 918 37	1.327 200 69
SAO	9011	−31 56 33.228	294 53 38.949	608.	621.0	SA69	+13.0	V.DLOR	2.280 660 87	−4.914 576 54	−3.355 368 76
SAO	9023	−31 23 30.8163	136 52 39.0156	137.91	136.9	AUGD	−1.0	LAGOON	−3.977 646 16	3.725 145 80	−3.303 143 65
SAO	9027	−16 27 54.365	288 30 26.578	2450.23	2484.4	SA69	+34.2	AREQU2	1.942 854 16	−5.804 093 46	−1.796 855 06
SAO	9029	−05 55 38.616	324 50 08.660	45.34	71.4	SA69	+26.1	NATLBR	5.186 539 16	−3.653 857 98	−.654 281 74
SAO	9031	−45 53 11.028	292 23 12.215	186.54	172.5	SA69	−14.0	CHDRVD	1.693 869 60	−4.112 339 51	−4.556 606 80
SAO	9039	−05 55 38.616	324 50 09.401	41.6	67.7	SA69	+26.1	NATAL2	5.186 549 28	−3.653 837 23	−.654 281 36

Agency	Sta. no.	Latitude	Longitude	H_{msl} (m)	H_{ell} (m)	Datum	GH (m)	Name	X	Y (megameters)	Z
									a = 6 378 140.0 m		$1/f$ = 298.258
NOAA	6007	+38 45 36.725	332 54 21.064	53.3	53.3	GRAC	0.0	AZORES	4.433 563 44	−2.268 197 74	3.971 629 06
NOAA	6040	−12 11 57.91	096 49 47.08	4.4	4.4	ASTR	0.0	COCOIS	−.741 462 10	6.190 800 89	−1.338 974 41
NOAA	6045	−20 13 50.	057 25 15.	149.4	.	NSPC	.	MAURIT	3.223 895 00	5.045 104 82	−2.191 716 44
NOAA	6051	−67 36 03.08	062 52 24.41	11.3	11.3	ASTR	0.0	MAWSON	1.111 359 85	2.169 307 95	−5.874 285 99
NOAA	6052	−66 16 45.12	110 32 04.61	18.0	18.0	ASTR	0.0	WILKES	−.902 551 77	2.409 545 73	−5.816 560 60
NOAA	6059	+02 00 35.622	202 35 21.962	2.75	.	XM67	.	XMASIS	−5.885 219 81	−2.448 507 30	.222 198 23
NOAA	6061	−54 16 39.515	323 30 42.531	4.2	.	SGRG	.	SOGEOR	3.000 591 10	−2.219 363 27	−5.154 853 86
NOAA	6072	+18 46 10.	098 58 15.	319.3	.	NSPC	.	TILAND	−.942 038 16	5.967 454 08	2.039 306 54

TABLE 9.16.—*Orbital Elements of Adopted Satellites*

Satellite	n (rev day^{-1})	i	e
7001701	13.800	5°.410	0.0880
7010901	14.811	15°.040	0.0165
6001301	13.454	28°.330	0.0166
5900101	11.460	32°.880	0.1650
6202901	9.126	44°.800	0.2428
6000902	12.197	47°.230	0.0114
6302601	14.108	49°.740	0.0600
6206001	13.345	50°.140	0.0070
6508901	11.968	59°.380	0.0717
6101501	13.870	66°.820	0.0080
6400101	13.920	69°.910	0.0015
6406401	13.746	79°.700	0.0129
6508101	13.805	87°.370	0.0743
6102801	8.677	95°.850	0.0121

TABLE 9.17.—*Coefficients of C_n Based on Kozai's (1964) Values*[a]

$C_2 = -1082.639$	$C_3 = 2.546$
$C_4 = 1.649$	$C_5 = 0.210$
$C_6 = 0.646$	$C_7 = 0.333$
$C_8 = 0.270$	$C_9 = 0.053$
$C_{10} = 0.054$	$C_{11} = -0.302$
$C_{12} = 0.357$	$C_{13} = 0.114$
$C_{14} = -0.179$	

[a] Given in units of 10^{-6}.

TABLE 9.18.—(O-C) *for Secular Motion and Their Differences*[a]

Satellite		(O-C)		I	II	1969	1962	1961	1959
7001701	$\dot{\omega}$ -----	−18060	±90	−57	271	29090	9540	18250	18840
	$\dot{\Omega}$ -----	10120	±70	−51	258	−17400	−5390	−9950	−10240
7010910	$\dot{\omega}$ -----	−2200	±800	−1530	−857	−4700	100	6200	6900
	$\dot{\Omega}$ -----	5160	±100	−83	99	−2160	−1450	−5560	−5900
6001301	$\dot{\omega}$ -----	170	±100	43	61	40	−300	−670	−90
	$\dot{\Omega}$ -----	−125	±5	−4	−10	−1	59	−611	−928
5900101	$\dot{\omega}$ -----	32	±3	1	3	1	18	−129	278
	$\dot{\Omega}$ -----	−9	±3	2	7	0	10	−248	−488
6202901	$\dot{\omega}$ -----	40	±6	11	10	2	300	827	1013
	$\dot{\Omega}$ -----	7	±3	5	8	2	−39	−247	−395
6000902	$\dot{\omega}$ -----	170	±50	0	21	47	−287	770	1070
	$\dot{\Omega}$ -----	−1	±3	1	5	4	−43	−342	−594
6302601	$\dot{\omega}$ -----	920	±10	−1	−6	−52	2650	4900	5290
	$\dot{\Omega}$ -----	1	±3	0	−2	19	261	−2	−352
6206001	$\dot{\omega}$ -----	600	±60	16	84	60	2230	4180	4500
	$\dot{\Omega}$ -----	−42	±3	1	2	8	−56	−437	−740
6508901	$\dot{\omega}$ -----	−110	±10	−1	−29	−26	1460	3180	3285
	$\dot{\Omega}$ -----	−70	±3	0	−6	−7	−670	−1465	−1670
6101501	$\dot{\omega}$ -----	−300	±80	14	97	65	−81	1900	2500
	$\dot{\Omega}$ -----	22	±3	−1	−1	3	−1252	−2815	−3057
6400101	$\dot{\omega}$ -----	600	±800	729	718	620	−600	580	−500
	$\dot{\Omega}$ -----	56	±8	10	6	9	−1073	−2703	−2921
6406401	$\dot{\omega}$ -----	−400	±100	−95	−231	−110	−2000	−4000	−4300
	$\dot{\Omega}$ -----	90	±10	9	9	15	−220	−1351	−1467
6508101	$\dot{\omega}$ -----	620	±30	15	100	−8	300	−3290	−3630
	$\dot{\Omega}$ -----	50	±3	−2	−9	−27	35	−306	−337
6102801	$\dot{\omega}$ -----	−35	±50	−47	−47	−47	−340	−915	−1008
	$\dot{\Omega}$ -----	−2.9	±0.5	0.6	0.7	0.6	62.7	192.3	212.6

[a] Given in units of 10^{-6} degrees per day.

TABLE 9.19.—(O-C) *for Amplitudes of* $\left.\begin{matrix}cos\\sin\end{matrix}\right\}$ 2ω *Terms and Their Differences*[a]

Satellite		(O-C)	I	II	1969	1962	1961	1959
5900101	ω	0.3 ± 0.5	−0.2	−0.2	−0.3	−0.6	1.5	1.4
	Ω	−2 ± 2	−1	−2	−2	−1	−4	−4
	i	−3 ± 6	−4	−4	−5	−4	3	3
	e	0 ± 1	1	1	1	1	−4	−4
6202901	ω	−0.1 ± 0.3	−0.2	−0.2	−0.2	−0.8	−2.5	−2.7
	Ω	−1 ± 1	1	1	1	−8	−14	−14
	i	4 ± 4	5	4	4	−3	−14	−15
	e	0 ± 1	0	0	0	5	12	12
6000902	ω	−3 ± 4	−2	−2	−2	−6	−10	−10
	e	0 ± 1	0	0	0	0	1	1
6302601	ω	−6 ± 2	−1	0	0	−14	−23	−23
	Ω	2 ± 2	3	3	3	−2	−3	−3
	i	−1 ± 3	1	1	1	−4	−6	−6
	e	3 ± 2	−3	−3	−3	12	20	20
6205001	ω	3 ± 6	7	6	6	−5	−13	−13
	e	1 ± 1	1	1	0	2	3	3
6508901	ω	6 ± 2	1	2	2	−22	−49	−50
	Ω	4 ± 2	2	2	0	9	10	10
	i	5 ± 5	4	4	4	−3	−11	−11
	e	−4 ± 1	2	1	1	30	62	63
6101501	ω[b]	−1 ± 2	−1	0	0	−3	0	0
	e	1 ± 2	0	0	−1	3	−1	−1
6406401	ω[b]	0 ± 2	0	0	0	−1	−1	−1
	e	4 ± 4	3	4	3	5	7	7
6508101	ω	7 ± 3	3	4	3	12	0	0
	Ω	1 ± 1	1	0	0	2	2	2
	i	−2 ± 8	−2	−2	−2	−2	−2	−2
	e	6 ± 2	1	−2	−1	−11	3	3

[a] Given in units of 10^3 degrees for ω, 10^4 degrees for Ω, 10^5 degrees for i, and 10^6 degrees for e per day.

[b] For these satellites, ω is in units of 10^2 degrees.

TABLE 9.20.—(O-C) *for Amplitudes of* $\left.\begin{matrix}cos\\sin\end{matrix}\right\}\omega$ *Terms and Their Differences*[a]

Satellite		(O-C)	I	II	1969	1962	1961	1959
7001701	ω	70 ± 5	−2	0	−126	−104	−85	−87
	Ω	−190 ± 30	0	−28	−248	−570	−168	−237
	i	430 ± 30	−34	−31	740	900	480	550
	e	−91 ± 6	−5	−5	−149	−179	−99	−112
7010901	ω	45 ± 30	9	41	160	−411	232	112
	Ω	−18 ± 45	−44	−48	0	10	9	7
	i	−170 ± 300	−166	−170	−181	−120	−190	−177
	e	28 ± 20	18	27	61	−102	83	49
6001301	ω	4 ± 1	0	0	0	46	314	241
	Ω	0 ± 3	2	2	0	3	−10	−7
	i	0 ± 30	0	0	0	−2	−16	−12
	e	1.6 ± 1.0	0.5	0.5	0.6	13.5	90.7	69.8
5900101	ω	−1.7 ± 0.3	0.0	0.3	0.0	4.8	22.4	17.2
	Ω	−2 ± 2	2	1	2	−7	−87	−58
	i	1 ± 5	−3	−3	−4	−8	−64	−57
	e	−3.1 ± 0.5	−0.3	−0.7	−0.1	3.2	40.0	35.6
6202901	ω	−0.1 ± 0.2	0.0	0.0	−0.1	−1.2	−4.0	6.1
	Ω	2 ± 3	2	3	3	16	5	31
	i	−2 ± 3	−5	−4	−4	−11	−26	−78
	e	± 0.8	0.2	0.0	0.2	4.2	15.2	49.7
6000902	ω	−19 ± 3	−4	−4	−10	42	1	315
	Ω	1 ± 1	1	1	0	3	4	6
	i	−2 ± 6	−2	−2	−6	−3	−2	−6
	e	−2.0 ± 0.6	1.0	1.0	0.3	10.5	2.4	64.8
6302601	ω	−17 ± 2	0	−4	−1	9	−17	86
	Ω	−6 ± 1	0	0	1	20	52	60
	i	14 ± 15	10	11	10	6	12	−19
	e	−12 ± 1	0	−1	2	16	−6	99
6206001	ω	−59 ± 4	0	5	0	187	122	931
	Ω	−2 ± 2	−2	−2	−2	0	3	4
	i	0 ± 10	0	0	0	−1	0	−4
	e	−8 ± 1	−1	0	−1	22	14	113
6508901	ω	3 ± 4	7	7	0	119	264	486
	Ω	10 ± 2	3	3	2	−10	8	−29
	i	−8 ± 8	−9	−9	−7	−40	−80	−144
	e	−4 ± 1	0	0	−2	127	292	555

TABLE 9.20.—*(Cont'd)*

Satellite		(O-C)	I	II	1969	1962	1961	1959
6101501	ω^b	−19 ± 5	−11	−11	−8	−46	−265	−413
	Ω	−3 ± 4	2	2	0	7	17	29
	i	0 ± 5	0	0	0	1	7	11
	e	−11 ± 1	0	0	4	−48	−354	−560
6400101	ω^b	−200 ± 10	6	3	1	−72	−445	−593
	e	−58 ± 3	−4	−5	−9	−24	−122	−161
6406401	ω	−110 ± 20	23	36	30	23	510	930
	Ω	6 ± 3	1	1	1	5	11	16
	i	0 ± 8	0	0	0	0	−2	−3
	e	−34 ± 5	−4	−2	−2	−4	106	199
6508101	ω	60 ± 2	1	−1	3	64	197	296
	Ω	20 ± 1	0	2	2	16	26	32
	i	−10 ± 10	−9	−9	−10	−10	−13	−16
	e	60 ± 3	−4	−5	−2	67	231	354
6102801	ω	−30 ± 50	−48	−47	−40	15	390	663
	Ω	−2 ± 2	−2	−2	−2	−2	−3	−4
	i	−6 ± 7	−6	−6	−6	−6	−6	−5
	e	3.0 ± 1.5	−0.7	−0.6	0.0	12.5	91.8	149.2

[a] Given in units of 10^3 degrees for ω, 10^4 degrees for Ω, 10^5 degrees for i, and 10^6 degrees for e per day.

[b] For these satellites, ω is in units of 10^2 degrees.

TABLE 9.21.—*Assumed Accuracy for SE III*

Data	Weight	Remarks
Baker-Nunn	4″	
Smoothed Baker-Nunn	2″	
SAO laser	5 m	Taken before 1970, observed before 1970
CNES laser	10 m	Taken before 1970, observed before 1970
GSFC laser	5 m	Taken before 1970, observed before 1970
ISAGEX laser	2 m	1971 International Campaign
Gravity anomalies	$\langle A \rangle \frac{13.5}{nA}$ mGal	n is the number of 1° × 1° squares in each 5° × 5° mean
Model (zero) anomalies	$\langle A \rangle \frac{27}{A}$ mGal	A is the area

TABLE 9.22.—*Smithsonian Atomic Time Defined With Respect to WWV and UTC (USNO)*[a,b]

Interval			A (sec)	B (sec/day)	T_0 (mod. J.d.)
$(A.S - WWV) = A + B\,(T - T_0)$ before September 20, 1967					
1961 Jan.	01.0—1961 Jul.	01.0	1.458 858	+ 0.001 296 000	$(T - 37\,300.0)$
1961 Jul.	01.0—1961 Jul.	13.0	1.693 434	+ 0.001 292 000	$(T - 37\,480.0)$
1961 Jul.	13.0—1961 Aug.	01.0	1.694 215	+ 0.001 245 000	$(T - 37\,480.0)$
1961 Aug.	01.0—1961 Sep.	21.0	1.643 160	+ 0.001 280 000	$(T - 37\,480.0)$
1961 Sep.	21.0—1961 Oct.	01.0	1.641 500	+ 0.001 300 000	$(T - 37\,480.0)$
1961 Oct.	01.0—1961 Nov.	01.0	1.642 184	+ 0.001 290 764	$(T - 37\,480.0)$
1961 Nov.	01.0—1962 Jan.	01.0	1.643 272	+ 0.001 289 444	$(T - 37\,480.0)$
1962 Jan.	01.0—1962 Apr.	01.0	1.865 000	+ 0.001 123 200	$(T - 37\,650.0)$
1962 Apr.	01.0—1962 Jul.	01.0	1.864 620	+ 0.001 126 800	$(T - 37\,650.0)$
1962 Jul.	01.0—1963 Jan.	01.0	1.864 704	+ 0.001 126 370	$(T - 37\,650.0)$
1963 Jan.	01.0—1963 Nov.	01.0	2.292 725	+ 0.001 118 458	$(T - 38\,030.0)$
1963 Nov.	01.0—1964 Jan.	01.0	2.392 725	+ 0.001 118 458	$(T - 38\,030.0)$
1964 Jan.	01.0—1964 Apr.	01.0	2.800 962	+ 0.001 293 560	$(T - 38\,395.0)$
1964 Apr.	01.0—1964 Jul.	01.0	2.900 766	+ 0.001 295 716	$(T - 38\,395.0)$
1964 Jul.	01.0—1964 Sep.	01.0	2.901 518	+ 0.001 292 659	$(T - 38\,395.0)$
1964 Sep.	01.0—1964 Oct.	01.0	3.001 518	+ 0.001 292 659	$(T - 38\,395.0)$
1964 Oct.	01.0—1965 Jan.	01.0	3.001 589	+ 0.001 296 048	$(T - 38\,395.0)$
1965 Jan.	01.0—1965 Mar.	01.0	3.575 732	+ 0.001 296 000	$(T - 38\,761.0)$
1965 Mar.	01.0—1965 Jul.	01.0	3.675 732	+ 0.001 296 000	$(T - 38\,761.0)$
1965 Jul.	01.0—1965 Sep.	01.0	3.775 732	+ 0.001 296 000	$(T - 38\,761.0)$
1965 Sep.	01.0—1966 Jan.	01.0	3.875 732	+ 0.001 296 000	$(T - 38\,761.0)$
1966 Jan.	01.0—1967 Jan.	01.0	3.348 772	+ 0.002 592 000	$(T - 39\,126.0)$
1967 Jan.	01.0—1967 Sep.	20.0	5.294 852	+ 0.002 592 000	$(T - 39\,491.0)$
$[A.S - UTC\,(USNO) = A + B\,(T - T_0)]$ after September 27, 1967					
1967 Sep.	20.0—1968 Jan.	01.0	5.294 688	+ 0.002 592 000	$(T - 39\,491.0)$
1968 Jan.	01.0—1968 Feb.	01.0	6.240 768	+ 0.002 592 000	$(T - 39\,856.0)$
1968 Feb.	01.0—1969 Jan.	01.0	6.140 768	+ 0.002 592 000	$(T - 39\,856.0)$
1969 Jan.	01.0—1970 Jan.	01.0	7.089 440	+ 0.002 592 000	$(T - 40\,222.0)$
1970 Jan.	01.0—1971 Jan.	01.0	8.035 520	+ 0.002 592 000	$(T - 40\,587.0)$
1971 Jan.	01.0—1972 Jan.	01.0	8.981 600	+ 0.002 592 000	$(T - 40\,952.0)$
1972 Jan.	01.0—1972 Jul.	01.0	10.035 280	+ 0.000 000 000	$(T - 41\,317.0)$

[a] From M. R. Pearlman, J. M. Thorp., C. R. H. Tsiang, D. A. Arnold, C. G. Lehr, and J. Wohn.

[b] Since September 20, 1967, SAO's satellite observations have been referred to UTC(USNO). Before that date, observations were referred to time of emission of WWV signals (WWV-emitted). Both timing systems are readily available for use in the field, yet both have occasional discontinuities which make them inappropriate for analysis.

When the satellite-tracking program began in the late 1950's, uniform time standards such as A1 and their differences from WWV emitted (and later UTC) were not available in a timely fashion. However, the intended relations between WWV (and later UTC) and the uniform time standard A1 were published regularly. SAO has used these intended relations to generate a facsimile of A1 from WWV and UTC data.

TABLE 9.23.—*Accuracy of an Observation as a Function of Topocentric Angular Velocity*

Cycle rate (sec)	Associated topocentric velocity of object (arc-sec sec^{-1})	With VLF and portable clocks		With VHF	
		Along track	Across track	Along track	Across track
32	0– 250	1".8	1".8	1".8	1".8
16	250– 500	1".8	1".8	2".1	1".8
8	500–1000	1".9	1".8	2".3	1".8
4	1000–2000	1".9	1".8	2".7	1".8
2	>2000	2".0	1".8	3".7	1".8

TABLE 9.24.—*Sensitivity Coefficients for Satellite 6701401*[a]

e = 0.084 313 0 A = 7614 km
I = 39°.454 59 perigee = 594 km
n = 13.064 356 apogee = 1878 km

m \ ℓ	11	12	13	14	15	16	17	18	19	20
1	154	229	121	75	139	160	66	69	118	67
2	113	43	61	94	58	35	59	46	0	33
3	52	78	65	25	54	43	12	18	39	26
4	66	34	19	39	38	14	10	27	0	0
5	38	28	51	29	0	23	10	0	0	18
6	65	48	42	14	27	19	0	17	0	0
7	68	62	61	45	10	0	18	16	0	0
8	46	62	45	37	18	12	0	0	18	0
9	21	30	46	64	55	53	23	0	0	0
10	0	0	29	44	43	58	37	32	0	0
11	0	0	8	16	27	48	47	57	48	44
12		0	0	21	44	64	89	101	75	99
13			425	1203	2987	4758	8014	9531	12277	11613
14				0	0	20	47	77	111	145
15					0	0	0	0	16	20
16						0	0	0	0	0
17							0	0	0	0
18								0	0	0
19									0	0
20										0

[a] Given in units of meters, with $|\mathfrak{C}_{\ell m}| \times 10^6$.

TABLE 9.25.—*Results of Complete Network Adjustment*

Interstation direction	Direction cosines			σ_ψ^2 (μrad)	σ_μ^2 (μrad)	$\sigma_{\psi\mu}$ (μrad)	No. obs.
	x	y	z				
			SAO Network				
8015-8019	0.008 826 76	0.991 566 88	−0.129 295 09	4378.25	3682.33	409.04	29
8015-9004	0.403 688 17	−0.775 736 75	−0.485 044 69	29.21	17.80	7.03	122
8015-9066	−0.696 237 98	0.308 764 57	0.648 010 12	552.99	204.51	−61.20	133
8015-9074	−0.723 132 48	0.499 652 76	0.476 892 59	54.68	21.55	−18.85	25
8015-9080	−0.612 142 61	−0.551 268 92	0.566 907 41	90.07	42.32	18.81	67
8015-9091	0.010 166 06	0.955 062 10	−0.296 231 40	24.96	25.68	0.97	30
8019-9004	0.375 702 50	−0.815 399 14	−0.440 422 38	8.99	5.46	2.27	301
8019-9091	0.010 266 10	0.950 679 22	−0.310 005 84	23.46	12.23	−1.87	61
9001-9007	0.553 303 12	−0.101 336 83	−0.826 792 90	7.19	4.91	−1.16	35
9001-9009	0.867 353 66	−0.148 829 84	−0.474 918 21	5.08	6.60	−3.13	183
9001-9010	0.965 435 98	−0.166 946 59	−0.200 155 43	12.00	14.31	−7.74	154
9001-9012	−0.795 296 06	0.559 031 40	−0.234 495 37	9.01	9.63	6.26	187
9001-9113	−0.839 865 57	0.498 415 57	0.214 959 85	119.75	227.49	110.69	20
9001-9114	0.109 263 14	0.685 666 26	0.719 668 92	41.57	18.51	−0.64	74
9001-9117	−0.716 762 03	0.649 994 62	−0.252 505 81	8.64	19.81	7.90	16
9002-9008	−0.263 480 98	0.264 768 12	0.927 618 25	23.08	145.74	−37.94	7
9002-9028	−0.038 627 03	0.316 476 94	0.947 813 43	52.37	119.71	21.28	25
9004-9006	−0.559 029 19	0.824 219 14	−0.090 272 72	8.87	8.85	−3.97	14
9004-9008	−0.326 789 15	0.937 481 22	−0.119 740 60	13.50	8.84	−6.96	139
9004-9009	−0.441 426 33	−0.813 880 96	−0.377 810 25	25.76	27.96	20.26	43
9004-9010	−0.627 485 32	−0.766 807 91	−0.135 158 44	26.73	28.14	18.57	41
9004-9028	−0.037 913 83	0.849 029 88	−0.526 982 74	18.85	15.61	−1.99	35
9004-9029	0.014 976 95	−0.573 627 21	−0.818 979 56	68.03	29.79	21.05	42
9004-9051	−0.189 212 79	0.980 621 32	0.050 797 07	2160.68	2169.11	−1375.13	47
9004-9066	−0.479 672 65	0.695 552 78	0.534 902 31	22.93	10.64	−5.24	192
9004-9074	−0.607 317 21	0.624 696 01	0.490 836 73	18.11	7.63	−4.83	65
9004-9080	−0.670 338 78	0.237 785 34	0.702 925 36	29.78	9.92	0.41	164
9004-9091	−0.192 739 02	0.979 763 41	0.053 993 83	3.29	3.55	−1.53	442
9004-9115	−0.689 044 82	0.398 593 75	0.605 260 49	74.58	28.34	−8.14	60
9005-9006	0.915 236 02	0.388 002 15	−0.108 615 64	44.80	34.23	32.36	61
9005-9012	−0.247 353 66	−0.939 455 40	−0.237 149 14	106.27	176.50	−114.45	25
9005-9117	−0.390 770 14	−0.849 194 96	−0.355 199 42	182.41	189.44	−154.07	16
9006-9008	0.911 043 75	−0.412 181 49	0.010 281 02	37.46	20.76	16.35	172
9006-9028	0.828 975 55	−0.321 287 02	−0.457 792 73	22.65	23.59	10.19	28

TABLE 9.25.—*(Cont'd)*

Interstation direction	Direction cosines			σ_ψ^2 (μrad)	σ_μ^2 (μrad)	$\sigma_{\psi\mu}$ (μrad)	
	x	y	z				
9006–9091	0.712 325 15	−0.683 388 19	0.159 917 01	20.83	36.31	14.13	10
9006–9115	0.360 690 12	−0.836 686 48	0.412 138 77	16.89	16.71	7.12	19
9007–9009	0.098 443 23	−0.004 084 91	0.995 134 28	4.04	9.65	2.17	263
9007–9010	−0.202 184 39	0.042 403 31	0.978 429 06	4.88	5.94	1.92	86
9007–9011	0.185 005 71	0.487 139 75	−0.853 503 22	17.65	9.35	5.14	437
9007–9029	0.799 740 13	0.530 146 21	0.281 710 37	14.15	32.67	2.56	74
9007–9031	−0.076 686 54	0.521 089 04	−0.850 050 22	31.70	22.18	1.86	32
9008–9028	0.567 329 00	−0.163 038 12	−0.807 190 42	69.25	59.45	15.59	25
9008–9051	0.442 138 26	−0.853 475 28	0.275 850 87	7168.06	6510.27	6102.56	13
9008–9080	0.109 946 43	−0.918 531 30	0.379 752 59	38.24	25.92	−8.53	8
9008–9115	−0.056 819 15	−0.847 191 43	0.528 240 73	30.33	16.42	8.31	38
9009–9010	−0.631 057 97	0.106 627 28	0.768 372 60	10.73	18.06	6.43	248
9009–9011	0.006 033 03	0.189 216 50	−0.981 916 86	7.28	2.47	0.50	201
9009–9029	0.707 260 24	0.521 304 13	−0.477 519 59	39.98	35.77	2.00	12
9009–9114	−0.614 261 56	0.410 481 04	0.673 934 76	8.47	10.52	3.09	13
9010–9029	0.721 923 97	0.333 948 56	−0.606 056 22	22.19	20.40	2.74	6
9010–9114	−0.580 737 58	0.553 105 20	0.597 342 87	19.62	15.65	5.54	38
9011–9029	0.698 052 66	0.302 858 53	0.648 844 50	52.36	41.72	−13.65	7
9011–9031	−0.376 336 08	0.514 540 22	−0.770 467 07	198.44	140.41	27.09	9
9012–9021	0.774 021 22	−0.586 319 09	0.239 000 17	75.78	18.83	−12.52	29
9012–9113	0.754 823 45	−0.555 631 45	0.348 590 37	23.64	21.19	14.81	14
9012–9114	0.801 985 13	−0.202 846 07	0.561 848 14	22.01	17.31	−0.17	24
9012–9117	−0.370 330 01	0.884 135 37	−0.284 886 53	49.17	46.84	27.96	216
9021–9113	−0.685 370 68	0.605 320 01	0.404 789 73	175.96	211.14	9.22	57
9021–9117	−0.692 362 28	0.674 539 06	−0.256 186 51	50.43	26.94	19.65	8
9028–9091	−0.087 279 58	−0.544 704 02	0.834 074 22	105.67	28.64	−3.90	37
9029–9031	−0.664 370 01	−0.087 213 96	−0.742 297 93	23.64	25.10	−2.78	26
9066–9074	−0.722 593 68	0.537 777 49	0.434 342 89	94.27	33.43	−29.12	13
9066–9080	−0.457 869 96	−0.782 066 08	0.422 762 05	120.67	109.92	26.05	27
9074–9077	0.776 325 65	0.194 165 54	−0.599 681 77	453.01	147.30	−165.47	42
9074–9091	0.675 716 06	0.295 891 28	−0.675 171 21	45.42	22.62	6.25	43
9077–9091	0.583 629 63	0.370 871 86	−0.722 378 38	187.65	121.07	−53.33	30
9113–9114	0.522 340 01	0.510 153 75	0.683 303 79	126.10	106.70	38.12	30
9113–9117	−0.669 105 98	0.660 671 02	−0.340 310 14	16.21	29.22	10.95	16

TABLE 9.25.—*(Cont'd)*

Interstation direction	Direction cosines			σ_ψ^2 (μrad)	σ_μ^2 (μrad)	$\sigma_{\psi\mu}$ (μrad)
	x	y	z			
6001-6002	0.141 867 57	−0.835 578 65	−0.530 737 14	4.88	2.13	0.12
6001-6003	−0.685 613 65	−0.614 208 86	−0.390 744 68	5.55	2.03	0.41
6001-6004	−0.901 363 80	0.366 090 55	−0.231 346 07	7.88	2.47	1.52
6001-6006	0.591 183 24	0.802 114 53	−0.084 348 41	10.68	2.69	−1.90
6001-6007	0.853 151 78	−0.192 741 70	−0.484 750 12	6.83	2.27	−0.37
6001-6016	0.773 269 54	0.481 076 40	−0.413 061 40	2.81	0.81	−0.44
6001-6065	0.809 558 20	0.488 080 94	−0.326 178 66	3.99	1.22	−1.02
6001-6123	−0.970 854 20	0.230 905 62	−0.064 223 96	19.08	6.47	−1.12
6002-6003	−0.934 936 56	0.299 816 54	0.189 746 36	3.10	2.95	1.48
6002-6007	0.790 059 49	0.613 005 38	−0.005 513 94	7.15	6.25	−1.91
6002-6008	0.589 564 10	−0.090 689 02	−0.802 614 27	4.37	3.76	−2.32
6002-6009	0.035 287 76	−0.333 951 82	−0.941 929 38	9.39	4.10	0.51
6002-6038	−0.840 626 18	−0.207 333 06	−0.500 360 51	4.85	4.12	1.11
6002-6111	−0.992 430 15	0.045 147 65	−0.114 210 70	6.70	6.52	2.33
6002-6134	−0.992 422 07	0.045 119 01	−0.114 292 19	6.19	5.00	1.27
6003-6004	−0.379 650 63	0.921 024 95	0.087 054 20	10.44	3.59	0.62
6003-6011	−0.768 297 61	0.317 940 94	−0.555 546 88	4.80	3.85	2.16
6003-6012	−0.542 340 66	0.753 078 57	−0.372 477 21	3.33	1.88	0.59
6003-6038	−0.010 322 05	−0.578 100 31	−0.815 900 41	5.50	2.64	−0.78
6003-6111	−0.225 140 91	−0.618 652 34	−0.752 715 65	34.64	18.77	12.08
6003-6123	0.075 002 12	0.906 419 74	0.415 665 66	11.48	8.39	0.56
6003-6134	−0.225 131 46	−0.618 590 94	−0.752 768 94	31.12	17.64	−4.62
6004-6012	−0.540 783 78	0.268 965 14	−0.797 001 04	18.71	5.13	−2.83
6004-6013	0.069 330 48	0.903 078 62	−0.423 842 30	9.58	8.25	3.02
6004-6123	0.786 132 00	−0.482 393 72	0.386 384 23	35.88	8.81	−4.98
6006-6007	0.544 571 14	−0.698 573 02	−0.464 153 00	7.50	3.40	−0.04
6006-6015	0.115 085 63	0.854 379 21	−0.506 745 95	5.03	3.21	0.14
6006-6016	0.787 806 62	0.167 660 50	−0.592 664 06	4.78	1.88	0.10
6006-6065	0.858 757 69	0.040 345 30	−0.510 791 05	7.60	3.14	0.19
6007-6016	0.127 976 51	0.991 267 29	−0.031 798 92	5.87	4.76	−1.86
6007-6055	0.325 134 21	0.134 399 75	−0.936 068 62	2.37	2.18	−0.80
6007-6063	0.518 127 69	0.148 082 01	−0.842 386 74	7.86	3.39	−2.96
6007-6064	0.320 536 02	0.783 539 87	−0.532 279 94	2.68	2.70	−0.75
6007-6065	−0.069 163 60	0.970 784 14	0.229 770 66	13.69	6.15	−0.88
6007-6067	0.154 021 10	−0.283 547 61	−0.946 508 46	3.36	2.86	1.14
6008-6009	−0.889 382 39	−0.393 627 48	−0.232 500 28	10.72	17.99	8.22
6008-6019	−0.320 491 21	0.071 535 74	−0.944 546 46	3.83	3.77	−1.25
6008-6067	0.615 252 90	0.614 120 14	−0.494 287 69	15.83	20.35	1.79
6009-6019	0.267 472 01	0.357 525 69	−0.894 781 60	6.28	5.31	3.34
6009-6020	−0.723 867 36	0.204 650 56	−0.658 888 60	10.08	11.65	−1.01
6009-6038	−0.849 821 14	0.150 178 73	0.505 223 10	7.40	9.49	3.01
6009-6043	0.015 902 71	0.463 052 32	−0.886 188 27	4.27	1.63	0.70
6011-6012	−0.102 697 51	0.993 954 29	−0.038 834 06	7.10	6.36	2.10
6011-6022	−0.154 186 69	0.342 233 00	−0.926 878 11	2.36	4.39	0.66

TABLE 9.25.—*(Cont'd)*

Interstation direction	Direction cosines			σ_ψ^2 (μrad)	σ_μ^2 (μrad)	$\sigma_{\psi\mu}$ (μrad)
	x	y	z			
6011–6038	0.713 571 02	−0.699 157 90	−0.044 661 29	4.93	4.11	−1.83
6011–6059	−0.203 146 66	−0.021 289 30	−0.978 916 85	12.93	3.89	1.67
6011–6111	0.753 727 27	−0.565 465 17	0.334 879 59	8.14	8.17	−2.05
6011–6134	0.753 729 93	−0.565 502 25	0.334 810 98	5.65	5.50	−2.71
6012–6013	0.609 450 15	0.724 692 18	0.321 545 90	13.41	8.85	4.80
6012–6022	−0.055 106 45	−0.545 974 12	−0.835 987 76	2.57	4.53	0.36
6012–6023	0.216 399 64	0.586 471 64	−0.780 526 88	4.01	7.30	0.90
6012–6059	−0.006 268 11	−0.898 976 36	−0.437 952 29	2.41	3.97	−1.42
6013–6015	0.996 026 91	0.052 213 03	0.072 140 17	3.28	3.62	0.01
6013–6040	0.485 672 28	0.356 024 41	−0.798 353 97	2.08	3.88	0.87
6013–6047	0.071 906 80	0.439 043 73	−0.895 583 62	8.33	7.00	4.50
6013–6072	0.760 880 82	0.535 459 13	−0.366 529 53	4.36	8.55	1.81
6013–6078	−0.370 956 05	−0.449 044 19	−0.812 865 87	0.94	12.01	−3.04
6015–6016	0.590 837 46	−0.806 324 68	0.027 415 57	2.95	2.82	1.04
6015–6040	−0.528 142 99	0.275 666 07	−0.803 164 49	1.65	2.08	−0.07
6015–6042	0.630 855 74	−0.130 742 05	−0.764 805 57	2.44	2.82	0.60
6015–6045	0.103 102 95	0.100 120 56	−0.989 618 94	1.27	0.81	0.32
6015–6064	0.676 713 19	−0.559 380 10	−0.478 699 44	1.74	1.85	0.53
6015–6065	0.394 666 49	−0.888 635 25	0.233 593 13	5.57	2.35	−0.21
6015–6072	−0.839 965 71	0.360 824 97	−0.405 293 67	2.98	4.19	−1.46
6015–6073	0.143 282 86	0.325 434 15	−0.934 645 73	2.72	1.85	−0.69
6015–6075	0.224 226 76	0.178 325 99	−0.958 082 57	2.84	1.86	0.81
6016–6042	0.001 109 29	0.676 082 54	−0.736 825 06	4.38	3.04	−0.43
6016–6063	0.246 574 17	−0.790 990 05	−0.559 942 79	3.84	2.99	1.33
6016–6064	0.405 181 93	0.108 489 72	−0.907 776 18	5.65	3.07	0.89
6016–6065	−0.571 507 16	−0.414 589 06	0.708 163 45	25.62	8.62	1.65
6019–6020	−0.988 544 61	−0.104 406 02	0.108 990 57	8.63	9.11	−4.07
6019–6043	0.390 990 19	0.558 928 98	−0.731 248 97	6.16	2.42	−0.23
6019–6061	0.216 670 72	0.811 860 39	−0.542 159 11	7.88	3.46	0.54
6019–6067	0.698 038 94	0.302 827 21	0.648 873 89	3.70	6.55	2.34
6019–6069	0.573 249 08	0.813 330 71	−0.099 391 40	14.67	10.84	5.58
6020–6038	−0.055 058 66	−0.058 182 22	0.996 786 52	9.75	3.90	−1.14
6020–6039	−0.886 798 99	0.450 925 46	0.101 261 01	46.24	84.34	−48.70
6020–6043	0.761 603 48	0.406 532 67	−0.504 669 51	12.13	7.22	2.77
6022–6023	0.229 398 44	0.969 946 65	0.081 116 30	3.97	4.22	0.22
6022–6031	0.447 512 00	0.473 203 10	−0.758 822 66	6.38	3.96	−1.71
6022–6039	0.550 539 48	−0.793 608 11	−0.259 022 11	9.48	15.45	6.00
6022–6059	0.092 732 48	−0.626 945 87	0.773 524 12	3.29	6.17	−0.26
6022–6060	0.310 640 87	0.873 041 83	−0.375 899 20	4.53	5.01	−0.95
6022–6078	0.065 258 85	0.985 289 47	−0.157 942 84	70.31	78.59	53.19
6023–6031	0.140 307 20	−0.645 359 19	−0.750 883 09	1.84	1.15	0.56
6023–6032	0.730 220 42	0.292 459 45	−0.617 450 90	4.71	2.62	−0.99
6023–6040	0.872 900 05	0.486 554 80	−0.036 192 95	3.22	4.69	−0.30
6023–6047	0.544 131 75	0.520 276 13	0.658 204 67	7.08	11.72	1.73
6023–6060	0.088 571 50	−0.456 559 81	−0.885 272 97	2.49	2.26	1.09
6023–6072	0.722 203 86	0.382 400 25	0.576 360 68	2.75	3.73	1.36

TABLE 9.25.—*(Cont'd)*

Interstation direction	Direction cosines			σ_v^2 (μrad)	σ_μ^2 (μrad)	$\sigma_{v\mu}$ (μrad)
	x	y	z			
6023-6078	−0.344 213 95	−0.901 266 78	−0.263 125 35	38.04	54.65	−32.36
6031-6032	0.421 012 31	0.865 343 95	0.271 897 94	2.21	2.25	−0.79
6031-6039	0.103 770 02	−0.935 883 55	0.336 680 52	7.68	9.08	3.79
6031-6051	0.948 773 86	0.223 489 34	−0.223 339 85	3.13	1.18	−0.29
6031-6052	0.868 470 44	0.386 519 64	−0.310 421 76	5.11	2.65	−1.05
6031-6053	0.868 120 23	−0.167 691 87	−0.467 168 82	6.20	2.29	0.62
6031-6060	−0.182 484 01	0.792 220 53	0.582 311 10	5.04	2.87	1.64
6031-6078	0.519 787 53	0.108 042 39	0.847 436 00	16.60	7.33	1.37
6032-6040	0.562 738 04	0.453 120 81	0.691 380 81	14.56	10.49	−4.02
6032-6044	0.856 098 02	−0.293 452 46	−0.425 419 60	11.72	9.87	−1.56
6032-6045	0.978 994 41	0.029 690 27	0.201 713 74	2.66	3.32	−0.96
6032-6047	−0.231 903 26	0.115 244 64	0.965 887 96	2.44	5.19	1.81
6032-6052	0.388 697 91	−0.650 824 51	−0.652 182 02	7.61	2.97	0.06
6032-6060	−0.751 113 54	−0.658 575 02	0.045 906 50	3.72	3.86	1.59
6038-6039	−0.305 337 11	0.238 502 97	−0.921 892 39	3.38	10.38	−1.16
6038-6059	−0.711 967 36	0.610 648 24	−0.346 714 88	3.44	3.33	1.84
6038-6134	−0.155 550 27	0.526 537 55	0.835 800 41	7.65	3.15	1.93
6039-6059	−0.523 780 88	0.478 273 00	0.704 917 39	7.29	16.49	−6.47
6040-6045	0.940 828 58	−0.271 770 48	−0.202 441 09	2.41	3.92	−1.07
6040-6047	−0.757 459 32	−0.238 511 17	0.607 756 37	6.92	9.42	−0.49
6040-6060	−0.719 063 73	−0.609 502 87	−0.333 846 68	2.87	3.23	0.49
6040-6072	−0.058 895 96	−0.065 862 14	0.996 089 08	8.00	9.57	0.10
6040-6073	0.979 007 93	−0.058 625 46	0.195 208 96	8.03	11.93	−2.38
6040-6075	0.960 512 05	−0.210 583 46	0.181 854 89	3.21	4.45	−1.29
6042-6045	−0.449 127 82	0.288 406 76	−0.845 639 25	2.23	2.36	0.15
6042-6064	0.426 834 35	−0.893 595 14	0.138 925 02	7.17	8.16	−0.92
6042-6068	0.046 510 08	−0.327 935 56	−0.943 554 49	2.02	3.55	−0.14
6042-6073	−0.739 897 12	0.509 802 26	−0.438 923 58	2.79	3.51	−0.32
6042-6075	−0.553 708 69	0.541 789 04	−0.632 353 80	5.24	9.84	1.47
6043-6050	−0.130 891 08	0.852 415 41	−0.506 216 84	39.52	14.49	−6.23
6043-6061	0.758 559 97	0.649 959 05	−0.046 260 24	21.33	11.80	1.07

TABLE 9.25.—*(Cont'd)*

Interstation direction	Direction cosines			σ_ψ^2 (μrad)	σ_μ^2 (μrad)	$\sigma_{\psi\mu}$ (μrad)	No. obs.
	x	y	z				
6044–6045	0.554 878 31	0.355 385 18	0.752 204 38	14.61	15.53	−2.69	
6044–6051	0.007 253 12	−0.883 713 18	−0.467 972 66	67.30	23.18	−2.08	
6045–6051	−0.411 896 51	−0.560 884 05	−0.718 157 61	4.08	2.14	−0.29	
6045–6068	0.605 912 70	−0.773 097 59	−0.187 589 76	4.79	5.03	−1.35	
6045–6073	−0.613 372 05	0.459 201 80	0.642 579 51	7.17	7.74	2.24	
6045–6075	0.219 418 94	0.111 565 29	0.969 230 89	13.52	7.81	−2.45	
6047–6072	0.863 993 41	0.214 776 50	0.455 397 01	8.25	9.11	3.04	
6050–6053	−0.666 360 22	0.735 231 19	−0.124 093 36	26.19	5.54	3.75	
6050–6061	0.943 372 93	0.120 914 00	0.308 913 11	44.80	21.02	−11.51	
6051–6052	−0.992 556 05	0.118 412 41	0.028 477 98	20.63	11.42	4.14	
6051–6053	−0.788 602 68	−0.604 920 10	−0.110 351 64	7.70	3.72	0.10	
6051–6061	0.390 885 48	−0.908 327 49	0.148 827 80	12.32	4.36	−0.77	
6051–6068	0.783 976 60	0.098 864 04	0.612 867 51	3.95	1.37	−0.67	
6052–6053	−0.187 775 83	−0.965 112 61	−0.182 477 11	12.18	5.73	1.01	
6052–6060	−0.824 242 87	0.081 916 08	0.560 279 80	4.14	1.63	0.39	
6053–6060	−0.661 296 78	0.476 791 55	0.579 099 64	2.98	1.20	−0.48	
6055–6063	−0.092 868 60	−0.111 882 65	0.989 372 37	6.33	6.52	1.12	
6055–6064	−0.024 459 13	0.821 692 72	0.569 405 67	2.34	4.58	0.72	
6055–6067	−0.406 559 49	−0.908 368 02	0.097 861 77	7.36	8.80	0.44	
6055–6069	−0.356 833 86	0.151 782 89	−0.921 754 60	32.27	18.85	3.97	
6061–6067	0.420 033 59	−0.275 587 72	0.864 652 07	5.97	4.53	1.70	
6061–6068	0.357 797 96	0.839 136 75	0.409 670 76	7.54	3.33	0.91	
6061–6069	0.749 334 62	0.428 916 57	0.504 507 89	53.39	28.14	16.96	
6063–6064	0.039 855 27	0.995 945 04	−0.080 653 84	3.07	3.81	−1.04	
6063–6067	−0.234 403 11	−0.604 571 06	−0.761 281 16	4.17	7.76	−0.64	
6064–6068	−0.216 482 33	0.242 737 19	−0.945 628 92	2.77	4.03	1.71	
6068–6069	−0.027 253 14	−0.962 401 53	−0.270 260 18	26.89	19.09	−9.25	
6068–6075	−0.398 041 64	0.689 693 01	0.604 885 45	5.43	5.59	0.88	
6072–6073	0.706 617 35	0.016 091 77	−0.707 412 87	4.53	6.29	1.63	
6072–6075	0.863 257 60	−0.138 517 63	−0.485 385 60	2.94	3.89	0.66	
6073–6075	0.894 816 33	−0.418 523 78	0.155 375 66	14.38	17.76	−0.98	

TABLE 9.26a.—*Accuracy Estimates for BC-4 Geometrical Network Station-Station Vectors*[a]

Line	σ_1^2 (μrad)	σ_2^2 (μrad)	δ^2 (μrad)	k^2
6002–6003	3.0	36.73	26.52	1.34
6002–6007	14.8	6.70	51.48	4.79
6002–6008	3.8	4.07	4.03	1.02
6002–6009	15.4	6.74	7.65	0.69
6002–6038	12.0	4.48	10.71	1.30
6002–6111	13.0	6.61	7.63	0.78
6003–6004	15.1	7.01	112.06	10.14
6003–6011	6.9	4.33	6.83	1.22
6003–6012	298.0	2.61	62.48	0.42
6003–6038	5.3	4.07	7.99	1.71
6003–6111	17.1	26.70	1.38	0.06
6003–6123	10.0	9.94	0.45	0.05
6003–6134	195.7	24.38	232.13	2.11
6004–6012	31.0	11.92	104.81	4.88
6004–6013	8.8	8.92	15.37	1.73
6004–6123	37.9	22.34	88.76	2.95
6006–6007	27.9	5.45	41.13	2.47
6006–6015	13.7	4.12	15.36	1.72
6006–6016	6.4	3.33	52.79	10.85
6006–6065	4.5	5.37	4.49	0.91
6007–6016	14.4	5.32	24.89	2.52
6007–6055	77.9	2.27	21.76	0.54
6007–6063	5.2	5.62	4.86	0.90
6007–6064	38.5	2.69	178.65	8.67
6007–6065	33.2	9.92	31.07	1.44
6007–6067	17.7	3.11	61.90	5.95
6008–6009	16.5	14.36	12.03	0.78
6008–6019	2.7	3.80	4.78	1.47
6008–6067	21.0	18.09	0.82	0.04
6009–6019	10.3	5.79	2.96	0.37
6009–6020	17.3	10.87	32.65	2.32
6009–6038	16.0	8.45	20.84	1.70
6009–6043	20.6	2.95	28.89	2.45
6011–6012	12.5	6.73	54.35	5.66
6011–6022	165.6	3.38	2.70	0.03
6011–6038	20.5	4.52	22.72	1.82
6011–6059	6.0	8.41	1.17	0.16
6011–6111	86.6	8.16	8.05	0.17
6011–6134	9.3	5.57	0.83	0.11
6012–6013	23.3	5.09	4.10	0.29
6012–6022	7.1	3.55	9.71	1.82
6012–6023	8.0	5.66	9.95	1.46
6012–6059	4.0	3.19	10.43	2.90
6013–6015	195.8	3.45	174.15	1.75
6013–6040	17.3	2.98	53.68	5.29
6013–6047	7.3	7.66	7.18	0.96
6013–6072	8.0	6.46	2.09	0.29
6013–6078	25.1	6.48	46.25	2.93
6015–6016	5.3	2.88	9.40	2.30
6015–6040	9.8	1.87	3.89	0.67
6015–6042	2.7	2.63	3.56	1.34
6015–6045	11.1	1.04	2.47	0.41
6015–6064	8.9	1.79	49.22	9.21
6015–6065	6.6	3.96	34.65	6.56
6015–6072	3.3	3.59	8.29	2.41
6015–6073	4.3	2.28	2.00	0.61
6015–6075	7.0	2.35	32.89	7.04
6016–6042	84.3	3.71	247.16	5.62
6016–6063	17.2	3.42	90.14	8.74
6016–6064	3.9	4.36	1.47	0.36
6016–6065	14.8	17.12	30.86	1.93
6019–6020	31.4	8.87	159.21	7.91
6019–6043	2.8	4.29	3.84	1.08
6019–6061	5.3	5.67	6.77	1.23
6019–6067	6.8	5.12	13.95	2.34
6019–6069	82.0	12.76	6.34	0.13
6020–6038	11.0	6.82	30.71	3.45
6020–6039	113.8	65.29	11.62	0.13
6020–6043	11.9	9.68	1.02	0.09
6022–6023	17.5	4.09	83.06	7.69
6022–6031	12.5	5.17	18.19	2.06
6022–6039	29.0	12.46	15.01	0.72
6022–6059	3.1	4.73	0.72	0.18
6022–6060	16.3	4.77	36.84	3.50
6022–6078	808.0	74.45	2970.60	6.73
6023–6031	11.1	1.49	11.13	1.77
6023–6032	4.9	3.66	52.75	12.32
6023–6040	30.2	3.96	65.25	3.76
6023–6047	17.8	9.40	63.17	4.64
6023–6060	1.6	2.38	2.09	1.05
6023–6072	94.9	3.24	268.78	5.48
6023–6078	663.6	46.34	1521.11	4.29
6031–6032	4.2	2.23	4.71	1.47
6031–6039	122.9	8.38	153.07	2.33
6031–6051	139.4	2.16	136.70	1.93
6031–6052	8.9	3.88	4.46	0.70
6031–6053	4.6	4.25	3.86	0.87
6031–6060	3.3	3.96	2.36	0.65
6031–6078	13.3	11.97	0.10	0.01
6032–6040	31.0	12.53	20.85	0.96
6032–6044	10.1	10.79	0.52	0.05
6032–6045	41.3	2.99	233.71	10.55
6032–6047	7.1	3.81	3.72	0.68
6032–6052	21.4	5.29	191.15	14.32
6032–6060	5.6	3.79	9.99	2.13
6038–6039	9.2	6.88	2.18	0.27
6038–6059	19.6	3.38	205.25	17.86
6038–6134	3.6	5.40	0.82	0.18
6039–6059	26.4	11.89	4.27	0.22
6040–6045	3.8	3.16	1.67	0.48
6040–6047	18.2	8.17	21.08	1.60
6040–6060	73.6	3.05	12.64	0.33
6040–6072	21.3	8.79	25.05	1.67
6040–6073	22.5	9.98	37.66	2.32
6040–6075	17.6	3.83	31.92	2.98
6042–6045	2.7	2.30	0.53	0.21

TABLE 9.26a.—*(Cont'd)*

Line	σ_1^2 (μrad)	σ_2^2 (μrad)	δ^2 (μrad)	k^2
6042–6064	9.6	7.67	8.74	1.01
6042–6068	2.8	2.78	1.55	0.56
6042–6073	162.0	3.15	720.92	8.73
6042–6075	15.5	7.54	23.07	2.00
6043–6050	19.1	27.00	58.35	2.53
6043–6061	29.9	16.57	78.65	3.38
6044–6045	74.5	15.07	19.43	0.43
6044–6051	38.3	45.24	0.16	0.00
6045–6051	8.2	3.11	1.14	0.20
6045–6068	5.0	4.91	0.50	0.10
6045–6073	6.5	7.46	0.53	0.08
6045–6075	7.6	10.67	6.83	0.75
6047–6072	8.2	8.68	13.27	1.57
6050–6053	51.3	15.86	512.41	15.26
6050–6061	32.7	32.91	174.32	5.31
6051–6052	22.2	16.02	11.87	0.62
6051–6053	4.8	5.71	6.28	1.20
6051–6061	20.4	8.34	32.94	2.29
6051–6068	2.5	2.66	8.36	3.24
6052–6053	7.1	8.96	1.59	0.20
6052–6060	6.2	2.88	3.66	0.81
6053–6060	27.8	2.09	6.33	0.42
6055–6063	6.0	6.42	2.28	0.37
6055–6064	4.6	3.46	11.38	2.82
6055–6067	5.9	8.08	0.71	0.10
6055–6069	23.5	25.56	4.41	0.18
6061–6067	238.0	5.25	1099.08	9.04
6061–6068	29.9	5.44	51.15	2.89
6061–6069	53.0	40.76	40.50	0.86
6063–6064	3.3	3.44	1.29	0.38
6063–6067	10.8	5.97	0.86	0.10
6064–6068	18.8	3.40	35.10	3.16
6068–6069	297.5	22.99	27.68	0.17
6068–6075	128.7	5.51	339.50	5.06
6072–6073	27.8	5.41	61.70	3.72
6072–6075	240.5	3.41	397.15	3.26
6073–6075	31.7	16.07	16.28	0.68
			k^2 ave =	2.60

[a] σ_1^2 and σ_2^2 are accuracy estimates before and after network adjustment, δ^2 is the square of the difference between the estimates, and k^2 is the scaling factor.

TABLE 9.26b.—*Accuracy Estimates for SAO Geometrical Network Station-Station Vectors*[a]

Line	n	σ_1^2 (μrad)	σ_2^2 (μrad)	δ^2 (μrad)	k^2	Line	n	σ_1^2 (μrad)	σ_2^2 (μrad)	δ^2 (μrad)	k^2
8015-8019	29	1514.4	4031.7	3114.8	1.12	9006-9091	10	30.0	28.6	38.6	1.32
8015-9004	122	7.2	23.4	44.9	2.93	9006-9115	19	5.9	16.8	201.5	17.75
8015-9066	133	79.2	378.5	258.9	1.13	9007-9009	263	1.1	6.9	1.5	0.38
8015-9074	25	37.2	38.1	487.9	12.96	9007-9010	86	2.3	5.5	0.6	0.15
8015-9080	67	20.8	66.2	217.4	5.00	9007-9011	437	1.7	13.5	0.1	0.01
8015-9091	30	10.6	25.3	0.01	0.00	9007-9029	74	1.2	24.1	10.6	0.84
8019-9004	301	0.9	7.2	0.6	0.15	9007-9031	32	3.5	27.0	0.4	0.03
8019-9091	61	4.0	17.9	2.3	0.21	9008-9028	25	16.7	64.3	6.4	0.16
9001-9009	183	1.0	5.8	1.3	0.38	9008-9080	8	233.1	32.1	453.1	3.42
9001-9010	154	2.1	13.1	6.8	0.89	9008-9115	38	6.4	23.3	33.4	2.25
9001-9012	187	1.6	9.4	0.8	0.15	9009-9010	248	2.2	14.4	0.1	0.01
9001-9113	20	32.3	174.1	195.2	1.89	9009-9011	201	1.3	4.9	0.2	0.06
9001-9114	74	5.8	30.0	11.7	0.65	9009-9114	13	21.5	9.5	13.8	0.89
9001-9117	16	11.7	14.4	85.3	6.54	9010-9029	6	59.6	24.9	79.9	1.89
9002-9008	7	19.3	84.3	369.4	7.13	9010-9114	38	7.4	17.6	146.4	11.71
9002-9028	25	11.0	86.0	40.6	0.84	9011-9029	7	734.0	47.9	6252.8	15.99
9004-9006	14	43.2	8.9	44.9	1.72	9011-9031	9	141.1	169.9	78.5	0.50
9004-9008	139	2.8	11.2	20.8	2.97	9012-9021	29	12.5	47.4	10.6	0.35
9004-9009	43	8.0	27.0	0.6	0.03	9012-9113	14	8.2	22.6	8.0	0.52
9004-9010	41	6.9	27.5	1.8	0.10	9012-9114	24	9.8	19.7	31.8	2.16
9004-9028	35	8.2	17.2	83.5	6.57	9012-9117	216	5.8	48.2	3.3	0.12
9004-9029	42	18.0	49.7	0.7	0.02	9021-9113	57	23.1	193.3	4.9	0.05
9004-9066	192	3.3	16.8	24.2	2.41	9021-9117	8	126.0	39.1	800.1	9.69
9004-9074	65	7.3	12.8	90.0	8.96	9028-9091	37	13.3	67.1	290.4	7.22
9004-9080	164	3.4	19.8	7.2	0.62	9029-9031	26	12.6	24.6	2.6	0.14
9004-9091	442	0.6	3.4	0.7	0.35	9066-9074	13	89.9	63.9	461.7	6.00
9004-9115	60	7.7	51.4	21.0	0.71	9066-9080	27	34.1	115.3	68.3	0.91
9005-9006	61	4.8	89.5	0.01	0.00	9074-9077	42	41.0	299.8	15.6	0.09
9005-9012	25	35.0	141.6	98.0	1.11	9074-9091	43	11.7	34.0	204.3	8.94
9005-9117	16	45.5	186.4	108.2	0.93	9077-9091	30	22.6	154.1	11.9	0.13
9006-9008	172	4.2	29.1	0.9	0.05	9113-9114	30	45.0	116.7	424.6	5.25

k^2 ave = 2.65

[a] n is the number of observations, σ_1^2 and σ_2^2 are accuracy estimates before and after network adjustment, δ^2 is the square of the angular difference between the two estimates, and k^2 is the scaling factor (σ_1, σ_2, and δ are in microradians).

TABLE 9.27.—*Coefficients of Zonal-Harmonic Coefficients in Equations for $\dot{\omega}$ and $\dot{\Omega}$*

Satellite		J_2	J_4	J_6	J_8	J_{10}	J_{12}	J_{14}	J_{16}	J_{18}	J_{20}	J_{22}	J_{24}	J_{26}	J_{28}	J_{30}	J_{32}	J_{34}	J_{36}
7001701	$\dot{\omega}$	11 306	−21 362	28 183	−31 767	32 678	−31 593	29 139	−25 835	22 092	−18 218	14 437	−10 903	7 717	−4 936	2 585	−665	−842	1 968
	$\dot{\Omega}$	−5 691	10 807	−14 617	16 932	−18 043	18 215	−17 685	16 649	−15 268	13 667	−11 950	10 197	−8 473	6 828	−5 299	3 913	−2 688	1 632
7010901	$\dot{\omega}$	12 165	−20 770	21 325	−14 509	3 882	6 305	−12 812	14 276	−11 222	5 463	756	−5 539	7 823	−7 500	5 223	−2 046	−967	3 043
	$\dot{\Omega}$	−6 414	11 751	−13 867	12 620	−8 995	4 414	−194	−2 781	4 171	−4 117	3 065	−1 574	144	891	−1 393	1 397	−1 052	547
6001301	$\dot{\omega}$	7 625	−5 479	−2 224	6 043	−3 260	−1 675	3 731	−2 045	−744	1 979	−1 213	−223	952	−671	−17	424	−348	38
	$\dot{\Omega}$	−4 671	5 169	−2 137	−945	1 924	−1 071	−157	703	−487	17	249	−211	37	84	−88	26	27	−36
5900101	$\dot{\omega}$	4 868	−1 560	−2 711	2 473	409	−1 902	926	665	−1 045	244	535	−517	−14	357	−230	−87	214	−85
	$\dot{\Omega}$	−3 236	2 540	−200	−1 095	787	106	−522	274	141	−264	85	114	−131	13	78	−61	−11	48
6202901	$\dot{\omega}$	1 836	1 040	−823	−645	400	342	−204	−179	107	94	−57	−50	31	27	−17	−14	9	8
	$\dot{\Omega}$	−1 717	301	512	−127	−208	60	97	−31	−48	16	24	−9	−13	5	7	−3	−4	1
6000902	$\dot{\omega}$	2 753	2 685	−1 224	−2 302	317	1 425	39	−763	−121	373	106	−171	−71	73	42	−30	−23	11
	$\dot{\Omega}$	−2 864	261	1 168	−16	−480	−37	194	34	−76	−21	29	12	−11	−6	4	3	−1	−1
6302601	$\dot{\omega}$	3 245	5 104	−765	−6 141	−1 782	4 990	3 273	−3 127	−3 678	1 374	3 334	−72	−2 612	−717	1 794	1 073	−1 055	−1 122
	$\dot{\Omega}$	−3 855	−145	2 333	645	−1 331	−761	677	685	−272	−540	41	385	77	−250	−124	144	128	−68
6206001	$\dot{\omega}$	2 741	4 130	−334	−4 065	−1 359	2 597	1 845	−1 190	−1 593	289	1 095	139	−632	−264	305	243	−112	−173
	$\dot{\Omega}$	−3 334	−187	1 667	489	−747	−441	278	301	−69	−174	−9	89	27	−39	−24	14	16	−3
6508901	$\dot{\omega}$	605	2 454	2 144	39	−1 392	−1 096	−10	604	438	−12	−240	−161	12	92	57	−7	−34	−20
	$\dot{\Omega}$	−2 076	−976	260	562	239	−92	−163	−64	32	50	18	−12	−16	−5	4	3	2	−2
6101501	$\dot{\omega}$	−641	1 893	4 419	4 327	1 628	−1 619	−3 300	−2 743	−816	1 016	1 750	1 305	295	−544	−809	−548	−82	264
	$\dot{\Omega}$	−2 240	−2 037	−809	331	811	657	219	−150	−284	−211	−57	62	98	67	14	−25	−34	−21
6400101	$\dot{\omega}$	−1 176	774	3 506	4 737	3 659	1 074	−1 486	−2 816	−2 596	−1 330	132	1 095	1 294	884	237	−292	−518	−449
	$\dot{\Omega}$	−1 971	−2 044	−1 205	−210	457	653	495	196	−60	−184	−179	−102	−14	43	58	43	16	−6
6406401	$\dot{\omega}$	−2 341	−2 483	−1 458	12	1 376	2 310	2 708	2 622	2 189	1 576	931	363	−68	−342	−471	−487	−427	−326
	$\dot{\Omega}$	−996	−1 298	−1 252	−1 026	−735	−455	−224	−59	44	96	110	101	79	55	33	15	2	−5
6508101	$\dot{\omega}$	−2 814	−3 984	−4 371	−4 299	−3 969	−3 508	−2 998	−2 491	−2 016	−1 588	−1 213	−893	−626	−406	−229	−90	18	−99
	$\dot{\Omega}$	−261	−375	−422	−431	−417	−392	−360	−327	−293	−260	−230	−201	−175	−152	−131	−112	−96	−81
6102801	$\dot{\omega}$	−903	−637	−331	−144	−53	−15	−2	2	2	1	1	0	0	0	0	0	0	0
	$\dot{\Omega}$	194.2	144.5	82.4	41.7	19.6	8.7	3.7	1.5	0.6	0.2	0.1	0.0	0.0	0.0	0.0	0.0	0.0	0.0

TABLE 9.28.—*Coefficients of Zonal-Harmonic Coefficients in Equations for ω, Ω, I, and e*

Satellite		J_3	J_5	J_7	J_9	J_{11}	J_{13}	J_{15}	J_{17}	J_{19}	J_{21}	J_{23}	J_{25}	J_{27}	J_{29}	J_{31}	J_{33}	J_{35}	J_{37}
7001701	ω	−5	12	−23	36	−50	63	−75	84	−90	93	−93	90	−85	77	−69	60	−50	40
	Ω	−211	381	−471	484	−436	347	−235	116	−1	−103	190	−258	307	−337	350	−348	334	−310
	I	203	−384	507	−573	592	−576	537	−484	423	−360	299	−241	190	−144	105	−72	45	−24
	e	−38	72	−95	107	−110	107	−100	90	−79	67	−56	45	−35	27	−20	13	−8	4
7010901	ω	−378	668	−753	644	−410	141	87	−229	275	−241	157	−59	−25	79	−97	86	−57	22
	Ω	−12	12	5	−31	54	−66	60	−40	12	16	−35	43	−38	25	−8	−7	18	−21
	I	38	−68	76	−64	41	−13	−9	23	−27	23	−15	5	3	−8	9	−8	5	−2
	e	−109	192	−216	183	−115	38	26	−66	77	−67	42	−15	−8	22	−26	23	−15	5
6001301	ω	−647	569	−67	−290	286	−76	−97	122	−47	−29	49	−25	−7	19	−12	−1	7	−5
	Ω	−2	−12	22	−12	−6	16	−11	−1	9	−7	1	4	−4	1	2	−2	1	1
	I	33	−29	3	15	−14	4	5	−6	2	1	−2	1	0	−1	1	0	0	0
	e	−187	164	−19	−84	82	−21	−28	35	−13	−8	14	−7	−2	5	−3	0	2	−1
5900101	ω	−77	53	14	−47	24	15	−26	8	12	−14	1	9	−7	−1	6	−3	−2	3
	Ω	9	−128	122	13	−103	65	25	−62	25	24	−34	7	18	−17	−1	12	−8	−3
	I	290	−143	−71	114	−33	−38	39	−4	−19	14	2	−9	5	2	−4	1	2	−2
	e	−193	95	48	−76	22	25	−26	3	12	−9	−1	6	−3	−2	3	−1	−1	1
6202901	ω	−74	−15	45	6	−25	−3	13	1	−7	−1	4	0	−2	0	1	0	−1	0
	Ω	103	−150	−66	96	33	−52	−16	28	8	−15	−4	8	2	−4	−1	2	1	−1
	I	319	98	−124	−31	45	11	−18	−4	8	2	−3	−1	2	0	−1	0	0	0
	e	−215	−66	83	21	−30	−7	12	3	−5	−1	2	1	−1	0	0	0	0	0
6000902	ω	−1365	−828	698	451	−269	−221	94	103	−29	−46	8	20	−1	−8	0	4	0	−1
	Ω	7	−9	−9	7	7	−4	−4	2	2	−1	−1	0	1	0	0	0	0	0
	I	16	10	−8	−5	3	3	−1	−1	0	1	0	0	0	0	0	0	0	0
	e	−271	−165	138	89	−53	−44	18	20	−6	−9	2	4	0	−2	0	1	0	0
6302601	ω	−305	−325	189	293	−61	−227	−17	159	55	−100	−68	55	66	−22	−55	1	42	11
	Ω	52	−57	−109	40	126	−1	−112	−32	84	50	−52	−54	25	49	−5	−39	−7	28
	I	91	97	−52	−82	14	58	6	−37	−14	21	15	−10	−12	3	9	0	−6	−2
	e	−311	−332	179	282	−49	−200	−20	126	47	−71	−50	34	42	−11	−31	−1	21	6

TABLE 9.28.—*(Cont'd)*

Satellite		J_3	J_5	J_7	J_9	J_{11}	J_{13}	J_{15}	J_{17}	J_{19}	J_{21}	J_{23}	J_{25}	J_{27}	J_{29}	J_{31}	J_{33}	J_{35}	J_{37}
6206001	ω	−2466	−2550	1113	1803	−168	−1033	−175	509	224	−213	−174	68	109	−8	−59	−11	28	13
	Ω	6	−6	−11	3	10	1	−7	−3	4	3	−2	−2	0	2	0	−1	0	0
	I	10	10	−5	−7	1	4	1	−2	−1	1	1	0	0	0	0	0	0	0
	e	−301	−311	136	220	−20	−126	−21	62	27	−26	−21	8	13	−1	−7	−1	3	2
6508901	ω	−268	−862	−417	160	309	126	−66	−106	−39	26	37	12	−10	−13	−4	4	5	1
	Ω	213	80	−186	−212	−32	108	97	8	−47	−37	−1	19	14	0	−7	−5	0	3
	I	77	249	119	−40	−78	−32	14	23	8	−5	−7	−2	2	2	1	−1	−1	0
	e	−314	−1019	−489	164	320	130	−57	−93	−34	19	27	9	−6	−8	−2	2	2	1
6101501	ω^a	−265	744	1046	652	48	−345	−396	−215	6	134	137	67	−10	−50	−46	−20	6	18
	Ω	−30	−40	−9	34	52	36	2	−26	−32	−18	1	14	15	7	−2	−7	−7	−3
	I	7	−20	−29	−18	−1	9	11	6	0	−4	−4	−2	0	1	1	1	0	0
	e	−370	1037	1459	909	68	−480	−551	−299	9	185	190	92	−14	−68	−64	−27	8	25
6400101	ω^a	−1447	1211	2666	2438	1244	−17	−771	−899	−598	−170	154	280	238	114	−6	−74	−83	−54
	Ω	−3	−5	−3	1	4	5	3	1	−2	−3	−2	−1	0	1	1	1	0	0
	I	1	−1	−2	−2	−1	0	1	1	0	0	0	0	0	0	0	0	0	0
	e	−378	317	698	638	326	−4	−202	−235	−157	−45	40	73	62	30	−2	−19	−22	−14
6406401	ω	−1750	−1123	−378	169	477	585	557	454	323	197	94	20	−26	−48	−54	−48	−38	−26
	Ω	−7	−15	−20	−21	−17	−12	−6	0	4	6	7	6	5	3	2	1	0	−1
	I	5	3	1	−1	−1	−2	−2	−1	−1	−1	0	0	0	0	0	0	0	0
	e	−394	−252	−85	38	107	130	124	101	71	43	21	4	−6	−10	−12	−10	−8	−6
6508101	ω	−318	−307	−261	−214	−173	−138	−109	−85	−65	−49	−36	−26	−17	−11	−5	−1	2	4
	Ω	−9	−22	−35	−45	−53	−57	−59	−59	−57	−54	−50	−46	−42	−37	−33	−29	−25	−22
	I	8	7	6	5	4	3	2	1	1	1	1	0	0	0	0	0	0	0
	e	−401	−377	−309	−242	−185	−139	−104	−76	−55	−39	−27	−18	−11	−7	−3	−1	1	2
6102801	ω	−1388	−638	−242	−81	−23	−5	0	1	1	0	0	0	0	0	0	0	0	0
	Ω	2	3	3	2	1	0	0	0	0	0	0	0	0	0	0	0	0	0
	I	−2	−1	0	0	0	0	0	0	0	0	0	0	0	0	0	0	0	0
	e	−293	−135	−51	−17	−5	−1	0	0	0	0	0	0	0	0	0	0	0	0

[a] For these satellites, ω is in units of 10^2 degrees.

TABLE 9.29.—*Coefficients of Zonal-Harmonic Coefficients in Equations for ω, Ω, I, and e*

Satellites		J_2	J_4	J_6	J_8	J_{10}	J_{12}	J_{14}	J_{16}	J_{18}	J_{20}	J_{22}	J_{24}	J_{26}	J_{28}	J_{30}	J_{32}	J_{34}	J_{36}
7001701	ω	0	0	0	0	1	−2	3	−4	6	−7	9	−11	12	−13	14	−15	15	−15
	Ω	0	−1	6	−15	25	−37	46	−54	57	−57	53	−46	36	−24	12	1	−13	23
	I	0	−1	6	−15	26	−39	52	−64	74	−81	85	−87	86	−82	77	−70	63	−55
	e	0	0	−1	3	−5	7	−10	12	−14	15	−16	16	−16	15	−14	13	−12	10
7010901	ω	0	−1	6	−13	20	−23	22	−15	6	4	−12	16	−15	11	−5	−1	6	−8
	Ω	0	0	0	0	0	0	−1	1	−2	2	−1	1	0	−1	2	−2	1	−1
	I	0	0	1	−1	2	−2	2	−2	1	0	−1	2	−2	1	0	0	1	−1
	e	0	0	−2	4	−6	7	−6	4	−2	−1	3	−4	4	−3	1	0	−2	2
6001301	ω	0	−4	10	−9	0	9	−9	2	4	−6	2	2	−3	2	1	−1	1	0
	Ω	0	0	0	0	0	0	0	0	0	0	0	0	0	0	0	0	0	0
	I	0	0	1	0	0	0	0	0	0	0	0	0	0	0	0	0	0	0
	e	0	1	−3	3	0	−3	3	−1	−1	2	−1	0	1	0	0	0	0	0
5900101	ω	0	−5	9	−4	−6	9	−2	−5	6	0	−4	3	1	−3	1	1	−2	1
	Ω	0	−2	−5	15	−11	−7	17	−8	−8	12	−3	−7	7	0	−5	4	1	−3
	I	0	−20	33	−9	−21	24	−2	−14	11	1	−8	4	2	−4	1	2	−2	0
	e	0	13	−22	6	14	−16	2	9	−7	−1	5	−3	−1	3	−1	−1	1	0
6202901	ω	0	−8	2	8	−3	−5	2	3	−2	−2	1	1	−1	−1	0	0	0	0
	Ω	0	2	−18	3	18	−4	−12	3	8	−2	−4	1	2	−1	−1	0	1	0
	I	0	−40	5	34	−6	−18	4	8	−2	−4	1	2	−1	−1	0	0	0	0
	e	0	27	−4	−23	4	12	−3	−6	1	3	−1	−1	0	1	0	0	0	0
6000902	ω	0	−10	−2	13	2	−9	−2	5	2	−3	−1	1	1	−1	0	0	0	0
	Ω	0	0	0	0	0	0	0	0	0	0	0	0	0	0	0	0	0	0
	I	0	0	0	0	0	0	0	0	0	0	0	0	0	0	0	0	0	0
	e	0	2	0	−3	0	2	0	−1	0	1	0	0	0	0	0	0	0	0
6302601	ω	0	−14	−9	27	19	−25	−26	16	27	−6	−25	−2	20	7	−14	−10	8	10
	Ω	0	1	−3	−3	6	7	−6	−10	4	11	0	−11	−3	9	5	−6	−6	3
	I	0	−4	−3	8	6	−7	−7	4	8	−1	−6	−1	5	2	−3	−2	2	2
	e	0	14	9	−27	−19	24	25	−14	−26	5	22	3	−17	−7	11	8	−6	−8

TABLE 9.29.—*(Cont'd)*

Satellites		J_2	J_4	J_6	J_8	J_{10}	J_{12}	J_{14}	J_{16}	J_{18}	J_{20}	J_{22}	J_{24}	J_{26}	J_{28}	J_{30}	J_{32}	J_{34}	J_{36}
6206001	ω	0	−13	−9	20	15	−14	−16	6	13	−1	−9	−2	5	3	−2	−2	1	2
	Ω	0	0	0	0	0	0	0	0	0	0	0	0	0	0	0	0	0	0
	I	0	0	0	0	0	0	0	0	0	0	0	0	0	0	0	0	0	0
	e	0	2	1	−2	−2	2	2	−1	−2	0	1	0	−1	0	0	0	0	0
6508901	ω	0	−22	−53	−16	35	38	5	−20	−18	−1	9	7	0	−4	−3	0	2	1
	Ω	0	4	−1	−12	−10	4	12	7	−3	−7	−3	2	4	1	−1	−2	−1	1
	I	0	−6	−16	−5	10	11	2	−5	−5	0	2	2	0	−1	−1	0	0	0
	e	0	26	65	19	−41	−44	−7	22	19	1	−9	−7	0	3	2	0	−1	−1
6101501	ω	0	4	78	114	62	−33	−97	−92	−34	29	59	47	13	−18	−29	−21	−4	9
	Ω	0	0	0	0	0	0	0	0	0	0	0	0	0	0	0	0	0	0
	I	0	0	0	0	0	0	0	0	0	0	0	0	0	0	0	0	0	0
	e	0	−1	−11	−16	−9	5	14	13	5	−4	−8	−7	−2	2	4	3	1	−1
6400101	ω	0	−5	30	62	60	24	−19	−47	−47	−27	0	20	25	18	5	−5	−10	−9
	Ω	0	0	0	0	0	0	0	0	0	0	0	0	0	0	0	0	0	0
	I	0	0	0	0	0	0	0	0	0	0	0	0	0	0	0	0	0	0
	e	0	0	−1	−2	−2	−1	1	1	1	1	0	−1	−1	0	0	0	0	0
6406401	ω	0	−11	−11	−2	8	17	22	23	20	15	9	4	0	−3	−5	−5	−4	−3
	Ω	0	0	0	0	0	0	0	0	0	0	0	0	0	0	0	0	0	0
	I	0	0	0	0	0	0	0	0	0	0	0	0	0	0	0	0	0	0
	e	0	2	2	1	−2	−4	−5	−5	−4	−3	−2	−1	0	1	1	1	1	1
6508101	ω	0	−13	−21	−25	−26	−25	−23	−20	−17	−14	−11	−8	−6	−4	−2	−1	0	1
	Ω	0	0	−1	−2	−4	−5	−6	−7	−8	−9	−9	−9	−9	−8	−8	−7	−7	−6
	I	0	0	−1	−1	−1	−1	−1	0	0	0	0	0	0	0	0	0	0	0
	e	0	16	26	31	31	29	26	22	18	14	11	8	6	4	2	1	0	−1
6102801	ω	0	−7	−5	−3	−1	0	0	0	0	0	0	0	0	0	0	0	0	0
	Ω	0	0	0	0	0	0	0	0	0	0	0	0	0	0	0	0	0	0
	I	0	0	0	0	0	0	0	0	0	0	0	0	0	0	0	0	0	0
	e	0	1	1	1	0	0	0	0	0	0	0	0	0	0	0	0	0	0

TABLE 9.30.—*Resonant Periods*

Resonant with order (m)	Satellite	Inclination (deg)	Period (days)
9	6102801	95	2.90
12	6100401	39	15.0
12	6000902	47	15.5
12	6508901	59	7.2
12	6506301	69	3.3
12	6507801	144	2.3
13	6701401	39	9.4, 10.9, 13.1, . . .
13	6503201	41	5.6
13	6701101	40	1.6
13	6206001	50	5.3
13	6800201	105	6.3
13	6600501	89	1.8
13	6304901	90	2.5
14	6701101	40	2.6
14	6302601	50	12.2
14	6101501	67	3.84
14	6101502	67	3.76
14	6400101	70	4.9
14	6406401	80	2.9
14	6408101	87	3.8
14	6600501	89	2.2

TABLE 9.31.—*Additional Parameters Determined*

Relation to the dynamical system	Translation parameters (m)	Rotation parameters about the axis (μrad)	Scale parameter
SAO geometrical	$X = -6.66$	$\epsilon_X = 0.70 \pm 1.56$	
	$Y = -14.88$	$\epsilon_Y = 0.84 \pm 1.24$	
	$Z = -9.90$	$\epsilon_Z = -0.40 \pm 1.43$	
BC–4 geometrical	$X = -11.25 \pm 9.60$	$\epsilon_X = 1.76 \pm 0.96$	
	$Y = -16.63 \pm 9.58$	$\epsilon_Y = -0.65 \pm 0.65$	
	$Z = -6.79 \pm 13.74$	$\epsilon_Z = -2.20 \pm 0.82$	
JPL		$\epsilon_Z = -3.43 \pm 1.02$	$0.18 \times 10^{-6} \pm 0.55 \times 10^{-6}$

TABLE 9.32.—*Geocentric Coordinates*

Station	*X* (Mm)	*Y* (Mm)	*Z* (Mm)	σ (m)	Location
7050	1.130 673 9	−4.831 373 5	3.994 101 0	1.81	Greenbelt, USA
1021	1.118 030 8	−4.876 321 3	3.942 973 0	1.81	Blossom Point, USA
7060	−5.068 964 1	3.584 106 1	1.458 744 3	2.88	Guam, USA
8816	4.654 336 9	1.959 179 0	3.884 358 5	2.26	Stephanion, Greece
8818	5.426 328 1	−0.229 326 6	3.334 606 4	6.07	Colomb-Bechar, Algeria
8015	4.578 327 7	0.457 974 8	4.403 179 7	2.07	Haute Provence, France
8815	4.578 370 7	0.457 959 1	4.403 135 5	2.07	Haute Provence, France
8809	4.578 348 4	0.457 965 9	4.403 157 9	2.07	Haute Provence, France
9001	−1.535 768 6	−5.166 989 0	3.401 042 5	2.44	Organ Pass, USA
9901	−1.535 768 8	−5.166 989 0	3.401 042 5	2.44	Organ Pass, USA
9002	5.056 126 7	2.716 513 6	−2.775 788 3	1.79	Olifantsfontein, Rep. S. Afr.
9902	5.056 126 5	2.716 513 5	−2.775 788 3	1.79	Olifantsfontein, Rep. S. Afr.
9022	5.056 120 7	2.716 524 3	−2.775 787 0	1.79	Olifantsfontein, Rep. S. Afr.
9003	−3.983 778 3	3.743 093 9	−3.275 561 0	2.49	Woomera, Australia
9023	−3.977 766 8	3.725 106 1	−3.303 028 3	2.16	Island Lagoon, Australia
9004	5.105 591 9	−0.555 230 0	3.769 662 5	3.06	San Fernando, Spain
8804	5.015 612 0	−0.555 252 3	3.769 631 2	3.06	San Fernando, Spain
9005	−3.946 690 6	3.366 295 7	3.698 833 4	6.26	Tokyo, Japan
9025	−3.910 434 2	3.376 357 4	3.729 220 2	6.26	Dodaira, Japan
9006	1.018 204 4	5.471 104 5	3.109 621 9	2.77	Naini Tal, India
9007	1.942 776 9	−5.804 089 4	−1.796 931 1	2.11	Arequipa, Peru
9907	1.942 777 0	−5.804 089 8	−1.796 931 2	2.11	Arequipa, Peru
9027	1.942 771 8	−5.804 096 1	−1.796 909 4	2.11	Arequipa, Peru
9008	3.376 892 9	4.403 982 3	3.136 257 8	5.08	Shiraz, Iran
9009	2.251 823 7	−5.816 915 7	1.327 163 5	4.42	Curacao, Antilles
9010	0.976 287 0	−5.601 394 7	2.880 234 7	2.86	Jupiter, USA
9011	2.280 591 3	−4.914 573 5	−3.355 423 0	3.19	Villa Dolores, Argentina
9012	−5.466 059 8	−2.404 278 8	2.242 180 5	2.72	Maui, USA
9912	−5.466 063 0	−2.404 278 7	2.242 172 7	2.72	Maui, USA
9021	−1.936 773 8	−5.077 708 3	3.331 902 4	3.16	Mt. Hopkins, USA
9921	−1.936 772 7	−5.077 705 3	3.331 907 6	3.16	Mt. Hopkins, USA
9028	4.903 765 2	3.965 216 0	0.963 868 0	4.85	Addis Ababa, Ethiopia
9029	5.186 459 7	−3.653 866 0	−0.654 334 7	3.86	Natal, Brazil
9929	5.186 459 9	−3.653 866 2	−0.654 334 8	3.86	Natal, Brazil
9039	5.186 469 8	−3.653 845 2	−0.654 334 4	3.86	Natal, Brazil
9031	1.693 805 4	−4.112 332 6	−4.556 653 1	5.24	Comodoro Rivadavia, Arg.
9091	4.595 167 5	2.039 466 0	3.912 658 7	4.11	Dionysos, Greece
9930	4.595 223 4	2.039 448 2	3.912 612 1	4.11	Dionysos, Greece
9030	4.595 214 5	2.039 448 0	3.912 622 0	4.11	Dionysos, Greece
8019	4.579 476 7	0.586 618 8	4.386 412 7	10.40	Nice, France
8010	4.331 304 7	0.567 521 8	4.633 101 2	3.67	Zimmerwald, Switzerland
9431	3.183 884 5	1.421 475 3	5.322 802 1	20.57	Riga, Latvia
9432	3.907 436 6	1.602 441 7	4.763 886 4	83.31	Uzhgorod, USSR
8011	3.920 168 9	−0.134 732 3	5.012 714 3	13.26	Malvern, U.K.
9425	−2.450 008 9	−4.624 414 9	3.635 028 8	3.70	Rosman, USA
9424	−1.264 845 1	−3.466 879 7	5.185 454 1	10.87	Cold Lake, Canada
9426	3.121 276 0	0.592 642 3	5.512 710 9	12.63	Harestua, Norway
9427	−6.007 407 9	−1.111 859 1	1.825 736 9	7.25	Johnston Is., USA
DSS11	−2.351 447 1	−4.645 070 6	3.673 760 0	3.80	California, USA
DSS12	−2.350 460 6	−4.651 969 9	3.665 624 7	3.80	California, USA
DSS14	−2.353 639 3	−4.641 333 2	3.677 048 3	3.77	California, USA
DSS41	−3.978 702 1	3.724 858 7	−3.302 208 1	2.78	Australia

TABLE 9.32.—*(Cont'd)*

Station	X (Mm)	Y (Mm)	Z (Mm)	σ (m)	Location
DSS42	−4.460 966 9	2.682 428 4	−3.674 613 8	6.05	Australia
DSS51	5.085 447 5	2.668 250 2	−2.768 726 1	4.73	So. Africa
DSS61	4.849 241 1	−0.360 297 2	4.114 867 3	3.64	Spain
DSS62	4.846 698 7	−0.370 214 9	4.116 890 5	3.66	Spain
6001	0.546 586 2	−1.389 973 0	6.180 232 9	11.15	Thule, Greenland
6002	1.130 768 8	−4.830 836 0	3.994 700 2	2.38	Beltsville, USA
6003	−2.127 825 1	−3.785 847 4	4.656 027 9	7.52	Moses Lake, USA
6004	−3.851 769 9	0.396 430 5	5.051 335 4	19.38	Shemya, USA
6006	2.102 948 2	0.721 679 1	5.958 176 5	13.56	Tromsø, Norway
6007	4.433 654 6	−2.268 140 7	3.971 641 0	12.86	Azores, Portugal
6008	3.623 253 6	−5.214 231 1	0.601 517 4	12.95	Paramaribo, Netherlands
6009	1.280 845 5	−6.250 943 5	−0.010 827 7	15.17	Quito, Ecuador
6011	−5.446 010 4	−2.404 397 9	2.242 216 3	3.12	Maui, USA
6012	−5.858 525 1	1.394 529 5	2.093 790 2	13.96	Wake Is., USA
6013	−3.565 847 0	4.120 728 3	3.303 421 8	7.56	Kanoyá, Japan
6015	2.604 378 6	4.444 166 7	3.750 317 1	10.37	Mashhad, Iran
6016	4.896 413 6	1.316 178 8	3.856 666 2	10.87	Catania, Italy
6019	2.280 642 9	−4.914 536 6	−3.355 441 9	3.54	Villa Dolores, Argentina
6020	−1.888 600 6	−5.354 864 7	−2.895 771 6	19.81	Easter Is., Chile
6022	−6.099 943 6	−0.997 320 8	−1.568 598 2	12.65	Tutuila, Am. Samoa
6023	−4.955 351 8	3.842 266 6	−1.163 859 8	8.96	Thursday Is., Australia
6031	−4.313 801 0	0.891 364 6	−4.597 282 7	9.29	Invercargill, New Zealand
6032	−2.375 370 7	4.875 567 2	−3.345 405 6	10.59	Caversham, Australia
6038	−2.160 977 9	−5.642 694 7	2.035 352 3	8.65	Revilla Gigedo, Mexico
6039	−3.724 752 5	−4.421 198 5	−2.686 105 0	22.12	Pitcairn Is., U.K.
6040	−0.741 936 4	6.190 810 5	−1.338 557 8	13.24	Cocos Is., Australia
6042	4.900 772 8	3.968 249 0	0.966 330 3	4.93	Addis Ababa, Ethiopia
6043	1.371 393 5	−3.614 735 8	−5.055 969 1	12.76	Cerro Sombrero, Chile
6044	1.098 926 5	3.684 646 5	−5.071 883 5	23.43	Heard Is., Australia
6045	3.223 459 4	5.045 345 3	−2.191 811 9	9.30	Mauritius, U.K.
6047	−3.361 922 1	5.365 826 1	0.763 621 4	12.76	Zamboanga, Philippines
6050	1.192 697 6	−2.450 987 7	−5.747 074 4	19.81	Palmer Sta., Antarctic
6051	1.111 361 9	2.169 282 1	−5.874 353 0	13.95	Mawson Sta., Antarctic
6052	−0.902 571 8	2.409 550 0	−5.816 569 5	13.80	Wilkes Sta., Antarctic
6053	−1.310 821 8	0.311 286 0	−6.213 299 2	13.45	McMurdo Sta., Antarctic
6055	6.118 349 5	−1.571 738 4	−0.878 618 1	11.14	Ascension Is., U.K.
6059	−5.885 323 7	−2.448 337 7	0.221 658 4	10.63	Christmas Is., U.K.
6060	−4.751 620 6	2.792 084 7	−3.200 181 2	3.19	Culgoora, Australia
6061	2.999 939 6	−2.219 352 6	−5.155 279 4	15.33	So. Georgia, U.K.
6063	5.884 483 9	−1.853 489 1	1.612 843 2	11.17	Dakar, Senegal
6064	6.023 411 3	1.617 937 3	1.331 725 4	9.89	Fort Lamy, Chad
6065	3.213 585 2	0.820 835 9	4.702 766 2	12.59	Hohenpeissenberg, W. Ger.
6067	5.186 415 4	−3.653 927 5	−0.654 297 7	4.13	Natal, Brazil
6068	5.084 848 9	2.670 346 3	−2.768 114 4	2.38	Johannesburg, Rep. S. Afr.
6069	4.978 443 0	−1.086 860 7	−3.823 181 6	26.56	Tristan Da Cunha, U.K.
6072	−0.941 663 5	5.967 461 5	2.039 307 2	13.65	Chiang Mai, Thailand
6073	1.905 165 3	6.032 287 8	−0.810 736 5	12.02	Chagos, Archipelg
6075	3.602 847 1	5.238 244 8	−0.515 950 7	11.39	Seychelles, U.K.
6078	−5.952 304 1	1.231 941 2	−1.925 939 0	22.93	New Hebrides, U.K.
6111	−2.448 849 2	−4.667 968 5	3.582 746 1	3.83	Wrightwood, USA
6123	−1.881 781 5	−0.812 422 7	6.019 588 6	17.73	Point Barrow, USA
6134	−2.448 902 9	−4.668 058 6	3.582 440 8	3.89	Wrightwood, USA

TABLE 9.33.—*Comparison of BC-4 Geometrical Solution With the Combination Solution*[a]

Station	Weight	Differences					
		ΔX	ΔY	ΔZ	North	East	Height
6001	12.22	−0	− 0	4	0	− 0	4
6002	5.54	12	−13	9	1	−15	13
6003	9.03	0	− 4	− 0	− 2	2	2
6004	20.01	2	− 9	1	3	9	− 0
6006	14.45	−6	−12	4	11	−10	0
6007	13.80	−6	− 5	− 1	1	− 7	− 3
6008	13.88	2	− 4	− 4	− 5	0	4
6009	15.97	5	− 5	− 1	− 1	4	6
6011	5.89	15	4	4	9	2	−13
6012	14.83	7	− 2	1	4	0	− 6
6013	9.06	−1	− 8	12	13	6	1
6015	11.51	−5	− 9	7	12	0	− 4
6016	11.96	−5	−11	3	8	−10	− 4
6019	6.13	13	3	− 5	− 3	13	5
6020	20.43	3	5	− 6	− 8	1	− 2
6022	13.60	7	6	− 1	− 3	− 4	− 8
6023	10.26	−2	3	0	1	− 1	4
6031	10.55	−2	4	− 9	− 4	− 4	9
6032	11.71	1	7	− 4	− 0	− 4	6
6038	9.99	4	5	− 1	0	2	− 6
6039	22.68	4	7	− 4	− 7	− 2	− 5
6040	14.15	−1	− 0	− 0	− 0	1	− 0
6042	7.02	−3	− 7	5	6	− 3	− 6
6043	13.70	11	8	− 8	− 8	13	4
6044	23.96	4	7	− 5	3	− 2	10
6045	10.56	−5	− 1	− 7	− 8	3	− 1
6047	13.70	−0	− 0	5	5	0	1
6050	20.43	10	2	− 6	− 0	10	6

TABLE 9.33.—*(Cont'd)*

Station	Weight	Differences ΔX	ΔY	ΔZ	North	East	Height
6051	14.82	5	4	−10	1	− 2	12
6052	14.68	4	5	− 9	− 0	− 5	10
6053	14.35	3	5	−12	− 5	− 5	11
6055	12.21	−9	0	11	10	− 1	−11
6059	11.75	9	5	− 2	− 2	− 1	−11
6060	5.93	−3	3	− 8	− 5	− 1	8
6061	16.12	8	3	− 4	1	8	6
6063	12.24	−8	− 2	0	2	− 4	− 7
6064	11.08	−6	−12	5	7	−10	− 7
6065	13.55	−6	−12	4	9	−11	− 2
6067	6.49	−5	13	10	9	7	−13
6068	5.54	−4	− 3	−24	−24	− 0	5
6069	27.03	−8	2	5	− 0	0	−10
6072	14.54	−3	− 1	9	9	4	1
6073	13.02	−7	− 2	0	0	6	− 4
6075	12.44	−4	− 2	1	1	1	− 4
6078	23.47	−8	3	9	12	− 1	5
6111	6.30	3	2	7	8	2	1
6123	18.42	1	−13	2	− 3	12	3
6134	6.33	4	12	6	12	− 1	− 7
					rms: 7.35	6.33	7.10
					Total rms: 12.02		

	Parameters determined		
	X	*Y*	*Z*
Translation (m)	16.32 ± 1.22	23.21 ± 1.22	−4.68 ± 1.22
Rotation (arc-sec)	−0.101 ± 0.050	0.086 ± 0.050	0.368 ± 0.046
		Scale (ppm) = 1.17 ± 0.19	

[a] Given in units of meters. The standard error of unit weight, σ_0, is 0.823.

TABLE 9.34.—*JPL–SAO Differences*

Rotation: -3.43 ± 1.02 μrad
Scale: $1.8 \times 10^{-7} \pm 5.5 \times 10^{-7}$

Station	R (m)	λ (m)
DSS 11	−0.81	2.69
DSS 12	−0.66	2.63
DSS 14	−0.86	2.57
DSS 41	4.31	−0.21
DSS 42	0.51	1.66
DSS 51	0.96	−3.03
DSS 61	−0.26	2.10
DSS 62	−0.31	2.31

TABLE 9.35.—*Translation, Rotation, and Scale Parameters for the Four Major Datums*

Datum	Number of stations	Translation (m)			Rotation (arc-sec)			Scale correction (ppm)	σ_0	σ (m)
		X	Y	Z	Azimuth	E–W	N–S			
NA27	10	−31.4	154.0	176.3	0.09	−0.62	−0.23	1.78	0.67	8
		±1.9	±2.2	±1.9	±0.24	±0.69	±0.24	±1.13		
EU50	17	−85.4	−111.1	−131.9	0.56	−0.51	−0.22	2.60	0.59	16
		±2.0	±1.9	±2.0	±0.21	±0.35	±0.22	±0.92		
SA69	8	−75.3	−3.3	−52.2	−0.33	−0.13	−0.33	−1.39	0.61	14
		±2.5	±2.6	±2.5	±0.21	±0.27	±0.33	±0.99		
AGD	7	−118.2	−38.6	+119.6	0.23	0.82	−0.22	2.33	0.35	5
		±1.5	±1.4	±1.4	±0.26	±0.41	±0.31	±1.22		

TABLE 9.36.—*Standard Deviations of Datum-Height Comparisons*

Datum	σ (m)
NAD27	3.07
SAD69	2.69
AGD	1.25
EU50	8.90
Average	3.98

TABLE 9.37.—*Comparison of Coordinates Determined in Both SE II and SE III*[a]

Station	Weight	Difference					
		X	*Y*	*Z*	North	East	Height
7050	7.23	1	− 6	− 9	−12	0	− 0
8015	5.41	−0	7	0	0	7	0
9001	5.58	−8	4	0	1	− 9	− 1
9002	7.23	1	− 0	− 3	− 2	− 1	2
9003	6.50	0	0	4	3	− 0	− 1
9004	5.86	3	− 3	− 4	− 5	− 3	0
9005	11.80	3	− 8	− 1	3	4	− 7
9006	9.42	0	− 2	− 2	− 1	− 1	− 3
9007	7.31	5	−10	3	6	1	10
9008	10.33	−1	2	6	5	2	4
9009	8.28	−2	1	4	5	− 1	− 1
9010	5.76	−1	1	− 4	− 3	− 1	− 3
9011	9.55	5	− 2	5	7	3	1
9012	7.51	−3	− 1	8	6	− 0	6
9021	15.33	11	− 6	−13	−13	12	− 5
9023	6.38	1	− 2	5	3	0	− 5
9028	12.94	14	11	− 4	− 6	0	17
9029	12.61	0	−11	− 7	− 7	− 9	7
9031	15.89	5	− 7	− 1	5	2	7
8010	7.90	−5	8	7	8	9	2
8011	16.03	−9	4	5	11	3	− 1
9425	7.92	4	3	− 6	− 2	2	− 8
9424	16.19	−5	2	−13	− 7	− 5	−11
9426	21.18	−4	− 2	8	8	− 1	5
9427	16.66	−2	− 4	5	4	4	4
				rms:	6.62	5.02	6.37
				Total rms:	10.47		

	Parameters determined		
	X	*Y*	*Z*
Translation (m)	−1.69 ± 1.19	3.76 ± 1.18	0.04 ± 1.18
Rotation (arc-sec)	−0.039 ± 0.047	−0.043 ± 0.049	−0.059 ± 0.044
	Scale (ppm) ≡ −0.26 ± 0.18		

[a] The systematic translation, rotation, and scale differences were removed before the differences were computed (in units of meters). The standard error of unit weight σ_0, is 0.662.

TABLE 9.38.—*Comparison of Spin-Axis Distances*

Using SAO station 9001 and geodetic tie	5 492 412.489 m
Using McDonald lunar laser	5 492 416.0 ± 3 m
Difference	−3.51 m

TABLE 9.39.—*Solutions for Even-Order Harmonics*[a]

J_2	J_4	J_6	J_8	J_{10}	J_{12}	J_{14}	J_{16}	J_{18}	J_{20}	J_{22}	J_n	n	$\sum$(residuals)^2
−3	30	−94	66	−178	161	−78	43	−77	−108	75			
±1	±2	±3	±4	±4	±3	±8	±7	±9	±9	±13			114
−3	31	−97	68	−178	155	−74	30	−75	−104	72	31		
±1	±2	±3	±4	±4	±5	±7	±10	±6	±9	±12	±17	24	106
−3	30	−94	67	−177	161	−76	43	−74	−108	73	−9		
±1	±2	±3	±4	±4	±3	±8	±7	±9	±9	±13	±20	26	113
−2	30	−89	61	−181	162	−80	35	−83	−132	80	94		
±1	±2	±3	±3	±3	±2	±6	±6	±5	±8	±9	±17	28	67
−3	28	−92	61	−178	167	−80	44	−75	−104	97	−61		
±1	±2	±3	±4	±4	±4	±7	±7	±6	±9	±15	±28	30	103
−3	29	−94	67	−176	159	−82	41	−76	−111	75	33		
±1	±2	±3	±4	±4	±3	±8	±7	±6	±9	±12	±25	32	110
−3	30	−94	66	−178	162	−78	40	−78	−107	74	14		
±1	±2	±3	±4	±4	±3	±7	±9	±7	±9	±12	±33	34	113
−2	31	−94	65	−183	165	−74	34	−102	−119	92	199		
±1	±1	±2	±2	±2	±2	±4	±4	±5	±5	±7	±22	36	39

[a] In units of 10^{-9}. Corrections are given for $n < 14$. Note that $J_n = -C_n$.

TABLE 9.40.—*Solutions for Odd-Order Harmonics*[a]

J_3	J_5	J_7	J_9	J_{11}	J_{13}	J_{15}	J_{17}	J_{19}	J_{21}	J_{23}	J_n	n	$\sum$(residuals)^2
6	−20	−12	−109	15	−222	104	−227	83	−70	111			
±3	±5	±7	±8	±7	±7	±11	±11	±12	±14	±21			53.7
8	−23	−8	−106	10	−210	88	−210	78	−83	137	−41		
±3	±4	±7	±7	±7	±10	±13	±13	±11	±13	±18	±20	25	49.4
3	−15	−18	−98	19	−226	121	−237	101	−78	101	−58		
±3	±4	±7	±8	±6	±7	±11	±11	±12	±11	±13	±20	27	44.7
5	−19	−12	−107	17	−222	107	−227	84	−64	103	−16		
±3	±5	±7	±8	±7	±7	±11	±11	±12	±14	±17	±23	29	53.0
6	−20	−11	−109	15	−220	106	−227	87	−72	115	−23		
±3	±4	±7	±8	±7	±8	±10	±11	±12	±12	±14	±28	31	52.8
7	−22	−11	−109	13	−219	102	−218	78	−69	124	−47		
±3	±4	±7	±8	±7	±8	±10	±12	±12	±12	±16	±32	33	51.1
5	−18	−19	−101	10	−225	105	−220	99	−83	145	−134		
±3	±4	±7	±7	±6	±7	±9	±10	±11	±11	±15	±36	35	40.6
6	−21	−11	−109	15	−222	102	−225	86	−66	110	−30		
±3	±4	±7	±8	±7	±7	±11	±11	±13	±13	±13	±44	37	53.1

[a] In units of 10^{-9}. Corrections are given for $n \leq 13$. Note that $J_n = -C_n$.

TABLE 9.41.—(O-C) *for Secular Motion and Their Differences*[a]

Satellite		(O-C)		I	II	1969	1963	1961	1959
7001701	$\dot{\omega}$	−18 060	± 90	−57	271	29 090	9 540	18 250	18 840
	$\dot{\Omega}$	10 120	± 70	−51	258	−17 400	−5 390	−9 950	−10 240
7010901	$\dot{\omega}$	−2 200	± 800	−1 530	−857	−4 700	100	6 200	6 900
	$\dot{\Omega}$	5 160	± 100	−83	99	−2 160	−1 450	−5 560	−5 900
6001301	$\dot{\omega}$	170	± 100	43	61	40	−300	−670	−90
	$\dot{\Omega}$	−125	± 5	−4	−10	−1	59	−611	−928
5900101	$\dot{\omega}$	32	± 3	1	3	1	18	−129	278
	$\dot{\Omega}$	−9	± 3	2	7	0	10	−248	−488
6202901	$\dot{\omega}$	40	± 6	11	10	2	300	827	1 013
	$\dot{\Omega}$	7	± 3	5	8	2	−39	−247	−395
6000902	$\dot{\omega}$	170	± 50	0	21	47	−287	770	1 070
	$\dot{\Omega}$	−1	±3	1	5	4	−43	−342	−594
6302601	$\dot{\omega}$	920	± 10	−1	−6	−52	2 650	4 900	5 290
	$\dot{\Omega}$	1	± 3	0	−2	19	261	−2	−352
6206001	$\dot{\omega}$	600	± 60	16	84	60	2 230	4 180	4 500
	$\dot{\Omega}$	−42	± 3	1	2	8	−56	−437	−740
6508901	$\dot{\omega}$	−110	± 10	−1	−29	−26	1 460	3 180	3 285
	$\dot{\Omega}$	−70	± 3	0	−6	−7	−670	−1 465	−1 670
6101501	$\dot{\omega}$	−300	± 80	14	97	65	−81	1 900	2 500
	$\dot{\Omega}$	22	± 3	−1	−1	3	−1 252	−2 815	−3 057
6400101	$\dot{\omega}$	600	± 800	729	718	620	−600	580	−500
	$\dot{\Omega}$	56	± 8	10	6	9	−1 073	−2 703	−2 921
6406401	$\dot{\omega}$	−400	± 100	−95	−231	−110	−2 000	−4 000	−4 300
	$\dot{\Omega}$	90	± 10	9	9	15	−220	−1 351	−1 467
6508101	$\dot{\omega}$	620	± 30	15	100	−8	300	−3 290	−3 630
	$\dot{\Omega}$	50	± 3	−2	−9	−27	35	−306	−337
6102801	$\dot{\omega}$	−35	± 50	−47	−47	−47	−340	−915	−1 008
	$\dot{\Omega}$	−2.9	± 0.5	0.6	0.7	0.6	62.7	192.3	212.6

[a] Given in units of 10^{-6} per day.

TABLE 9.42.—(O-C) *for Amplitudes of* $\left.\begin{matrix}cos\\sin\end{matrix}\right\}$ 2ω *Terms and Their Differences*[a]

Satellite		(O-C)	I	II	1969	1963	1961	1959
5900101	ω	0.3 ± 0.5	−0.2	−0.2	−0.3	−0.6	1.5	1.4
	Ω	−2 ± 2	−1	−2	−2	−1	−4	−4
	I	−3 ± 6	−4	−4	−5	−4	3	3
	e	0 ± 1	1	1	1	1	−4	−4
6202901	ω	−0.1 ± 0.3	−0.2	−0.2	−0.2	−0.8	−2.5	−2.7
	Ω	−1 ± 1	1	1	1	−8	−14	−14
	I	4 ± 4	5	4	4	−3	−14	−15
	e	0 ± 1	0	0	0	5	12	12
6000902	ω	−3 ± 4	−2	−2	−2	−6	−10	−10
	e	0 ± 1	0	0	0	0	1	1
6302601	ω	−6 ± 2	−1	0	0	−14	−23	−23
	Ω	2 ± 2	3	3	3	−2	−3	−3
	I	−1 ± 3	1	1	1	−4	−6	−6
	e	3 ± 2	−3	−3	−3	12	20	20
6206001	ω	3 ± 6	7	6	6	−5	−13	−13
	e	1 ± 1	1	1	0	2	3	3
6508901	ω	6 ± 2	1	2	2	−22	−49	−50
	Ω	4 ± 2	2	2	0	9	10	10
	I	5 ± 5	4	4	4	−3	−11	−11
	e	−4 ± 1	2	1	1	30	62	63
6101501	[b]ω	−1 ± 2	−1	0	0	−3	0	0
	e	1 ± 2	0	0	−1	3	−1	−1
6406401	[b]ω	0 ± 2	0	0	0	−1	−1	−1
	e	4 ± 4	3	4	3	5	7	7
6508101	ω	7 ± 3	3	4	3	12	0	0
	Ω	1 ± 1	1	0	0	2	2	2
	I	−2 ± 8	−2	−2	−2	−2	−2	−2
	e	−6 ± 2	−1	−2	−1	−11	3	3

[a] Given in units of 10^3 degrees for ω, 10^4 degrees for Ω, 10^5 degrees for I, and 10^6 for e, per day.
[b] For these satellites, ω is in units of 10^7 degrees.

TABLE 9.43.—(O-C) *for Amplitudes of* $\left.\begin{matrix}cos\\sin\end{matrix}\right\}$ *ω Terms and Their Differences*[a]

Satellite		(O-C)	I	II	1969	1963	1961	1959
7001701	ω	−70 ± 5	−2	0	−126	−104	−85	−87
	Ω	−190 ± 30	0	−28	−248	−570	−168	−237
	I	430 ± 30	−34	−31	740	900	480	550
	e	−91 ± 6	−5	−5	−149	−179	−99	−112
7010901	ω	45 ± 30	9	41	160	−411	232	112
	Ω	−18 ± 45	−44	−48	0	10	9	7
	I	−170 ± 300	−166	−170	−181	−120	−190	−177
	e	28 ± 20	18	27	61	−102	83	49
6001301	ω	4 ± 1	0	0	0	46	314	241
	Ω	0 ± 3	2	2	0	3	−10	−7
	I	0 ± 30	0	0	0	−2	−16	−12
	e	1.6 ± 1.0	0.5	0.5	0.6	13.5	90.7	69.8
5900101	ω	−1.7 ± 0.3	0.0	0.3	0.0	4.8	22.4	17.2
	Ω	−2 ± 2	2	1	2	−7	−87	−58
	I	1 ± 5	−3	−3	−4	−8	−64	−57
	e	−3.1 ± 0.5	−0.3	−0.7	−0.1	3.2	40.0	35.6
6202901	ω	−0.1 ± 0.2	0.0	0.0	−0.1	−1.2	−4.0	6.1
	Ω	2 ± 3	2	3	3	16	5	31
	I	−2 ± 3	−5	−4	−4	−11	−26	−78
	e	1.5 ± 0.8	0.2	0.0	0.2	4.2	15.2	49.7
6000902	ω	−19 ± 3	−4	−4	−10	42	1	315
	Ω	1 ± 1	1	1	0	3	4	6
	I	−2 ± 6	−2	−2	−6	−3	−2	−6
	e	−2.0 ± 0.6	1.0	1.0	0.3	10.5	2.4	64.8
6302601	ω	−17 ± 2	0	−4	−1	9	−17	86
	Ω	−6 ± 1	0	0	1	20	52	60
	I	14 ± 15	10	11	10	6	12	−19
	e	−12 ± 1	0	−1	2	16	−6	99
6206001	ω	−59 ± 4	0	5	0	187	122	931
	Ω	−2 ± 2	−2	−2	−2	0	3	4
	I	0 ± 10	0	0	0	−1	0	−4
	e	−8 ± 1	−1	0	−1	22	14	113
6508901	ω	3 ± 4	7	7	0	119	264	486
	Ω	10 ± 2	3	3	2	−10	8	−29
	I	−8 ± 8	−9	−9	−7	−40	−80	−144
	e	−4 ± 1	0	0	−2	127	292	555
6101501	[b]ω	−19 ± 5	−11	−11	−8	−46	−265	−413
	Ω	−3 ± 4	2	2	0	7	17	29
	I	0 ± 5	0	0	0	1	7	11
	e	−11 ± 1	0	0	4	−48	−354	−560
6400101	[b]ω	−200 ± 10	6	3	1	−72	−445	−593
	e	−58 ± 3	−4	−5	−9	−24	−122	−161
6406401	ω	−110 ± 20	23	36	30	23	510	930
	Ω	6 ± 3	1	1	1	5	11	16
	I	0 ± 8	0	0	0	0	−2	−3
	e	−34 ± 5	−4	−2	−2	−4	106	199
6508101	ω	60 ± 2	1	−1	3	64	197	296
	Ω	20 ± 1	0	2	2	16	26	32
	I	−10 ± 10	−9	−9	−10	−10	−13	−16
	e	60 ± 3	−4	−5	−2	67	231	354
6102801	ω	−30 ± 50	−48	−47	−40	15	390	663
	Ω	−2 ± 2	−2	−2	−2	−2	−3	−4
	I	−6 ± 7	−6	−6	−6	−6	−6	−5
	e	3.0 ± 1.5	−0.7	−0.6	0.0	12.5	91.8	149.2

[a] Given in units of 10^3 degrees for ω, 10^4 degrees for Ω, 10^5 degrees for *I*, and 10^6 for *e*, per day.
[b] For these satellites, ω is in units of 10^2 degrees.

TABLE 9.44.—*Comparison of Results*[a]

Solution	J_2	J_4	J_6	J_8	J_{10}	J_{12}	J_{14}	J_{16}	J_{18}	J_{20}	J_{22}	J_{36}
1959	1082.1	−2.15										
1961	1082.19	−2.13										
	±3	±5										
1963	1082.48	−1.84	0.39	−0.02								
	±4	±9	±9	±7								
1964	1082.639	−1.649	0.646	−0.270	−0.054	−0.357	0.179					
	±6	±16	±30	±50	±50	±44	±63					
1969	1082.628	−1.593	0.502	−0.118	−0.354	−0.042	−0.073	0.187	−0.231	−0.005		
	±2	±7	±14	±20	±25	±27	±28	±26	±22	±22		
1973 I	1082.637	−1.618	0.552	−0.205	−0.237	−0.192	0.105	0.034	−0.102	−0.119	0.092	0.199
	±1	±1	±2	±2	±2	±2	±4	±4	±5	±5	±7	±22
1973 II	1082.636	−1.619	0.552	−0.204	−0.232	−0.196	0.101	0.043	−0.077	−0.108	0.075	
	±1	±2	±3	±4	±4	±3	±8	±7	±9	±9	±13	
Cazenave *et al.* (1971)	1082.637	−1.619	0.558	−0.209	−0.233	−0.188	0.085	0.048	−0.137	−0.087		
	±4	±10	±17	±24	±26	±27	±34	±43	±44	±52		

Solution	J_3	J_5	J_7	J_9	J_{11}	J_{13}	J_{15}	J_{17}	J_{19}	J_{21}	J_{23}	J_{35}
1959	−2.20											
	±8											
1961	−2.29	−0.23										
	±2	±2										
1963	−2.562	−0.064	−0.470	0.117								
	±7	±7	±10	±11								
1964	−2.546	−0.210	−0.333	−0.053	0.302	−0.114						
	±20	±25	±39	±60	±35	±84						
1969	−2.538	−0.230	−0.361	−0.100	0.202	−0.123	−0.174	0.085	−0.216	0.145		
	±4	±7	±15	±23	±35	±49	±61	±65	±53	±29		
1973 I	−2.541	−0.228	−0.352	−0.154	0.312	−0.339	0.105	−0.220	0.099	−0.083	0.145	−0.134
	±3	±4	±7	±7	±6	±7	±9	±10	±11	±11	±15	±36
1973 II	−2.540	−0.230	−0.345	−0.162	0.317	−0.336	0.104	−0.227	0.083	−0.070	0.111	
	±3	±3	±7	±8	±7	±7	±11	±11	±12	±17	±21	
Cazenave *et al.* (1971)	−2.543	−0.226	−0.365	−0.118	0.236	−0.202	−0.081	−0.027	−0.112	0.106		
	±5	±7	±12	±13	±12	±14	±21	±23	±23	±15		

[a] Given in units of 10^{-6}.

TABLE 9.45.—*Fully Normalized Tesseral-Harmonic Coefficients for the Potential*[a]

Harmonic	Value	Harmonic	Value	Harmonic	Value	Harmonic	Value
$\overline{C}_{2,2}$	2.3799 −06	$\overline{S}_{2,2}$	−1.3656 −06	$\overline{C}_{3,1}$	1.9977 −06	$\overline{S}_{3,1}$	2.2337 −07
$\overline{C}_{3,2}$	7.7830 −07	$\overline{S}_{3,2}$	−7.5519 −07	$\overline{C}_{3,3}$	4.9011 −07	$\overline{S}_{3,3}$	1.5283 −06
$\overline{C}_{4,1}$	−5.1748 −07	$\overline{S}_{4,1}$	−4.8140 −07	$\overline{C}_{4,2}$	3.4296 −07	$\overline{S}_{4,2}$	6.7174 −07
$\overline{C}_{4,3}$	1.0390 −06	$\overline{S}_{4,3}$	−1.1923 −07	$\overline{C}_{4,4}$	−1.0512 −07	$\overline{S}_{4,4}$	3.5661 −07
$\overline{C}_{5,1}$	−5.3667 −08	$\overline{S}_{5,1}$	−7.9973 −08	$\overline{C}_{5,2}$	5.9869 −07	$\overline{S}_{5,2}$	−3.9910 −07
$\overline{C}_{5,3}$	−5.8429 −07	$\overline{S}_{5,3}$	−1.6338 −07	$\overline{C}_{5,4}$	−1.1583 −07	$\overline{S}_{5,4}$	−4.5393 −08
$\overline{C}_{5,5}$	1.3956 −07	$\overline{S}_{5,5}$	−8.6841 −07	$\overline{C}_{6,1}$	−7.2166 −08	$\overline{S}_{6,1}$	1.7756 −08
$\overline{C}_{6,2}$	2.4670 −08	$\overline{S}_{6,2}$	−4.0654 −07	$\overline{C}_{6,3}$	4.4139 −09	$\overline{S}_{6,3}$	2.9055 −08
$\overline{C}_{6,4}$	−1.0003 −07	$\overline{S}_{6,4}$	−3 .0297 −07	$\overline{C}_{6,5}$	−1.3504 −07	$\overline{S}_{6,5}$	−6.0964 −07
$\overline{C}_{6,6}$	−2.9136 −08	$\overline{S}_{6,6}$	−2.6327 −07	$\overline{C}_{7,1}$	2.3532 −07	$\overline{S}_{7,1}$	5.5634 −08
$\overline{C}_{7,2}$	2.0425 −07	$\overline{S}_{7,2}$	1.7321 −07	$\overline{C}_{7,3}$	2.1994 −07	$\overline{S}_{7,3}$	−3.4644 −07
$\overline{C}_{7,4}$	−2.8617 −07	$\overline{S}_{7,4}$	−2.7738 −07	$\overline{C}_{7,5}$	3.4727 −08	$\overline{S}_{7,5}$	8.7014 −08
$\overline{C}_{7,6}$	−2.7496 −07	$\overline{S}_{7,6}$	8.5865 −08	$\overline{C}_{7,7}$	−2.4856 −08	$\overline{S}_{7,7}$	−8.8968 −09
$\overline{C}_{8,1}$	1.0946 −08	$\overline{S}_{8,1}$	4.8429 −08	$\overline{C}_{8,2}$	1.1084 −07	$\overline{S}_{8,2}$	1.0359 −07
$\overline{C}_{8,3}$	−8.8578 −08	$\overline{S}_{8,3}$	−5.0715 −08	$\overline{C}_{8,4}$	−2.2315 −07	$\overline{S}_{8,4}$	2.6511 −07
$\overline{C}_{8,5}$	1.5318 −07	$\overline{S}_{8,5}$	8.1158 −08	$\overline{C}_{8,6}$	−9.7542 −08	$\overline{S}_{8,6}$	2.8082 −07
$\overline{C}_{8,7}$	2.0498 −07	$\overline{S}_{8,7}$	2.4592 −07	$\overline{C}_{8,8}$	1.6967 −07	$\overline{S}_{8,8}$	9.3261 −08
$\overline{C}_{9,1}$	1.8099 −07	$\overline{S}_{9,1}$	4.1091 −08	$\overline{C}_{9,2}$	−2.2013 −08	$\overline{S}_{9,2}$	2.4215 −09
$\overline{C}_{9,3}$	−9.9252 −08	$\overline{S}_{9,3}$	−2.3085 −08	$\overline{C}_{9,4}$	−4.0867 −08	$\overline{S}_{9,4}$	−3.8525 −08
$\overline{C}_{9,5}$	−5.8957 −08	$\overline{S}_{9,5}$	3.6834 −09	$\overline{C}_{9,6}$	4.8812 −08	$\overline{S}_{9,6}$	1.1115 −07
$\overline{C}_{9,7}$	−1.9880 −07	$\overline{S}_{9,7}$	−1.4978 −07	$\overline{C}_{9,8}$	2.3523 −07	$\overline{S}_{9,8}$	9.6355 −09
$\overline{C}_{9,9}$	−3.4533 −08	$\overline{S}_{9,9}$	5.9502 −08	$\overline{C}_{10,1}$	8.9008 −08	$\overline{S}_{10,1}$	−6.0157 −08
$\overline{C}_{10,2}$	−3.7256 −08	$\overline{S}_{10,2}$	−6.3676 −08	$\overline{C}_{10,3}$	−1.3307 −07	$\overline{S}_{10,3}$	−7.2728 −08
$\overline{C}_{10,4}$	−2.1887 −08	$\overline{S}_{10,4}$	−7.8408 −08	$\overline{C}_{10,5}$	−6.1509 −09	$\overline{S}_{10,5}$	−1.1904 −07
$\overline{C}_{10,6}$	−9.4142 −08	$\overline{S}_{10,6}$	−1.1728 −08	$\overline{C}_{10,7}$	1.8525 −07	$\overline{S}_{10,7}$	2.1656 −08
$\overline{C}_{10,8}$	1.0887 −09	$\overline{S}_{10,8}$	7.0781 −09	$\overline{C}_{10,9}$	7.8473 −08	$\overline{S}_{10,9}$	5.6381 −09
$\overline{C}_{10,10}$	1.3321 −07	$\overline{S}_{10,10}$	9.8839 −08	$\overline{C}_{11,1}$	−1.2194 −08	$\overline{S}_{11,1}$	7.5463 −08
$\overline{C}_{11,2}$	−2.0255 −08	$\overline{S}_{11,2}$	−6.2998 −08	$\overline{C}_{11,3}$	−1.0988 −09	$\overline{S}_{11,3}$	−3.8098 −08
$\overline{C}_{11,4}$	1.5676 −08	$\overline{S}_{11,4}$	−1.9551 −07	$\overline{C}_{11,5}$	−1.8591 −09	$\overline{S}_{11,5}$	6.1113 −08
$\overline{C}_{11,6}$	6.3601 −08	$\overline{S}_{11,6}$	−2.6457 −08	$\overline{C}_{11,7}$	−3.3761 −08	$\overline{S}_{11,7}$	−1.2825 −07
$\overline{C}_{11,8}$	−1.3634 −08	$\overline{S}_{11,8}$	4.5229 −08	$\overline{C}_{11,9}$	2.1256 −08	$\overline{S}_{11,9}$	6.6721 −08
$\overline{C}_{11,10}$	5.2555 −08	$\overline{S}_{11,10}$	−7.7401 −08	$\overline{C}_{11,11}$	8.6996 −08	$\overline{S}_{11,11}$	−2.5691 −08
$\overline{C}_{12,1}$	−5.6935 −08	$\overline{S}_{12,1}$	−6.6159 −08	$\overline{C}_{12,2}$	−9.7424 −08	$\overline{S}_{12,2}$	4.6341 −08
$\overline{C}_{12,3}$	1.5555 −07	$\overline{S}_{12,3}$	−4.8666 −08	$\overline{C}_{12,4}$	−5.0379 −08	$\overline{S}_{12,4}$	5.3568 −08
$\overline{C}_{12,5}$	8.1834 −08	$\overline{S}_{12,5}$	2.7932 −08	$\overline{C}_{12,6}$	−2.1177 −08	$\overline{S}_{12,6}$	3.5034 −08
$\overline{C}_{12,7}$	2.9751 −08	$\overline{S}_{12,7}$	3.1783 −08	$\overline{C}_{12,8}$	4.0190 −08	$\overline{S}_{12,8}$	5.6877 −08
$\overline{C}_{12,9}$	−1.1503 −07	$\overline{S}_{12,9}$	1.4508 −08	$\overline{C}_{12,10}$	−4.5921 −08	$\overline{S}_{12,10}$	−4.3264 −08
$\overline{C}_{12,11}$	−7.8443 −09	$\overline{S}_{12,11}$	−4.7858 −08	$\overline{C}_{12,12}$	−2.7617 −08	$\overline{S}_{12,12}$	−1.6808 −08
$\overline{C}_{13,1}$	8.6136 −09	$\overline{S}_{13,1}$	−3.2401 −08	$\overline{C}_{13,2}$	−1.0679 −08	$\overline{S}_{13,2}$	−9.0670 −08
$\overline{C}_{13,3}$	−3.2361 −08	$\overline{S}_{13,3}$	4.9286 −08	$\overline{C}_{13,4}$	3.9852 −08	$\overline{S}_{13,4}$	−1.0608 −07
$\overline{C}_{13,5}$	4.0047 −08	$\overline{S}_{13,5}$	3.8114 −08	$\overline{C}_{13,6}$	−2.1906 −08	$\overline{S}_{13,6}$	−1.1321 −08
$\overline{C}_{13,7}$	−7.6933 −08	$\overline{S}_{13,7}$	1.1140 −08	$\overline{C}_{13,8}$	−2.7448 −09	$\overline{S}_{13,8}$	1.4309 −08
$\overline{C}_{13,9}$	−1.1588 −08	$\overline{S}_{13,9}$	7.2989 −08	$\overline{C}_{13,10}$	4.1979 −09	$\overline{S}_{13,10}$	7.6769 −09
$\overline{C}_{13,11}$	−5.4381 −08	$\overline{S}_{13,11}$	1.3450 −08	$\overline{C}_{13,12}$	−4.6633 −08	$\overline{S}_{13,12}$	7.9963 −08
$\overline{C}_{13,13}$	−6.8944 −08	$\overline{S}_{13,13}$	7.1891 −08	$\overline{C}_{14,1}$	−1.4359 −08	$\overline{S}_{14,1}$	5.2390 −08

[a] Values given as coefficient and exponent of 10.

TABLE 9.45.—*(Cont'd)*

Harmonic	Value	Harmonic	Value	Harmonic	Value	Harmonic	Value
$\overline{C}_{14,2}$	−1.5908 −08	$\overline{S}_{14,2}$	−2.7374 −09	$\overline{C}_{14,3}$	9.6915 −08	$\overline{S}_{14,3}$	−2.5631 −08
$\overline{C}_{14,4}$	−2.9864 −08	$\overline{S}_{14,4}$	−3.8189 −09	$\overline{C}_{14,5}$	−1.3828 −09	$\overline{S}_{14,5}$	−5.8680 −08
$\overline{C}_{14,6}$	−1.3872 −08	$\overline{S}_{14,6}$	−2.7976 −08	$\overline{C}_{14,7}$	7.1056 −08	$\overline{S}_{14,7}$	2.4043 −09
$\overline{C}_{14,8}$	−1.8779 −08	$\overline{S}_{14,8}$	−5.8750 −08	$\overline{C}_{14,9}$	−2.4322 −08	$\overline{S}_{14,9}$	6.0461 −08
$\overline{C}_{14,10}$	2.8985 −08	$\overline{S}_{14,10}$	−3.4224 −08	$\overline{C}_{14,11}$	8.2611 −08	$\overline{S}_{14,11}$	−1.9627 −09
$\overline{C}_{14,12}$	1.1751 −09	$\overline{S}_{14,12}$	−3.0967 −08	$\overline{C}_{14,13}$	3.0793 −08	$\overline{S}_{14,13}$	4.7620 −08
$\overline{C}_{14,14}$	−6.5969 −08	$\overline{S}_{14,14}$	3.3030 −09	$\overline{C}_{15,1}$	2.9358 −08	$\overline{S}_{15,1}$	−1.6691 −08
$\overline{C}_{15,2}$	−1.2291 −08	$\overline{S}_{15,2}$	−6.8963 −08	$\overline{C}_{15,3}$	−5.8921 −08	$\overline{S}_{15,3}$	4.477 2 −08
$\overline{C}_{15,4}$	1.4876 −08	$\overline{S}_{15,4}$	7.0359 −09	$\overline{C}_{15,5}$	3.6806 −08	$\overline{S}_{15,5}$	−8.4051 −09
$\overline{C}_{15,6}$	1.0081 −08	$\overline{S}_{15,6}$	−3.0473 −08	$\overline{C}_{15,7}$	3.0439 −08	$\overline{S}_{15,7}$	1.5775 −08
$\overline{C}_{15,8}$	−6.8884 −08	$\overline{S}_{15,8}$	6.0808 −08	$\overline{C}_{15,9}$	−4.5169 −08	$\overline{S}_{15,9}$	5.5556 −08
$\overline{C}_{15,10}$	6.2126 −08	$\overline{S}_{15,10}$	−7.1799 −09	$\overline{C}_{15,11}$	−4.4724 −08	$\overline{S}_{15,11}$	−3.4391 −09
$\overline{C}_{15,12}$	−4.2025 −08	$\overline{S}_{15,12}$	5.9072 −09	$\overline{C}_{15,13}$	−4.1654 −08	$\overline{S}_{15,13}$	−5.5892 −09
$\overline{C}_{15,14}$	9.5654 −09	$\overline{S}_{15,14}$	−2.7145 −08	$\overline{C}_{15,15}$	−5.6358 −08	$\overline{S}_{15,15}$	3.4895 −08
$\overline{C}_{16,1}$	−9.9588 −09	$\overline{S}_{16,1}$	5.4160 −08	$\overline{C}_{16,2}$	5.5086 −09	$\overline{S}_{16,2}$	4.9455 −08
$\overline{C}_{16,3}$	5.4189 −08	$\overline{S}_{16,3}$	5.4887 −09	$\overline{C}_{16,4}$	4.6176 −08	$\overline{S}_{16,4}$	3.6270 −08
$\overline{C}_{16,5}$	−2.4432 −08	$\overline{S}_{16,5}$	2.9671 −08	$\overline{C}_{16,6}$	−3.7203 −09	$\overline{S}_{16,6}$	−2.0786 −08
$\overline{C}_{16,7}$	−2.2794 −09	$\overline{S}_{16,7}$	3.0609 −09	$\overline{C}_{16,8}$	−1.0459 −07	$\overline{S}_{16,8}$	−4.4731 −08
$\overline{C}_{16,9}$	2.4845 −08	$\overline{S}_{16,9}$	−8.6262 −08	$\overline{C}_{16,10}$	−3.9928 −08	$\overline{S}_{16,10}$	−4.5058 −09
$\overline{C}_{16,11}$	−2.0848 −08	$\overline{S}_{16,11}$	2.9738 −08	$\overline{C}_{16,12}$	1.5930 −08	$\overline{S}_{16,12}$	−1.2703 −08
$\overline{C}_{16,13}$	2.5280 −08	$\overline{S}_{16,13}$	6.6240 −09	$\overline{C}_{16,14}$	−1.4852 −08	$\overline{S}_{16,14}$	−8.1713 −09
$\overline{C}_{16,15}$	−7.7425 −08	$\overline{S}_{16,15}$	−2.6491 −08	$\overline{C}_{16,16}$	−1.8538 −08	$\overline{S}_{16,16}$	−2.2310 −08
$\overline{C}_{17,1}$	8.6593 −09	$\overline{S}_{17,1}$	−4.1093 −08	$\overline{C}_{17,2}$	−9.0769 −09	$\overline{S}_{17,2}$	−2.7205 −08
$\overline{C}_{17,3}$	−7.7864 −09	$\overline{S}_{17,3}$	−1.7913 −08	$\overline{C}_{17,4}$	−4.3231 −08	$\overline{S}_{17,4}$	6.8203 −08
$\overline{C}_{17,5}$	4.1513 −08	$\overline{S}_{17,5}$	−2.5453 −08	$\overline{C}_{17,6}$	−4.5453 −08	$\overline{S}_{17,6}$	−1.7273 −08
$\overline{C}_{17,7}$	1.6938 −08	$\overline{S}_{17,7}$	−3.3752 −08	$\overline{C}_{17,8}$	4.1231 −08	$\overline{S}_{17,8}$	5.8792 −09
$\overline{C}_{17,9}$	−4.3119 −08	$\overline{S}_{17,9}$	−1.5974 −08	$\overline{C}_{17,10}$	−1.0844 −08	$\overline{S}_{17,10}$	5.5628 −08
$\overline{C}_{17,11}$	−4.4136 −08	$\overline{S}_{17,11}$	−4.3123 −09	$\overline{C}_{17,12}$	3.1661 −08	$\overline{S}_{17,12}$	6.2982 −09
$\overline{C}_{17,13}$	2.5147 −08	$\overline{S}_{17,13}$	9.7728 −09	$\overline{C}_{17,14}$	−5.5945 −09	$\overline{S}_{17,14}$	7.2604 −09
$\overline{C}_{17,15}$	4.9113 −08	$\overline{S}_{17,15}$	3.1958 −08	$\overline{C}_{17,16}$	−2.3540 −08	$\overline{S}_{17,16}$	−1.5882 −08
$\overline{C}_{17,17}$	−9.0191 08	$\overline{S}_{17,17}$	−9.4775 −09	$\overline{C}_{18,1}$	−2.3557 −08	$\overline{S}_{18,1}$	−7.4536 −08
$\overline{C}_{18,2}$	−9.4249 −09	$\overline{S}_{18,2}$	3.0353 −08	$\overline{C}_{18,3}$	−3.5003 −08	$\overline{S}_{18,3}$	−2.0464 −08
$\overline{C}_{18,4}$	2.9433 −08	$\overline{S}_{18,4}$	−4.4672 −08	$\overline{C}_{18,5}$	1.7511 −09	$\overline{S}_{18,5}$	−6.0367 −09
$\overline{C}_{18,6}$	2.3931 −08	$\overline{S}_{18,6}$	−4.4966 −09	$\overline{C}_{18,7}$	−7.8040 −10	$\overline{S}_{18,7}$	−8.2010 −09
$\overline{C}_{18,8}$	5.3819 −08	$\overline{S}_{18,8}$	−2.2106 −08	$\overline{C}_{18,9}$	−3.6120 −10	$\overline{S}_{18,9}$	−5.0562 −09
$\overline{C}_{18,10}$	4.2146 −08	$\overline{S}_{18,10}$	7.8924 −09	$\overline{C}_{18,11}$	2.4981 −08	$\overline{S}_{18,11}$	2.3183 −08
$\overline{C}_{18,12}$	−6.2242 −09	$\overline{S}_{18,12}$	6.6025 −09	$\overline{C}_{18,13}$	−2.6685 −08	$\overline{S}_{18,13}$	−4.2500 −08
$\overline{C}_{18,14}$	9.1191 −09	$\overline{S}_{18,14}$	−3.3129 −08	$\overline{C}_{18,15}$	−4.1521 −08	$\overline{S}_{18,15}$	−1.7610 −08
$\overline{C}_{18,16}$	2.4850 −08	$\overline{S}_{18,16}$	−4.8182 −09	$\overline{C}_{18,17}$	3.5357 −08	$\overline{S}_{18,17}$	−4.7166 −08
$\overline{C}_{18,18}$	−3.4701 −10	$\overline{S}_{18,18}$	5.0554 −08	$\overline{C}_{19,12}$	3.6058 −08	$\overline{S}_{19,12}$	−3.4421 −09
$\overline{C}_{19,13}$	9.6876 −09	$\overline{S}_{19,13}$	−6.6095 −08	$\overline{C}_{19,14}$	7.6389 −09	$\overline{S}_{19,14}$	−2.7649 −08
$\overline{C}_{20,13}$	2.7630 −08	$\overline{S}_{20,13}$	3.2389 −08	$\overline{C}_{20,14}$	3.3687 −08	$\overline{S}_{20,14}$	−6.5741 −08
$\overline{C}_{21,13}$	−1.9799 −08	$\overline{S}_{21,13}$	−3.0711 −08	$\overline{C}_{21,14}$	1.6623 −08	$\overline{S}_{21,14}$	8.7215 −09
$\overline{C}_{22,13}$	−7.9435 −09	$\overline{S}_{22,13}$	4.1452 −09	$\overline{C}_{22,14}$	2.8516 −09	$\overline{S}_{22,14}$	−4.2148 −08
$\overline{C}_{23,13}$	−1.3236 −08	$\overline{S}_{23,13}$	−4.8892 −09	$\overline{C}_{23,14}$	−2.1148 −08	$\overline{S}_{23,14}$	2.2010 −08
$\overline{C}_{24,14}$	3.4668 −09	$\overline{S}_{24,14}$	2.2983 −08				

TABLE 9.46.—*Comparison of SE III With Satellite Observations*[a]

Epoch (MJD)	σ(m)	n	Epoch (MJD)	σ(m)	n
	6508901 (GEOS-A) A/m = 0.05				
41 000	4.1	289	41 010	7.7	523
41 002	5.5	367	41 012	9.8	577
41 004	3.2	314	41 014	9.2	715
41 006	8.9	601	14 016	4.1	425
41 008	10.6	696	41 018	3.6	221
	6800201 (GEOS-B) A/m = 0.05				
41 038	2.4	249	41 048	3.8	304
41 040	6.5	533			
41 042	7.8	681	41 052	2.8	388
41 044	6.3	651	41 054	6.6	602
41 046	2.7	441			
	6701401 (DID) A/m = 0.1				
41 072	10.3	467	41 080	7.4	621
41 074	9.9	332	41 082	6.9	764
41 076	16.3	341	41 084	4.9	427
41 078	17.0	254	41 086	3.6	519

[a] n is number of observations used.

TABLE 9.47.—*Comparison of SE III Combination Solution With Surface Gravity*[a]

Solution	ℓ,m	$\langle(g_t - g_s)^2\rangle$	$\langle g_t g_s\rangle$	$\langle g_s^2\rangle$	D	$\langle g_t^2\rangle$	$E\ (e_s^2)$	$E\ (e_t^2)$	$E\ (\delta g^2)$	n
SE II[b]	16	75	184	186	163	253	2	11	63	≥20
SE II	16	187	177	229	203	311	52	13	122	(306 anomalies)[c]
SE III	18	105	221	236	237	311	15	13	77	----------
SE III	10	195	150	192	163	302	42	24	129	≥ 1
	14	174	174	220	198	302	47	24	103	(1183 anomalies)
	18	156	202	258	237	302	56	24	75	----------
SE III	10	184	183	205	163	345	22	19	143	≥10
	14	151	215	236	198	345	20	19	111	(659 anomalies)
	18	117	255	281	237	345	26	19	63	----------
SE III	10	186	151	176	163	311	25 (24)	13	148	≥20
	14	146	182	200	198	311	17 (21)	13	116	(306 anomalies)
	18	105	221	236	237	311	15 (18)	13	77	----------

[a] Given in mGal^2.
[b] From the available data, there were 935, 369, and 136 gravity anomalies with $n \geq 1$,10, and 20 1° × 1° anomalies.
[c] Here, n is the number of 1° × 1° mean gravity anomalies used to obtain 5° × 5° mean gravity anomalies.

TABLE 9.48.—*Surface-Gravity Residuals for an $\ell = m = 36$ Potential From Numerical Quadrature*[a]

Degree of reference field	$\langle(g_t - g_s)^2\rangle$ $n = 1$	$n = 20$	$\langle(g_s - g_{ref})^2\rangle$ $n = 0$	$E\,(e_s^2)$
0	28	29	12	-----
6	38	39	12	10
8	53	54	20	25
10	56	53	21	24
14	61	50	19	21
18	70	48	16	18
Anomalies used	1183	306	471	-----

[a] Given in mGal^2.

TABLE 9.49.—*Comparison With Independent Surface-Gravity Data*[a]

Comparison field, g_c	Maximum ℓ, m	n	$\langle(g_t - g_s)^2\rangle$	$\langle g_t g_s\rangle$	$\langle g_t^2\rangle$	D	$\langle g_c^2\rangle$	$E\,(e_s^2)$	$E\,(e_t^2)$	$E\,(\delta_n^2)$	Region
SE III	18	3726	147	209	284	237	282	75	13	59	North Atlantic
SE III	18	1794	145	188	232	237	290	44	13	88	Indian Ocean
Averages								64 ≈ 3 m		68	

[a] Given in mGal^2.